

Promotors: Prof. dr. ir. Jan Pieters

Ghent University (UGent)

Department of Biosystems Engineering

Dr. ir. Peter Demeyer

Institute for Agricultural and Fisheries Research (ILVO)

Technology and Food Science Unit – Agricultural Engineering

Dean: Prof. dr. ir. Marc Van Meirvenne

Rector: Prof. dr. Anne De Paepe

Philippe Van Overbeke

**Development of a reference method for ventilation rate
measurements in a naturally ventilated test facility**

Thesis submitted in fulfilment of the requirements for the degree of Doctor (PhD) in Applied
Biological Sciences

Dutch translation of title:

Ontwikkeling van een referentiemethode voor ventilatiedebietsmetingen in een natuurlijk geventileerde testconstructie

Van Overbeke P. (2015). Development of a reference method for ventilation rate measurements in a naturally ventilated test facility. *PhD Thesis*. Ghent University, Belgium.

ISBN-number: 978-90-5989-846-2

The author and the promoters give the authorisation to consult and to copy parts of this work for personal use only. Every other use is subject to the copyright laws. Permission to reproduce any material contained in this work should be obtained from the author.

Voorwoord - Preface

Al wie in dit dankwoord terecht komt weet inmiddels dat er aan mij geen groot schrijver verloren is gegaan. Ik hou het dus maar “bondig” en bijgevolg sowieso onvolledig.

Als eerste wil ik uiteraard mijn promotoren bedanken:

Peter, heel erg bedankt om in de beginjaren zoveel moeite te steken in het ontcijferen van mijn chaotische teksten en om toch de verborgen achterliggende structuur te vinden. En met beginjaren bedoel ik dus slechts die eerste 4,5 jaar. Het was een zeer aangename samenwerking en ik hoop dat we die in volgende projecten zeker kunnen verderzetten.

Jan, jouw vermogen om zeer snel de juiste beslissingen te nemen stond vaak lijnrecht tegenover mijn besluiteloosheid. Ik wil je dan ook oprecht bedanken voor alle doorgehakte knopen en het geduld om naar alle twijfels te luisteren. Eén van je quotes was “gelukkig hebben ze niet gewacht op de uitvinding van de atoomklok om een horloge te maken”. Stiekem hoop ik toch ergens in de referentielijst te staan wanneer ze dan toch uiteindelijk die “atoomklok” uitvinden.

Ook de jury wil ik bedanken voor de kritische blik op mijn doctoraat. Jullie commentaren hebben dit doctoraat op zijn minst vollediger en duidelijker gemaakt.

Rolinde, bij jou heb ik mijn eerste stappen in het onderzoek gezet. Alles startte met een professioneel gesprek met massa’s verkeerd interpreteerbare termen. Wij hebben ons beiden toen zeer serieus gehouden, maar dat zal zowat de laatste keer geweest zijn. Bedankt voor alle steun in mijn eerste ILVO jaren en voor het kleurrijke woord “inkakken”. Het heeft de voorbije weken al meermaals exact de lading gedekt.

Merlijn, je bent zeer snel overgegaan van collega naar een echte vriend. Ik heb op veel vlakken van jou kunnen leren, zowel tijdens jouw ILVO dagen als erna. Jouw doorzettingsvermogen tijdens de laatste maanden van je doctoraat zijn een echte inspiratie geweest. Als blijk van vriendschap vind ik nu wel dat je de referentie naar mijn doc op je rug mag laten tatoeëren.

Bear, we hebben weinig woorden nodig. Je luistert als ik er nood aan heb, zwemt als er gezwommen moet worden en geeft poomsea’s in wezens die het verdienen.

Jonas, er is heel wat gebeurt de voorbije vier jaar. Desondanks stond je altijd klaar om mij af te leiden met boeiende verhalen. Mijn verhalen zijn daarentegen doorheen deze 4 jaar toch wel wat eenzijdiger geworden. Hoog tijd dus om eindelijk samen die Triglav te beklimmen. Maar laten we dat vooral eerst samen eens uitgebreid op café bespreken.

Samyr, alhoewel je constant bezig lijkt te zijn met het oprichten van nieuwe bedrijven of organiseren van events, maakte je toch steeds tijd vrij voor mij. Bij deze raad ik dan ook iedereen aan om naar The Lounge in Eeklo te gaan voor al uw netwerkevents. Een beetje product placement verdient toch wel wat drankbonnetjes zou ik zeggen ;-).

Dieter, een CD en een optreden waarbij de politie bijna is gebeld voor geluidsoverlast. Geef toe, al bij al niet slecht gedaan van ons ILVO bandje. Er zat wat in, misschien wordt het nu tijd om het er terug uit te halen. En ja, ik geef het nu ook officieel en schriftelijk toe, ik ben jaloers op Charlene.

Eva, Ik ben ontelbare keren je bureau binnengelopen voor kleine en grote vragen en steeds had je ofwel direct een antwoord of maakte je toch de tijd om er één te vinden. En ik ben lang niet de enige voor wie je dat doet. Onmisbaar is een groot woord, maar kijk, het past nog juist terecht in deze zin.

Ingrid, je mag je binnenkort weer verwachten aan sms-en om 3u 's nachts. Hopelijk gaan we dan ook eindelijk eens beiden op hetzelfde moment in Gent rondhangen.

Veerle, bedankt voor alle raad doorheen de jaren, en dat over gelijk welk onderwerp. Jouw lach die vaak te horen was tot in mijn bureau, heeft veel stressmomenten doorbroken.

Heel erg bedankt aan Bert, Sophie, Ingrid en Mariska van de "ILVO fun brigade" (we moeten echt een andere naam vinden). Mijn bijdrage was dit jaar minimaal, dus bedankt om mij nog niet buiten te smijten. Volgend jaar ben ik terug met volle goesting!

Raphael, from now on when people ask me how things are going, I hope that I can, just as you always do, say with a big smile "not too bad". Luciano, I think we can all agree that you will get very far, as a researcher and as a baker. In your short time at ILVO you were always ready to help everyone with both these skills.

Caroline, een schoon kostuum, een fake horloge en een mistige muur, meer kan een mens toch niet wensen. Alhoewel een proper toilet ook tof was geweest.

Aan alle technici, ik heb veel van jullie bijgeleerd. Bv. waarom ik niet met mijn handen in mijn zakken mocht rondlopen. Als ingenieur ging mijn grootste plezier in de eerste plaats naar het ontwerpen van alle mogelijke testopstellingen. Jullie stonden altijd klaar om daar een kritische blik op te werpen. Meer dan eens zijn die ontwerpen dan ook achteraf grondig aangepast. Ik kom jullie allemaal wel eens persoonlijk bedanken, begin volgende week, donderdag of vrijdag.

Fusees, ik heb jullie zelf laten beslissen wat er in mijn dankwoord moest komen. Bij deze: "Ik bedank de fusees voor hun jarenlange steun en toeverlaat. Zonder hen waren er geen inspirerende avonden vol

drank geweest waar ik het grootste licht heb gezien om dit doctoraat te schrijven - Naomi.” Dat vat het inderdaad wel zowat samen.

Gerlinde, waar moet ik beginnen...Ik ga hier al geen grappige anekdotes verspillen want wees er maar zeker van dat ze op allemaal op jouw presentatie terecht zullen komen. Dan maar direct over naar de emotionele zaken. We verstaan elkaar ondertussen met zeer weinig woorden maar dat hield ons toch niet tegen om er zeer veel te gebruiken. We hebben ongelofelijk veel afgelachen, misschien veel van de stress, maar toch ook gewoon om de dwaaste dingen eerst. We namen samen vele hordes, stuikten er af en toe keihard met ons gezicht tegen, maar elke overwinning werd ook samen gevierd. Je wist mij als geen ander te blijven motiveren. De dagen dat je niet recht tegenover mij zat verliepen misschien een efficiënter maar ze waren opmerkelijk een pak minder aangenaam. Nog een jaartje en het is uw beurt. Hopelijk zit ik dan nog altijd recht tegenover jou en kan ik de wederdienst bewijzen.

Zoals reeds vermeld, dit dankwoord is verre van volledig. Er zijn nog zovele collega's, vrolega's en vrienden die hier uitgebreider zouden moeten instaan. Aan allen bedankt, voor de kleinste afleidingen tijdens de koffiepauze tot de grootste verwondering tijdens de karaoke avond op weekend.

Willy en Hilde, ik ben toch echt wel met mijn gat in de boter gevallen als het op schoonouders aankomt. Hilde, jij met de emotionele steun gecombineerd met een koffie en een koekske en Willy met een nuchtere kijk op de zaak (behalve als de kabouter langskomt).

Padre en moedre, uiteraard was ik zonder jullie constante steun doorheen de jaren nooit zover geraakt. Toch wel mijn excuses voor alle kopzorgen en al die keren dat ik langskwam en enkel tijd had om te eten en direct terug door moest gaan. Jullie verdienen veel meer tijd van mij en ik hoop deze vanaf nu ook meer te kunnen geven. Als jullie uiteraard niet alweer op reis vertrokken zijn ;).

Zus, Peter, Emile en Elodie, het wordt hoog tijd om mijn broer-, schoonbroer-, pepe- en nonkelniveau terug op te krikken. Ik zal binnenkort nog eens mijn zwembroek moeten gaan verslijten op de glijbanen in Rozebroeken ter compensatie.

Om in schoonheid te eindigen...Jeezy, je hebt doorheen de voorbije vier jaar veel moeten verdragen, met deze laatste weken als hoogtepunt. Een paar zinnen in een dankwoord zijn zeker niet genoeg, maar ze staan hier toch wel schoon vereeuwigd (en dan nog in de bib van UGent ook!). We hebben al veel horen zeggen dat dit toch wel een relatietest moet zijn. Ik denk dat je hier dan met ferme onderscheiding geslaagd zal zijn. Ik kan iedereen die een doctoraat wil maken ten stelligste aanraden om een (andere) psychologe als vriendin te hebben, het kan ferm van pas komen. Alle plannen die we maakten en die altijd eindigden met “dat is dan iets voor na het doctoraat hé”...Wel het is zover! Wanneer vertrekken we?

Table of contents

LIST OF SYMBOLS AND ABBREVIATIONS.....	VII
SAMENVATTING	XI
SUMMARY.....	XVII
CHAPTER 1. GENERAL INTRODUCTION.....	1
1.1. Indoor climate requirements.....	2
1.2. Indoor climate control through natural ventilation.....	3
1.3. Emissions from naturally ventilated animal houses	18
1.4. Problem statement	1
1.5. Research objectives	3
1.6. Thesis outline.....	4
CHAPTER 2. EXPERIMENTS UNDER CONDITIONS OF MECHANICAL VENTILATION: MANUAL 2D APPROACH.*	5
2.1. Introduction	6
2.2. Materials and Methods	6
2.3. Results & Discussion	16
2.4. Conclusions.....	21
CHAPTER 3. EXPERIMENTS UNDER CONDITIONS OF MECHANICAL VENTILATION: AUTOMATED 3D APPROACH*	23
3.1. Introduction	24
3.2. Materials and Methods	24
3.3. Results & Discussion	34
3.4. Conclusions.....	41
CHAPTER 4. EXPERIMENTS UNDER CONDITIONS OF NATURAL VENTILATION: CROSS VENTILATED TEST ROOM*	43
4.1. Introduction	44
4.2. Materials and Methods	44
4.3. Results & Discussion	55

4.4.	Conclusions.....	68
CHAPTER 5. EXPERIMENTS UNDER CONDITIONS OF NATURAL VENTILATION: CROSS AND RIDGE VENTILATED TEST FACILITY*		71
5.1.	Introduction	72
5.2.	Materials and Methods	72
5.3.	Results and Discussion	79
5.4.	Conclusions.....	89
CHAPTER 6. EXPERIMENTS UNDER CONDITIONS OF NATURAL VENTILATION: COMPLEMENTARY DATA-ANALYSIS TOWARDS REDUCED MEASUREMENT TECHNIQUES 91		
6.1.	Introduction	92
6.2.	Methods.....	92
6.3.	Results and discussion.....	93
6.4.	Conclusions.....	105
CHAPTER 7. GENERAL DISCUSSION AND FUTURE PERSPECTIVES.....		107
7.1.	Development of the measuring method.....	108
7.2.	Transferability to commercial animal houses.....	114
7.3.	Future perspectives	116
REFERENCES.....		119
CURRICULUM VITAE.....		133
PUBLICATIONS.....		134

List of symbols and abbreviations

Abbreviations

2DS	2D ultrasonic anemometer
3DS	3D ultrasonic anemometer
ACNV	Automated control of natural ventilation
CFD	Computational Fluid Dynamics
CTP	Combined traverse plane
H-guide	The horizontal guidance of the automated measuring frame
PAN	Programmatic Approach Nitrogen
SD	Standard deviation
SW	South-West
TP	Traverse plane
TF	Translocated measuring frame
V-guide	The vertical guidance of the automated measuring frame

Symbols

Subscripts for Velocities (V)

avg	Average air velocity in a vent (m/s)
c	Average of continuous velocity through an elementary surface (m/s)
i_{\perp}	Velocity component normal to elementary surface “i” (m/s)
i+	Time weighted averages of air velocities in elementary surface “i” contributing to the inflow rate (m/s)
i-	Time weighted averages of air velocities in elementary surface “i” contributing to the outflow rate (m/s)
isd	Standard deviation of $V_{i_{\perp}}$ (m/s)
o	Governing outside wind velocity at the height of a side vent (m/s)
r	Air velocity at the longitudinal central axis of the ridge, (m/s)
s	Average of sampled velocity through an elementary surface (m/s)

Subscripts for airflow rates (Q)

2DS	Airflow rate measured by the 2DS in wind tunnel (m ³ /h)
3DS	Airflow rate measured by the 3DS in wind tunnel (m ³ /h)
avg	Average of total building in- and outflow rate (m ³ /h)
imp	Airflow rate measured by a free running impeller (m ³ /h)
in	Total building inflow rate (m ³ /h)
m	Mass flow rate (g/s)

out	Total building outflow rate (m ³ /h)
th	Airflow rate due to buoyancy forces (m ³ /h)
total	Airflow rate due to buoyancy and wind forces combined (m ³ /h)
vA	Airflow rate through Vent A, (m ³ /h)
vB	Airflow rate through Vent B, (m ³ /h)
vdi	Airflow rate measured by the VDI2041 reference technique (m ³ /h)
w	Airflow rate due to wind forces (m ³ /h)

Miscellaneous

A	Opening area of a vent (m ²)
A _{eff}	Area of the vent that acts as an outlet relative to its total area (%)
A _i	Area of elementary surface “i”, (m ²)
C _d	Discharge Coefficient (-)
d	The inner diameter of the orifice (m)
D	The outer diameter of the orifice (m)
E _{mv}	Relative measurement error on the air velocity through an elementary surface, (%)
E _q	Relative measurement error on the airflow rate, (%)
É	Opening effectiveness (-)
f	Rotational frequency of the impeller (Hz)
F	Conversion factor provided by Fancom (-)
g	Gravitational acceleration (m/s ²)
H _d	Vertical distance between side vent and ridge vent (m)
I	Number of iterations of the vent traverse (-)
m	Number of vents (-)
n	Number of elementary surfaces (-)
N _{mv}	Number of measuring volumes (-)
p _{atm}	Atmospheric pressure (Pa)
PF	Pipe Factor (-)
Δp	differential pressure (Pa)
R	Specific gas constant (J/(Kg K))
R ₂₀	Data remaining under the limit of 20% relative error (%)
S _i	Trial “i” of the applied sampling strategy on the complete dataset
t ₀	Time at which the first traverse of the vents starts (s)
t _i	Time past after “I” traverses (s)
t _m	Measuring time per measuring volume, (s)
t _{tr}	Travel time of the sensor, (s)
t _{tot}	Total measuring time, (s)

T_i	Temperature inside the animal house (K)
T_o	Temperature outside the animal house (K)
UF	Unsteadiness of the airflow (%)

Greek symbols

κ	The isentropic exponent (-)
ε	Upstream expansibility factor (-)
ρ	Density of the fluid (kg/m ³)

Samenvatting

Het binnenklimaat van stallen kan grotendeels gekarakteriseerd worden door middel van vijf hoofdparameters: licht, temperatuur, relatieve vochtigheid, samenstelling van de lucht en het patroon van de luchtstromen. In een goed ontworpen stal zal het ventilatiesysteem het merendeel van deze factoren beïnvloeden, aangezien de luchtuitwisseling overtollige warmte en vochtigheid zal verwijderen, samen met stof en schadelijke gassen zoals NH_3 , CO_2 , CH_4 , N_2O en H_2S . De gassen die in stallen worden geproduceerd zijn niet alleen schadelijk voor de dieren en landbouwers, maar kunnen ook een negatieve impact hebben op het milieu wanneer deze worden uitgestoten. Er moet dus een optimum gevonden worden tussen een geschikt binnenklimaat handhaven en bovenmatige uitstoot verhinderen. In een natuurlijk geventileerde stal, is het ventilatiedebiet grotendeels afhankelijk van klimaatomstandigheden zoals windsnelheid, de windinvalshoek en verschillen tussen de binnen- en buitentemperatuur. Deze hoogst veranderlijke omstandigheden bemoeilijken de ontwikkeling van betrouwbare meet- en controletechnieken voor het ventilatiedebiet. Geen van de reeds bestaande technieken wordt momenteel algemeen aanvaard als referentietechniek om de uitstoot van natuurlijk geventileerde stallen te bepalen. Het is duidelijk dat een referentiemeettechniek voor het ventilatie- en emissiedebiet in natuurlijk geventileerde stallen nodig is om een ondubbelzinnig regelgevend kader te creëren voor landbouwers, wetgevers en onderzoekers. De algemene doelstelling van deze verhandeling was daarom het ontwikkelen van een referentiemethode voor metingen van het ventilatiedebiet in een natuurlijk geventileerde testomgeving.

Een snelheidsprofiel in een natuurlijk geventileerde opening wordt gekenmerkt door ruimtelijke en temporele variabiliteit. Daarom werd een stapsgewijze aanpak gevolgd, bestaande uit twee hoofdcomponenten, met name experimenten in een windtunnel in stabiele omstandigheden en experimenten in het veld in een natuurlijk geventileerde testomgeving. De experimenten in de windtunnel richtten zich hoofdzakelijk op de karakterisering van de ruimtelijke variabiliteit van de snelheidsprofielen, terwijl bij de experimenten in het veld zowel de ruimtelijke als temporele variabiliteit bestudeerd werden. Bij alle experimenten werd gekozen voor het toepassen van ultrasone anemometers wegens hun robuustheid, nauwkeurigheid en kostprijs.

Aangezien er geen referentiemeettechniek bestaat voor natuurlijk geventileerde luchtdebieten, werd er beslist om in een eerste stadium een referentie voor mechanisch geventileerde luchtdebieten te gebruiken. VDI2041 werd gekozen als referentietechniek voor alle experimenten in de windtunnel en was gebaseerd op verschildrukmetingen over een meetflens. Er werden verschillende windtunnelopstellingen gebouwd.

In een eerste reeks experimenten in de windtunnel werd een opstelling ontwikkeld om het luchtsnelheidsprofiel te meten in een uitstroomopening van 0.5m x 1.0m. In dit stadium vonden de

metingen plaats binnenin de ventilatieopening waar alleen de snelheidscomponent loodrecht op het uitstroomoppervlak bijdraagt tot het ventilatiedebiet. De luchtsnelheden werden gemeten met een 2D ultrasone anemometer.

Het basisprincipe van de methode voor debietsmetingen bestond uit het doorlopen van het uitstroomoppervlak (traverse) van de opening met de ultrasone anemometer om zo het snelheidsprofiel te bepalen, op basis waarvan het debiet kon worden berekend. Het aantal meetlocaties om een snelheidsprofiel nauwkeurig op te meten, d.w.z. de meetdensiteit, was essentieel voor de betrouwbaarheid van de methode. Een goed gekozen meetdensiteit zou borg moeten staan voor de brede waaier aan snelheidsprofielen die in natuurlijk geventileerde ventilatieopeningen kunnen voorkomen. Er werden 20 meetlocaties gekozen in het uitstroomoppervlak. De methode werd onderworpen aan verschillende snelheidsprofielen (vorm en stabiliteit van de luchtsnelheden). Geen hiervan had een aanzienlijke impact op de nauwkeurigheid van de methode en de relatieve verschillen tussen ventilatiedebieten gemeten met de VDI2041-referentie en de ontwikkelde methode bleven in alle gevallen onder de 10%.

Door de noodzaak om een meetmethode te ontwikkelen voor grotere ventilatieopeningen die representatiever zijn voor de praktijk en de noodzaak om de methode te automatiseren, was een tweede reeks experimenten in de windtunnel noodzakelijk. Er werd een windtunnel gebouwd met een uitlaatopening van 0.5m x 3.0 m. Er werd een automatisch sensorkader ontwikkeld dat bestond uit een verticaal en horizontaal lineair geleidingssysteem. Bovenop de verticale geleiding kon een ultrasone anemometer gemonteerd worden, waardoor de sensor een effectieve reikwijdte kreeg van 0.7m x 4.0 m. De beweging van het automatisch sensorkader werd gecontroleerd door een PLC en kon dag en nacht in werking blijven zonder enige tussenkomst van de operator. Wegens praktische beperkingen moesten de luchtsnelheidsmetingen direct achter het uitstroomoppervlak van de ventilatieopeningen worden genomen. De luchtstroom, die niet langer beperkt werd door de wanden van de tunnel, kon uitwaaiëren, wat zorgde voor een meer uitgesproken 3D karakter in vergelijking met de unidirectionele stroom binnenin de tunnel. Er werd aangetoond dat het 3D karakter van de stroom in rekenschap diende gebracht te worden door gebruik te maken van een 3D ultrasone sensor. Deze sensor liet toe om de X- en Z- componenten van de luchtsnelheid (Z is de verticale component) aan de randen van het uitstroomoppervlak te meten bovenop de Y-componenten loodrecht op het uitstroomoppervlak. De methode werd onderworpen aan diverse snelheidsprofielen die werden verkregen door verschillende ventilatiedebieten aan te leggen en door obstructies in de tunnel te plaatsen die de profielen verstoorden. Hoewel het relatieve verschil tussen ventilatiedebieten gemeten met de VDI2041-referentie en de ontwikkelde methode licht toenam voor sterk heterogene snelheidsprofielen, bleven de verschillen onder de 10% voor alle experimenten in zowel de opening van 0.5m x 1.0m als 0.5m x 3.0m.

Het was niet mogelijk om in een windtunnelopstelling zowel de temporele en spatiale variabiliteit van een natuurlijk geventileerd opening te onderzoeken. Daarom werd een natuurlijk geventileerde testconstructie gebouwd. De geometrie van dit gebouw werd gebaseerd op een sectie van een natuurlijk geventileerde varkensstal en had een lengte x breedte x nokhoogte van 12.0m x 5.0 x 4.9m (interne afmetingen). Het had twee zijopeningen van 0.5m x 4.5m en een nokopening van 0.3m x 4.0m.

In een eerste reeks experimenten werd een dwars geventileerde testkamer (TK) gebouwd binnenin de testconstructie met twee zijopeningen van 0.5m x 1.0m. De TK had een lengte x breedte x hoogte van 4.0m x 5.0m x 2.9m. Deze kamer werd gebouwd om de luchtdichtheid beter te kunnen controleren en om de invloeden van natuurlijke ventilatie op kleinere schaal te onderzoeken. De meetmethode ontwikkeld in de windtunnelexperimenten, d.w.z. een automatisch sensorkader met een 3D ultrasone anemometer, werd overgebracht naar beide zijopeningen van de TK. De meetdensiteit bleef onveranderd. De manier waarop de data verzameld werd, moest echter worden aangepast om rekening te kunnen houden met de constant veranderende windsnelheid en windinvalshoek en de daaruit resulterende luchtsnelheidsprofielen. De meest efficiënte combinatie van bemonsteringstijd per meetlocatie en van het aantal herhalingen waarmee de volledige zijopening werd opgemeten, werd experimenteel bepaald. 24 verschillende bemonsteringsstrategieën werden onderzocht, waarvan de strategie om elke meetlocatie gedurende 10s op te meten en het volledige doorlopen van de zijopeningsmeting 10 maal te herhalen, de beste resultaten opleverde. Aangezien er geen referentie voor natuurlijk geventileerde ventilatiedebieten bestaat, was de enige manier om de nauwkeurigheid van de methode te beoordelen het instroomdebiet met het uitstroomdebiet te vergelijken. Uitgaande van een onsamendrukbaar medium zonder interne productie, zouden in- en uitstroomdebiet gelijk moeten zijn. Het verschil tussen het totale instroom- en uitstroomdebiet van het gebouw werd uitgedrukt als een relatieve meetfout. Er werd aangetoond dat windinvalshoeken parallel aan de ventilatieopeningen luchtsnelheidsprofielen kunnen veroorzaken waarbij een opening deels in- en uitlaat is. Door de in- en uitstroomdebieten in eenzelfde opening van elkaar te onderscheiden, werd er met dergelijke gevallen rekening gehouden. Voor een totaal van 1005 ventilatiedebieten, gemeten bij een grote verscheidenheid aan windinvalshoeken en windsnelheden, werd een gemiddelde relatieve meetfout van $4\pm 7\%$ gevonden. Bovendien werd aangetoond dat ook in omstandigheden van natuurlijke ventilatie, de meting van de X- en de Z- componenten van de luchtsnelheid aan de randen van de openingen noodzakelijk was om dergelijk lage relatieve fouten te verkrijgen.

Aangezien werd aangetoond dat de methode toepasbaar in in natuurlijk geventileerde openingen, werd de stap gezet naar metingen in de volledige testconstructie. Eerst werd een opstelling gebruikt met een gesloten nok, een zijopening van 0.5m x 1.0m en een zijopening van 0.5m x 3.0m. Hier deed de kleinere zijopening dienst als referentie. Een relatieve meetfout van $5\pm 8\%$ toonde aan dat de methode ook toepasbaar is op grotere openingen. In een tweede opstelling hadden beide zijopeningen een

oppervlakte 0.5m x 3.0m en werd de nok volledig geopend. Een meetmethode voor het ventilatiedebiet door de nok werd ontwikkeld gebruik makend van 8 ultrasone 2D sensoren die over de longitudinale as van de 4.0m lange nok werden verdeeld. Aangezien de sensoren slechts de luchtsnelheid in het centrum van de breedte van de nok maten, moest een reductiefactor worden bepaald die de verhouding tussen de luchtsnelheden in het centrum en de gemiddelde snelheid over de totale breedte van de nok gaf. Een reductiefactor van 0.78 werd bepaald via gedetailleerde metingen van het snelheidsprofiel over de breedte van de nok met hittedraad anemometers. Alle snelheidsmetingen in de nok werden vermenigvuldigd met deze factor vóór verdere verwerking. Voor deze opstelling was de relatieve meetfout op het totale ventilatiedebiet $8\pm 5\%$. Hieruit werd geconcludeerd dat ook de nokmetingen voldoende nauwkeurig waren. Metingen in een derde opstelling met ongelijke zijopeningen (0.5m x 1.0m en 0.5m x 3.0m) en een geopende nok werden uitgevoerd om de invloed van dergelijke asymmetrische configuratie te onderzoeken. Hier werd een relatieve meetfout van $-9\pm 7\%$ gevonden.

Het is praktisch en economisch onhaalbaar om de methode die in de testconstructie werd ontwikkeld over te brengen naar een commerciële stal. Het is duidelijk dat een sterk gereduceerde meetmethode nodig is. Een mogelijke benadering is om voorspellingsmodellen te ontwikkelen die slechts een beperkt aantal meetpunten vergen om het ventilatiedebiet en eventueel het luchtsnelheidsprofiel te bepalen. Er werden reeds enkele stappen in deze richting gezet. Zo bleek dat een meting van de luchtsnelheid in het longitudinale centrum van de nok gecombineerd met een lineair model zou kunnen volstaan om het ventilatiedebiet te bepalen. Een zelfde resultaat kon bekomen worden via een meting van de windsnelheid op een nabijgelegen meteomast gecombineerd met een lineair model. Er werd ook aangetoond dat dergelijke modellen van de zijopeningsconfiguratie afhankelijk waren. De hoge graad van detail waarin de snelheidsprofielen werden opgemeten toonde aan dat er een range van windinvalshoeken bestond waarin een zijopening een volledige uitlaat was en dat binnen deze range grote delen van het luchtsnelheidsprofiel als homogeen konden worden beschouwd. Echter, buiten deze range konden de ventilatieopeningen gelijktijdig een in- en uitlaat zijn, en dit met variërende ratio's. Deze range bleek afhankelijk te zijn van de zijopeningsconfiguratie. Deze informatie kan van groot belang zijn voor emissie experimenten, aangezien daar de locatie en de grootte van de uitlaatopeningen continu moeten gekend zijn.

Wegens de uitgebreidheid van de experimenten onder een grote verscheidenheid van externe omstandigheden werd een uniek referentie testplatform gecreëerd met een relatieve fout op het in- en uitlaatdebiet die binnen de 20% blijft. De diepgaande kennis van de snelheidsprofielen en de bijbehorende ventilatiedebieten door zowel zij- als nokopeningen, creëren mogelijkheden voor de ontwikkeling, het kalibreren en het valideren van nieuwe meettechnieken voor het ventilatiedebiet in natuurlijk geventileerde openingen. Deze technieken moeten worden ontworpen met het oog op de

overdracht naar commerciële stallen. Hoewel resultaten bekomen in ons testplatform geen definitieve conclusies zouden geven over hoe een nieuwe techniek in commerciële stallen zou presteren, kan het wel sterke aanwijzingen geven over de capaciteit van de techniek om om te gaan met de hoogst veranderlijke omstandigheden in de openingen.

Summary

The indoor climate of animal houses can be, to a large extent, characterized by means of 5 main parameters: light, temperature, relative humidity, air composition and airflow pattern. In a well-designed animal house the ventilation rate will influence most of these factors as the air exchange will remove excessive heat and moisture together with dust and harmful gases such as NH_3 , CO_2 , CH_4 , N_2O and H_2S . However, the gases produced in animal houses are not only harmful to the animals and farmers, but can also have negative effects on the environment. Therefore, without additional precautions, ventilation systems might induce environmental problems by emitting the pollutants. An optimum has to be found between maintaining a suitable indoor climate and preventing excessive emissions. In a naturally ventilated animal house, the airflow rate is largely dependent on climate conditions such as wind speed, wind incidence angle and indoor/ outdoor temperature differences. These highly variable conditions complicate the development of reliable measurement and control techniques for the airflow rate. Consequently, to this day, no generally accepted reference technique exists to measure the emissions from naturally ventilated farms. Therefore, also the reduction potentials of existing and new abatement techniques remain uncertain and prone to discussion. It is clear that a reference measuring technique for the ventilation and emission rate in naturally ventilated animal houses is necessary to construct an unambiguous regulatory framework aiding farmers, constructors, legislators and researchers. Hence the overall objective of this thesis was to develop a reference method for ventilation rate measurements in a naturally ventilated test facility towards application in naturally ventilated animal houses.

A velocity profile in a naturally ventilated vent is characterised by spatial and temporal variability. Therefore a stepwise research approach was followed consisting of two main parts, i.e. wind tunnel experiments under steady state conditions and field experiments in a naturally ventilated test facility. The wind tunnel experiments mainly focused on the characterisation of the spatial variability of the velocity profiles, whilst the field experiments under conditions of natural ventilation studied both spatial and temporal variability. Throughout all experiments it was opted to use ultrasonic anemometers on account of their robustness, accuracy and, price range.

As there was no reference for naturally ventilated airflows, it was decided to start the method development using a reference for mechanically ventilated flows. The VDI2041 was chosen as reference airflow rate measurement technique for all wind tunnel experiments and was based on differential pressure measurements over an orifice. Different wind tunnel set-ups were built.

In a first set of wind tunnel experiments a set-up was developed to measure the air velocity profile in a vent of 0.5m x 1.0m. At this stage the measurements took place within the vent, where only the velocity component normal to the outflow plane contributes to the airflow rate. The air velocities were measured with a 2D ultrasonic anemometer.

The basic principle of the airflow rate measuring method was to move the ultrasonic across the outflow plane of the vent, thus determining the velocity profile from which the airflow rate could be calculated. The number of measurements taken to accurately measure a velocity profile, i.e. the measurement density, was essential for the reliability of the method. A correctly chosen measurement density should account for the wide range of velocity profile shapes that can occur in naturally ventilated vents. A set of 20 measurement locations across the outflow plane were chosen. The method was subjected to different velocity profiles (shape and airflow unsteadiness). None of these had a considerable impact on the accuracy of the method and in all cases the relative differences in airflow rate between the VDI2041 reference and the developed method remained under 10%.

Due to the need of developing a measuring method for larger vents which are more representative of practice and the need of automating the method, a second set of wind tunnel experiments was necessary. A wind tunnel with an outlet opening of 0.5m x 3.0m was constructed. An automatic sensor frame was developed that consisted of a vertical and horizontal linear guiding system. On top of the vertical guidance an ultrasonic anemometer could be fitted giving the sensor an effective traversing range of 0.7m x 4.0m. The movement of the frame was controlled by a PLC and could run day and night without any influence of the operator. Due to practical limitations, the air velocity measurements had to be taken directly after the outlet plane of the vent. No longer contained by the borders of the tunnel, the airflow could fan out giving it a more 3D character as compared to the unidirectional flow inside the tunnel. Therefore, a method was developed using a Thies® 3D ultrasonic sensor. It was proven that by measuring the X- and Z-components (vertical velocity component) at the edges of the vent additional to the Y-components normal to the vent's outflow plane, the method accounted for the 3D character of the flow. The method was validated under diverse velocity profiles obtained by different airflow rates and different airflow obstruction set-ups in the tunnel. Although the relative difference between VDI2041 reference and the developed method slightly increased for strongly heterogeneous velocity profiles, it remained under 10% for all experiments in both the vent of 0.5m x 1.0m and 0.5m x 3.0m.

The temporal variability of a velocity profile in a naturally ventilated vent could not be examined in a wind tunnel set-up, hence a naturally ventilated test facility was built. The geometry of the building was based on a section of a naturally ventilated pig house and had a length x width x ridge height of 12.0m x 5.0m x 4.9m (internal dimensions). It had two side vents of 0.5m x 4.5m and a ridge vent of 0.3m x 4.0m.

In a first set of experiments a cross ventilated test room was built inside the test facility with side vents of 0.5m x 1.0m. The test room had a length x width x height of 4.0m x 5.0m x 2.9m. This room was built to have more controlled environment concerning airtightness and to examine the influence of natural ventilation on a smaller scale. The measuring method developed in the wind tunnel

experiments, i.e. the automatic sensor frame with a 3D ultrasonic anemometer, was transferred to both vents of the test room. The measurement density remained unchanged. However, the way in which the data was gathered needed to be adapted to account for the constantly changing conditions of wind speed and incidence angle and the resulting velocity profiles. This was done by experimentally determining the most effective combination of sampling time per sampling location and the number of traverse repetitions of the complete side vent. 24 different sampling strategies were examined, from which the strategy of measuring each sampling location within the vent for 10s and repeating the complete vent traverse for 10 times was found to be the most satisfactory. As there exists no reference for naturally ventilated airflow rates, the only way to assess the accuracy of the method was by comparing the inflow rate to the outflow rate. Evidently, when assuming an incompressible medium, the in –and outflow rates should be equal. The difference between the building's total inflow rate and the building's total outflow rate was expressed as a relative measurement error. It was shown that wind incidence angles parallel to the vents could induce velocity profiles where the vent was partly in- and outlet. By differentiating these two differently directed flows, such cases were effectively accounted for. For the total of 1005 airflow rates that were measured under a large variety of wind incidence angles and wind speeds, an average relative measurement error of $4\pm 7\%$ was found. Additionally it was proven, that also in conditions of natural ventilation, the measurement of the X- and Z- velocity components at the borders of the vents needed to be measured to obtain such low relative errors

As the method was proven to be applicable under naturally ventilated conditions, the step was made towards measurements in the complete test facility. First a set-up was used with a closed ridge, a side vent of 0.5m x 1.0m and a side vent of 0.5m x 3.0m. This way, the smaller side vent acted as a reference. A relative measurement error of $5\pm 8\%$ inferred that the method is also applicable on larger vents. In a second set-up both side vents were 0.5m x 3.0m large and the ridge was completely opened. An airflow rate measuring method for the ridge was developed using 8 ultrasonic 2D sensors equally distributed along the longitudinal axis of the 4.0m long ridge. As the sensors only measured in the centre of the ridge's width, a reduction factor needed to be determined that gave the ratio between the air velocities at the centre and the average velocity over the total width of the ridge. A reduction factor, i.e. the pipe factor (PF) of 0.78 was determined by detailed velocity profile measurements in the width of the ridge with hotwire anemometers. All velocity measurements in the ridge were multiplied by this PF before further processing. The relative measurement error on the total airflow rate for this set-up was $8\pm 5\%$ inferring that also the ridge measurement method was accurate. A third set-up (cross and ridge ventilated) was added to the experiments where the side vents had unequal areas, i.e. 0.5m x 1.0m and 0.5m x 3.0m, to examine the influence of such an asymmetrical configuration. Here a relative measurement error of $-9\pm 7\%$ was found.

It is practically and economically infeasible to transfer the method developed in the test facility to a commercial animal house. It is clear that a strongly reduced measuring method is still needed. A possible approach is to develop prediction models that only need a limited number of measuring points to determine the airflow rate and possibly the ventilation profile. Some first steps in this direction were taken. For example it was found that a measurement of the air velocity located in the longitudinal centre of the ridge combined with a linear model could be sufficient to determine the airflow rate. The same was true for a wind velocity measurement at a nearby meteoromast. On the other hand it was also shown that such a model was dependent on the side vent configuration. The high degree of detail in which the velocity profiles were measured also revealed that there exists a range of wind incidence angles in which a side vent was a complete outlet and that within this range large parts of the velocity profile can be considered homogeneous. However, outside this range, the vents serve simultaneously as both inlet and outlet with varying ratios. Again, these ranges seemed to be dependent on side vent configuration. This is important information when setting up emission rate experiments as in these cases the location and size of the outlets should be known at all times.

Due to the extensiveness of the experiments under a large variety of external conditions, a unique reference testing platform was created with a relative error that remains within 20%. The in depth knowledge of the velocity profiles and the associated airflow rates through each vent, creates possibilities for the development, the calibration and the validation of new airflow rate measurement techniques for natural ventilation. These techniques need to be designed to allow for the transferral to commercial animal houses. Although results from our reference testing platform would not give definitive conclusions on how a new technique would perform in real life animal houses, it can give strong indications on its ability to cope with the highly variable conditions in the vents.

Chapter 1. General Introduction

1.1. Indoor climate requirements

The world meat and milk consumption is rising whilst the farms are decreasing in numbers but increasing in size. In intensive livestock farming pigs and dairy cows are mainly kept in constructions designed to act as a shelter from rain, excessive heat, cold and wind gusts. Although some farms, in particular dairy farms, combine this with grazing time on neighbouring fields, in Europe the animals are predominantly kept indoors (EFSA, 2009). The indoor climate can be greatly characterized by means of five main factors: light, temperature, relative humidity, air composition and airflow pattern (EFSA, 2009). The influence of light will not be discussed here.

The influence of the indoor temperature on the well-being of the animals has been studied in detail (EFSA, 2009, 2007). Both cows and pigs are homoeothermic and strive to maintain a constant body temperature. For each animal there exists an optimal temperature range, referred to as the “Thermo-neutral zone”, where the production levels (weight gain, milk yield, etc.) are the highest. Within the thermo-neutral zone a “comfort zone” exists, in which, as the name implies, the animal feels most comfortable. Hence distinction is made between production efficiency and animal welfare. These ranges get narrower as the animal is smaller and/or younger. A continuous temperature control can thus be more critical for these young or small animals. It must be noted that, in general, most naturally ventilated animal houses, do not need additional heating. Indoor temperature and relative humidity are connected to some extent. They are both are highly influenced by the temperature and relative humidity of the inlet air (Wang et al., 2010), together with the heat and moisture produced by the animals or other sources. A higher relative humidity hinders the release of heat through evaporation, which makes it more difficult for most animals to cool down, possibly leading to heat stress. Also, moist environments will be a breeding ground for fungi and bacteria, which have a negative impact on animal production and health.

The air quality is negatively affected by pollutants released by the animals, including their manure (NH_3 , CO_2 , CH_4 , N_2O , H_2S and dust). The harmful effects of these gases on people and animals is well known (Schiffman et al., 2006) and guidelines for maximum concentrations exist (see Table 1-1). Mitigation techniques can be applied to lower the release of most gases (see 1.3.1).

The ventilation rate and the associated airflow pattern are often mentioned as the defining parameters of the indoor climate. In a well-designed animal house the ventilation rate will influence most indoor climate factors. It will remove excessive heat and moisture from the indoor air together with dust and harmful gases. However, an airflow that does not reach and refresh the polluted areas inside the animal house will be largely ineffective (Banhazi et al., 2008). Moreover, a badly guided airflow can even worsen the situation by influencing the fouling behaviour of the animals (Randall et al., 1983) or by increasing the airspeed over emitting surfaces (Morsing et al., 2008) (see also 1.3.1). Also cold draughts in the animal occupied zone caused by uncontrolled airflow patterns will increase the animals' sensitivity to cold weather. As a guideline, indoor airflows of approximately 0.2m/s to 0.6m/s

are accepted, depending on the ambient temperature (EFSA, 2009). Obtaining the desired ventilation rate without checking the airflow pattern can lead to severe shortcomings of the indoor climate. It is clear that well-controlled ventilation is essential to maintain an optimal indoor climate.

Table 1-1: Thresholds for air pollutants to protect humans and animals in an animal house atmosphere. Adapted from (EFSA, 2009)

Pollutant	Thresholds for animal	Thresholds for man
Ammonia	20 ppm	20 ppm
Hydrogen sulphide	0.5 ppm	10 ppm
Methane	-	-
Carbon monoxide	10 ppm	30 ppm
Carbon dioxide	3000 ppm	5000 ppm
Inhalable dust	-	4 mg/m ³

1.2. Indoor climate control through natural ventilation

Because this thesis focuses on pig and dairy farms, details on building structures will apply to these housing systems. However, the discussed general working principles of natural ventilation and control techniques can be applied to most naturally ventilated livestock houses.

1.2.1. Ventilation of animal houses

As discussed in section 1.1, maintaining an optimal indoor climate is essential for the wellbeing of the animals, which in its turn affects the daily production. The ventilation rate or air renewal rate is one of the major influential factors of the indoor climate as heat, moisture and pollutants such as NH₃, CO₂, CH₄, N₂O, H₂S and dust need to be removed. However, the pollutants produced in animal houses are not only harmful to the animals and farmers (Omland, 2002), but can also have negative effects on the environment. Therefore, without additional precautions, ventilation systems might induce environmental problems by emitting the pollutants. An optimum has to be found between maintaining a suitable indoor climate and preventing excessive emissions.

Two main types of ventilation systems are possible, i.e. mechanical and natural ventilation. Since its rise in the sixties, mechanical ventilation has been the main technique for controlling the indoor climate of pig and poultry housing systems. In mechanical ventilation, the ventilation rate is controlled through the adjustment of the rotational speed of fans often combined with the adjustment of valves. Adequate techniques have been developed to measure the ventilation rate (e.g. free running impeller) (Berckmans et al., 1992; Vranken and Berckmans, 1998; Gates et al., 2004; Hoff et al., 2009), which can be used in a feedback loop of the fan for a more precise control. Although mechanical ventilation is also a viable option for dairy farms, in Europe dairy houses are typically naturally ventilated (EFSA,

2009). The physical principles on which natural ventilation systems are based, are discussed in section 1.2.2. Since the seventies most pig houses in Flanders are mechanically ventilated. This is mainly because of the ease of setting up a fully automated and reliable climate control system and the increasing energy efficiency of the fans. On the other hand, Berckmans and Goedseels (1986) stated that the production results of mechanically ventilated pig houses were not proven to be significantly better than in naturally ventilated houses. However, at the time of this study, both the control of the fan's airflow rate and how this control should interact with the internal climate were still in an early stage of development. Due to the lack of more recent studies it is, therefore, not possible to draw any final conclusions on the subject of production results. Nonetheless, natural ventilation remains an attractive and potentially sustainable technology.

Because of the absence of fans, naturally ventilated houses have lower investment costs and a higher energy efficiency (Andonov et al., 2003a; Brockett and Albright, 1987). In mechanically ventilated pig buildings, 50% to 75% of the energy cost can be attributed to the use of fans (Innovatiesteunpunt, 2015). Naturally ventilated systems are therefore regarded in the IE Directive of the EU as a Best Available Technique (BAT) for energy use in intensive pig husbandry where possible to apply (IPPC, 2003). Another advantage of natural ventilation are the lower noise levels (Brockett and Albright, 1987; IPPC, 2003) inside the houses. A noisy environment can be harmful to the animal's health (EFSA, 2007). Also the lack of noise for the neighbourhood can help the general acceptance of the animal house in densely populated areas. In mechanically ventilated houses a power failure can be fatal as the supply of fresh air can come to a complete stop leading to dangerously high temperatures and concentrations of harmful gases. Built-in safeties exist that are designed to minimise the risk in these situations, e.g. automatic and complete opening of the inlet vents and/or alarming the farmer by a text-message and/or an alarm. However, many cases have been reported where the complete livestock had suffocated (Louwagie, 2015). This is partly due to the small sizes of the inlet vents. In wind still conditions these vents might not deliver sufficient air renewal, even when they are completely opened. A naturally ventilated housing system does not have this disadvantage as these buildings have much larger vents that are designed to deliver an adequate air renewal rate even in wind still conditions (see section 1.2.3). Because of the large variety of available housing systems, be it mechanically or naturally ventilated, it is difficult to give definitive numbers on maintenance costs. However, the larger number of devices that can wear and tear in mechanical ventilation systems, specifically the fans, means another possible advantage for naturally ventilated systems. In times where the awareness for bio- and ecological farming is growing, the use of natural ventilation is also gaining proponents. Aside from possible advantages for the animals, the view of an animal housing with very large openings can be more appealing to the general public as compared to mechanically ventilated buildings which are more sealed off. This is especially true for small farms that aim for the local sales market.

For a large number of farmers, all of these advantages will not offset the seemingly higher controllability of the indoor climate in mechanically ventilated houses. Indeed, an adequate control of the airflow rate remains difficult even with a correct choice in building structure of the naturally ventilated building combined with a well-adjusted automation system (see section 1.2.3 and 1.2.4). Note that natural ventilation will not be applicable in all types of housing systems. Especially in livestock houses with large animal densities during periods of heat stress, natural ventilation might not be a feasible solution as the high demand in ventilation capacity cannot be guaranteed. In these cases a combination of mechanical and natural ventilation is possible by installing additional fans (hybrid ventilation). A characteristic of mechanical ventilation is that the fans can force out all of the polluted indoor air through a relatively small outlet. This is in contrast to natural ventilation where the polluted air leaves the building through very large openings. In light of the recent developments concerning air pollution originating from agriculture (see 1.3) there exist emission reduction techniques that require the use of mechanical ventilation. For example, in air scrubbers the polluted air needs to be pushed or drawn through a relatively small opening filled with packing material. This packing causes a large differential pressure that can only be overcome with fans. In some cases, to obtain or renew the production permits, the required ammonia reduction percentage is so high that air scrubbers seem, for now, the only viable option (Industrial Emission Directive 2010/75/EU, 2015). Applying natural ventilation is no longer possible in these cases. However, as an intermediate solution air scrubbers are currently being developed for application in naturally ventilated animal houses where the ventilation system is transformed to a hybrid system or a completely mechanically ventilated system.

1.2.2. The natural ventilation process

The ventilation process in naturally ventilated buildings, refreshing the indoor air volume and keeping the temperature and relative humidity within limits, is fuelled by two processes: the wind effect and the stack effect (a.k.a buoyancy or chimney). Both effects are caused by the differential pressure between the in- and outside of the building. Because the building acts as an obstruction to the free wind, typically positive and negative pressures build up on the windward and leeward side of the building, respectively. Typically large vents are located at the windward and leeward sides of the building causing an in- and outflow through the respective vents (wind effect). Due to the heat production of the animals, possibly combined with a heat influx caused by solar radiation, the air inside the housing heats up and rises to the ridge. This causes a drop in pressure at the lower levels (stack effect). A vent along the ridge acts as an outlet for the heated air and fresh air enters through the vents at the sidewalls. Generally, all vents run along almost the entire length of the building.

The respective contributions of stack and wind effect to the total airflow rate are dependent on the building design and orientation and the governing indoor and outdoor conditions. The airflow rate delivered by the wind effect can be many times higher than that from a purely stack effect driven ventilation (Bjerg et al., 2013a). Hence, from a certain wind speed or range of wind speeds on, the

stack effect is negligible relative to the wind effect. However, different values have been reported: $>1.8\text{m/s}$ (Papadakis et al., 1996); between 1-2 m/s (Boulard et al., 1996); from $u/\sqrt{\Delta T} > 1$ (Kittas et al. 1997) with ‘ u ’ the wind speed in m/s and ‘ ΔT ’ the indoor/outdoor temperature difference in K or °C.

1.2.3. Effect of building design and orientation

1.2.3.1. *Vent models and sizes*

A variety of side wall vent systems are available. However, all of them have the same basic function, i.e. to limit or increase the airflow rate according to the demand respectively by reducing or increasing the permeability of the vent area. In dairy farms one of the most common systems consists of large windscreens that vary in size to change the opening height. Space boarding is another popular system where the vent is covered with small vertical boards. The spaces between the boards can be varied by installing a movable second row of boards. In pig farms the side vents can be more complex. Here the vents have an additional and equally important role, namely the guidance of the airflow away from the pigs. Pigs are very sensitive to cold draughts and without proper airflow guidance the cold inflowing air can drop down quickly into the animal occupied zone. Different designs of ridge openings exist, distinguished mainly by their ability to keep out rain and snow without obstructing the outflow (Graves and Brugger, 1995). In some ridge systems the permeability of the ridge can be adjusted by valves.

The size of the openings is chosen depending on the required indoor conditions which are animal species specific. There exist target values for the airflow rate determined mainly by animal characteristics (CIGR, 1992; Van Gansbeke, 2014). Hellickson et al., (1983) stated that the variability of the outside conditions limits the adaptability of a theoretical equation for the determination of the ventilation rate due to wind forces. However, empirical or semi-empirical equations do exist to give an approximation of the ventilation rate caused by the stack or the wind effect or the combination of both [1.1 to 1.3].

$$Q_{th} = C_d A \sqrt{2 g H_d \frac{T_i - T_o}{T_i}} \quad [1.1]$$

$$Q_w = \acute{E} A V_o \quad [1.2]$$

$$Q_{total} = \sqrt{Q_{th}^2 + Q_w^2} \quad [1.3]$$

With Q_{th} the airflow rate due to the buoyancy forces (m^3/s); C_d the discharge coefficient(/); A the opening area of the vent (m^2); g the gravitational acceleration (m/s^2); H_d the vertical distance between the side vents and the ridge vent (m); T_i and T_o the temperature inside and outside the animal house respectively (K); Q_w the airflow rate due to wind forces (m^3/s); \acute{E} the opening effectiveness (/); V_o the

governing outside wind velocity at the height of the side vent (m/s); Q_{total} the airflow rate due to wind and buoyancy effect combined (m^3/s).

Although different adaptations of these equations exist, the area of the vent (A) is always variable in both the equation for wind and stack effect. Therefore, they can also be used as a design tool to determine minimum and maximum opening sizes. To estimate the necessary maximum vent sizes, a worst case scenario, i.e. low wind speeds on a hot day, can be assumed. In this situation the small difference between in- and outside temperature and the low wind speeds reduce the stack and wind effect, respectively, to a minimum. According to equation [1.3], the area A that delivers the minimum required airflow rate with a temperature difference close to zero and low wind speeds, is the necessary maximum opening size.

When combining equations [1.1] and [1.2] into equation [1.3], 4 parameters can be seen to be influenced by the building design: C_d , \acute{E} , A (Etheridge, 2012) and H_d . C_d and \acute{E} are similar (Yu et al., 2002) as they both give an estimate on how the airflow rate is reduced as a ratio between real flow and theoretical flow through a specific vent.

Generally a value for the opening effectiveness \acute{E} between 0.5 and 0.6 is recommended for perpendicular winds and 0.25 to 0.35 for diagonal winds (ASHRAE, 2009). As it is assumed that the wind incidence angle is rarely continuously perpendicular to the vents, an \acute{E} of 0.35 is recommended for agricultural buildings (Hellickson et al., 1983). Bucklin et al. (1991) give a more detailed description as they express the \acute{E} as proportional to the wind incidence angle.

Yu et al. (2002), Nääs et al. (1998) and Verlinde et al. (1998) developed algorithms to predict the opening effectiveness. They found that \acute{E} decreases with higher wind speeds, wind incidence angles deviating from perpendicular to the inlet opening, a decreasing ratio height to length of the vent and larger roof slopes. The roughness of the surrounding field has only limited influence on \acute{E} .

The discharge coefficient for a vent generally lies between 0.60 and 0.75 for sharp edged openings (Freire et al., 2013) and accounts for the losses due to friction, turbulence and other related factors in the vent (Teclé et al., 2013). The C_d is determined by the ratio between the actual airflow rate and the theoretical airflow rate through a vent and therefore has to be determined experimentally (Heiselberg, 2006a; Inard et al., 1996). Some values of C_d for different studies can be found summarised in Karava et al. (2011), Heiselberg, (1901), Roy et al. (2002) and Pearson and Owen (1994). Karava et al. (2011) conclude in their review paper that the discharge coefficient is dependent on opening porosity, opening shape and location on the building, wind incidence angle and Reynolds number. They also state that using a constant C_d , as is done in some textbooks and studies, can be a source of error.

It is clear that C_d as well as \acute{E} are parameters that change according to the building design. However, designing a building, or estimating the possible ventilation rate, requires the a priori knowledge of these parameters (Fracastoro et al., 2002) whilst an exact determination is only possible when the building is already built. A margin of error should therefore always be incorporated in the design.

It must be noted that the ventilation rate will not only be affected by the building envelope and its vents but also by the flow obstructions inside the animal house. The larger the vents the more this will have a considerable impact (Chu and Chiang, 2013) Not only the ventilation rate but also the indoor airflow pattern is affected by the vents' sizes and location. Bangalee et al. (2013) showed that a larger ventilation rate does not always ensure a better air renewal rate when the location of the inlet in relation to the outlet is not optimal. Morsing et al. (2002) proved that the height of the wall between the top of the ventilation opening and the eaves could significantly alter the airflow pattern. It was shown that this height could guide the inflowing air jet away or towards the animal occupied zone. The height of the vent will also influence the homogeneity of the indoor air (Norton et al., 2010). A homogenous distribution of the air characteristics can make the control of the indoor climate more efficient (see 1.2.4).

1.2.3.2. Roof design

The roof slope, together with the width of the building, has an influence on the stack effect due to the increase in vertical distance between side vents and ridge opening. It will also have an effect on the solar radiation that is captured and therefore the heating of the housing (Cooper et al., 1998). Higher inclination angles will result in higher pressures at the windward side of the building (Heiselberg, 2006b) which will cause an increase in ventilation rate due to the wind effect (Perén et al. 2015). However higher roof slopes will increase construction costs. As a rule of thumb the roof slope has to be at least 25% (Albright, 1990) and an optimum has to be found between stack effect effectiveness and building costs. Roof insulation has some obvious advantages such as reducing the impact of solar radiation in summer and heat loss in winter and preventing condensation on the inside of the roof which would otherwise have a negative impact on the building structure and could cause the growth of fungi. However, its application also brings less apparent disadvantages. For example, condensation under the roof can be a signal for the farmer that the relative humidity is too high and, therefore, the airflow rate too low. Insulation removes this signal, sometimes leading to under ventilated animal houses (Van Gansbeke, 2014). Additional relative humidity sensors might be necessary to overcome this problem.

1.2.3.3. Building orientation and surroundings

Many studies have shown the influence of the wind incidence angle on the ventilation rate e.g. De Paepe et al. (2013), Larsen et al. (2011), Teitel et al. (2008). The maximum ventilation rate is generally obtained for wind incidence angles perpendicular to the vents. Of course the incidence angle cannot be controlled. It is therefore important to orient the large side wall openings towards the predominant wind direction in that area to make maximum use of the potential of natural ventilation (Choinière & Munroe, 1990; Hellickson & Walker, 1983). In Flanders the predominant wind direction is SW and occurs during $\pm 30\%$ of the time. Animal houses that are not oriented correctly can have large problems maintaining an adequate indoor climate as winds blowing parallel to the vents give a more heterogeneous indoor airflow pattern than winds blowing perpendicular to the vents (Choiniere and Munroe, 1994). In these cases, a vent can be an inlet and outlet simultaneously (Linden, 1999). The possibility of creating still air zones where the air is not refreshed heightens and the heterogeneity of the indoor air characteristics enlarges. This will negatively influence the automatic control systems that assume a homogeneous distribution (see 1.2.4). Although these situations are unavoidable, their occurrence can be influenced by choosing the correct building orientation.

However, these recommendations apply for buildings that do not have large obstructions in their vicinity. Obstructions, such as shelterbelts or other buildings, can have a large influence on the indoor airflow pattern (Fiedler et al., 2013). When expanding a farm, it is not always possible to build the animal houses in the optimal location and orientation. In these cases a well-designed obstruction can also help in guiding the airflow towards the vents and ameliorate the airflow pattern (Allard, 1998).

1.2.4. Control techniques

Once the building's structure is determined, the only parameters that will be easily changed are the height of the side vent openings or the position of the in- and outlet valves and in some cases the width of the ridge vent. A consequence of the mostly large dimensions of the vents (see 1.2.2) is that without proper control of the opening size, the ventilation rate can be many times larger than is actually required (Monteny and Hartung, 2007; Shen et al., 2013a). Especially in manually controlled systems where the farmer is often inclined to prefer the air to be as fresh as possible as this causes a more pleasant working environment. When cold draughts are avoided and the indoor climate remains within the comfort or thermoneutral zone, this is not necessarily a problem for the animals. However, these larger ventilation rates are possibly associated with larger NH_3 emission rates (see 1.3.1). Therefore the optimal ventilation rate should be the lowest possible rate where the animals are still within their comfort zone.

Achieving this merely through experience of the farmer without an automated system that relies on measurements of the indoor and/or outdoor climate parameters is nearly impossible. Although ACNV systems (Automated Control of Natural Ventilation) have been studied as early as in 1984 (Strøm and Morsing, 1984) and a lot of models have been proposed (Andonov et al., 2003b; Brockett and Albright, 1987; Daskalov et al., 2005; Hoff, 2004; Kizil et al., 2002; Shen et al., 2013; van't Klooster and Heitlager, 1994; van't Klooster, 1996), they are still not standard in naturally ventilated pigs or cattle houses. Therefore, the vents are mostly manually adjusted by the farmer when climate conditions change during the day. However, these adjustments are not always optimal, as in windy conditions the vents are often closed to a minimum to reduce a possible downdraft on the animals, which in its turn results in poor indoor climate conditions (Morsing et al., 2002). Additionally, weather changes occurring at night might pass by unnoticed by the farmer. The most advanced commercially available ACNV systems account for rainfall, wind speed and wind incidence angle at ridge height, temperature and/or indoor CO_2 concentration and/or relative humidity. Certain systems will stimulate adjustments by the farmers to allow for a more farm specific control. It must be noted that a correct application of an ACNV system will have a steep learning curve and a close cooperation between farmers and ACNV suppliers is needed to reach the maximum potential of these systems. However, even then the performance of these systems is not always optimal.

Automatically adjusting the vent sizes correctly under varying outdoor conditions remains difficult. The ACNV systems are mostly based on lumped parameter models (see Fig. 1-1), designed to calculate the ideal ventilation opening size (Bjerg et al., 2013b). These models consider the air in the housing as a whole and do not account for spatial variations of the measured factors. Indeed, when the indoor air composition would be homogeneous, it would not be necessary to know the exact ventilation rate (when ignoring possible emission effects). As long as the sensor outputs that

characterize the indoor climate remain within their permitted limits, the air exchange rate is considered to be in the correct range.

However, as wind speed, angle and vent size will affect the indoor airflow patterns, the air quality throughout the animal house will not be homogeneous due to incomplete mixing (Barber and Ogilvie, 1982; Calvet et al., 2014; Ngwabie et al., 2009). As a consequence the sensors delivering the CO₂ and/or temperature and/or relative humidity information might under- or overestimate the need for a higher ventilation rate. Finding sensor locations that will deliver representative values under all circumstances is a difficult task (Shen et al., 2012; Takai et al., 2013; Zhang et al., 2010) and can only be partly solved by using more sensors, making the system more complex and expensive.

Therefore, knowledge of the airflow rate in combination with the indoor airflow pattern, under all circumstances, would be an essential stepping stone for the improvement of ACNV systems. Finding a purely theoretical model that can give an accurate prediction of the pattern and flow rate is infeasible at present and full scale measurements would be necessary. Some techniques/models exist to give an online estimate of the airflow rate and are discussed in section 1.2.5.

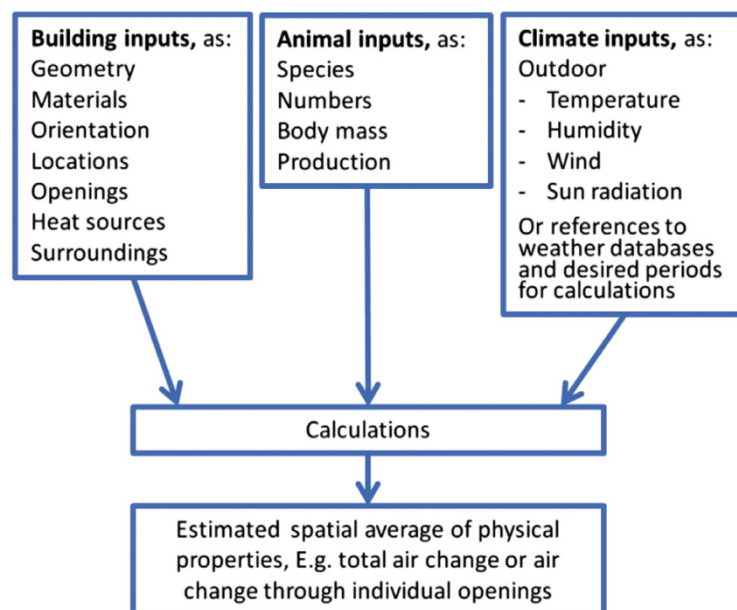


Fig. 1-1: Simplified flow chart for a lumped parameters model to calculate air change in a naturally ventilated livestock building (Bjerg et al., 2013b)

1.2.5. Measurement of the ventilation rate

As aforementioned, knowledge of the ventilation rate through a naturally ventilated building would be a stepping stone towards a more controllable indoor climate through better automated adjustment of ventilation opening size and possibly even airflow pattern. Over- or under-ventilation could then be avoided, which in its turn could have an influence on the emission rate.

1.2.5.1. Research approaches

There are several approaches used to investigate the ventilation rate in naturally ventilated buildings: experiments in real life operational buildings or full size mock-up buildings, wind tunnel studies, models and numerical simulations using Computational Fluid Dynamics (CFD). Although these approaches can provide useful information, a combination is often necessary to compensate for the limitations of each technique.

Scaled models in wind tunnels have been used to study the airflow patterns in (Choiniere et al., 1988) and around the model (Ntinis et al., 2014) or the ventilation rate through the model (De Paepe et al., 2013, 2012). The evident advantage of a wind tunnel is the control of the simulated weather parameters such as wind direction, wind speed and temperature. Although Ji et al. (2011) have incorporated fluctuating wind angles in their wind tunnel experiments, the large majority of wind tunnel tests are performed under steady state conditions. Ji et al. (2011) stated that the natural variations occurring in wind angle could have a significant influence on the ventilation performance. Therefore experiments under steady state conditions should be analysed accordingly. The small size of the scale model poses a limit to the variety of measurement methods or degree of detail that can be investigated. Mostly very delicate hotwire anemometers or small pressure tubes are applied. The more robust sensors that could be applied on full scale installations are often too large for scale models. There exist non-intrusive sensor techniques such as particle image velocimetry. Although this technique can deliver detailed results, the limitations as described by Cao et al. (2014) show that its application is still very demanding.

Numerical simulations using CFD can also give an estimate of the ventilation rate under specific boundary conditions and many different building designs can be tested. However, CFD simulations cannot be regarded as proof per se, but still need to be validated by real life or wind tunnel measurements. This is strongly emphasized in the reviews by Norton et al. (2007) and Blocken (2014). Both wind tunnel experiments and CFD approaches can give insight into the factors influencing the airflow rate but cannot deliver a measurement method ready for use in practice. Models such as those used to estimate the necessary opening size (see 1.2.2), can also be used for the estimation of the ventilation rate. As discussed, these models generally need parameters, such as the discharge coefficient or opening effectiveness, that are difficult to determine and that vary depending on external climate conditions and building design. Hence, they should be experimentally determined and validated in the animal house before using them in a model.

Therefore, regardless of the research approach, experiments in real life naturally ventilated animal houses are indispensable. One way is to perform experiments in a real life occupied barn. Due to the large amount of known and unknown influential parameters in such buildings it can be difficult to draw correct conclusions without expensive and time-consuming measurement campaigns (Heber et al., 2001). Also, the presence of the animals can impede some measurement locations, especially in the animal occupied zone, or substantially increase the effort of taking such measurements (Fiedler et al.,

2013). Furthermore, gases like NH_3 or dust can be harmful for the correct functioning of sensors in the long term (Hinz and Linke, 1998), increasing the experimental cost or lowering the reliability of the sensors.

As an intermediate step also full size mock up buildings can be used. Experiments in mock up buildings can become gradually more complex by adjusting the indoor structure to emulate conditions of a real animal house. There is the possibility to add pen equipment, heat sources to simulate the presence of animals (Bjerg et al., 2000), controlled release of gases such as ammonia or CO_2 to simulate emissions from manure or the exhalation of the animals. Also the larger size of the building allows the use of a large variety of sensor equipment, from the relatively small cup anemometers to the larger 3D ultrasonic sensors. This will increase the transferability of the developed measuring methods to commercial animal houses as these types of robust sensors will also be applicable there. Extensive studies were already performed in such buildings at the Silsoe Research institute in the “Silsoe structures building” and the “Cube” (Demmers et al., 2001; Hoxey and Richards, 1995; Richards and Hoxey, 2012; Straw, 2000). There the focus mainly lied on pressure distributions on buildings.

1.2.5.2. Prerequisites of the measuring technique

As will be discussed in 1.3.3 the ventilation rate is also an important aspect of the most common emission rate measurement techniques. However, distinction has to be made between measuring techniques for the application in control systems and techniques as a part of an emission quantification method. A control technique will need updated results at least every few minutes whilst a daily average could be sufficient for the determination of the emission rate (Estelles et al., 2010a). Evidently a control technique needs to be applied permanently whilst emission rate determination, depending on legislation, will only need to be performed periodically. Also the accuracy is a determining factor. As mentioned in section 1.2.1, there is a certain range in which the indoor climate can fluctuate without harming the animals. Therefore, the accuracy of the control technique needs to be adapted to the specific needs of the animals, thus possibly reducing the complexity or cost of the method. For example, the broader comfort zone of cows could result in less demanding control techniques than for pigs that have a narrower comfort zone. On the other hand, the accuracy of the emission rate measuring technique is of great importance as it can have serious consequences for the draft of new or the enforcement of existing legislation (see section 1.3.2).

1.2.5.3. Direct and indirect measuring techniques

Irrespective of their use for control or emission quantification purposes, ventilation rate measurement techniques on full scale buildings can be divided into direct and indirect techniques. The direct techniques measure a parameter directly linked to the airflow rate such as air velocity in the vent. Although dynamic pressure can also be translated into an airflow rate, the small pressure differences occurring in naturally ventilated openings make this method less reliable. The air velocity can be

measured in a variety of ways, e.g. propeller gauges, sonic and hotwire anemometers (see **Fout! Verwijzingsbron niet gevonden.**). Most of the off-the-shelf anemometers give point measurements. To determine the ventilation rate these measurements are multiplied by the vent area of which they are assumed to be representative (Joo et al., 2014; Molina-Aiz et al., 2009). This can result in large errors when the velocity profile in that area is not homogeneous. Especially in naturally ventilated vents this homogeneity cannot be expected due to the constantly changing wind incidence angles. Each chosen measuring point will have a stochastically changing significance in its contribution to the total calculated airflow rate (Shen et al., 2012b). The more heterogeneous the velocity profile is, the more sensors will be needed to give a correct airflow rate. However, this implies that the profile should already be known to some extent before the tests start. An assessment has to be made on how many sensors will give the necessary amount of detail without causing a considerable obstruction of the vent. The use of CFD modelling could help in these cases, but often the choice seems to be made on sensor availability. The vent area assumed to be representative of a point velocity measurement differs greatly among different studies from 2.1m² (Molina-Aiz et al., 2009); 2.6m² (Boulard et al., 1998); 1.1m² (Teitel et al., 2008a), 8.5m² (Teitel et al., 2005) in greenhouses. In livestock buildings sometimes areas of 100m² were taken by Joo et al. (2014). Kiwan et al. (2012) studied the effect of sensor placement in the vent opening. They stated that *“it is more important to measure the air velocity at different points within an opening to obtain representative data for the whole opening than to measure at a high number of openings which are located in very similar positions”*. Still, important knowledge gaps exist on the subject of animal houses and particularly with regard to the effect of measurement positions within the respective openings. It must be noted that there have been research efforts to develop air velocity or airflow rate sensors that do not rely on point measurements but rather on line or even surface area measurements. Doing so, part of the heterogeneity of the velocity profile could be captured by the sensor. Two distinct methods were found. One concerns a heat dissipation method developed by Özcan et al. (2009) and further adapted by Lule et al., (2014). Heat is generated from a line source located in the vent. The relation between temperature distribution and airflow rate could be found by capturing the two-dimensional temperature distribution around the ventilation opening by infrared thermal imaging. Their results show that the ventilation rate can be predicted with an error of 8% under controlled conditions by using a data-based mechanistic approach. However, it is not clear how such a technique could be used on large vents such as those in cattle farms. The other technique is based on ultrasonic transit times or, in more complex applications, ultrasonic tomography. These techniques are mainly used to measure gas flow rates through pipes (Drenthen and de Boer, 2001; Kurniadi and Trisnobudi, 2006) but might also be applicable for natural ventilation purposes. Ozcan (2011) has applied such a technique to a round duct with the intention of using this set-up in naturally ventilated buildings. An airflow rate measurement error of 9% was found under controlled conditions for heterogeneous velocity profiles through a round duct. However, no further

developments have been published. None of these innovative techniques have been tested in naturally ventilated animal houses and are, therefore, not directly transferable without further in depth research. Indirect measuring methods such as mass balance methods (Demmers et al., 2000 ; Kiwan et al., 2013; Samer et al., 2011) are commonly used to give an estimate of the ventilation rate. They include heat and moisture balance methods and tracer gas tests with naturally occurring tracers such as CO₂ and artificially inserted tracers such as SF₆. There exist three types of tracers gas tests, e.g. tracer gas decay, constant concentration and constant injection method. For the tracer gas decay test the animal house is sealed off and filled with tracer gas which is mixed with the indoor air until a homogenous gas concentration is found throughout the animal house. When the vents are opened again, the rate of tracer concentration decay is a measure for the ventilation rate. This method does not allow a continuous measurement. For the constant concentration method, the concentration of the tracer gas is measured at various locations. The amount of tracer that is necessary to maintain that concentration is a measure of the ventilation rate. Therefore, the valve controlling the tracer injection rate has to be adjusted automatically and continuously whilst measuring the gas concentrations. Due to changing ventilation rates it is challenging to maintain a constant concentration throughout the whole animal house. Therefore, this method is not recommended for use in naturally ventilated buildings. The constant injection method is the most commonly used one and allows a semi-continuous measurement of the ventilation rate, i.e. until the tracer gas runs out (Ogink et al., 2013). The CO₂ mass balance method uses CO₂ emitted by the animals and the manure as a natural tracer gas. Therefore, the advantage of the method is that the “tracer” is often released more homogeneously throughout the stable without the need of a complex release system. However, the accuracy of the models needed to predict the amount of CO₂ that is released from the different sources remains a problem (Kiwan et al., 2013).

The tracer concentrations should be measured at the outlet openings and corrected for background concentrations measured at the inlets. As mentioned above, these in- and outlet locations vary according to the wind incidence angle. In principle a vent can be determined to be an in- or outlet by comparing the concentration in the vent to the outside concentration of fresh air. Outlets should have higher concentration of the tracer gas. However recirculation, influences of surrounding emission sources and in the case of CO₂ small differences between indoor and outdoor concentrations make this approach less reliable.

The results of tracer gas techniques are very variable and mainly depend on the sampling positions and the mixing of the indoor air with the tracer (Van Buggenhout *et al.*, 2009). An extended review on uncertainty analysis and error sources of these indirect ventilation rate measuring techniques is given by Calvet et al. (2013). Good results are found when tracer gas tests are compared with reference techniques for mechanical ventilation (summarised by Ogink et al., 2013). However, as there is no reference technique for natural ventilation (Ogink et al., 2013), they cannot be validated in these conditions. Ozcan (2011) mentions inaccuracies from 10% to 230% for tracer gas tests.

Overall, it can be stated that a reliable and continuous quantification of the ventilation rate is difficult to achieve with these techniques because they do not sufficiently take into account the continuous fluctuations in the airflow rate and the characteristics of non-perfectly mixed fluids. Indirect methods are not suited for long term measurements and are therefore mostly used for research purposes.

1.2.5.4. Ultrasonic anemometers: applications in agriculture

As mentioned in 1.2.5.3 the air velocity can be measured in a variety of ways. The most common anemometers are cup, vane, hotwire and ultrasonic anemometers. The prerequisites of an anemometer fit for the use in naturally ventilated animal houses are a.o. robustness, accuracy and the ability to measure the direction of the flow.

Although there exist very accurate hotwires that are also able to indicate flow directions, they are in general too fragile and expensive to be used in outdoor conditions. Cup and vane anemometers are robust but are not able to measure the direction of the flow. Furthermore, these sensors rely on the correct functioning of their mechanical (rotating) parts. In the sometimes dusty conditions of an animal house, the sensors' bearings might become clogged. Although they can certainly be used for short term measurements in combination with a wind vane, longer measurement periods will therefore require regular cleaning and even recalibration. This is in stark contrast to the robust ultrasonic anemometers which have no moving parts and are made to last without the need for calibration (Ozcan, 2011). An ultrasonic sensor measures the air velocity by sending an acoustic pulse from one piezoelectric transducer to another. The time it takes for the acoustic pulse to travel between those transducers, i.e. the transit time, is a measure for the air velocity. Flows travelling in the opposite sense of the pulse increase the transit time and vice versa. Flows traveling perpendicular to the path between two transducers do not influence the travelling time. With one transducer pair, a 1D sensor is created. Therefore, for a 3D sensor, 3 pairs are necessary. These 3D sensors will deliver the total wind velocity decomposed into its X-, Y- and Z-velocity components. Furthermore, the measuring frequency of the ultrasonic sensor can be very high, as this frequency only depends on the speed at which the acoustic pulses can be sent and received. This allows turbulence measurements for studies concerning e.g. heat transfer and the mixing and transport of pollutants within the animal house.

Ultrasonic sensors have been widely used in ventilation studies in agriculture, especially in greenhouse production. In many of these studies the sensors are placed in or at the ventilation openings in order to measure the ventilation rate or to study the flow patterns through these openings (López et al., 2011a, 2011b; Molina-Aiz et al., 2009; Teitel et al., 2005). In other studies the ultrasonic sensors are distributed throughout the building to measure the internal flow patterns (Boulard et al., 2000; López et al., 2012a, 2012b; Wang and Deltour, 1999; Wang et al., 1999). The data gathered in these studies allowed to examine the relation between buoyancy and wind effect and the influence of e.g. building geometry, obstructions in the surroundings, wind incidence angle and speeds, vent characteristics, etc. on the ventilation rates and patterns. Also the turbulence of the airflow at the vents was characterized

to study the contribution of turbulence to the overall sensible heat transfer and to provide a database for future validations of CFD based simulations.

All above mentioned studies are performed on greenhouses. The interest in this sector is related to the need for a very precise control of the indoor climate to ensure crop growth. Furthermore, a homogeneous distribution of temperature, relative humidity and gases are needed to obtain uniform growth throughout the greenhouse. Also in animal production, more and more attention is being paid to an optimal indoor (micro)environment (see 1.1). According to Bjerg and Sørensen (2008) the modern demands of airflow in livestock buildings are related to air distribution, control, energy efficiency, and air velocity in the animal occupied zone. Samer et al. (2011b) state that there are several procedures that should be implemented to meet these demands: determining and limiting air velocity at animal level, homogenizing air velocity distribution and direction in the entire barn, determining whether air velocity distribution inside and close to the inlet are similar, investigating air velocity profiles and turbulences, and reducing air velocity at floor level at high ventilation rates without increasing the pressure drop over the inlet.

Although the ultrasonic sensor would be an ideal tool to study abovementioned topics, few studies in naturally ventilated animal houses can be found where these sensors are applied for more than determining the surrounding wind conditions. However, some studies have clearly proven the sensors' applicability by delivering important insights into the relation between external wind conditions and airflow rates and patterns. For example, Fiedler et al. (2013) measured air velocities throughout the animal occupied zone of a naturally ventilated dairy barn. They found a relation between heterogeneous airflow patterns and climatic conditions within the animal house and the outside wind direction (25° from normal to the vent). However, they state that more data is necessary to identify the factors causing changes in the airflow patterns and rates. Norton et al. (2009) took detailed ultrasonic anemometer measurements of the internal airflow patterns in a naturally ventilated $\frac{1}{2}$ scale duopitch building to validate CFD predictions. This study confirms the relation between internal climate heterogeneities and wind incidence angles other than normal to the vents. In this study it was also shown that the airflow rate through the vents does not necessarily represents the actual air renewal rate as short circuiting between the vents can occur. Joo et al. (2014) measured the airflow rates through the vents of a naturally ventilated dairy barn by multiplying velocities measured in the vents by an area for which these velocities were assumed to be representative. Although these areas were sometimes as large as 100m^2 , this representativeness was not thoroughly checked. They found that the air inflow rates were, in general, higher than the outflow rates. It was also shown that using an on-site weather station and an ultrasonic sensor in the centre of each vent could be a possible simplified approach for determining the ventilation rates. Ndegwa et al. (2008) performed similar experiments as Joo et al. (2014) and found that averaging the in- and outflow rates results in a reasonable measurement of the ventilation rates.

No studies could be found that give a detailed image of the velocity profiles in the vents of full scale animal houses (not accounting for CFD simulations). However, such a velocity profile is the link between outdoor and indoor conditions. Therefore, a more in depth knowledge concerning what influences the profile's heterogeneity could deliver insights useful for the measurement, distribution and control of the airflow rate. Furthermore, from a detailed velocity profile the minimal measuring density can be deduced necessary to obtain a reliable estimate of the ventilation rate.

1.3. Emissions from naturally ventilated animal houses

As discussed in 1.2, the indoor climate of an animal house needs to be controlled and maintained between certain limits of, amongst others, temperature, relative humidity and concentrations of harmful gases. The main influencing factor is the ventilation rate as it refreshes the indoor air and removes pollutants such as NH₃, CO₂, CH₄, N₂O, H₂S and dust. Consequently, these pollutants are emitted into the environment causing harm to fauna and flora. National and international regulations exist to enforce the mitigation of the emission of harmful gases (see 1.3.2). A source oriented approach is necessary to reduce the release of these pollutants as much as possible (see 1.3.1). How these emission rates are currently measured is discussed in section 1.3.3.

1.3.1. Mitigation techniques

Pollutants in livestock facilities have two main sources: the animals themselves and the manure they produce. NH₃, CO₂, CH₄, N₂O, H₂S are all gases that are released from manure, either under aerobic and/or anaerobic conditions. Additionally CO₂ is also released through the animal's exhalation (Philippe and Nicks, 2015) and up to 80% of the emitted CH₄ originates from enteric fermentation (Ngwabie et al., 2014). Dietary strategies can reduce the enteric CH₄ production and have been reviewed by Boadi et al. (2004). To reduce the emissions originating from manure there exists an array of mitigation techniques. They can be subdivided into three main mitigating strategies: 1) Changing the properties or composition of the manure, 2) reducing the contact surface and exposure time of manure to the indoor air and 3) creating an indoor climate that does not stimulate the release of pollutants.

Most of these techniques focus on NH₃ reduction. The first strategy can be accomplished through e.g. adaptation in the animals diet, avoiding contact between urine and faeces to counter the formation of NH₃, lowering the temperature of manure through cooling elements, lowering the pH of the manure. The second strategy can be accomplished through e.g. frequent removal of manure from the pits and/or solid floors, reducing the emitting surface through the application of e.g. sloped pit walls, solid floors covering the manure pits beneath the animals. More information concerning abovementioned techniques can be found in e.g. Sommer et al. (2013) and UNECE (2014). As the focus of this general introduction lies on the link between airflow rates or patterns and the indoor climate, these techniques will not be discussed further.

However, the indoor climate itself also has an impact on the emission rate which leads to the third strategy. Reducing the air velocities over the emitting surface of slatted or solid floors and pits can lower the emission rate of NH_3 considerably (Rong et al., 2009). It should be noted that it is not necessarily the ventilation rate that is the key factor. When large airspeeds over emitting surfaces are avoided through a well-controlled airflow pattern, the ventilation rate might not need to be decreased. However, with current techniques the airflow pattern is not easily controlled, especially not in dairy farms due to their large and naturally ventilated vents. In these cases lowering the ventilation rate, without compromising the indoor climate, is the best option to lower internal air speeds. Wu et al. (2012) found a significant linear relation between NH_3 emission and ambient temperature. Hence by controlling the indoor climate and avoiding unwanted high temperatures, emissions might be lowered. Nevertheless, concerning the third strategy, Philippe and Nicks (2015) rightfully stated that the indoor climate parameters should be primarily controlled to fulfil the physiological needs of the animals. Only in second order it should be examined whether the indoor climate could be adjusted to diminish emissions.

Unlike mechanically ventilated animal houses the use of end of pipe techniques is scarce but rising. This is mainly due to the variability of the outlet location and the large differential pressure differences that are necessary to overcome airscrubbers and biobeds.

In any case, research efforts should be aimed at “front of pipe” techniques, as they do not only lower the emission rate but help in maintaining a healthy indoor climate for animals and farmers.

More detailed information on the formation of pollutants and on mitigation strategies can be found in Monteny et al. (2006), Ndegwa et al. (2008);, Philippe et al. (2011) and Webb et al. (2005).

1.3.2. Impact and regulatory aspects

The pollutants emitted from an animal house can have a considerable effect on the surrounding and even global environment. In the vicinity of the barn the emitted ammonia can cause soil acidification and eutrophication, thus damaging the ecosystem. CO_2 , CH_4 , N_2O contribute to the greenhouse effect which can cause severe climate changes and increase the occurrence of extreme weather phenomena.

In more densely populated areas odours from animal houses are becoming an increasing problem.

Agriculture is considered to be responsible for the contribution of 93% and 18% of ammonia and methane emissions, respectively, in Europe (EEA, 2014). The negative effects on the environment have brought about international legislation (Kyoto-Protocol, 1998; NEC-Directive, 2001). In Flanders this has reached a culmination point in April 2014 with the acceptance of the specific conservation objectives (in Dutch: specifieke instandhoudingsdoelstellingen (S-IHD)). This program was created as an answer to the NATURA2000 framework which imposes a predetermined area of “protected special areas of conservation” in Europe. In Flanders some animal husbandry farms are located in or near these protected and nitrogen sensitive areas. The PAN (2014) program (programmatische aanpak stikstof) has been created to set regulations and eventually compensations for this sector in specific.

In light of this program approximately 970 farmers have recently been informed that when they have to renew their licenses, an emission reduction of 30% will be imposed. Additionally for about 70 farms, the license renewal will be rejected with closure as a result. In Flanders emission abatement techniques in animal husbandry are already enforced through national legislation (MB, 2004) to reach the European goals. However, these techniques do not apply for naturally ventilated dairy farms. Unfortunately it is mostly these farms that are targeted by the PAN. Therefore there is an urgent need for specific abatement techniques. Parallel there is a need for measuring techniques to accurately quantify the efficiency of the abatement techniques and the emission rate in general. Without these measuring techniques, legislators are forced to base their decisions on numbers provided by models, generalisations of earlier studies and simplifications. As mentioned in 1.2.5 and 1.3.3 the accuracy of existing measuring techniques for determining the ventilation rate cannot be guaranteed as no reference method exists.

1.3.3. Measurement of the emission rate

An extensive review on measurement techniques for the emission rate in naturally ventilated animal houses by Phillips et al. (2001), discussing techniques up to 2000, was updated by Ogink et al. (2013) up to 2013. Ogink et al. (2013) distinguished five techniques:

- 1) product of measured differential concentration and ventilation rate
- 2) tracer gas ratio method
- 3) direct measurements using passive flux samplers
- 4) flux chamber methods
- 5) combination of downwind measurement and dispersion modelling

For the first technique the measurement of the ventilation rate can be carried out by applying direct and indirect techniques as discussed in 1.2.5.3. The measurement of the differential concentration (inlet vs outlet) of the pollutant of interest is subjected to the same inaccuracies as the ventilation rate measurement by tracer gases. Such methods assume a homogenous pollutant or tracer distribution across the vents and a fixed in or- outlet character of that vent. Both assumptions can lead to large errors, especially when the wind incidence angle is not perpendicular to the vents. In these cases, a measurement of the wind velocity profile in the vents is essential to know the exact locations of the in- and outlets. Such a measurement could be used simultaneously to determine the airflow rate. Due to the multitude of emission sources e.g. animals and manure, the pollutants could be considered homogeneously released throughout the animal house. However, this does not necessarily imply a homogenous indoor distribution. Certain airflow patterns can induce “dead zones” of still air (Daskalov et al., 2005), where the pollutant concentration can build up affecting in its turn the heterogeneity of the concentration profile in the vents. The number of measuring points in the vents will be proportional to the uncertainty of the method (Joo et al., 2014). In any case finding

representative locations to measure the inlet and outlet concentrations remains a challenge. The causes of the uncertainties associated with this method are shown in Fig. 1-2.

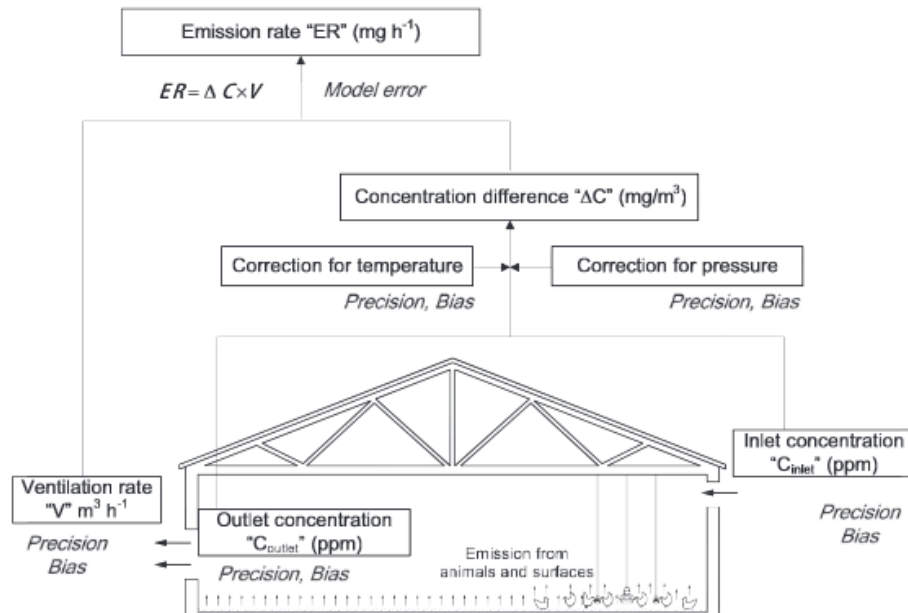


Fig. 1-2: Uncertainty diagram concerning the determination of gas emissions from livestock buildings. Potential sources of random errors (precision) and systematic errors (bias) are indicated. Figure adapted from Calvet et al.(2013).

The tracer gas ratio method is based on the assumption that the ratio between the release rates of the pollutant and the injection rate of the tracer gas is equal to the ratio of the pollutant and tracer gas concentrations (both corrected for background concentrations) (Mosquera et al., 2005). Hence, a big advantage of this method is that it does not require knowledge of the ventilation rate, thus avoiding the uncertainties associated with such a measurement. Also, a perfectly homogenous distribution of tracer and pollutant throughout the animal house is not necessary as long as both behave in the same manner. Therefore, a prerequisite is that the applied tracer gas and pollutant are thoroughly mixed and have a similar distribution of sources and similar transport and dispersion properties. The difficulty of the ratio method lies in fulfilling these criteria (Scholtensa et al., 2004). Although no homogenous distribution is necessary, the measuring points should be located where the mixing of tracer and pollutant is optimal. Ogink et al. (2013) stated that the most representative sampling locations are situated at the outlets. Therefore, a determination of the velocity profiles in the vents remains advisable to avoid errors due to the changing in- and outlet character of the vents. However, it must be noted that Mendes et al.(2015) found that measuring the concentrations above the animal occupied zone would also deliver satisfactory results. This would be a viable option when it is impossible to determine the in- or outlet locations.

Passive flux samplers for NH₃ are tubes internally coated with acid that capture the NH₃ at a rate proportional to the NH₃ concentration and the wind velocity flowing through the tube. These tubes

only perform optimally when the air is flowing directly towards them (Ogink et al., 2013). Therefore a fixed wind incidence angle is necessary. Additionally, the samplers need a longer sampling time required for the diffusion reaction. The method is therefore, on the one hand, not suited for long term measurements where changes in wind incidence angles can be expected. On the other hand it is also not suited for measurements where short term variations in the emission rates are to be examined.

The flux chamber method is used to single out certain parts of the animal house. A small chamber is positioned over the location of interest resulting in a controlled environment where the emission rate can be determined. However due to the high spatial variability of the emission sources and strengths, multiple locations inside the animal house need to be sampled when a representative average over the whole building is wanted. The amount of measurements and their locations are difficult to determine. Additionally the presence of these flux chambers disturbs the normal airflow patterns, potentially altering the emission rate of the measured locations. Therefore, it is not recommended to use these flux chambers to determine the total emission rate of an animal house.

Dispersion modelling uses concentration measurements downwind of the animal house to calculate the emission rate. As these measurements should be taken at large distances (e.g. 100m) downwind, the wind incidence angle determines the location of these sampling points. Therefore the surroundings of the animal house can impede such measurements when no open field is present. Also, when more animal houses are located closely together, their individual contributions to the total emission rate will be difficult to assess.

A practical emission monitoring technique should be robust, low maintenance and able to deliver reliable results whilst relying on only few measuring points. Most abovementioned measuring techniques could potentially be very accurate. However, large heterogeneities of velocity profiles and gas concentration distributions are common in naturally ventilated animal houses. Therefore, the amount of measuring locations to take this fully into account would be so high that these methods would at least become highly impractical and expensive. Being able to measure a detailed velocity profile in a naturally ventilated vent would be a stepping stone towards reducing the need for such high measuring densities. As mentioned in 1.2.5.4, in depth knowledge concerning what influences the velocity profile's heterogeneity could deliver insights into the distribution of the airflow rate which can be linked to the gas concentration distribution. Furthermore, it is only from a detailed velocity profile that the minimal measuring density, necessary to obtain a reliable estimate of the ventilation rate, can be deduced.

1.4. Problem statement

In light of sustainable livestock production, the management of a naturally ventilated animal house needs to be focused at lowering the emissions of pollutants whilst keeping an optimal indoor climate. This has to be approached from three sides. Firstly, a farmer needs full and automated control of the air renewal rate. In this way he can be sure that, whilst keeping the exhaust airflow at an optimal level, the animals will not be harmed as an adequate air renewal rate is guaranteed (EFSA, 2009). Secondly, new source oriented techniques need to be developed to diminish the release of the pollutants from manure (Philippe and Nicks, 2015; Philippe et al., 2011). Lastly, the emission rate of animal houses needs to be measured accurately to give the possibility to base the legislation on reliable numbers in order to be effective. All three approaches have a strong connection to the airflow rate and the associated wind velocity profiles in the vents. Most common emission rate measurement techniques, for instance, rely on an accurate determination of the ventilation rate and the location of the in- and outlets (Ogink et al., 2013). For the research on source oriented approaches, the emission rate of animal houses where the mitigation techniques are applied can give insight into the reduction potential of these techniques. In mechanically ventilated animal houses there exist accurate techniques which can serve as reference techniques to determine the airflow rate. Also the locations of the outlets are known and constant. These are both factors that contribute largely to the reliability of the emission rate determination (Groot Koerkamp et al., 1998). This is in stark contrast with naturally ventilated animal houses where variations in e.g. wind speed and wind direction have a large influence on the airflow rate and outlet locations (Linden, 1999). As a result of these variable conditions, there is no reliable measurement technique for the airflow rate to this day. Consequently, no generally accepted reference technique exists to measure the emissions from naturally ventilated animal houses. Therefore, also the reduction potentials of existing and new abatement techniques remain uncertain and prone to discussion. It is clear that a reference measuring technique for the ventilation and emission rate in naturally ventilated animal houses is necessary to construct an unambiguous regulatory framework aiding farmers, constructors, legislators and researchers. This is acknowledged throughout the scientific community and extensively discussed in the special issue of Biosystems Engineering on 'Emissions from Naturally Ventilated Livestock Buildings' (November 2013). This issue emphasizes the importance of accurate practical measuring techniques for the ventilation rate and draws the attention to the lack of a reference measuring method to validate such techniques (Calvet et al., 2013; Ogink, Mosquera, Calvet, & Zhang, 2013). In this respect, Takai et al. (2013) concluded that one pillar of future research must be the development of practical field methods that can be used as reference standards. The development of a reference method for measuring the airflow rate in naturally ventilated animal houses, would be a key milestone for both the quantification of the emissions and the further development of adequate measuring and control techniques.

Takai et al. (2013) also concluded that a dedicated facility needs to be established that can be used to obtain precise reference measurements of ventilation rates in naturally ventilated buildings. The authors state that such a facility would enable researchers to investigate and determine error sources and underlying mechanisms for measurement inaccuracies. This knowledge would be an essential tool for the development and selection of measuring techniques with higher accuracy and lower costs.

1.5. Research objectives

The overall objective is to develop a reference method for ventilation rate measurements in a naturally ventilated test facility towards application in naturally ventilated animal houses.

Sub-objectives

- The test facility should be built in a way representative of a commercial animal house, i.e. with side and ridge vents. This should allow to gain insights that are transferable to these commercial buildings concerning the airflow rate distribution among the vents.
- The reference technique should be developed for both side vents and ridge vents measurements.
- In this set-up the reference technique should give detailed information on airflow rate and velocity profiles in the vents under varied wind conditions. The location of the outlets should be known at all times.

1.6. Thesis outline

A measuring technique for the ventilation rate through rectangular vents will be developed, capable of coping with heterogeneous velocity profiles. As no reference exists for naturally ventilated flows, this technique will be validated with a reference technique for mechanical ventilation (Chapter 2). A fully automated version of the airflow rate measuring technique will be developed to allow for an automated measurement of rectangular vents. Again a validation with a reference technique for mechanical ventilation will be necessary. The method will be validated for heterogeneous velocity profiles and larger vents (Chapter 3). A naturally cross ventilated testing room will be built where the fully automated measuring technique will be applied. The development of the airflow rate measuring method will be focussed on the capability of measuring the temporal and spatial variability of velocity profiles (Chapter 4). A dedicated naturally cross and ridge ventilated test facility will be built, equipped with the automated ventilation rate measuring technique. The usability of the method in more representative circumstances (larger vents and internal volume, sloped roof and ridge opening) will be determined. A technique will be developed for measuring the ventilation rate through the ridge, accounting for the velocity profile through that ridge (Chapter 5). Although it is not within the scope of this research to develop a method directly transferable to commercial animal houses, a first step towards a possible simplified measuring strategy will be taken. Therefore, the velocity profiles that will be determined in Chapter 5 will be examined in more detail. Especially the influence of wind direction will be discussed (Chapter 6). A more elaborate discussion will be held on why certain choices concerning the development of the measuring method were made and how these choices relate to the existing literature. Also the transferability of the developed method to commercial animal houses will be discussed, ending with some recommendations for future research (Chapter 7).

Chapter 2. Experiments under conditions of mechanical ventilation: Manual 2D approach.*

*Adapted from: Van Overbeke, P., Pieters, J.G., De Vogeleer, G., Demeyer, P., 2014b. Development of a reference method for airflow rate measurements through rectangular vents towards application in naturally ventilated animal houses: Part 1: Manual 2D approach. *Comput. Electron. Agric.* 106, 31–41. doi:10.1016/j.compag.2014.05.005

2.1. Introduction

Velocity profiles in ventilation openings induced by natural ventilation can be heterogeneous and will change according to e.g. wind incidence angles and speeds (De Paepe et al., 2013). Therefore, the challenge in measuring the velocity profile in a naturally ventilated vent is twofold: finding a method that can (1) cope with the large variety in the profile characteristics and (2) deal with the temporal variability of these profiles. In this chapter the first challenge (1) was studied as an initial step in the development of a robust and accurate technique that can act as a reference for airflow rate measurements through rectangular sections. This implied the subsection of the method to a variety of velocity profiles in order to determine the appropriate sensor locations.

2.2. Materials and Methods

In order to determine the accuracy of a method, we need a reliable reference. As this was impossible to obtain under conditions of natural ventilation, experiments conducted under mechanical ventilation were needed. Evidently, the conditions in such experiments are not fully representative of the conditions under natural ventilation as these mechanically induced airflows are constant in speed and direction and therefore different from the continuously changing wind (Larsen, 2006). Nevertheless, at the current state-of-the-art there was no real alternative and such experiments can procure valuable insights into the behaviour of the examined measuring method under different conditions, albeit in steady state. Therefore, first a test installation based on mechanically induced airflows was developed for this specific application (See 2.2.1).

Some airflow rate measuring techniques have already been developed especially for the application in naturally ventilated vents. These techniques have been discussed in 1.2.5.3 and none of them are ready for use in practice. Therefore, rather than to invest a large amount of time in the development of a completely new sensor, it was decided to use an existing sensor technique i.e. ultrasonic anemometry for the development of a new method (See 2.2.1.3). Ultrasonic anemometry was suggested by Ogink et al. (2013) and Takai et al. (2013) for direct velocity measurements due to its robustness and has been used in the field by many authors (Fiedler et al., 2013; López et al., 2011a; Samer et al., 2011b; Wang et al., 1999). According to a Thies Clima Manual of a 2D ultrasonic anemometer it was advisable to install the sensor at a minimum distance of 1 meter to surrounding objects. Ignoring this advice could lead to echoing when the sound packages meet reflecting surfaces, resulting in incorrect measurements. As this would be a limiting factor in sensor location, the influence of walls in the vicinity (<1.00m) of the sensor was examined in a first experiment (See 2.2.2.1).

Because of the relatively large size of a 2D ultrasonic sensor, measurements of the air velocity close to walls (<0.05m) was difficult. Thus, part of the velocity profile information could be lost due to an incomplete measurement. This could lead to an overestimation of the airflow rates, especially near the edges where the biggest velocity gradients are to be expected as the velocity is zero at the borders. In a

second experiment (See 2.2.2.2), a comparison was made between an airflow rate measuring method with a 2D ultrasonic sensor and a hotwire method with a finer measuring grid to gain insight into the possible loss of information.

As stated in the introduction the measuring method should be able to cope with different velocity profile characteristics, e.g. airflow unsteadiness and velocity distributions. The unsteadiness of an air velocity profile (UF) is a measure of its instability over time. In a third experiment (See 2.2.2.3) the effect of the UF on the airflow rate measured by the developed method was studied.

In a fourth experiment (See 2.2.2.4), the ability of the chosen measuring set-up with the 2D ultrasonic anemometer to accurately measure different airflow rates was determined using the airflow reference system following the VDI2041. Since a free running impeller was part of the test installation and is a reference method to determine the airflow rate and thus emissions through a mechanical ventilation shaft, this method was also included in the experimental set-up.

In a last experiment (See 2.2.2.5) a closer look was taken at the side wall effects in an attempt to explain the deviations found in previous experiments.

2.2.1. Overall set-up of the test installation

The test installation consisted of four airflow rate measurement techniques (see Fig. 2-1): a reference technique based on a differential pressure measurement over an orifice following the guidelines of VDI2041 (see 2.2.1.1), a free running impeller (see 2.2.1.2), the method developed with a 2D ultrasonic sensor (see 2.2.1.3) and a hotwire method (See 2.2.1.4), with the last two methods making use of a manual measuring frame.

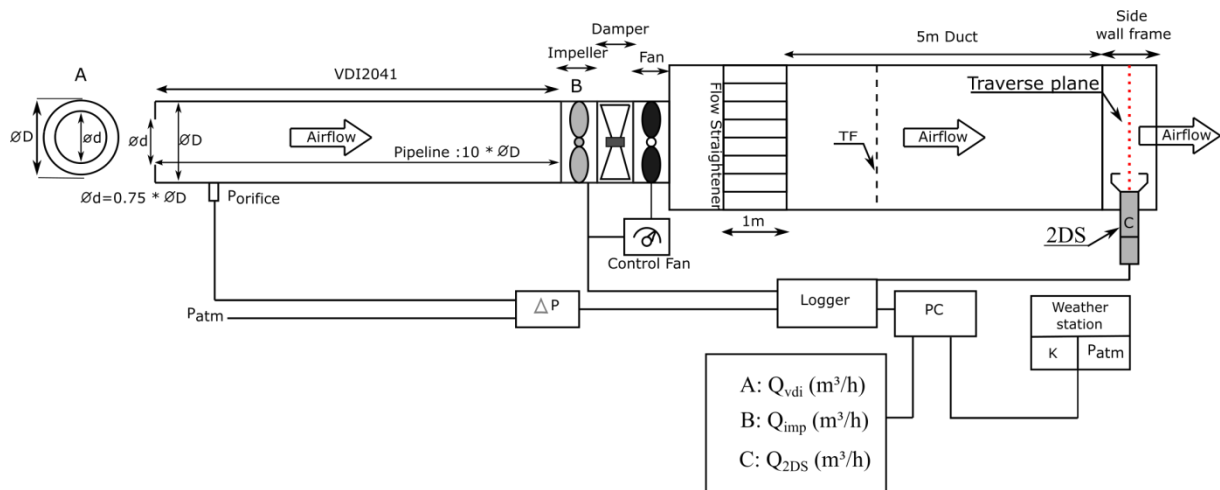


Fig. 2-1: General set-up with three simultaneous airflow rate measurement systems: A) differential pressure over an orifice according to the VDI2041 (Q_{vdi}), B) free running impeller (Q_{imp}) and C) the developed method with a 2D ultrasonic sensor (Q_{2DS}). In a fourth method the ultrasonic sensor was replaced by a 2D hotwire. With $\varnothing d$ and $\varnothing D$ the inner and outer diameters of the orifice (m), respectively. With $P_{orifice}$, P_{atm} and ΔP the static pressure downstream of the orifice, the atmospheric pressure and the differential pressure between the previous, respectively (Pa). A weather station measured the temperature (K) and P_{atm} . The side wall frame could be placed at the end of the duct or inside the duct at the location marked with TF.

The airflow was produced by an axial fan (See 2.2.1.2). Two set-ups were constructed, one for the lowest airflow rates (1000m³/h to 1500m³/h) with a fan, impeller and pipeline diameter of 35cm (\varnothing 35

set-up) and one for the higher rates ($1500\text{m}^3/\text{h}$ to $6500\text{m}^3/\text{h}$) with a fan, impeller and pipeline diameter of 56cm ($\text{Ø} 56$ set-up). Both set-ups could be fitted at the inlet of the airflow duct. This duct guided the airflow to the plane where measurements were taken by means of a traversing movement of an anemometer. This plane was referred to as the traverse plane. Three rectangular ventilation ducts were constructed with a height of 0.5m and a width of 1.0m . Two ducts had a length of 2.0m and one a length of 1.0m . These three ducts can be combined in any order to form an airtight duct of up to 5.0m long. The heights of the ducts were chosen in order to represent a section of an in- or outlet side vent of a naturally ventilated pig barn. The horizontal walls were made of smooth plywood and the vertical walls of polymethyl methacrylate. The transparency of the sidewalls ensured correct placement of the sensors in the tunnel and visibility of the smoke propagation during smoke tests. A flow straightener made of plywood was positioned inside the tunnel in order to diminish the influence of the airflow swirl caused by the axial fan. The flow straightener was located 0.3m behind the inlet of the duct and had a length of 1m with a mesh size of $0.05\text{m} \times 0.05\text{m}$.

Two sensor frames were developed to guide the traverse movement of the sensor described in 2.2.1.3 and 2.2.1.4. One frame of $0.5\text{m} \times 1.0\text{m} \times 0.2\text{m}$ was meant to simulate a section of the sidewall vents and is referred to as the side wall frame (Fig. 2-2). The second frame of $0.15\text{m} \times 1.00\text{m} \times 0.50\text{m}$ was meant to simulate a section of the ridge opening and is referred to as the ridge frame (Fig. 2-3).

The sidewall frame could be placed at the end of the airflow duct or between tunnel parts thus creating the possibility to measure inside the tunnel. The vertical walls were made of polymethyl methacrylate. The bottom horizontal wall had a sled in which the sensor was fixed and was further covered with canvas in order to minimize air leakage. The horizontal movement was carried out by turning the left or right handle, rolling up the canvas and moving the sled. The vertical positioning was carried out by placing the sensor higher in the sled. The sled could be adapted to hotwires or ultrasonic sensors.

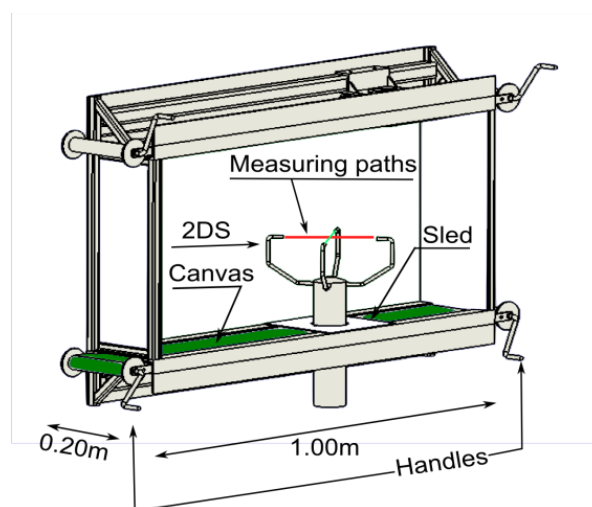


Fig. 2-2: Side wall frame with 2D ultrasonic anemometer (2DS). By moving the handles the sled was moved left or right. To measure higher or lower inside the frame, the 2DS was put higher or lower in the sled. The frame could be placed at the end of the duct or between duct parts.

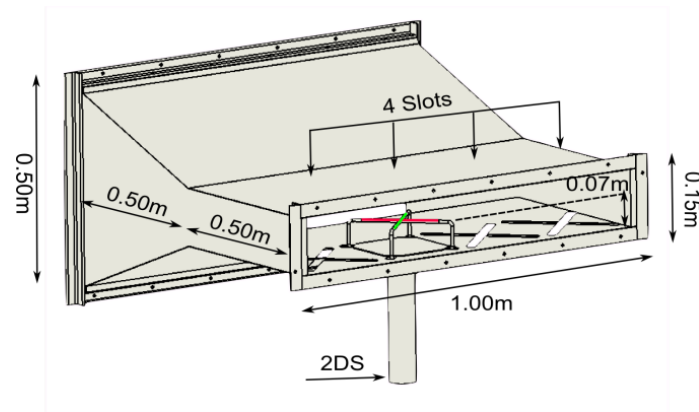


Fig. 2-3: Ridge frame with 2D ultrasonic anemometer (2DS). The 2DS could be placed in one of the four slots. The frame could only be placed at the end of the duct.

In the ridge frame, the air velocity sensors could be placed in four slots distributed over the length of the outflow opening and centrally placed over the height of the sensor frame. During measurements the three unused slots were covered to minimize air leakages. This frame could only be mounted at the end of the airflow duct.

2.2.1.1. Airflow calibration system (VDI 2041)

A method described by the standard VDI 2041 was chosen as a reference for the airflow rate measurements and has a combined standard measurement uncertainty of 3.0% (VDI2041). This standard is based on a differential pressure measurement over a standardized orifice and is further referred to as VDI2041. The steel orifices used in these experiments meet the requirements of DIN EN ISO, 5167-2:2004-01 (2003). As the VDI2041 imposes a pipeline length of at least 10 times the outer diameter of the orifice, the Ø35cm and Ø56cm set-up had a pipe length of 4.0m and 6.0m, respectively. The maximum diameter ratio (inner diameter/outer diameter of the orifice) of 0.75 was chosen for both set-ups to minimize the pressure build-up. The polyethylene pipes came in lengths of 1.0m. The different pipe pieces were coupled with ring pieces to form a smooth interconnection. The outlet of the pipe was connected to the impeller.

The pressure difference over the orifice was measured with a calibrated (11/2011) Dimed P26 differential pressure sensor ($-100..100\text{Pa} \pm 0.3\%$) for pressures below 100Pa. A Testo400 differential pressure sensor ($0..1000\text{Pa} \pm 30\text{Pa}$) was used for higher pressures. Both had a measuring frequency of 1Hz. The Testo400 was compared to a calibrated (06/2012) Dimed P26 ($-1000..1000\text{Pa} \pm 0.3\%$). The average value of 600 measurements made with both devices at 1Hz only differed by 2Pa at an average pressure difference of 255Pa. The Testo400 was not connected to the logger and could not log separate values but gave the average value of the measurements made at 1Hz after a predefined period. This made it impossible to calculate the standard deviations (SD). These missing standard deviations were indicated by “/”. The differential pressure over the orifice was measured throughout the whole duration of each experiment. Temperature and atmospheric pressure were obtained from a weather

station located next to the test installation. As both parameters were not expected to vary considerably during these short measurements (approximately 30 to 60 minutes) they were only registered once after each measurement. The airflow rate Q_{vdi} was calculated using equations [2.1 to 2.3] (VDI2041).

$$\varepsilon = 1 - 0.41 \frac{\Delta p}{\kappa p_{atm}} \quad [2.1]$$

$$Q_m (\text{g/s}) = C_d \varepsilon \pi \frac{d^2}{4} (2 \Delta p \rho)^{0.5} \quad [2.2]$$

$$Q_{vdi} (\text{m}^3/\text{h}) = 3600 \frac{Q_m}{\rho} \quad [2.3]$$

With ε the upstream expansibility factor (-); Δp the differential pressure over the orifice (Pa); κ the isentropic exponent (-); ρ the density of the fluid (kg/m^3) calculated with following equation: $\rho_{atm} / (R * T)$. With p_{atm} the atmospheric pressure (Pa), R the specific gas constant ($\text{J}/(\text{Kg} * \text{K})$) and T the temperature (K); Q_m the mass flow rate (g/s); C_d the discharge coefficient (-); d the inner diameter of the orifice (m). The calculations were made with $C_d = 0,6$ (VDI2041) and $\kappa = 1.4$ (for diatomic molecules) (Carter, 2001) and $R = 287,1$. The standard deviation of the air flow rate was calculated based on the fluctuations of Δp for the duration of each experiment (see 2.2.2.4).

2.2.1.2. Airflow generation and control

Direct current fans were chosen since their propeller speed is stable, even at low speeds, and can be adjusted almost steplessly. Two direct current axial fans (Fancom® IF Ø35cm and Ø56cm) with respective working ranges of up to 3540 m^3/h and 12300 m^3/h at 0Pa were used to produce different steady airflow rates. The pressure build-up of the orifice (max. 256Pa) reduced the working range of the Ø56cm fan to almost 6500 m^3/h . The fans were combined with their respective free running impeller systems. Two Fancom® ATM-Units (Impeller + Control Damper) were used (Ø35cm and Ø56cm). The impellers have working ranges of 125 m^3/h to 3500 m^3/h (Ø35cm) and 350 m^3/h to 11000 m^3/h (Ø56cm). The imposed airflow rates ranged from 1000 m^3/h to 6500 m^3/h and correspond to an average speed of 0.55 to 3.6m/s, respectively, in the outlet opening (0.5 m^2) of the airflow duct. This range was chosen to represent the average air speed velocity in Belgium which lies between 2 and 7m/s depending on the region (KMI, 2015). Higher speeds were not attainable as the fan reached its limits due to the pressure build-up caused by the orifice.

The rotational speed of the fan was automatically controlled and stabilized by a Fancom® ITM-iF unit that uses the feedback signal of the impeller. The impeller sends a frequency signal which is a measure of the airflow rate. From this logged frequency (f), the average value and standard deviation of the flow rate were calculated using the following equation provided by Fancom® [2.4]:

$$Q_{imp} (\text{m}^3/\text{h}) = (f/4) 60 F \quad [2.4]$$

Where F is a conversion factor calculated by Fancom® during the calibration of their impellers that converts the frequency of the impeller to the supplied airflow rate. f is the mean turning frequency of the impeller (Hz). F is 1.74 and 5.16 for the Ø35cm and Ø56cm impellers, respectively. The frequency signal was logged at 1Hz and checked with an oscilloscope to ensure correct functioning.

2.2.1.3. 2D ultrasonic method (2DS method)

A 2D ultrasonic anemometer or 2DS (Thies® 4.3820.02.300) was selected (See Fig. 2-4:A). Due to the measuring principle of the 2DS, temperature, air pressure and absolute air humidity had no or only a small influence on the air speed measurements and were therefore not taken into account (Thies Clima manual). According to the manufacturer the 2DS had an air velocity accuracy of ± 0.1 m/s below 5m/s and $\pm 2\%$ of the measured value above 5m/s (RMS-mean over 360°). The sensor was able to detect the direction of the airflow with an accuracy of $\pm 1^\circ$. An extra calibration conducted by Deutsche WindGuard Wind Tunnel Services GmbH (calibration mark 22997; D-K-15140-01-00 ; 10/2011) showed a standard uncertainty of max. 0.05m/s in a range of 0.557m/s to 5.470m/s.

The traverse area of 0.5mx1.0m (side wall frame) was divided into 20 areas or elementary surfaces (Fig. 2-4:D). All areas were consecutively measured for 2 minutes at 1Hz (De Paepe et al., 2012). Each time the sensor was manually moved to the next measuring point. The ultrasonic sensor was placed within each area so the intersection of the measuring paths coincided with the centres of these areas. The transducer arms were placed at an angle of 45° with respect to the sidewalls. As the sensor was placed inside the duct, only the vector normal to the traverse plane had to be accounted for (Fig. 2-4:C). Every normal vector ($V_{i\perp}$) was multiplied by its accompanying area A_i (m²) after which the individual airflow rates were summed [2.5]. With n the number of elementary surfaces, i.e. 20 in this case. In every area the SD of the $V_{i\perp}$ was calculated (V_{isd}). The combined standard deviation from one complete traverse (SD Q_{2DS}) was calculated following equation [2.6].

$$Q_{2DS}(\text{m}^3/\text{h}) = \sum_{i=1}^n (V_{i\perp} A_i 3600) \quad [2.5]$$

$$\text{SD } Q_{2DS}(\text{m}^3/\text{h}) = \sqrt{\sum_{i=1}^n (V_{isd} A_i 3600)^2} \quad [2.6]$$

Due to the geometry of the 2D ultrasonic anemometer the lowest measuring point was situated 12cm above the bottom edge of the sensor frame. Therefore the lowermost 5 areas (area 1 to 5) were chosen larger. In these areas the measurements were taken 2cm above the area centre.

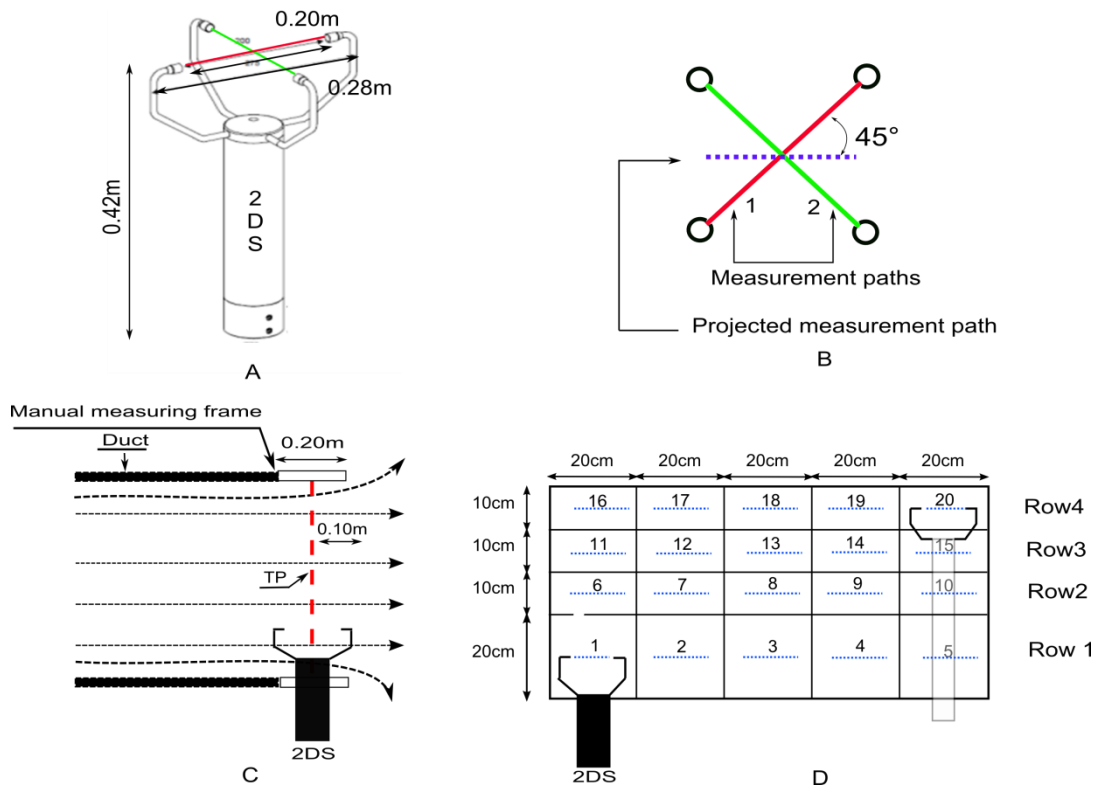


Fig. 2-4: A: 2DS geometry, with the measuring paths coloured red and green; B: Top view of the measuring paths of the 2DS. The paths cross where the traverse plane is located. Dotted blue line is the projection of the measuring paths on the traverse plane; C: Airflow through traverse plane (TP), all air passes through the TP before leaving the duct; D: Division of the traverse plane of the side wall frame into elementary surfaces with the projected measuring paths of the 2DS represented by dotted blue lines. Bottom row is larger as the 2DS could not go lower in the frame.

The traverse area of the ridge section (0.15m x 1.00m, see Fig. 2-5) was divided into 4 equal areas. The measurements were taken at a height of 7.5cm from the bottom. The measuring set-up of the method was equal to the set-up for the side wall frame.

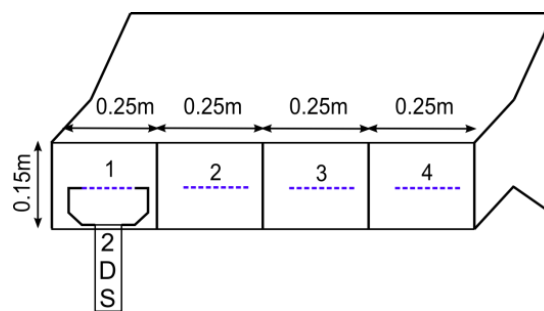


Fig. 2-5: Division of the traverse plane in the ridge frame with dotted blue lines the projected measuring paths of the 2DS.

2.2.1.4. Hotwire method

The traverse plane was divided into 66 areas (Fig. 2-6). A 2D hotwire (TSI® 8465) was used to measure the air velocities in the centre of each of these areas. This hotwire is considered 2D as, when it is set-up vertically, its measuring probe reacts mainly to flows from a horizontal plane at the height of the probe. However, this hotwire is not capable of giving the velocity components in that plane. Hotwires with such capabilities do exist, but these are in a much higher price range. The areas near the

walls were smaller to account for the influence of wall friction. Every point was logged for 2 min at 1Hz (De Paepe et al., 2012). In every area the mean velocity vector (m/s) and its SD were acquired. The airflow rate and its combined standard deviation were calculated using equations [2.5] and [2.6] applied to the hotwire method with $n=66$.

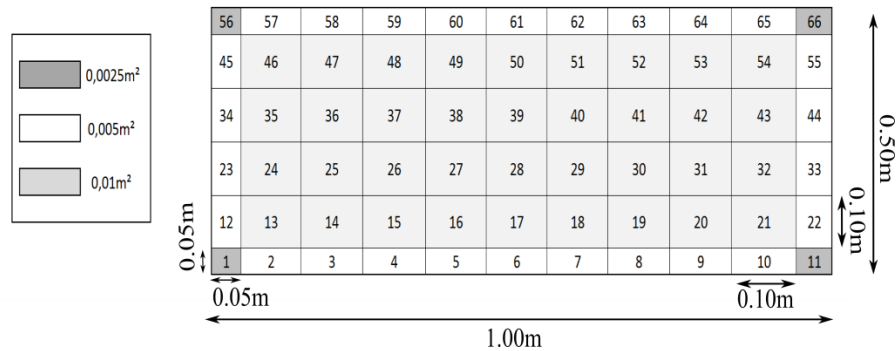


Fig. 2-6: Division of the traverse plane in the side wall frame into elementary surfaces for the 2D hotwire anemometer measurement density test. All hotwire point measurements were taken in the centre of the elementary surfaces.

2.2.2. Experiments for testing the validity of the 2DS method

During the period of June 2011 to June 2012, several tests were conducted to test the validity of the 2DS method. To evaluate these experiments, the relative measurement error (E_q) in % was used (Van Buggenhout et al., 2009) [2.7].

$$E_q = \frac{Q_{measured} - Q_{reference}}{Q_{reference}} 100 \quad [2.7]$$

Considering that these experiments are a first step towards the development of a reference method for the ventilation rate of naturally ventilated animal houses, a maximum relative measurement error of 10% was considered acceptable for these experiments.

The most influential parameter in each experiment was the fan rotation speed which was easily controlled. The reported standard deviations are therefore primarily the results of the small variations in fan rotation speed and airflow unsteadiness during one complete traverse. Although the SD are mentioned, they are not used for comparison purposes (except in 2.2.2.3), but give an idea of the stability of the airflow during one experiment. The orifice set-up was only installed for the experiments in 2.2.2.4. Each resulting airflow rate was calculated from data logged during one complete traverse movement. In each experiment (except 2.2.2.4) the desired airflow rate was manually selected by increasing the fan rotation speed with the Fancom® ITM-iF unit until the desired frequency of the impeller was reached. All measurements were taken at a frequency of 1Hz and logged by a Squirrel 2010 logger.

2.2.2.1. Sensor interference

To reduce the possibility of reflection of sound packages, the transducer arms were placed at an angle of 45° with respect to the walls (personal communication Thies®). To examine the influence of the surrounding walls, experiments were set up trying to induce errors through signal reflection. Four experiments were carried out. In each experiment the surrounding walls of the side wall frame were entirely covered by a different material: a rigid and smooth material, i.e. metal plates, a flexible and smooth material, i.e. rubber plates, a flexible and thin material, i.e. cloth and lastly the walls without additional materials i.e. polymethyl methacrylate and canvas. The air velocity was measured in areas 1, 5, 16 and 20 (Fig. 2-4:D) using a 2DS, each time for 2 minutes (De Paepe et al., 2012). These measuring locations were chosen because at these points interference was most likely to occur. As a reference, the air velocity was also measured in area 8, since less reflection was expected in this location. All experiments were performed at the same airflow rate, i.e. 1330 ± 25 m³/h.

2.2.2.2. Effect of the measurement density

A hotwire sensor is much smaller than a 2D ultrasonic sensor and can measure the air velocity in a much denser measuring grid. It was assumed that the hotwire method would deliver an airflow rate value that was closer to the true value. A comparison test was set-up between the hotwire method and the 2DS method at two different airflow rates.

2.2.2.3. Effect of airflow unsteadiness

The airflow unsteadiness was calculated by dividing the overall combined deviation by the mean air velocity. To examine the effect of UF, several adjustments were made to the test installation. The closer to the fan, the more the pulsing effect of the fan blades will have an influence on the flow. Therefore, to lower the UF, the duct was extended from 5m to 8m in steps of 1m by adding extra ducts. To increase the UF, 2 other set-ups were realized. First an obstruction (10 litre bucket) was placed in the tunnel at 0.50m upstream of the outlet at 0.35m from the left wall. The sole purpose of this obstruction was to increase the unsteadiness of the flow by an abrupt change in the mostly unidirectional flow inside the duct. Location and shape of this obstruction were rather arbitrarily chosen and had no additional purpose. In a second set-up the sensor frame was removed from the outlet and placed between 2 duct parts 3m downstream of the fan (TF in Fig. 2-1). Each test was carried out for 2 airflow rates, except for the obstruction experiment.

2.2.2.4. Effect of airflow rate

The effect of the airflow rate on the relative measurement error of the 2DS method was tested with the side wall frame (0.5mx1.0m) at 8 different airflow rates ranging from 1044m³/h to 6210m³/h. At the beginning of each experiment the desired airflow rate was manually selected by increasing the fan rotation speed with the Fancom® ITM-iF unit until the desired pressure difference over the orifice was reached. Airflow rates 1 and 2 were measured with the Ø35 set-up, airflow rates 3 to 8 with the

Ø56 set-up. The relative measurement error of the free running impeller systems were tested simultaneously with the side wall frame experiments.

With the ridge frame two airflow rates, 1447m³/h and 2596m³/h, were measured. As the Ø56 orifice was not yet available at that time, the Ø35 orifice was connected to the Ø56 fan and impeller by means of a transition box. This box might have disturbed the measurements of the impeller which were therefore not taken into account.

2.2.2.5. *Side wall effects*

The 2DS gives the average wind velocity over its measuring paths with a length of 0.2m (Komiya and Teerawanachai, 1993). These measurements must rather be seen as line instead of point measurements. As these paths are placed with an angle of 45° with respect to the traverse plane, the projected length that was captured by the sensor in this plane was 0.14m (Fig. 2-7:A).

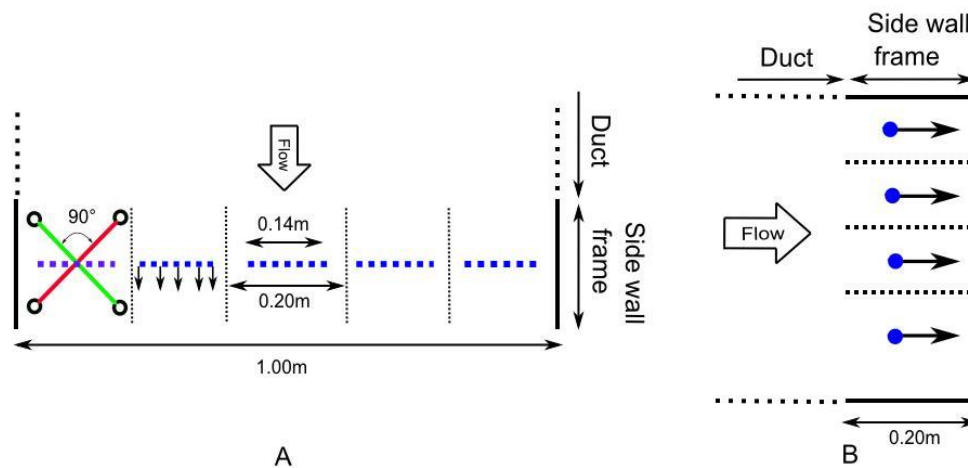


Fig. 2-7: A: Top view of the side wall frame, with the measuring paths of the 2DS in red and green and the projection of the paths on the traverse plane (dotted blue line). Almost the entire width of the vent is covered by such a measurement resulting in a high horizontal measuring density ; B: Side view of the side wall frame. From the side the projected measuring paths are similar to point measurements (blue dots), the vertical measuring density is, therefore, much lower than the horizontal density.

A horizontal traverse movement in the 2DS method (from area 1 to 5, 6 to 10, 11 to 15 and 16 to 20) consisted of 5 consecutive measuring points which meant that 70% ($5\text{m} \times 0.14\text{m} = 0.70\text{m}$) of the horizontal velocity profile was measured. On the other hand, a measurement in a vertical traverse could be seen as a point measurement (Fig. 2-7:B). This meant that the vertical traverse was captured by only 4 points. Together with the inability to measure the bottom 12cm, this led to the assumption that an overestimation could be caused by an insufficient measuring density in the vertical direction to fully account for the edge effects. Therefore, both the middle horizontal (areas 6 to 10) and vertical (areas 3, 8, 13 and 18) traverse movements were repeated with the 2DS and compared with higher density traverses (25 points each) using a calibrated 1D hotwire (TSI® 8455) (Fig. 2-8). The 5 points closest to the top and bottom wall in the vertical hotwire traverse movement were 1cm apart, the other points were taken every 2.5cm. In the horizontal hotwire traverse the 4 points closest to the left and right walls, starting at 2cm from each wall, were also 1cm apart, the other points 5cm. For every

traverse the ventilation rate was calculated. The surface areas were adjusted according to the number of measuring points.

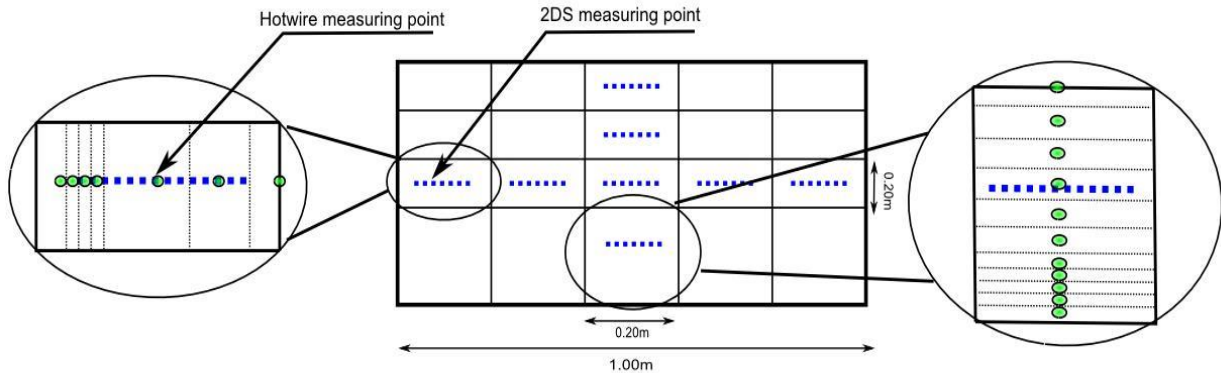


Fig. 2-8: The traverse plane of the side vent divided into elementary surfaces. A horizontal and vertical traverse is made with a 2DS and a hotwire. Measurement points for the 2DS are represented by the projection of its measuring paths (■■■■■■) and measuring points of the 1D hotwire by green dots (●). All hotwire point measurements are taken every 5cm in both the horizontal and vertical traverse (only shown for two elementary surfaces), except for the five measurements closest to each border which are taken every 2,5cm. This adds up to 25 measuring points in both the horizontal and vertical traverse.

2.3. Results & Discussion

2.3.1. Sensor interference test

Table 2-1 shows the air velocities and SD for the different wall coverings of the side wall frame. The largest difference between corresponding corner measurements was found in area 5 and amounted to 0.11m/s. As this was a single event and the remaining differences were not bigger than the measuring limit of the 2D sensor, it was concluded that a limited influence of reflection was to be expected under normal testing conditions where the walls are mainly polymethyl methacrylate and wood and in further research, concrete.

Table 2-1: Influence of different wall materials of the side wall frame on the velocities obtained by the 2DS in order to exclude the possible echoing of the acoustic signals against the duct wall which might lead to unreliable measurements.

Area (Fig.2-4D)	Rubber (SD) (m/s)	Steel (SD) (m/s)	Cloth (SD) (m/s)	Reference (SD) (m/s)
1	0.69 (0.10)	0.71 (0.13)	0.70 (0.17)	0.64 (0.13)
5	0.92 (0.16)	0.96 (0.15)	1.01 (0.14)	0.90 (0.16)
8	0.92 (0.09)	0.95 (0.10)	0.94 (0.11)	0.93 (0.10)
16	0.98 (0.16)	1.03 (0.16)	1.01 (0.17)	1.00 (0.17)
20	0.72 (0.12)	0.68 (0.12)	0.71 (0.11)	0.67 (0.12)

2.3.2. Effect of the measurement density

Fig. 2-9 and Fig. 2-10 show the velocities measured by the hotwire method and the 2DS method respectively, for two imposed airflow rates, i.e. approximately 1600m³/h and 3300m³/h. The curved velocity profile caused by the edge effects was visualized more clearly when using a higher

measurement density. Considering the large difference in methodology, the difference in airflow rates obtained by the two methods was limited (Table 2-2).

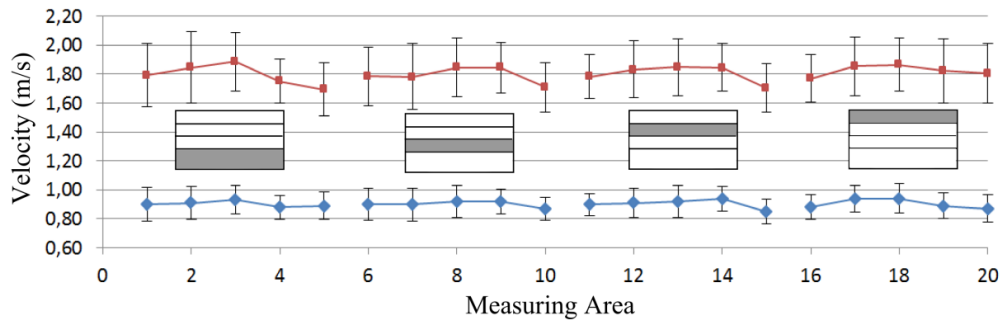


Fig. 2-9: Velocities measured by the 2DS method in the 20 elementary surfaces of the side wall frame, whiskers represent the SD. Two airflow rates were imposed: \blacklozenge 1600m³/h and \blacksquare 3300m³/h (approximately). The rectangle represents the traverse plane and the grey rectangles the row within the traverse plane on which the measurements are taken. The measurement areas can be found in Fig.2-4D.

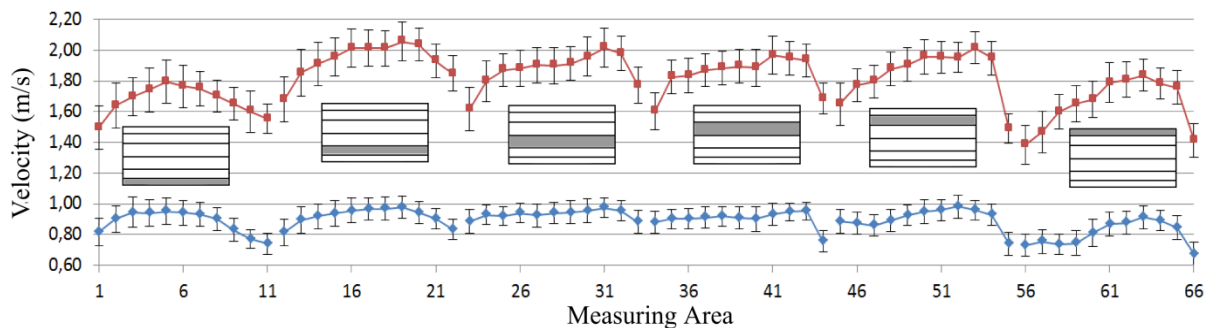


Fig. 2-10: Velocities measured in the 66 measuring areas by the hotwire method, whiskers represent the SD. Two airflow rates were imposed: \blacklozenge 1600m³/h and \blacksquare 3300m³/h (approximately). The rectangle represents the traverse plane and the grey rectangles the row within the traverse plane on which the measurements are taken. The measurement areas can be found in Fig.2-6.

Table 2-2: Comparison between 2 airflow rate measurement methods: 2DS method where the traverse plane is divided into 20 measuring areas and the hotwire method where the traverse plane is divided into 66 measuring areas. The hotwire method serves as the reference, with E_q the relative measurement error.

	2DS method (SD) (m ³ /h)	Hotwire method (SD) (m ³ /h)	E_q (%)
1	1625 (40)	1635 (15)	-0.6
2	3240 (85)	3340 (25)	-3.0

It should be noted that the used 2D hotwire was unable to measure the airflow direction. This could have led to an overestimation as it was necessary to calculate the airflow rate using only the vector normal to the traverse plane. Furthermore, the influence of the different sensor geometries could not be taken into account. Therefore, this experiment could not deliver conclusive proof for the correct choice in measurement density.

2.3.3. Effect of airflow unsteadiness

The experiment with the duct length of 5m was considered the reference for comparison purposes (see Table 2-3). The extension of the duct from 5 to 8m lowered the UF from 11% to 4%. The placement of

an obstruction in the tunnel (5m*) changed the shape of the velocity profile drastically and the UF increased to 33% for airflow rate 1. The measured velocities in this experiment are shown in Fig. 2-11. The grayscale gives an impression of the shape of the profile. The lee in the velocity profile clearly showed the asymmetrical positioning of the obstruction. This experiment also reinforced the proof that the measurement density was adequate as for two completely different velocity profiles (with and without obstruction) almost no difference was found in the airflow rate (5m and 5m*: $E_q = 2.2\%$). The translocation of the frame (TF in Fig. 2-1) from the outlet to 3m behind the fan increased the UF up to 22% for airflow rate 1. The largest relative measurement error was -2.3%. This indicates that airflow unsteadiness did not affect the 2DS method considerably under these conditions.

Table 2-3: Influence of airflow unsteadiness (UF) on the measurement of two imposed airflow rates. The UF was influenced by changing the duct length from 5 to 8m; by placing the side wall frame between duct parts (see Fig. 2-1, location marked with TF); by placing an obstruction (10L bucket) inside the duct (5m*). The reference set-up was the 5m duct without obstruction.

Imposed airflow rate	1: 1330m ³ /h		2: 2690m ³ /h	
Duct length	UF (%)	E_q (%)	UF (%)	E_q (%)
5m	11	reference	11	reference
6m	6	-2,3	10	-1,1
7m	7	-2,3	8	-1,1
8m	4	-1,1	4	0
5m*	33	+2,2	/	/
TF	22	+1.9	/	/

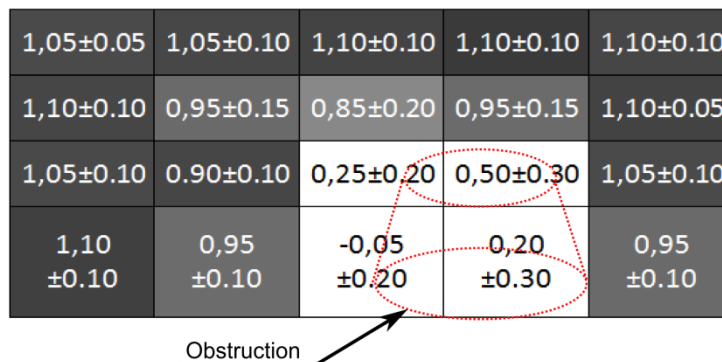


Fig. 2-11: Influence on the velocity profile of an obstruction placed 0.5m upstream of the outlet. The obstruction, a 10L bucket is drawn in red. In each elementary surface the average and SD of the measured velocities are shown (m/s). The greyscale is linked to the velocities and shows the lee in the profile caused by the obstruction.

2.3.4. Effect of airflow rate

Table 2-4 shows the measured values of the airflow rate for each side wall frame experiment as provided by the VDI2041, the 2DS method and the free running impeller, respectively. The relative measurement error of the 2DS method did not change much for different airflow rates and ranged from +4.0% to +6.9% while the relative measurement error of the free running impeller ranged from -12.1% to -5.2%. It should be taken into account that only one impeller of Ø35cm and Ø56cm was tested and that these results might not be representative of other impellers. Nevertheless, this gives an indication

that the use of an uncalibrated off-the-shelf impeller in emission rate experiments or for comparison with tracer gas experiments is not without risk (Heber, Ni et al. 2001; Hinz and Linke, 1998). It should be considered, however, that for the practical use as an airflow rate controller in mechanically ventilated animal houses the accuracy is sufficient.

Table 2-4 : Eight airflow rates measured simultaneously by three methods, i.e. VDI2041 as the reference (Q_{vdi}); 2DS method (Q_{2DS}) and free running impeller (Q_{imp}). The relative measurement errors E_{2DS} and E_{imp} , are given for the 2DS method and free running impeller, respectively.

	Q_{vdi} (SD) (m ³ /h)	Impeller	Q_{2DS} (SD) (m ³ /h)	E_{2DS} (%)	Q_{imp} (SD) (m ³ /h)	E_{imp} (%)
1	1040 (10)	Ø35	1105 (35)	+6.3	915 (25)	-12,1
2	1500 (15)	Ø35	1570 (45)	+4.6	1330 (25)	-10,8
3	1750 (20)	Ø56	1835 (25)	+4.9	1550 (75)	-11,3
4	2705 (45)	Ø56	2835 (35)	+4.8	2475 (75)	-8,0
5	3645 (15)	Ø56	3840 (45)	+5.3	3405 (75)	-6,4
6	4610 (/)	Ø56	4825 (50)	+4.6	4255 (75)	-7,4
7	5464 (/)	Ø56	5725 (65)	+4.7	5110 (75)	-6,6
8	6215 (/)	Ø56	6550 (60)	+5.4	5880 (75)	-5,2

Fig. 2-12 shows the velocity values obtained in the 20 measuring areas for airflow rates 3 to 8 in Table 2-4. During these tests the installation remained unchanged (Ø56 set-up) except for the airflow rates. Therefore the increasing velocity gradient at the walls was completely attributable to the augmentation of the airflow rate. However, this had a limited effect on the relative measurement error.

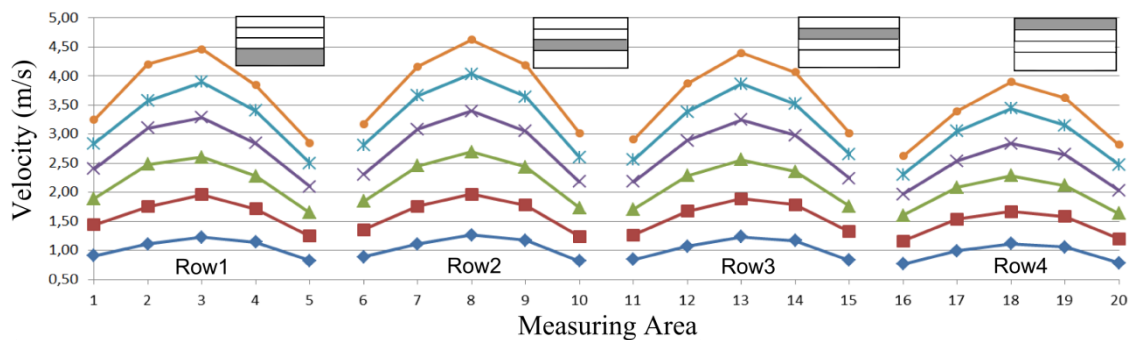


Fig. 2-12: Velocity measurements obtained by the 2DS method in the side wall frame: ◆ 1750m³/h, ■ 2750m³/h, ▲ 3645m³/h, × 4610m³/h, ★ 5464m³/h, ● 6215m³/h. The average standard deviation did not surpass 0.2m/s. The rectangle represents the traverse plane and the grey rectangles the row within the traverse plane on which the measurements are taken. The measurement areas can be found in Fig.2-4D.

The two airflow rates measured in the ridge frame (Table 2-5) showed a comparable relative measurement error as the side wall frame. Fig. 2-13 shows a relatively constant velocity over the length of the opening. The variation in velocity between the measurement areas was less than 0.05m/s. In the ridge frame the ratio between the circumference of the opening and its surface area was greater than in the side wall frame (15.3m⁻¹ vs. 6 m⁻¹). Hence a larger edge effect was to be expected. However, the relative measurement errors were still within the desired range.

Table 2-5: Two airflow rates measured by 2 methods simultaneously: VDI2041 as a reference and the 2DS method. With E_q the relative measurement error. The 2DS method was applied to the ridge frame.

	VDI2041 (SD) (m ³ /h)	2DS (SD) (m ³ /h)	E_q (%)
1	1445 (5)	1525 (10)	+5.3
2	2596 (/)	2770 (10)	+6.6

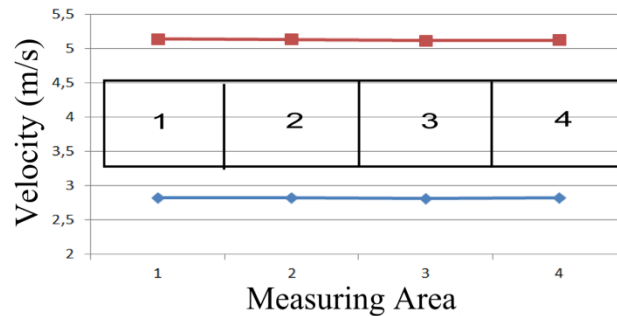


Fig. 2-13: Velocity measurements obtained by the 2DS method with two imposed airflow rates: \blacklozenge 1525m³/h, \blacksquare 2770m³/h. The average standard deviation did not surpass 0.04m/s. The measurement areas can be found in Fig. 2-5.

2.3.5. Side wall effects

In the experiments carried out with the VDI2041 as the reference, an overestimation of approximately 5% was found when using the 2DS method. The experiments in 2.3.2 show that a higher measuring density did not lower the measured airflow rate. However, the measuring grid was only considerably finer in the horizontal direction. This suggested that the origin of the overestimation could be mainly attributable to edge effects in the vertical direction. Indeed, the 2DS measurements showed a 1.6% and 4.8% higher airflow rate than the hotwire measurements for the horizontal (Fig. 2-15) and vertical (Fig. 2-14) traverse movement, respectively. This relatively higher difference for the vertical traverse strengthens the hypothesis that the relative measurement error of the total airflow rate was mostly due to unaccounted edge effects close to the top and bottom edge. Fig. 2-14 shows that the vertical “point” measurement of the 2DS in area 3 (Fig. 2-4:D) was less representative of its related sub-area. Fig. 2-15 shows that the average taken by the 2DS over its measuring paths can replace a much denser horizontal point velocity measurement. Overall, it could be concluded that a more detailed vertical traverse was needed to obtain the most accurate flow rate estimation. However, the extra obtained accuracy would entail a much higher execution time as more areas will have to be measured. This is unfavourable for later use in naturally ventilated vents as a more time consuming method will have a larger influence of the time-dependency of the velocity profile. The 20 points traverse was withheld. This experiment could not deliver conclusive proof for the influence of the vertical and horizontal traverse densities as the influence of the different sensor geometries could not be taken into account.

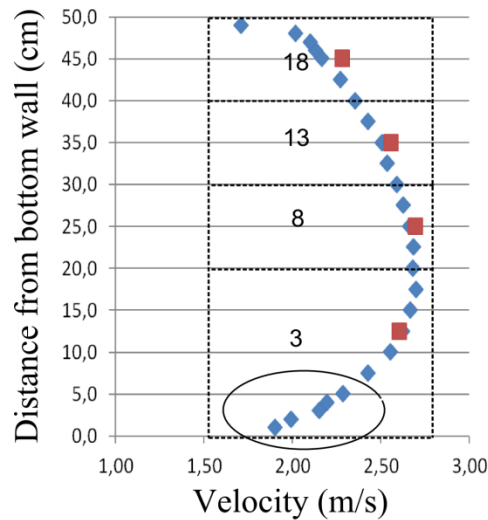


Fig. 2-14: Comparison between 2 vertical traverses in the side wall frame with different measuring densities: \blacklozenge represents measurements by the hotwire anemometer and \blacksquare measurements by the 2DS. The location of the measurement areas 3, 8, 13, 18 can be found in Fig. 2-4:D.

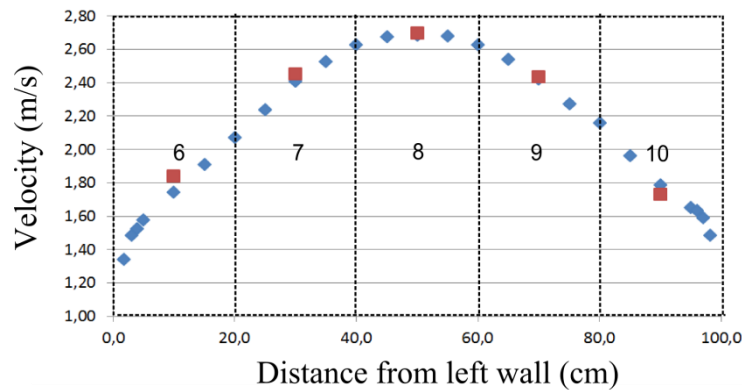


Fig. 2-15: Comparison between 2 horizontal traverses with different measuring densities: \blacklozenge represents measurements by the hotwire anemometer and \blacksquare measurements by the 2DS. The location of the measurement areas 6 to 10 can be found in Fig. 2-4:D.

2.4. Conclusions

The 2DS method accurately measured mechanically induced airflow rates in a range of 1040m³/h to 6215m³/h through a rectangular opening of 0.5m x 1.0m at the end of a 5.0m long duct. The relative measurement error remained under the self-imposed limit of 10% (max.: 6.3%). Possibly, a lower error can be obtained through additional air velocity measurements near the top and bottom wall of the opening. As the results were already below the 10% relative error limit, no additional measurements were deemed necessary at this point.

Tests under varying conditions of airflow unsteadiness (UF ranging from 4% to 33%) resulted in a maximum change in airflow rate of -2.3%. This indicates that variations in UF did not have a large impact on the 2DS method. Deliberately disturbing the velocity profile gave rise to an increase of the measured airflow by 2.2% as compared to the undisturbed flow. Experiments show that the 2D

ultrasonic sensor is applicable in the vicinity of walls without causing false measurements due to an echoing effect.

Tests performed on free running impellers with Ø35cm and Ø56cm showed that, for lower airflow rates (1040m³/h to 1750m³/h), relative measurement errors of up to -12% are possible. These errors were found to decrease with higher airflow rates. This indicates that the use of an uncalibrated off-the-shelf impeller is not without risk in emission rate experiments or for the validation of tracer gas experiments, especially at low airflow rates.

Chapter 3. Experiments under conditions of mechanical ventilation: Automated 3D approach*

*Adapted from: Van Overbeke, P., De Vogeleer, G., Pieters, J.G., Demeyer, P., 2014a. Development of a reference method for airflow rate measurements through rectangular vents towards application in naturally ventilated animal houses: Part 2: Automated 3D approach. *Comput. Electron. Agric.* 106, 20–30. doi:10.1016/j.compag.2014.05.004

3.1. Introduction

In Chapter 2 it was stated that the main challenges in measuring velocity profiles in a naturally ventilated vent are: (1) to cope with the large variety in velocity distributions and (2) to deal with the continuous and the temporal variability of these profiles. The first challenge (1) was partly addressed in Chapter 2 by imposing different steady state velocity profiles to a mechanically ventilated laboratory set-up with 2D anemometers. Chapter 3 further addresses the first challenge (1) concerning the variety in velocity distributions. The aim of this chapter was to further develop and adapt the airflow rate measurement method under conditions which are more representative of naturally ventilated openings with regard to vent size (i.e. larger vents), velocity profile (i.e. heterogeneous velocity distributions) and sensor position (i.e. measurements behind a vent instead of in the vent).

3.2. Materials and Methods

The test set-up built in Chapter 2 was adapted (Fig. 3-1) to perform experiments under conditions which are more representative of naturally ventilated animal houses, and this with regard to (1) vent size, (2) velocity profile and (3) sensor position. To further develop the method on a more representative vent scale (1), also a 3.0m wide tunnel was constructed next to the 1.0m wide tunnel (section 3.2.1.1). For practical reasons no tunnel wider than 3.0m could be built. The velocity profiles can have many shapes in a naturally ventilated opening (2) and are rarely completely unidirectional such as the profiles found in ventilation ducts. Therefore, some airflow obstructions were built (section 3.2.1.1) which could be placed inside the tunnels during the experiments. Size and location of the obstructions were rather arbitrarily chosen and had no other purpose than to change the velocity profile to a less unidirectional pattern.

To allow for continuous measurements with a high measurement density, and to limit manual labour and operator influence, the traverse sensor movement and data logging were fully automated. For this purpose an automated sensor frame was built (section 3.2.1.2). The used 2D and 3D sensors are described in section 3.2.1.3. Concerning the sensor position (3), it is impractical and almost infeasible to perform measurements within the actual ventilation openings without altering the vents. Therefore, measuring inside the duct was no longer an option. The best alternative was to measure as closely as possible to the in- or outlet of the vent. Consequently, the anemometers were placed directly behind the outlet of the ducts with the automated sensor frame as a support structure. At this position, however, the air can fan out giving the airflow a more pronounced 3D character. Therefore, the 2DS method developed in Chapter 2 was accordingly adapted (section 3.2.2) and also more advanced 3DS methods were developed (section 3.2.3).

As in Chapter 2, the standard VDI2041 (2001) was used as the reference to assess the accuracy of the examined airflow rate methods. The airflow rate was calculated following equations [2-1] to [2-3] in

Chapter 2. To evaluate the experiments, the relative measurement error (E) in % was used (Van Buggenhout et al., 2009) [3.1].

$$E_q = \frac{Q_{measured} - Q_{reference}}{Q_{reference}} 100 \quad [3.1]$$

Considering the practical applications in naturally ventilated animal houses, a maximum relative measurement error of 10% was regarded as acceptable. The standard deviations (SD) found in tables 3-1, 3-3 and 3-4 are a measure for the stability of the airflow during one complete traverse and do not represent the variability of the method.

3.2.1. Overall experimental set-up

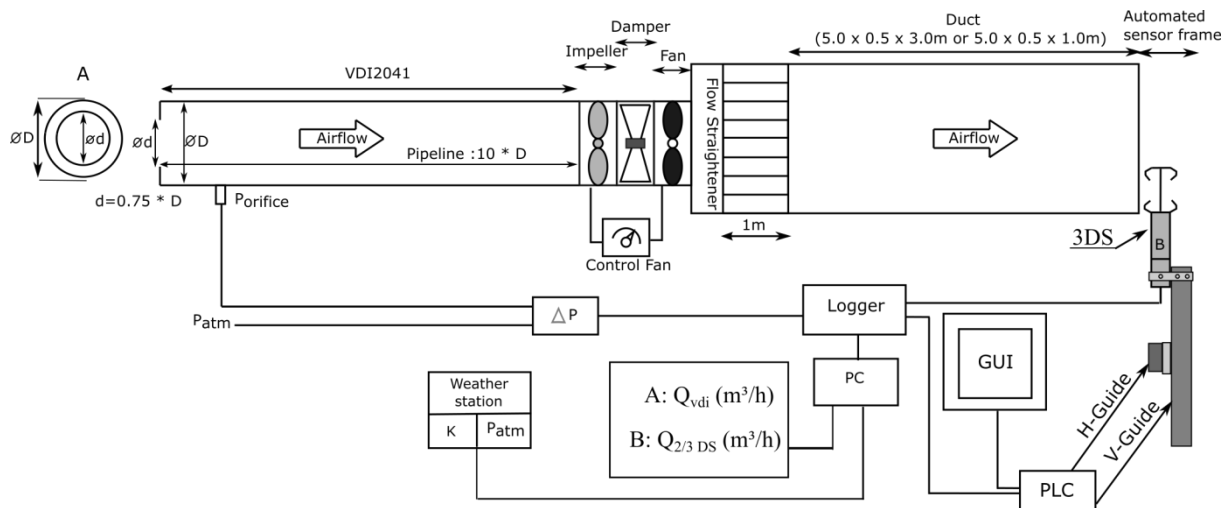


Fig. 3-1: Overall set-up with two simultaneous airflow rate measurement systems: A) differential pressure over an orifice according to the VDI2041 (Q_{vdi}) and B) the developed method with a 2D or 3D ultrasonic sensor (Q_{2DS} / Q_{3DS}). With $\varnothing d$ and $\varnothing D$ the inner and outer diameters of the orifice (m), respectively. With $P_{orifice}$, P_{atm} and ΔP the static pressure downstream of the orifice, the atmospheric pressure and the differential pressure between the previous, respectively (Pa). A weather station measured the temperature (K) and P_{atm} . An automatic sensorframe with a vertical (V-guide) and horizontal (H-guide) guidance, automatically moves the sensor across the vent opening. The frame is controlled with a graphical user interface (GUI) connected to a programmable logic control (PLC).

3.2.1.1. Wind tunnels

In addition to the 5.0m long tunnel with a 0.5m x 1.0m outlet opening (built in Chapter 2), a tunnel with a length of 5.0m and an outlet opening of 0.5m x 3.0m was constructed. The horizontal walls were made of smooth plywood and the vertical walls of polymethyl methacrylate.

In the 1.0m wide tunnel a flow straightener made of plywood was placed inside the tunnel in order to diminish the influence of the airflow swirl caused by the axial fan. It was positioned 0.3m behind the outlet of the fan and had a length of 1m with a mesh size of 0.05m x 0.05m. When the 3.0m wide tunnel was used, the part of the 1m wide tunnel with the flow straightener was placed at the centre of the inlet of the 3.0m wide tunnel (see Fig. 3-2). The two 1.0m wide openings at both sides of the flow straightener were sealed with triplex. The airtightness of the combination of the 3.0m wide tunnel,

flow straightener and VDI2041(2001) pipeline ($\varnothing 0.56\text{m}$ set-up, see Chapter 2) were tested by pressurising the installation and visualizing the air leakages through smoke tests.

To prove that the measuring method was able to deliver accurate results even when the velocity profiles have a more heterogeneous pattern, obstructions were placed inside the tunnels. The sole purpose of these obstructions was to cause abrupt changes the geometry of the velocity profile. For the 1.0m wide tunnel, a ramp was built to guide the airflow upward (Fig. 3-3:A: obstruction set-up 1). For the 3.0m wide duct, 3 small obstacles were placed together inside the duct at 0.50m upstream of the outlet. The locations of these obstacles were varied (see Fig. 3-3:B) to obtain three different obstruction set-ups and, therefore, three different profile shapes (obstructions 2,3 and 4).

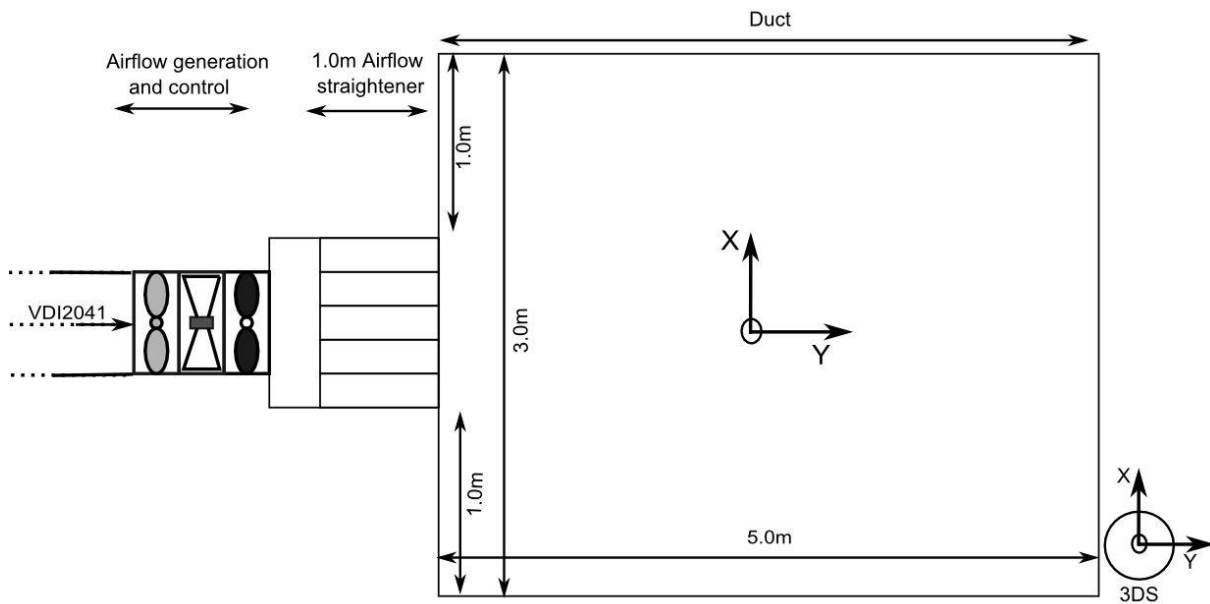


Fig. 3-2: Top view of the test installation with the 3.0m wide tunnel.

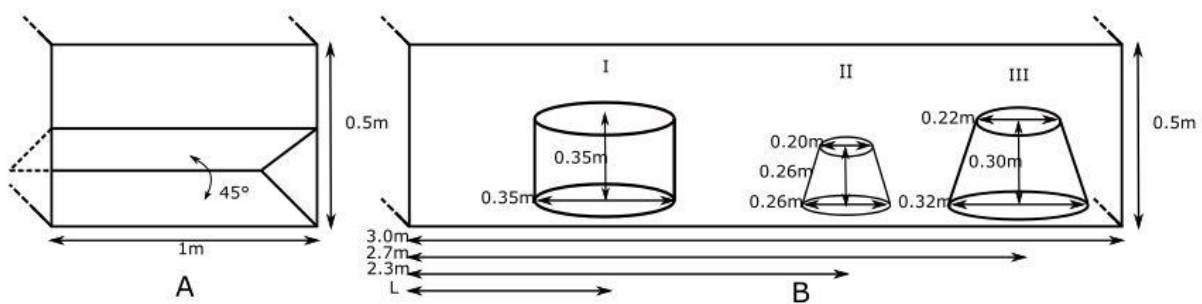


Fig. 3-3: **A:** Outlet of the 1.0m wide tunnel with obstruction set-up 1: upward guidance; **B:** Outlet of the 3.0m wide tunnel with the obstruction set-up composed of 3 buckets (I, II and III). Bucket I was moved to three different locations (L) to obtain three obstruction set-ups. For obstruction set-up 2 bucket I was located at $L = 1.8\text{m}$, for obstruction set-up 3: $L = 1.4\text{m}$ and for obstruction set-up 4: $L = 0.4\text{m}$. The sole purpose of these obstructions was to change the shape of the velocity profile.

3.2.1.2. Automated sensor frame and integrated data logging

The automated sensor frame consisted of a connected horizontal (4.5m, H-guide) and vertical (0.7m, V-guide) linear guidance system located at the outlet of the duct (see Fig. 3-4) . This allowed to scan an area of 4.5m x 0.7m by a sensor rigidly fixed with a sensor mount to the top of the V-guide. The sensor mount brought the sensors as close as possible to the outlet of the opening. A linear speed of up to 2m/s was obtainable. Therefore every location in the scan area could be reached in less than 3 seconds. The movement of the sensor was driven by 2 electro motors controlled by a Siemens Step 7® PLC program. The desired measuring locations could be reached within 1mm. It was possible to create different recipes within the PLC program, each containing a set of coordinates of the respective measuring points. A signal to the connected data logger (Datataker® DT85M) was given by the PLC when the sensor reached a pre-set coordinate, giving the authorization to start logging. After a predetermined and adjustable time the logging stopped and a signal was automatically given to move the sensor to the next coordinate after which the logging restarted. Therefore, no measurements were made during the movement of the sensor. The movement itself had a ramp up and ramp down to diminish the vibration of the sensor. It was assumed that due to these precautions no false measurements would be made attributable to residual sensor vibration or sensor movement. The control of the measurement variables (measuring time, number of measuring points, starting point) and sensor movement (choice of the recipe, start, stop) took place by means of a graphical user interface on a touchscreen. To simulate the effect of the building structure of a naturally ventilated animal house, a wall was placed in front of the tunnel. The opening in this wall was adaptable in order to have the same dimensions as these of the tunnel. The automated sensor frame was then fixed to this wall as would be the case in a barn. The wall mounts ensured a good alignment with respect to the opening.

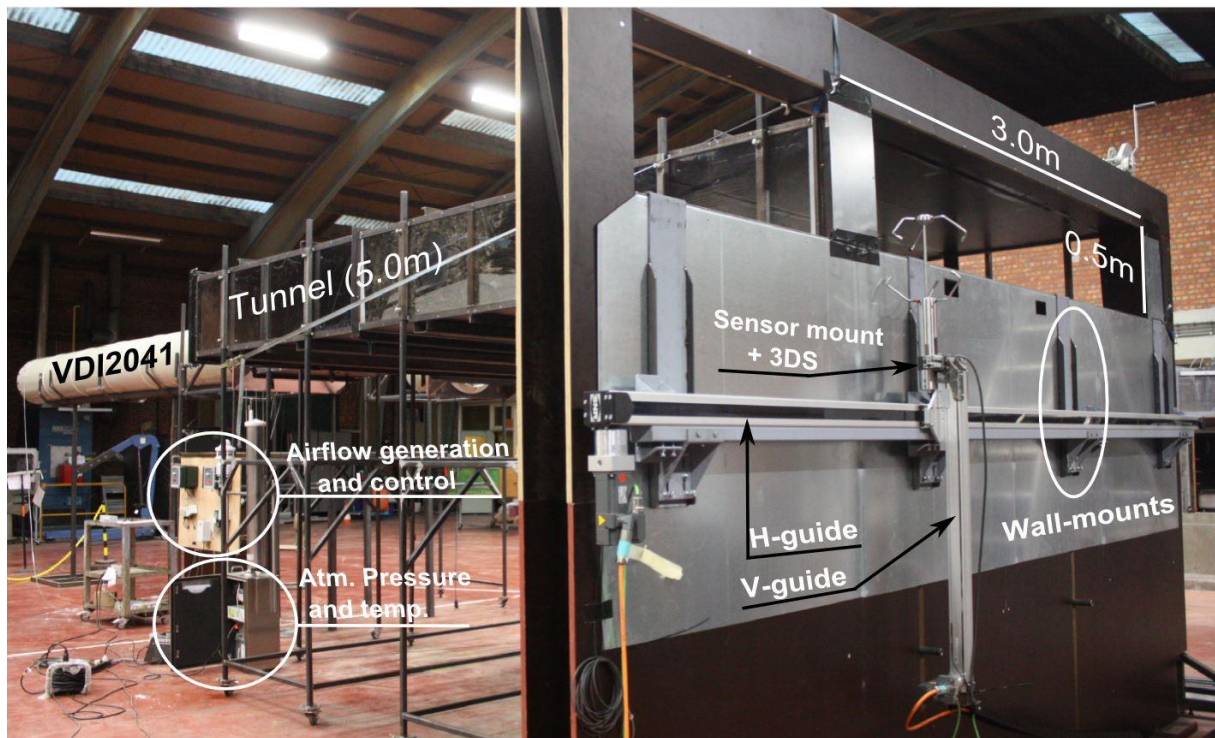


Fig. 3-4: Automated sensor frame on wall prepared for measurements in the 3m wide tunnel. For a schematic overview see Fig. 3-1.

3.2.1.3. *Sensors*

The 1D air velocity measurements were performed with a hotwire anemometer (TSI® air velocity transducer model 8455). This type of anemometer has a protective cap surrounding the fragile sensor wire. This cap is a blockage for air velocity components from other directions than those normal to the opening in the protective cap and the sensor is therefore referred to as the 1D hotwire. However, a small range of incidence angles other than normal could also have an influence on the signal (personal communication supplier TSI). Although the hotwire cannot be regarded as a true 1D sensor, it was assumed that the velocity reading was mainly attributable to the normal component. According to the manual the 1D hotwire has an accuracy of $\pm 2.0\%$ of the reading or $\pm 0.5\%$ of full scale of selected range. The selected range was 0.0 - 5.0m/s. The 2D air velocity measurements were made with a 2D ultrasonic anemometer or 2DS (Thies® 4.3820.02.300) (for more detailed information see Chapter 2). The 3D air velocity measurements were made with a Thies® 3D ultrasonic anemometer or 3DS (Thies® 4.3830.22.300). According to the manual the 3DS has a wind speed accuracy of ± 0.1 m/s below 5m/s and $\pm 2\%$ of the measured value above 5m/s (RMS-average over 360°). An additional calibration conducted by Deutsche WindGuard Wind Tunnel Services GmbH (calibration mark 22997; D-K-15140-01-00; 10/2011) showed a standard uncertainty of max. 0.05m/s in a range of 0.557m/s to 5.470m/s. The sensor is able to detect the direction of the airflow with an accuracy of $\pm 1^\circ$.

All movements of the sensors were made with the automated sensor frame. Once the sensor was installed on the frame it was not removed until the end of an experimental series. The atmospheric pressure and temperature needed for the calculation of the density of the air in Q_{vdi} (see Fig. 3-1 and

equations [2-2] and [2-3]) were checked once after every experiment on a weather station next to the installation as these parameters were not expected to vary considerably during the short measurements. All other measurements were taken at 1Hz and logged with the Datataker® DT85M.

3.2.2. Adapted 2DS method

The traverse plane is located 0.10m downstream of the outlet (see Fig. 3-5, TP2). TP1 indicates the traverse plane inside the duct as used in Chapter 2. TP2 coincides with the intersection of the 2DS's measuring paths when the sensor is placed on the automated sensor frame's V-guide. To be able to make a direct comparison with the tests carried out in Chapter 2, a similar test set-up was chosen with identical measuring areas (Fig. 3-6, areas 1 to 20). All areas were measured for 2 minutes (De Paepe et al., 2013). Every vector component normal to the traverse plane ($v_{i\perp}$) was multiplied by its respective area A_i (m^2) after which the individual airflow rates were summed ($n=20$) [3.2]. In every area the SD of the $V_{i\perp}$ was calculated (V_{isd}). The combined standard deviation from one complete traverse was calculated according to equation [3.3].

$$Q_{2DS}(m^3/h) = \sum_{i=1}^n (V_{i\perp} A_i 3600) \quad [3.2]$$

$$SD Q_{2DS}(m^3/h) = \sqrt{\sum_{i=1}^n (V_{isd} A_i 3600)^2} \quad [3.3]$$

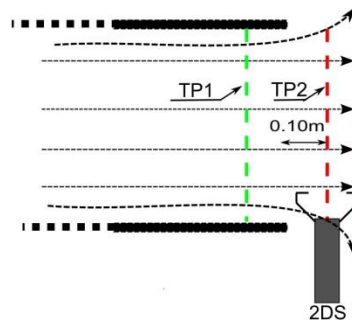


Fig. 3-5: The repositioning of the traverse plane from the position indicated by TP1 to the position indicated by TP2.

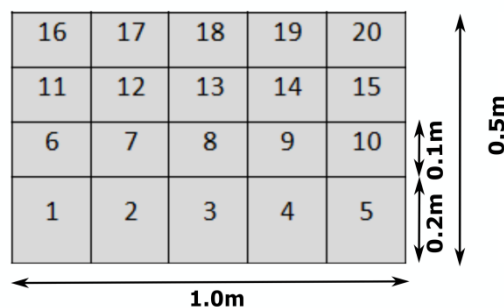


Fig. 3-6: Subdivision of the traverse plane into areas 1 to 20, for the adapted 2DS method. To allow comparison with the measurements in Chapter 2 the areas 1 to 5 are larger to obtain an identical subdivision of the traverse plane as in Chapter 2.

3.2.3. Developed 3DS methods

Different calculation techniques were developed based on the measurements by a 3D ultrasonic anemometer (3DS). An ultrasonic anemometer does not measure point velocities but the average velocity over each of its measuring paths (Komiya and Teerawatanachai, 1993). The 3DS has three of these paths and these are electronically transposed by the sensor's software into an orthogonal coordinate system identical to the coordinate system of the tunnel (see Fig. 3-2). The 6 transducers of the 3DS fit inside a cuboid of 0.25m x 0.25m x 0.125m (see Fig. 3-7). This cuboid will be referred to as the measuring volume and was the building block of the traverse based measurements of the developed methods. The X-, Y-, and Z- components provided by the sensor were considered to be representative of the average velocities through the side planes, the front plane, and the top and bottom plane of the measuring volume, respectively. The representativeness of this measuring volume was examined in 3.2.3.1.

Two airflow rate methods were developed to cope with the 3D character of the velocity profile: the Basic and Extended method (section 3.2.3.2 and 3.2.3.3). Each method provided in different relations between the velocity vectors and their corresponding measuring volume. A third method only took into account the Y-components of the Basic method (Y- method). This allowed to evaluate the influence of the other velocity components (X and Z) by comparison with the Basic and Extended method. All measurements with the 3DS were taken at 1Hz during 60s per measuring volume.

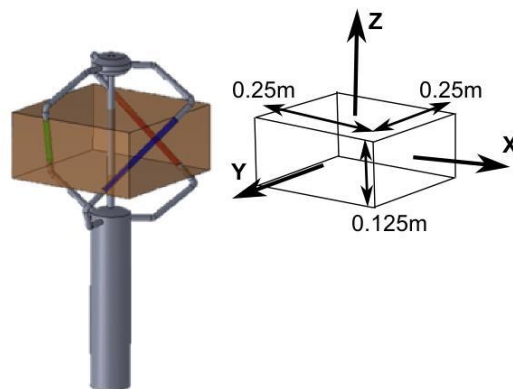


Fig. 3-7: 3D ultrasonic sensor with measuring paths coloured green, blue and red. The 6 transducers of the 3DS fit inside a cuboid (brown cuboid) which is referred to as the measuring volume. The velocity components (X, Y and Z) obtained with the 3DS are associated with the areas of the measuring volume to which they are perpendicular.

3.2.3.1. *Validity of the measuring volume approach*

The measuring volume approach was based on the assumption that the X, Y, Z velocity components as measured by the 3DS, were representative of the actual flows through the respective planes of the measuring volume. Since the airflow will mainly pass through the front plane of the measuring volume (Y-component) in the conducted experiments, this assumption was verified for the front plane through comparison with a 1D hotwire anemometer.

Both the 3DS and the 1D Hotwire were mounted on the V-guide of the automated sensor frame. A measuring volume was chosen at 2.37m from the left wall and 0.31m from the bottom wall of the 3m wide tunnel. The hotwire was positioned in such a way that it could traverse an area of 0.25m x 0.125m inside and 0.13m upstream of the front plane of that measuring volume (see Fig. 3-8). This area was divided into 20 equal sub-areas of 0.03 x 0.05m. An automated sensor frame motion recipe was written to alternately move the 3DS and the hotwire to specific measuring locations. One cycle consisted of the 3DS measuring the measuring volume for 60s followed by the hotwire measuring one of the 20 equal sub-areas inside that measuring volume for 60s. The 3DS returned every cycle to the same measuring volume, whereas the hotwire moved to the next sub-area. After 20 cycles, the measuring volume was measured 20 times for 60s by the 3DS, while the hotwire finished 1 traverse of the area composed of 20 sub-areas inside that measuring volume. This alternating movement was imposed to counter possible changes in the airflow during the experiment. Two airflow rate levels were imposed (approximately 4600 and 6000 m³/h, Table 3-2). A deviation of maximum 10% between the two methods was deemed acceptable. The SD's of the 3DS vector components were based on the 20 one minute averages made by the 3DS. These SD's represented the stability of the flow during the experiment. The SD's of the hotwire measurement represented the combined standard deviation of all 20 sub-areas measured by the hotwire.

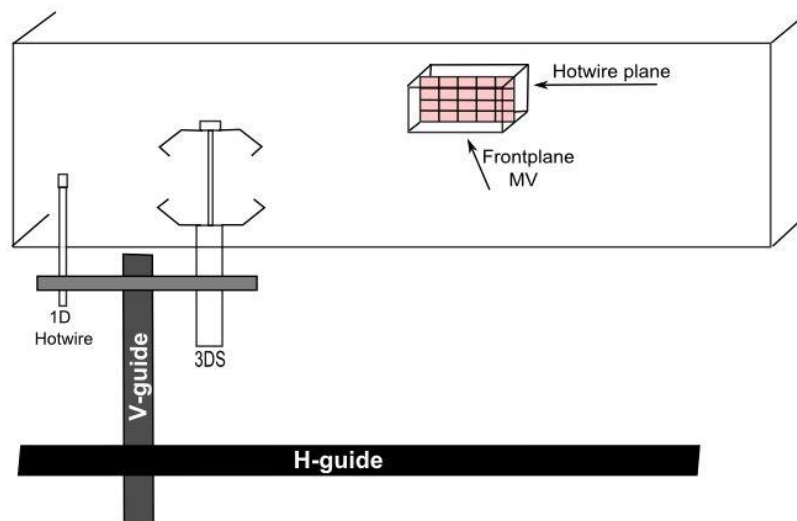


Fig. 3-8: Test set-up to alternately scan a measuring volume (MV) with a 3DS and a plane within that measuring volume with a 1D hotwire anemometer. The plane measured with the hotwire is divided into 20 elementary surfaces. These are consecutively sampled with the hotwire whilst alternating with the measurement of the MV with the 3DS.

3.2.3.2. 3DS Basic method

When the traverse plane is located inside the duct, evidently all air has to flow through that plane (Fig. 3-9 A). Therefore measuring the velocity component normal to the traverse plane multiplied by the area of that plane will deliver the total airflow rate. However, as the sensor is now located outside the

duct, also the traverse plane moves to this location. Behind the outlet of the duct the flow can fan out freely and only the forward oriented flows, i.e. parallel to the length axis of the duct, will flow through the traverse plane (Fig. 3-9 B). To measure the up-, down- and sideward oriented flows, traverse planes normal to these orientations are added to the original traverse plane. These planes virtually fill up the gap between the duct and the original traverse plane (Fig. 3-9 C). All air leaving the duct now has to flow through the combination of these different oriented traverse planes, i.e. the Combined Traverse Plane or CTP. The velocity Y- component was measured on the front plane, the X- component on the left and right side planes and the Z- component on the top and bottom planes (Fig. 3-9 D). The 3DS cannot measure the complete CTP at once. Therefore, the volume created by the CTP was subdivided into smaller volumes equal to the size of the 3DS's measuring volumes (Fig. 3-9 E). By doing so, the traverse planes themselves were subdivided into smaller elementary surfaces. In total, the CTP consisted of 32 or 80 elementary surfaces for the 1.0m or 3.0m wide tunnel, respectively. By traversing the CTP with the 3DS, the velocity components normal to all elementary surfaces were measured. The total airflow rate was calculated following equation [3.2]. The airflow rates that originate from inside the CTP and travel outward are referred to as positive airflow rates and are added to the total airflow rate. Airflow rates caused by returning flows originate from outside the duct and flow into the CTP. Therefore, these flows are considered as negative airflow rates and are subtracted from the total airflow rate. Such returning flows could be induced by nearby obstructions deflecting the airflow (Fig. 3-9 F). Each location within the CTP was measured for 1 minute after which the sensor was moved to the next location. This method is further referred to as the Basic method.

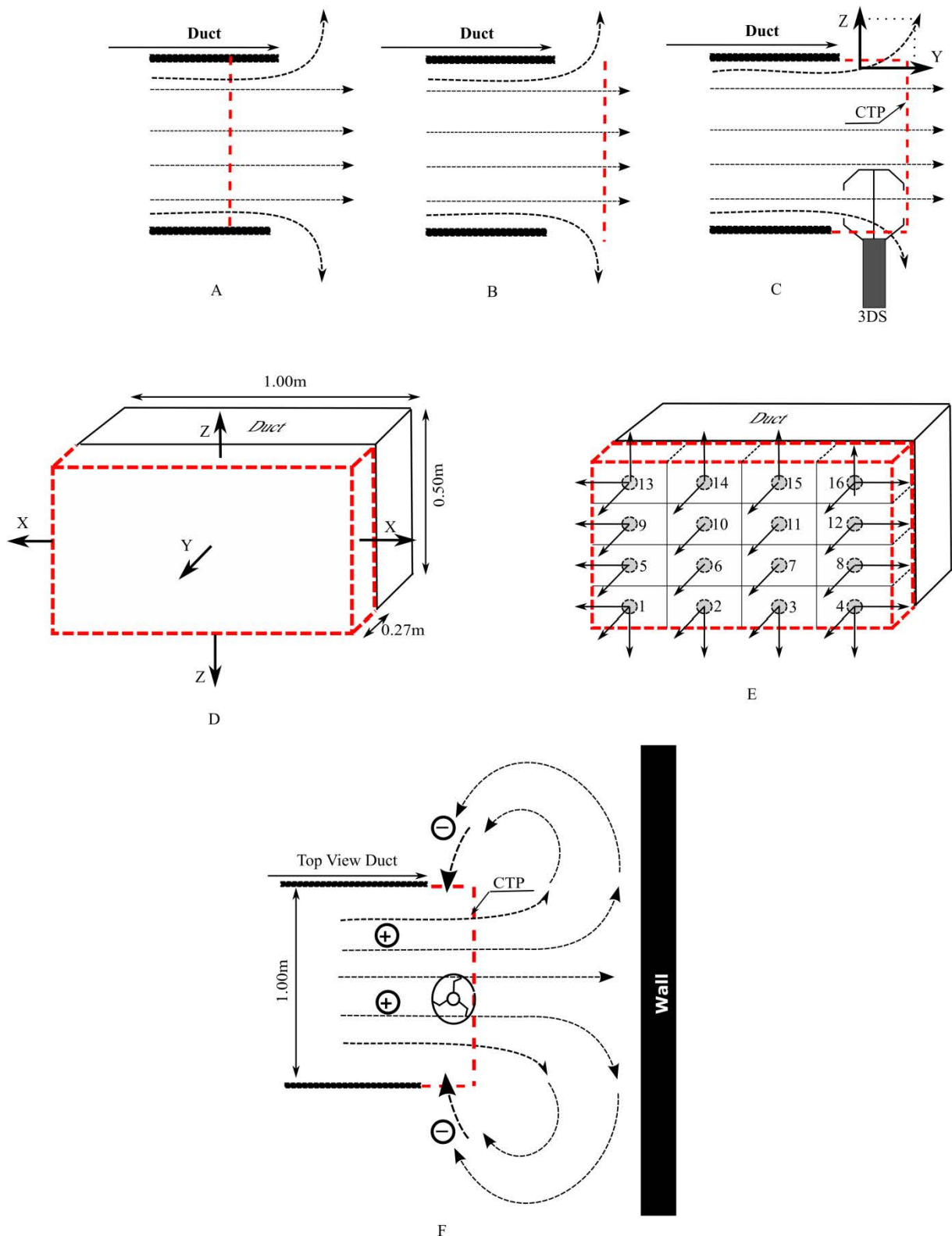


Fig. 3-9: The dashed red lines represent the traverse planes. **A:** Side view of the duct. When the traverse plane is located inside the duct all flow passes through that plane. **B:** When traverse plane is located outside the duct not all flow passes through that plane as it can escape undetected to the sides. **C:** Additional traverse planes to virtually envelop the flow. **D:** The combined traverse plane (CTP) through which all air has to flow. Differently oriented flows are measured at their associated traverse planes. **E:** Virtual volume created by the CTP is subdivided into 16 measuring volumes, which in their turn subdivide the traverse planes into 32 elementary surfaces. **F:** Top view of the duct. Possible returning flows due to obstructions. Returning flows are considered negative flows.

3.2.3.3. 3DS Extended method

In the Basic method a positive flow rate, originating from inside the CTP, first passes through a measuring volume before it travels through the virtual boundary set by the CTP. Returning flows, on the other hand, first pass through the CTP and then through the measuring volumes inside the CTP (Fig. 3-9 F). A new method is suggested to examine whether a different treatment of flows depending on their origin would influence the measurement result. In this method, further referred to as the Extended method, the outward directed or positive flows will only be accounted for in the measuring volumes located inside the CTP. Additional measuring volumes are added (measuring volumes A to P, Fig. 3-9 G), bordering the CTP, in which only the inward directed or negative flows will be accounted for. Therefore, in contrast to the basic method, every measured flow first has to pass a measuring volume before it passes the CTP and this independent of the flow direction. Due to the 2D movement of the automated sensor frame, it was not possible to add measuring volumes behind the front plane. Hence, these measurements remain the same as in the basic method.

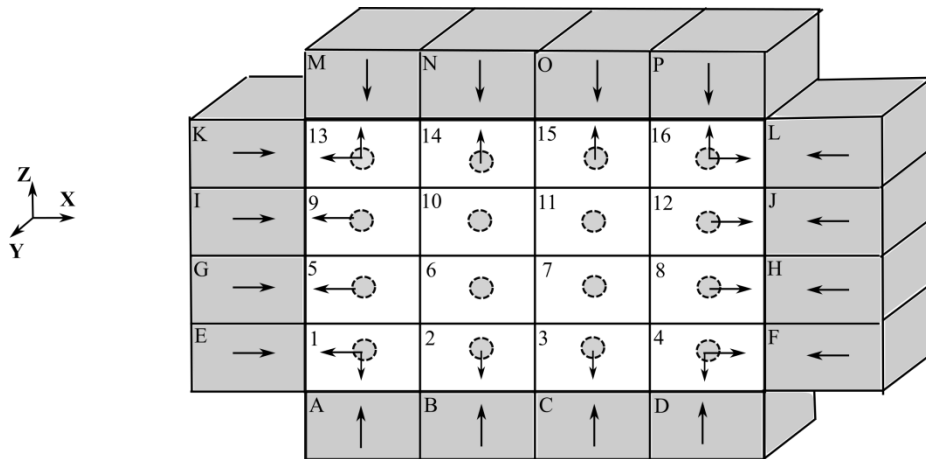


Fig. 3-10: Combined traverse plane of the Extended 3DS method in the 1m wide duct (areas 1 to 16 + areas A to P). Outward oriented flows (from duct to surroundings) are measured in the white measuring volumes (1 to 16) and are considered positive, inward oriented flows (from surroundings to duct) are measured in the grey measuring volumes (A to P) and are considered negative. The arrows represent the X- and Z-flow direction that will be measured in a measuring volume. When the direction is opposite the velocity is not accounted for. The grey circles represent the Y-components. These are measured irrespective of their direction.

3.3. Results & Discussion

3.3.1. Applicability of the adapted 2DS method

Table 3-1 gives the relative measurement error of the adapted 2DS method under different airflow rates and obstructions. These results show that the method delivered satisfactory results when there was no obstruction in the airflow (free flow). These results were similar to the measurements carried out inside the tunnel in Chapter 2, where the relative measurement errors were 4.8% and 5.3% for airflow rates of 2705m³/h and 3645m³/h. The 3D character of the outflowing air did not show a clear influence on the accuracy. This can be explained by the predominant Y-components which occurred in

the airflow jet 0.10m behind the outlet (see Fig. 3-11, left). Measuring the X- and Z- component would not have contributed to a meaningfully higher accuracy as the relative measurement errors are already well below the 10% limit. However, when obstruction set-up 1 forced the airflow away from its mostly perpendicular and thus unidirectional path, the relative measurement error increased up to -18.5%. This demonstrated that measuring only the Y-component (see Fig. 3-11, right) can cause a large underestimation of the airflow rate in disturbed airflows. It was evident that in this case the Z-component was necessary for an accurate measurement.

It should be noted that a 2DS gathers its information from line measurements. For extremely distorted velocity profiles, the chance of having larger velocity gradients throughout the profile increases. Therefore, the location of the line measurement, especially where the velocity profile shows sudden changes, will be of great importance. Consequently, every velocity profile will have its own optimal measuring locations. Even though the experiments with obstruction set-up 1 are an extreme example of a sudden alteration in the velocity profile, it can be expected that in naturally ventilated openings there exist no optimal static sampling locations as the profile changes continuously. This problem can be partly solved by introducing more measuring locations with the 2DS or by measuring with a 3DS. Although a 3DS also takes line measurements, these measurements are assumed representative of a larger area due to the distribution of these lines.

Table 3-1: Relative measurement error E_q (%) of the adapted 2DS method (Q_{2DS}) under different airflow rates and obstruction set-up 1 with VDI2041 (Q_{vdi}) as the airflow rate reference. Duct width is 1m. Measurement (Standard deviation);

Obstruction	Q_{vdi} (m ³ /h)	Q_{2DS} (m ³ /h)	E_q (%)
Free flow	2625 (25)	2760 (55)	+5.2
Free flow	3650 (35)	3780 (90)	+3.6
Free flow	4610 (45)	4785 (85)	+3.8
Obstruction 1	3450 (30)	2870 (50)	-16.8
Obstruction 1	4500 (45)	3665 (90)	-18.5

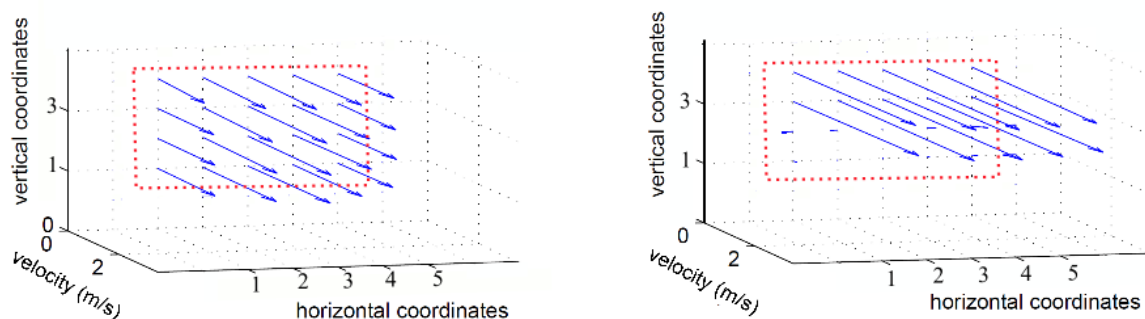


Fig. 3-11: Profile measurements with the adapted 2DS method in the 1m wide duct **Left:** velocity components normal to the traverse plane, free flow, 4610 m³/h; **Right:** velocity components normal to the traverse plane, obstruction set-up 1, 4500m³/h. Dotted line represents the outlet area.

3.3.2. Applicability of the developed 3DS methods

3.3.2.1. Validity tests of the measuring volume approach

Table 3-2 gives the three velocity components measured with the 3DS and the deviation between the Y-component and the hotwire measurement. It can be seen that the deviation between the 1D hotwire measurement and the Y-component of the 3DS remains under the 10% limit. This supports the assumption that the 3DS Y-component is representative of the average velocity on the front plane of the measuring volume. Side, top and bottom planes were not further investigated.

Table 3-2: Validity tests of the measuring volume approach under two imposed airflow rates (Q_{vdi}) (See Fig. 3-8). Measurement (Standard deviation); 3DS ultrasonic velocity components 3DS -X, -Y, -Z; Hotwire as the reference compared with 3DS-Y;

Q_{vdi} (m ³ /h)	3DS-X (m/s)	3DS-Y (m/s)	3DS-Z (m/s)	Hotwire (m/s)	Deviation(%) H and 3DS-Y
4600	0.01 (0.02)	2.21 (0.03)	0.40 (0.01)	2.31 (0.05)	-4.3%
6000	0.01 (0.02)	2.88 (0.03)	0.53 (0.02)	3.05 (0.06)	-5.6%

Although a calibrated 1D hotwire anemometer was used, these tests could not give conclusive proof of the correctness of the assumptions. For example, as the influence of the sensors on the velocity profile was not clear, it was not possible to be certain of the complete similarity of the velocity profiles measured with the hotwire and the 3DS. Also, as mentioned in 3.2.1.3, a small influence of velocity components other than the Y-component could not be ruled out.

3.3.2.2. Wind tunnel tests (1.0m)

Table 3-3 shows the relative measurement error of the Y-, Basic- and Extended method under different airflow rates and obstructions. Without obstructions (free flow), the additional measurements of the X- and Z- velocity components did not have a large influence, as was expected due to the primarily unidirectional perpendicular flow as can be seen in the vector plot in Fig. 3-12 (Left). On average, the Y-method showed a relative measuring error of $-2.5 \pm 1.0\%$ in these free flow experiments. The Y-method resulted in a slight systematic underestimation of the airflow rates, while the 2DS method gave rise to an overestimation. The mean relative measuring error of the Basic method in the free flow experiments was $4.7 \pm 1.4\%$ and showed no advantage compared to the Y-method. The mean relative measuring error of the Extended method was $3.0 \pm 1.5\%$ in the free flow experiments. None of the methods showed a clear dependence on the airflow rate.

When the directionality of the flow was changed by introducing obstruction set-up 1 in the tunnel, measuring only the Y- component proved to be insufficient as the relative measuring error reached the 10% limit. It is clear that in these cases the Y-method underestimated the airflow rate as it was not capable of capturing the upward oriented airflow. A smaller error was found when using either the Basic or Extended method. Overall, the Extended method showed the best results under most imposed

airflow rates and different velocity profiles as also the errors of the obstructed airflow experiments fell within the variation of the error of the free flow experiments. Fig. 3-12 (right) gives the velocity vector plot and clearly shows the influence of the obstruction set-up 1 on the direction of the vectors. Since the three 3DS methods were measured simultaneously, only the SD for the Basic method was given as a measure for the stability of the airflow.

Table 3-3 Relative measurement error E_q (%) of the Y-, basic- and extended method under different airflow rates and obstruction set-up 1. With VDI2041 (Q_{vdi}) as the airflow rate reference; 3DS Y: Y-method; 3DS B: Basic method; 3DS E: Extended method. Duct width is 1m. Measurement (Standard deviation)

Method	Obstruction	Q_{vdi} (m ³ /h)	Q_{3DS} (m ³ /h)	E_q (%)
3DS Y			1660	-3,8
3DS B	Free flow	1725 (10)	1770 (40)	2,6
3DS E			1735	0,6
3DS Y			3410	-1,7
3DS B	Free flow	3470 (30)	3665 (70)	5,6
3DS E			3625	4,5
3DS Y			3385	-3,1
3DS B	Free flow	3495 (30)	3632 (70)	3,9
3DS E			3595	2,9
3DS Y			4475	-2,1
3DS B	Free flow	4570 (55)	4815 (85)	5,4
3DS E			4725	3,4
3DS Y			4500	-1,6
3DS B	Free flow	4575 (40)	4855 (85)	6,1
3DS E			4750	3,8
3DS Y			3160	-9,8
3DS B	Obstruction1	3505 (35)	3765 (45)	7,4
3DS E			3650	4,1
3DS Y			4070	-11,1
3DS B	Obstruction1	4580 (60)	4890 (60)	6,8
3DS E			4680	2,2

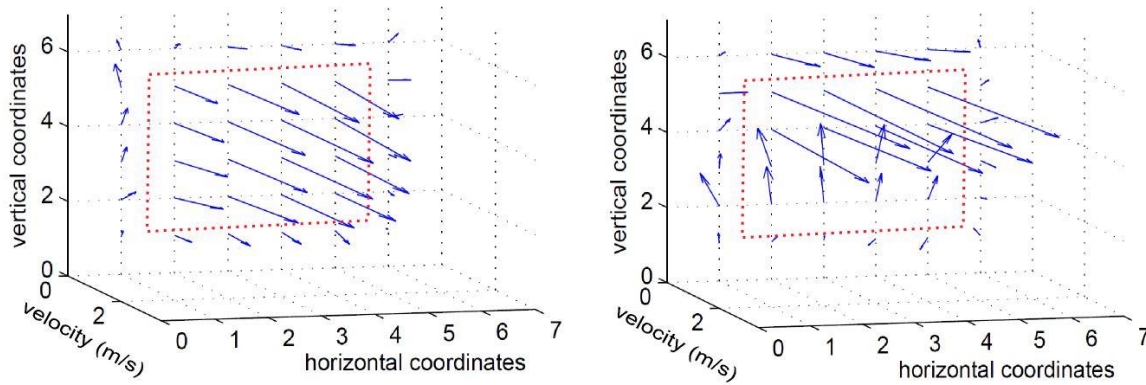


Fig. 3-12: Profile measurements with the 3DS in the 1m wide duct **Left:** 3D vector plot, Free flow, 4575m³/h; **Right:** 3D vector plot, Obstruction1, 4555m³/h. Dotted line represents the outlet area.

3.3.2.3. *Wind tunnel tests (3.0m)*

The width of the tunnels could have a large influence on the edge effects since the edge length vs. outflow area ratio diminished from 6.0m⁻¹ to 4.6m⁻¹ for the 1.0m and the 3.0m wide tunnel respectively. Table 3-4 shows the relative measurement error of the Y-, Basic- and Extended method under different airflow rates and obstructions. Since the three 3DS methods were measured simultaneously, only the SD for the Basic method was given as a measure for the stability of the airflow.

The Y-method showed a systematic overestimation of the airflow rate ($E_q = 12.1 \pm 0.6\%$), averaged over the eight experiments. In general it would be expected that the Y-method delivers an underestimation of the airflow rate as part of the flow can escape undetected in the upward or sideward direction. This was the case for obstruction set-up 1 in the 1m wide tunnel (see 3.3.2.2). However, in the 3m wide tunnel we see the opposite effect as the Y-method resulted in an overestimation. This suggests that there existed returning flows that resulted in flows entering through the side planes and leaving through the front plane. Furthermore these negative flows should be larger than the upward and sideward oriented positive flows. Otherwise the positive and negative flows would compensate one another. To visualise these possible flow patterns two 3D velocity vector plots are given. Fig. 3-13 shows the vector plot from a free flow experiment (5770m³/h, see Table 3-4). Because of a skewed alignment of the fan and the tunnel most of the airflow passed through the right side of the tunnel. In Fig. 3-14 the 3D vector plot for an obstructed flow is given (obstruction set-up 4, 5355m³/h, see Table 3-4). Here it can be seen that the majority of the airflow passed through the left side of the opening. In both cases a returning flow can be seen. For the vector plot in Fig. 3-14 it was found that 341m³/h escaped through the sides of the CTP whilst 1130m³/h entered through the side planes of the CTP. This means that 789m³/h of the flow caused by the returning flows had to exit through the front plane of the CTP. It is clear that this was the cause for the overestimation of the airflow rate by the Y-method. Similar results were found for the remaining experiments.

The mean relative measurement error of the Basic 3D method was $1.3 \pm 2.6\%$. The extended 3D method showed marginally better results with a mean relative measurement error of $-0.6 \pm 2.6\%$. As the relative measurement errors of the Basic and Extended method are so small that they do not have a practical significance, no further investigation was performed to identify the cause of these deviations. The different airflow rates as well as the different obstructions did not seem to influence the relative measurement errors of the three methods. The small relative measurement errors from the Basic and Extended method prove that the methods were capable of detecting and correctly processing the more complex velocity profiles, in contrast to the Y-method.

Table 3-4: Relative measurement error E_q (%) of the Y-, basic- and extended method under different airflow rates and obstructions. With VDI2041 (Q_{vdi}) as the airflow rate reference; 3DS Y: Y-method; 3DS B: Basic method; 3DS E: Extended method. Duct width is 3m. Measurement (Standard deviation)

Method	Obstruction	Q_{vdi} (m ³ /h)	Q_{3DS} (m ³ /h)	E_q (%)
3DS Y			3900	+12.2
3DS B	Free flow	3480 (30)	3535 (200)	+1.6
3DS E			3585	+3.1
3DS Y			4670	+11.6
3DS B	Free flow	4185 (40)	4355 (215)	+4.1
3DS E			4235	+0.8
3DS Y			6485	+12.4
3DS B	Free flow	5770 (55)	5915 (255)	+2.6
3DS E			5905	+2.5
3DS Y			4575	+11.0
3DS B	Obstruction 2	4120 (50)	4255 (210)	+3.3
3DS E			3970	-3.6
3DS Y			5940	+11.8
3DS B	Obstruction 3	5315 (45)	5425 (255)	+2.0
3DS E			5225	-1.8
3DS Y			5095	+13.3
3DS B	Obstruction 4	4495 (40)	4605 (245)	+2.5
3DS E			4470	-0.5
3DS Y			6030	+12.6
3DS B	Obstruction 4	5355 (56)	5240 (270)	-2.2
3DS E			5190	-3.1
3DS Y			6825	+11.8
3DS B	Obstruction 4	6100 (62)	5900 (280)	-3.3
3DS E			5945	-2.6

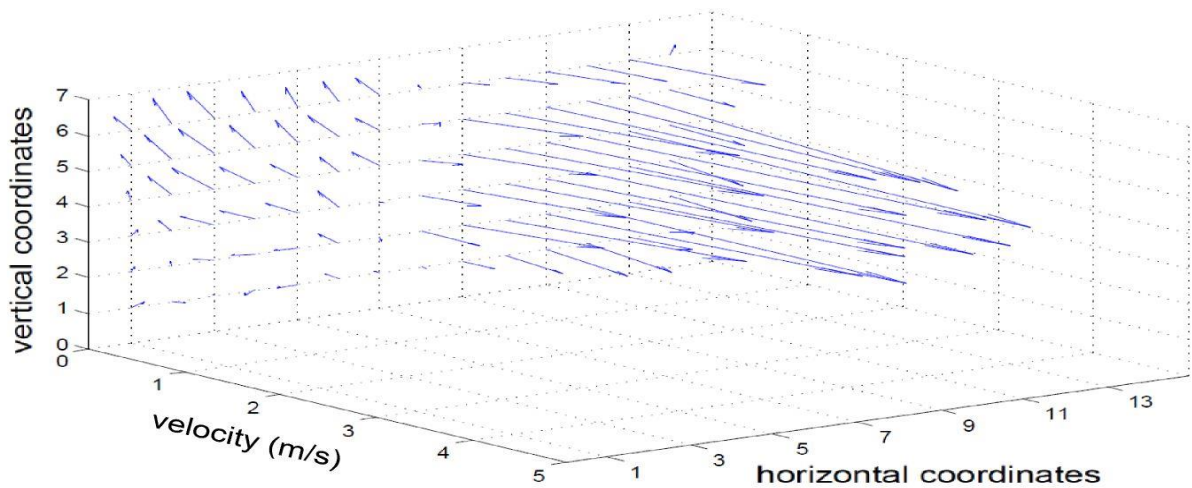


Fig. 3-13: 3D vector plot of velocities measured in the 3m wide tunnel, Free flow, 5770m³/h.

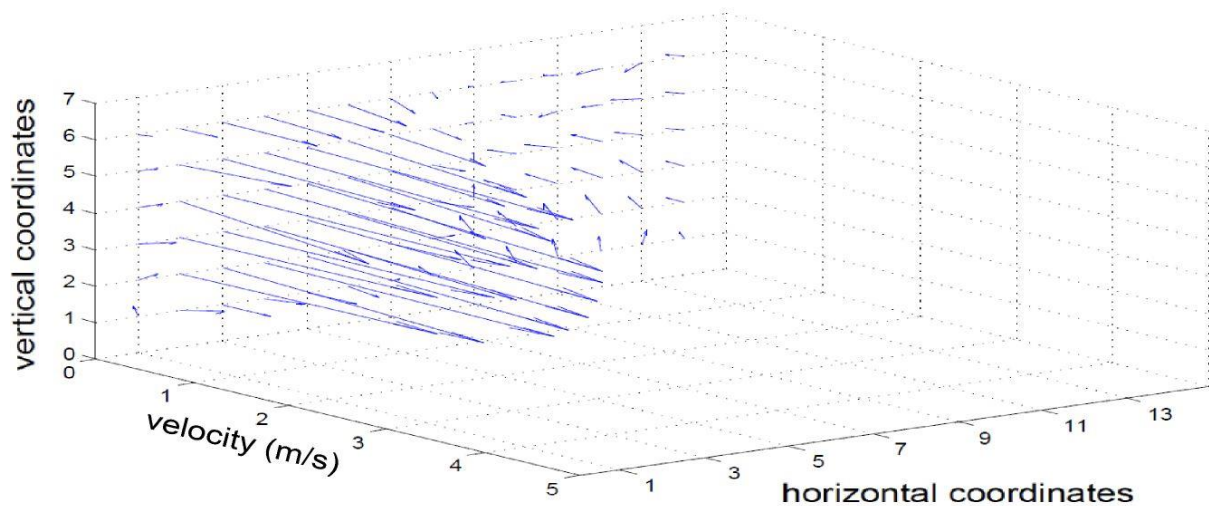


Fig. 3-14: 3D vector plot of velocities measured in the 3m wide tunnel, obstruction set-up 4, 5355m³/h.

3.3.3. General discussion

Compared to Chapter 2, the conducted series of experiments incorporated additional challenges in order to be more representative of naturally ventilated openings. The developed airflow rate methods proved to cope adequately with challenges concerning vent size, velocity profiles and sensor positions. Still further research is needed since these experiments were conducted under conditions of mechanical ventilation with airflow rates that were kept constant. Therefore, these methods are premature to be used as a reference technique for naturally ventilated openings. For the Basic and Extended method respectively, the execution times are approximately 48 and 80 minutes for a 3.0m x 0.5m opening. In this timespan it is most likely that the velocity profile could have changed significantly under conditions of natural ventilation. This lack of constant conditions could render the measured profiles to be insufficiently accurate. The next important challenge in measuring velocity

profiles in a naturally ventilated vent is therefore to deal with the temporal variability of the velocity profiles. This aspect needs to be investigated under conditions of natural ventilation. In order to tackle this challenge further research was conducted in a naturally ventilated test facility in which our developed 3DS method was incorporated (Chapter 4). In any case, when a very intensive sampling of a naturally ventilated vent is necessary to obtain meaningful conclusions, the developed automated sensor frame and 3DS methods will be valuable tools.

3.4. Conclusions

Different airflow rate measurement techniques were further adapted and developed under conditions which are more representative of naturally ventilated openings with regard to vent size, velocity profile and sensor position.

It is clear that positioning the sensor behind the outlet resulted in more complex 3D flows through the traverse plane. For the 1.0m wide tunnel and with disturbed velocity profiles, the 2D sensor measurements delivered unacceptably large relative measurement errors of up to -18.5%. Also, measuring only the Y-component (Y-method) at the 3.0m wide tunnel showed a systematic error of $12.1\pm 0.6\%$ for velocity profiles with different shapes and airflow rates. Therefore, it was further examined whether the additional information generated by the 3D sensor would result in a more reliable technique with smaller relative measurement errors under these conditions.

Two measuring methods were proposed to capture the 3D character of the airflows. Both the Basic method and the Extended method were based on traversing the outlet opening with a 3D sensor. Each method resulted in different relations between the velocity vectors and their corresponding sub-areas in the traverse planes. The Basic method showed a mean relative measurement error of $5.4\pm 1.7\%$ and $1.3\pm 2.6\%$ for a 1.0m and 3.0m wide duct, respectively, and for different undisturbed and disturbed airflows. The Extended method showed a mean relative measurement error of $3.1\pm 1.3\%$ and $-0.6\pm 2.6\%$ for a 1.0m and 3.0m wide duct, respectively, and for different undisturbed and disturbed airflows. Visualisation of the velocity profiles for the 3.0m wide duct evidenced that both the Basic and Extended method took into account returning flows. As all relative measuring errors remained under the 10% limit, both methods are to be considered satisfactory for measuring airflow rates through large openings regardless of the shape of the velocity profile. Therefore, the use of a 3D ultrasonic sensor is recommended when measuring airflow rates at the in- or outlets of naturally ventilated housing systems. As these methods are very labour intensive, a sensor frame was successfully developed that allowed an automated measurement.

Chapter 4. Experiments under conditions of natural ventilation: Cross ventilated test room*

*Adapted from: Van Overbeke, P., de Vogeleer, G., Brusselman, E., Pieters, J.G., Demeyer, P., 2015. Development of a reference method for airflow rate measurements through rectangular vents towards application in naturally ventilated animal houses: Part 3 : Application in a test facility in the open. Accepted in Computers and Electronics in Agriculture.

4.1. Introduction

In Chapter 3, two airflow rate measurement methods were developed, based on an automated traverse movement of a 3D ultrasonic anemometer across the outlet plane of the vent. However, these methods were not yet tested under conditions of natural ventilation, which are characterized by fluctuating wind speed and incidence angles. As the accuracy of both measuring methods did not differ considerably, the method with the fastest execution time was withheld. This method is further referred to as the Basic 3DS method. In Chapter 4 it is shown how the Basic 3DS method was applied to a naturally cross ventilated test room built inside a full size naturally ventilated mock-up building. The advantages of such an approach are discussed in chapter 1.2.5.1 and compared to similar set-ups in 7.1.1. The aim was to develop a new measuring method for the airflow rate that can take into account the variations of the external wind conditions by finding an appropriate sampling strategy for a sensor traversing the vents. This was achieved by (1) optimizing the sampling strategy using the Basic 3DS method in order to account for the temporal variations of the wind, (2) assessing the accuracy of the optimized method under a broad range of wind conditions, (3) examining the influence of wind speed and wind incidence angle on the airflow rate and (4) investigating whether the 3D velocity measurement could be replaced by a 2D or 1D velocity measurement without compromising a correct ventilation rate measurement.

4.2. Materials and Methods

4.2.1. Test Facility

4.2.1.1. The building

In this study a real scale section of a naturally ventilated pig house was mimicked. The geometry of a pig house was chosen because of its simple building design and relatively small ventilation openings compared to cattle houses. This building, further referred to as the test facility (see Fig. 4-1), was built at a site of the Institute for Agricultural and Fisheries Research in Merelbeke, Belgium (+50° 58' 38.56" N, +3° 46' 45.68" E; A on Fig. 4-2). This location was selected because of the absence of large flow disturbances such as buildings or rows of trees South-West (SW) of the facility, which is the prevailing wind direction in Flanders.

The test facility has internal dimensions of 12.0m × 5.3m × 4.9m (length x width x ridge height) and a volume of 251m³. No pen equipment was installed. Both concrete sidewalls have a ventilation opening of 4.5m by 0.5m with a depth of 0.2m (Vent A and Vent C, Fig. 4-1). No wind guidance systems or screens were installed in the vents. The vents are located at a height of 2.2m above the floor. They are oriented according to the SW – NE axis. This is the recommended positioning in practice in order to make maximum use of the potential of natural ventilation (Choinière and Munroe, 1990; Hellickson and Walker, 1983). The ridge opening has a length of 4.0m and a width of 0.3m. The test facility contained a smaller cross ventilated test room which was constructed by placing a wooden

wall, 4.0m behind the wall facing the South-West. The height of the test room was 2.9m with an internal volume of 61m³. The test room was closed with a suspended ceiling. The vent (Vent B) in the wooden wall was identical in size and location to the vents in the sidewalls of the test facility. This room was constructed to create a more controllable environment at this stage of the research whilst creating also the possibility to perform comparative measurements between a vent directly exposed to external conditions (Vent A) and an internal vent sheltered by a room on both sides (Vent B). The vent openings of the walls could be varied in size. In this study the opening size of both Vent A and Vent B was kept at 0.5m x 1.0m, Vent C was kept at 0.5m x 4.5m. The airtightness of the test room was examined by performing a standard blower door test (ASTM international E 779-03) at a pressurization of 4Pa and sealing the major leaks that were visualised through a smoke test. The results of the blower door tests indicated an effective leakage area of 0.0105m². No further attempts to diminish this leak were undertaken as its area only represented a small percentage (1%) of the combined size of the ventilation openings (2 x 0.5m²).

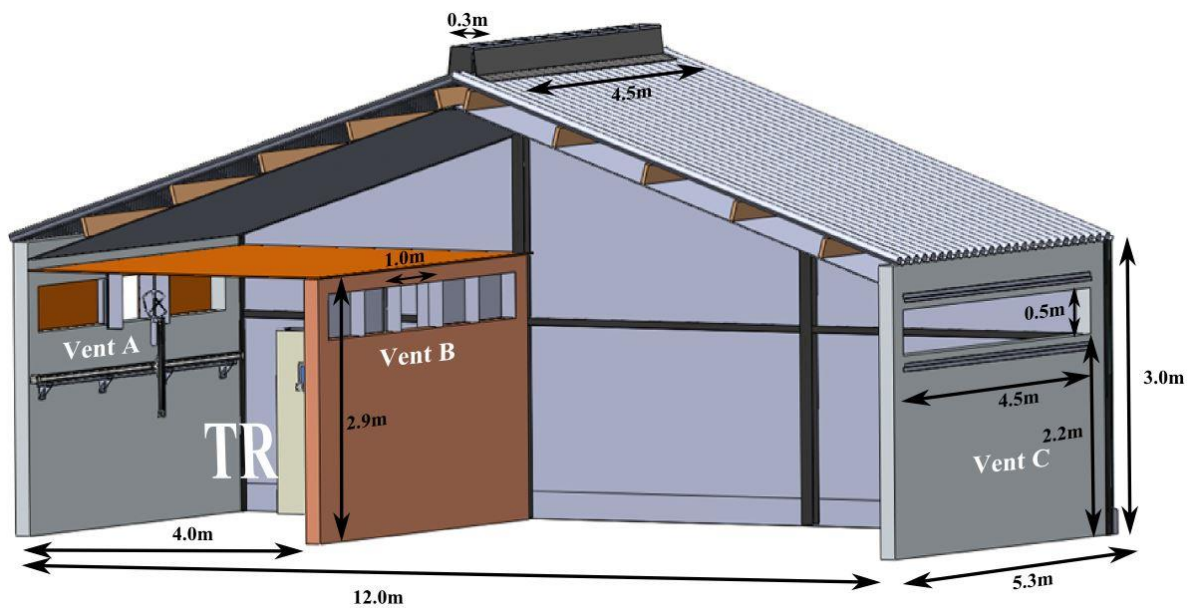


Fig. 4-1: 3D model of the naturally ventilated test facility at the Institute of Agricultural and Fisheries Research. A smaller test room (TR) was built inside the test facility to obtain a more controllable testing environment. An automatic sensorframe was installed at Vent A and B to allow an automated traverse movement of a 3D ultrasonic anemometer across the vent openings.



Fig. 4-2: Satellite image of test facility (A), a meteorological mast with a 2D ultrasonic sensor at a height of 10m (M) and nearest surrounding buildings (B, C, D and E) at the Institute of Agricultural and Fisheries Research. (Google Maps)

4.2.1.2. Air velocity sensors on automated sensor frame and meteorological mast

Two automated sensor frames, developed in Chapter 3, were attached to the inner walls of the test room, underneath vents A and B (Fig. 4-1). The automated sensor frame consisted of a vertical linear guidance of 0.7m attached to a horizontal linear guidance of 4.5m. The movement of the two guidances was automated by two PLC controlled servo motors. Every test was carried out with this fixed set-up, eliminating operator influences. On both sensor frames, a Thies ultrasonic 3D anemometer or 3DS (Thies 4.3830.22.300) was fixed on top of the vertical guidance. All sensor movements were made with the automated sensor frame with a positioning accuracy within 1mm.

A meteorological mast with a height of 10m was placed in the vicinity of the test facility (see Fig. 4-2, M) and equipped with a Thies ultrasonic 2D anemometer or 2DS (Thies 4.3820.02.300) on top.

All ultrasonic sensors were connected through a serial interface (half duplex mode), allowing a virtually simultaneous response of all sensors. The sensors had an internal measuring rate of 50Hz (2D sensor) and 33Hz (3D sensor). However, a moving average over 1s was continuously saved in the sensors' internal buffers. The value in this buffer was retrieved by the logger at 1Hz (Etheridge, 2012; Fiedler et al., 2013). A control connection was established between the logger and the control of the sensor movement to prevent measurements being taken whilst the sensor was moving.

For all ultrasonic sensors a coordinate system was chosen where the positive Y-component was aligned with the South-West wind direction (See Fig. 4-3). For illustrative purposes a South-West wind was taken equivalent to a wind incidence angle of 180° . A wind incidence angle of 90° was equal to a North-West wind. Airflow rates induced by flows moving from Vent A to Vent B were referred to as positive airflow rates. All polar plots of wind incidence angle and speed were based on

the coordinate system of the 3D or 2D sensor and are composed of the sensors' X- and Y-components (see Fig. 4-3).

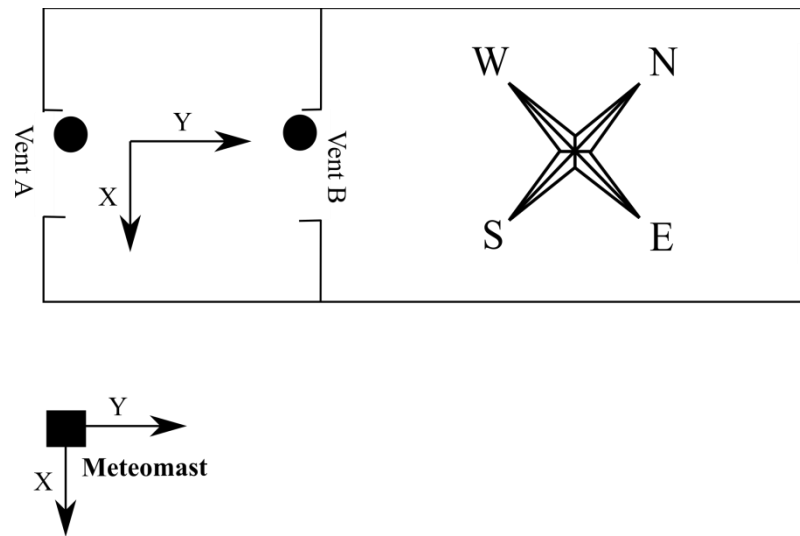


Fig. 4-3: Coordinate system of the ultrasonic sensors with respect to the wind directions, with ●: moving 3D ultrasonic anemometer in side vents A and B; ■: 2D ultrasonic anemometer on meteomast at height of 10m.

4.2.1.3. *Implementation of the Basic 3DS method*

Airflow rate measurements through the vents were initially performed with a set-up based on the Basic 3DS method as developed in Chapter 3. This method sampled the outflow surface behind the opening by traversing that area once with a 3D ultrasonic sensor mounted on the automated sensor frame.

The measurement volume of a 3D ultrasonic sensor was approximately 0.25m x 0.25m x 0.125m. To measure the outlet opening of 0.5m x 1.0m, 16 of these separate measuring volumes were considered to create the combined traverse plane. The velocity vector in the Y- direction was measured in every measuring volume. Additionally, the velocity vector in the X- direction or the Z- direction or both were measured for the measuring volumes at the edges. In total 32 velocity components were measured, which can be related to 32 elementary surfaces (Fig. 4-4). Such velocity components will be further referred to as e.g. VA-16-z (Ventilation opening A – measuring volume 16 – velocity component z).

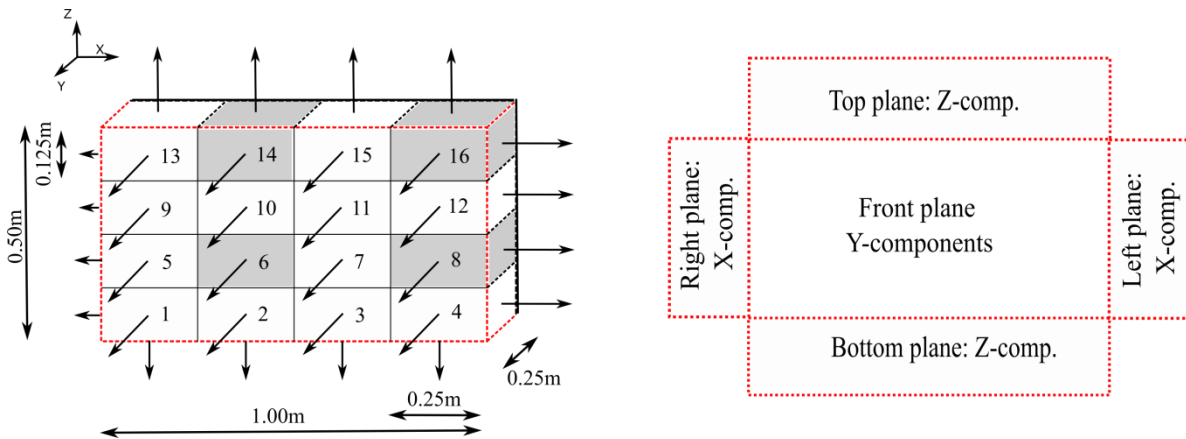


Fig. 4-4:Left: Front view of the combined traverse plane in Vent B, made up of 16 measuring volumes or 32 elementary surfaces. Four representative measuring volumes for Vent B in which continuous measurements were taken to determine the optimal sampling method are coloured grey (see 4.2.2) (for Vent A the mirrored image is applicable). **Right:** flat folded combined traverse plane, indicating the different traverse planes and the velocity components associated with these planes.

A full traverse of the combined traverse plane consisted of the consecutive measurement of the 16 measuring volumes by the 3DS. Each measuring volume was measured for a certain time (t_m). The total measuring time (t_{tot}) and airflow rate through Vent A (Q_{va}) and Vent B (Q_{vb}) could be calculated by equations [4.1] and [4.2], respectively.

$$t_{tot} (s) = N_{mv} (t_m + t_r) \quad [4.1]$$

$$Q_{vA/B} (m^3/h) = \sum_{i=1}^n (V_{i\pm} A_i 3600) \quad [4.2]$$

With N_{mv} : number of measuring volumes (16); t_m : the measuring time per measuring volume (s); t_r : average time to move sensor from one measuring volume to the next (2s); Q_{vA} (m^3/h) and Q_{vB} (m^3/h) the airflow rates through Vent A and Vent B, respectively; n : number of elementary surfaces (32); A_i : the area of the elementary surface “i” for which the normal velocity component was measured (m^2); $V_{i\pm}$: the average velocity component normal to an elementary surface “i” (m/s).

The Basic 3DS method was developed with the intention of taking into account the influence of returning airflows by differentiating positive and negative airflow velocities in X-, Y- and Z-directions. For example, a returned airflow could be characterized by a flow entering one or more measuring volumes through the side surfaces (X- or Z-direction) and that same flow leaving the measuring volumes through the front surfaces (Y-direction). As the flow in the X- or Z-direction is defined as a negative flow in this case, it will be subtracted from the total airflow rate, therefore compensating for the “false” flow rate through the front surfaces caused by returned flows. However, these are complex situations which need to be avoided as much as possible at this stage of the research. Therefore, a flange was built at the two vertical sides and the top horizontal side on the two

ventilation openings in order to obstruct flows from the X- and Z-directions and diminish these possible effects (see Fig. 4-5 and Fig. 4-6). Evidently, it was not possible to build a flange that completely bordered the vent as the vertical guide of the automated sensor frame needed to pass. The flange had a width, height and depth of 1.14m, 0.64m and 0.30m respectively.

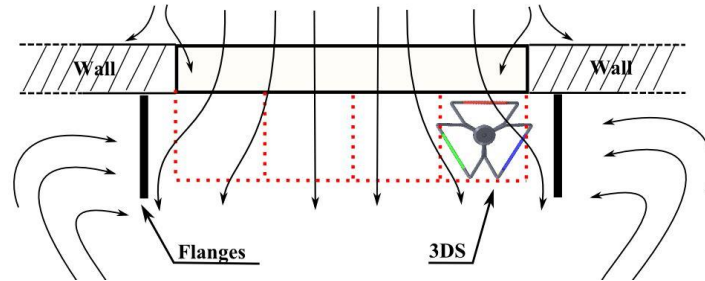


Fig. 4-5: Top view of the vent with flanges (dotted red line represents the composed traverse plane). A schematic impression is given of a possible returning airflow pattern shielded by the flanges.



Fig. 4-6: Vent B with flange and 3D ultrasonic sensor mounted on the vertical guidance of the automated sensor frame.

4.2.2. Optimization of the sampling strategy

The followed procedure to optimize the sampling strategy is illustrated in Fig. 4-7 based on real life measurements. The top graph in Fig. 4-7 shows continuous measurements (500s at 1Hz) of the air velocity in a certain measuring volume (here volume 6). This illustrates that the constantly changing external wind speed and direction are reflected in the unsteadiness of the velocity measured in the measuring volume. For a t_m of 20s (arbitrarily selected), t_{tot} equals 352s (equation [4.1]). When

applying the traverse motion of the ultrasonic anemometer to the vent, with the traverse starting at t_0 and ending at t_{tot} the sensor sequentially samples each measuring volume and passes through measuring volume 6 for only $1/16^{\text{th}}$ of the total measuring time. Such a ‘sampling window’ is illustrated by the red rectangle in the top graph of Fig. 4-7. It is clear that the average velocity measured during this short time interval at volume 6 might not be representative for the respective average velocity over the time period from t_0 to t_{tot} . To account for these unsteady conditions, the sampling strategy could be adapted in two ways: a) by increasing the sampling duration, i.e. increasing t_m , or b) by increasing the number of samples of each measuring volume, i.e. averaging over not only one traverse but over multiple traverses, further referred to as iterations (I). As the number of iterations evidently influences the total measuring time t_{tot} , equation [4.1] is adapted to equation [4.3].

$$t_{tot} = I N_{mv} (t_m + t_{tr}) \quad [4.3]$$

With N_{mv} : number of measuring volumes (16); t_m : the measuring time per measuring volume (s); t_{tr} : average time to move the sensor from one measuring volume to the next (2s). Increasing both I and t_m increases the total measuring time t_{tot} which could lead to even larger variations during the total measuring period. Therefore an optimal combination of t_m and number of iterations has to be found. Such a sampling strategy is illustrated in the bottom graph of Fig. 4-7. This graph shows the application of a sampling strategy with a t_m of 20s and 5 iterations applied to continuous measurements of the air velocity in measuring volume 6 for a period of 2000s at 1Hz.

In total 24 different combinations of I and t_m were tested to find the optimal sampling strategy (Table 4-1). A maximum was set for the total measuring time of approximately 30 minutes.

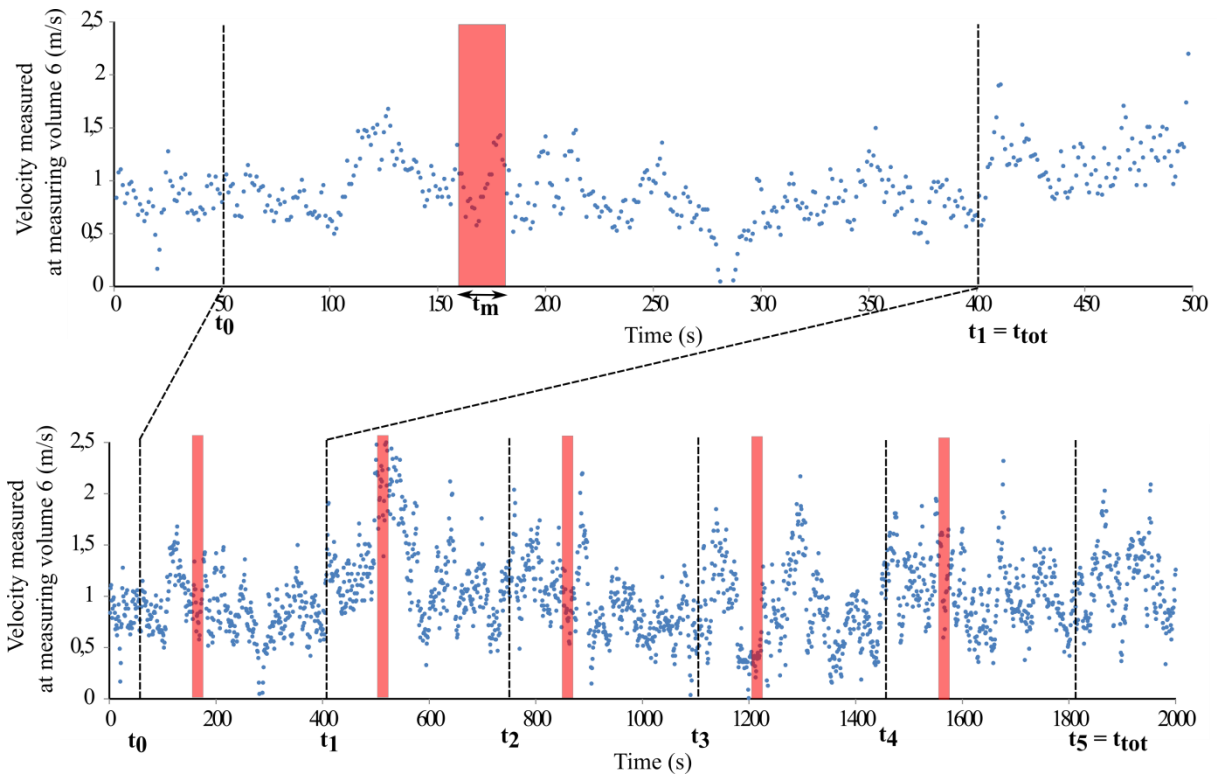


Fig. 4-7: Illustrative example of a continuous measurement of the air velocity (Y-component) in measuring volume 6 at 1 Hz (blue dots). **Top Graph:** The vertical dashed lines represent the start (t_0) and end (t_{tot}) time of a complete traverse movement of the ultrasonic sensor through the vent. The red rectangle illustrates the period in which the sensor stops in measuring volume 6. A measuring time per measuring volume (t_m) of 20s was chosen for illustrative purposes. **Bottom Graph:** Air velocity data for five consecutive traverses (t_0 to t_5) with the red rectangles representing the respective periods at which the sensor samples volume 6.

Table 4-1: Tested combinations of number of iterations (I) and measuring time per measuring volume (t_m) to find the optimal sampling strategy

I	1	2	3	4	5	6	8	10
t_m (s)	10, 35, 55, 75, 90	10, 15, 25, 35, 45, 55	10, 15, 25, 30, 35	10, 25	5, 20	10	5, 10	10

The sampling strategies were tested by applying them to a large dataset of continuous velocity measurements whereby different measuring volumes were measured for longer periods without moving the sensor. These measurements were performed in four measuring volumes in Vent A and B, i.e. 6, 8, 14 and 16 (grey areas in Fig. 4-4). These 4 volumes were considered to be a representative selection of all 16 measuring volumes. Depending on the type of measuring volume, other components of the air velocity were considered (Table 4-2). In each vent only one volume was measured at a time to prevent obstructed airflows. The experiments were carried out between August and December 2013 for periods of 4 to 16 days depending on the measuring volume. Some measurements were performed

longer as more interesting wind incidence angles were predicted (KMI), i.e. incidence angles other than the predominant one. Simultaneous measurements of the 2D anemometer on the metemast were processed in order to assess the variability in external wind speed and direction during the experiments.

Table 4-2: Components continuously measured at four representative measuring volumes (MV) in both Vent A and B (8 measuring volumes in total). Locations of the measuring volumes can be found in Fig. 4-4.

Continuously measured MV	Type	Similar MV's	Components measured
6	Inner MV	7, 10, 11	Y
8	Horizontal border MV	5, 9, 12	X, Y
14	Vertical border MV	2, 3, 15	Y, Z
16	Corner MV	1, 4, 13	X, Y, Z

For each sampling strategy, the average of all data over the period t_{tot} (V_c) was calculated and compared to the average (V_s) obtained by imposing the respective sampling strategy over that period. Applied to our illustration (bottom graph in Fig. 4-7) this implies that V_c is the average velocity over the period from t_0 to t_{tot} and V_s is the average velocity of all data measured within the red rectangles. Evaluation was performed using the relative measurements error $|E_{mv}|$ which is calculated following equation [4.4].

$$E_{mv} = \frac{V_s - V_c}{V_c} 100 \quad [4.4]$$

For each sampling strategy different E_{mv} values were obtained for different trials (S_i) performed over the complete dataset. The first trial (S_1) started at t_0 . In total S_i trials were performed starting respectively at $t_0 + (i-1)*t_m$. The trials stopped when $t_0 + (i-1)*t_m$ exceeded the end time of the dataset. For each sampling strategy, the percentage of trials was calculated for which $|E_{mv}|$ of max. 20%. This percentage is further referred to as R_{20} (%). For each of the 16 measured components, belonging to the 8 measuring volumes (4 for vent A and 4 for vent B), such a R_{20} value was obtained.

The influence of number of iterations on the R_{20} value was examined. Also the influence of the different combinations of I and t_m on the R_{20} value was examined. The method with the highest R_{20} value was chosen for further experiments.

Due to the use of a relative comparison method [4.4] small velocities could possibly result in high E_{mv} 's. The influence of these low velocities on the R_{20} was examined by calculating the E_{mv} for different reduced datasets for which average wind velocities (V_s or V_c) below certain respective limits (0.05, 0.1, 0.2, 0.3, 0.4 and 0.5 m/s) were omitted. This was only performed using the most promising sampling strategy.

4.2.3. Implementation and evaluation of the optimized sampling strategy

The airflow rates through Vents A and B were measured with the selected optimal sampling strategy determined in 4.3.1. According to the law of mass conservation the total influx of air into the test room had to be equal to the total outflow of air (Boulard et al., 1997), assuming an incompressible medium. Therefore, the accuracy of the method was assessed by the relative measurement error (E_q , see [4.5]) in % (Van Buggenhout et al., 2009).

$$E_q = \frac{Q_{vA} - Q_{vB}}{Q_{vB}} 100 \quad [4.5]$$

Where Q_{vA} (m^3/s) and Q_{vB} (m^3/s) were the airflow rates through Vent A and Vent B, respectively. Vent B was chosen as the reference based on measurements in 4.3.1.2. An acceptance criterion for the airflow rate measurement method had to be set. In the review of Calvet et al. (2013) an estimation of the standard uncertainty is given for different airflow rate measuring techniques in naturally ventilated buildings (techniques are discussed in 1.2.5.3). There it is shown that tracer gases can provide the lowest estimated uncertainties, i.e. 10 to 15%. For all other techniques the estimated uncertainties are higher. However, also for tracer gas techniques, much higher uncertainties (up to 230%) were found in other studies (Ozcan, 2011). When looking specifically at studies based on ultrasonic anemometer measurements, relative measurement errors between the in- and outfluxes of air through the vents are found ranging from 1 % (López et al., 2011b) over 19% (Joo et al., 2014) to 37% (Molina-Aiz et al., 2009). Based on expert judgement and abovementioned literature research, a relative measurement error between the airflow rates in Vents A and B (E_q , see [4.5]) of max. 20% was deemed acceptable as a criterion to evaluate our experimental results. The goal was to reach this criterion for the broadest range of wind incidence angles and speeds as possible.

The influence of the wind incidence angle and the average air velocity in the vent on E_q was studied. Also the influence of the external weather conditions (wind incidence angle and speed) on the airflow rate was examined. The necessity of taking a 3D measurement was studied by examining the contributions of the X-, Y- and Z-components to the total airflow rate under different wind incidence angles. The validity of using Vent B as a fixed reference was examined in more detail.

Also an alternative method of evaluating the optimized sampling strategy was examined by taking a different approach to calculate the relative measurement errors. Instead of comparing the airflow rate through Vent A to the airflow rate through Vent B (see equation [4.5]), the total building's inflow rates and total outflow rates (equation [4.6]) were compared (equation [4.7]). To accomplish this, the air velocities measured at the elementary surfaces were no longer averaged but split into a subset for air velocities contributing to an inflow rate and a subset for air velocities contributing to an outflow rate. The time weighted averages of the inflow and outflow subsets are referred to as v_{i+} and v_{i-} , respectively.

$$Q_{in} = \sum_{j=1}^m \sum_{i=1}^n (v_{i+} A_i \cdot 3600)_j \quad [4.6]$$

$$E_{q2} = \frac{Q_{in} - Q_{out}}{Q_{avg}} 100 \quad [4.7]$$

Where: Q_{in} : the total building inflow rate (m^3/h); m : the number of vents (2); n : number of elementary surfaces in the vent (32); v_{i+} : the time weighted average of the velocity component contributing to the inflow rate through elementary surface “i” (m/s); A_i : the area of the elementary surface “i” for which the velocity component was measured (m^2). Equation [4.6] was also used to calculate the total building outflow rate (Q_{out} , m^3/h) by substituting v_{i+} to v_{i-} , which was the time weighted average velocity component contributing to the outflow rate through an elementary surface “i”. Q_{avg} was taken as the reference ($Q_{avg} = (Q_{in} + Q_{out})/2$) in equation [4.7] (Ndegwa et al., 2008b).

4.3. Results & Discussion

4.3.1. Optimizing the sampling strategy

4.3.1.1. Experimental conditions

Fig. 4-8 gives an overview of frequency distribution of the wind speed and a polar plot of the wind direction at the meteomast during the experiments. A mean wind speed of (4.0 ± 2.4) m/s was found. The predominant wind direction was South to South-West. Consequently, Vent A and Vent B acted primarily as inlet and outlet, respectively.

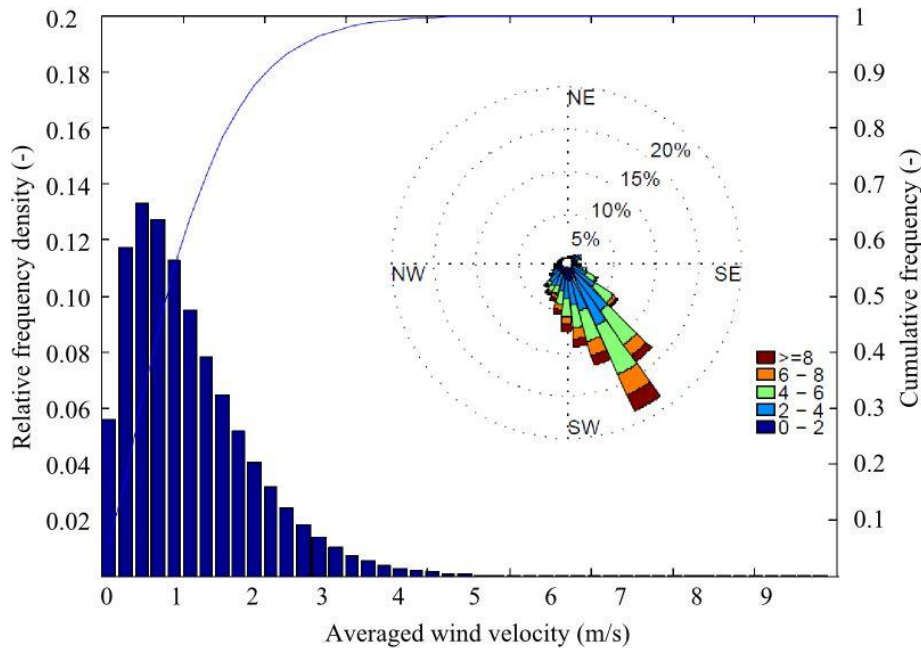


Fig. 4-8: Frequency distribution of the wind speed (m/s) and polar plot of the wind direction measured at the meteomast during all experiments for the determination of the optimal sampling strategy.

A more detailed view on the wind conditions in each separate experiment is given in Fig. 4-9. The horizontally adjacent plots of meteomast and measuring volumes represent simultaneously obtained data. The respective average velocities in the X-, Y- and Z-directions are given in the adjacent table. The component values used in the Basic 3DS method (see Fig. 4-4) are represented in bold. The wind incidence angles observed at measuring volume 6 and measuring volume 14 in Vent A, compared well with the meteomast data. This is in contrast to Vent B, where incidence angles closer to SW, and thus normal to the vent, were observed. This can be explained by the buffering effect of the test room, diminishing exterior influences at Vent B. This observed difference between Vents A and B was less clear at measuring volume 8, presumably because this measuring volume was positioned next to the vertical edge of the vent. Therefore, in Vent A, measuring volume 8 was partially shielded from the direct influence of a predominantly Southern wind. During the measurements at measuring volume 16, the wind came partly from the North resulting in less interpretable polar plots. The average velocities found for the X- and Z-components were in all cases considerably smaller than those for the Y-

components. This does not only mean that the X- and Z-components contributed less to total airflow rate than the Y-components, but that they could also lead to larger relative errors. These two effects combined resulted in a difficult interpretation of the R_{20} values.

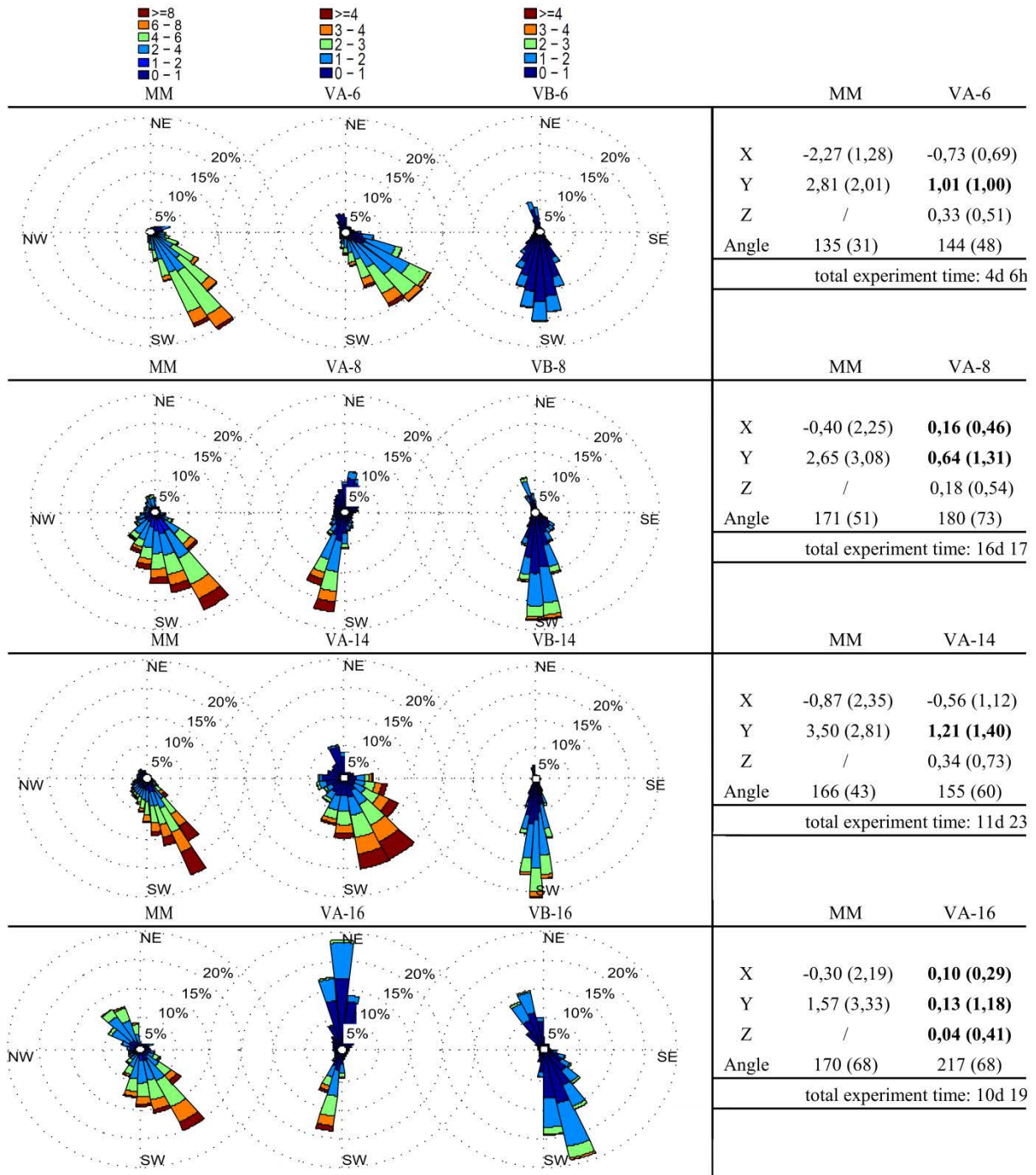


Fig. 4-9: Polar plots of wind direction from simultaneous measurements at the metemast and at different measuring volumes in Vent A and B. The velocity components X, Y and Z (m/s) and incidence angles (°) averaged over the total experimentation time are given together with their standard deviations (SD). The component values used in the Basic 3DS method are represented in bold.

4.3.1.2. *Minimising measurement error*

In order to assess the optimal sampling strategy, the measurement error (E_{mv}) was calculated for different combinations of I and t_m . The different sampling strategies are referred to via their I and t_m , e.g. an I of 5 and an t_m of 10 gives the 5x10 method. In Fig. 4-10 the influence of the number of iterations was examined (fixed t_m of 10s) in relation to the R_{20} . As the limit for the total measuring time was set at approximately 30min in this study, longer lasting sampling methods were not tested. Still, the trend in Fig. 4-10 shows that a higher number of iterations would possibly ameliorate the results, albeit an increasingly smaller gain. It can be seen that the lowest R_{20} values can be found for the X-components whilst the highest are found for the Y-components. No conclusions could be drawn for the Z-components as they varied from results as high as those of the Y-components to as low as the X-components. This distribution was maintained throughout the different sampling combinations. The generally lower R_{20} values for Vent A compared to Vent B can be attributed to the direct influence of the external wind conditions on Vent A, resulting in higher turbulence intensities at the windward side (Boulard et al., 2000; Teitel et al., 2008a). Evidently it is more challenging to find a correct sampling method under these conditions. Although in Vent B the differences between the 6x10 and the 10x10 method were very small, the 10x10 method was withheld because of the better results in Vent A.

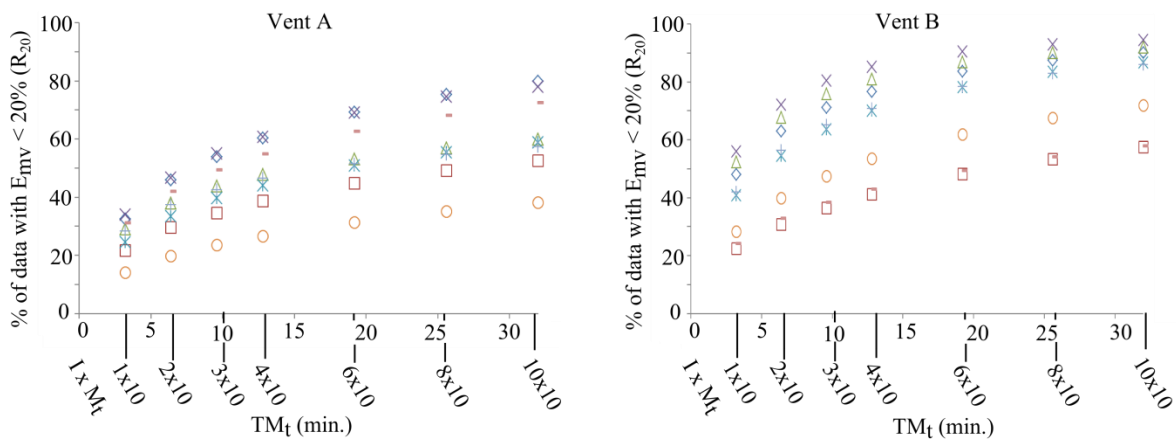


Fig. 4-10: Effect of increasing the number of iterations (fixed t_m of 10s) on the R_{20} values (%) at Vent A and B with $\diamond = 6\text{-Y}$; $\square = 8\text{-X}$; $\triangle = 8\text{-Y}$; $\times = 14\text{-Y}$; $\star = 14\text{-Z}$; $\circ = 16\text{-X}$; $+$ = 16-Y; $-$ = 16-Z.

In Fig. 4-11 it is shown, for combinations of I and t_m ($I \times t_m$) with a similar t_{tot} as the 10x10 method, that higher R_{20} values were obtained with a larger number of iterations (I) and thus a smaller t_m . The velocity components 6-Y, 14-Z and 16-X shown in Fig. 4-11 and other components measured but not shown, follow the same trend. The small differences in t_{tot} were inherently due to differences in the number of sensor movements (see [4.3]). From Fig. 4-10 and Fig. 4-11 we can conclude that the best results will be found for sampling strategies with a longer total measuring time which is divided in a high number of iterations.

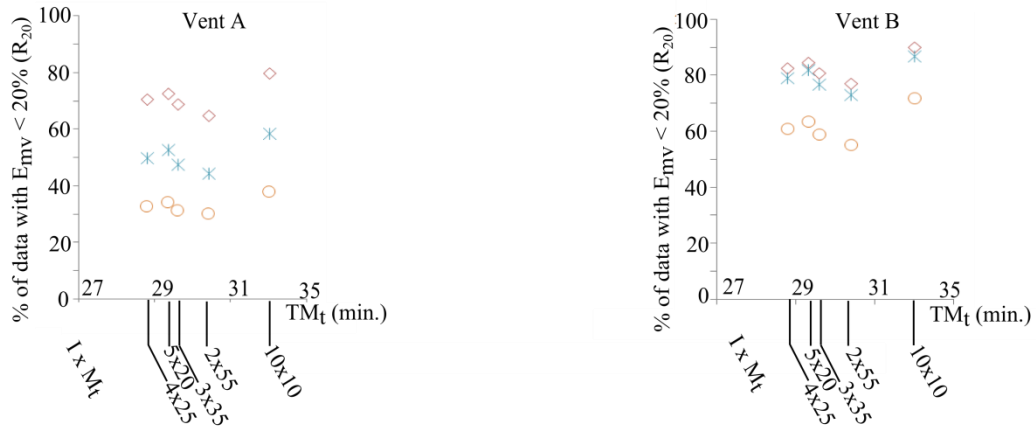


Fig. 4-11: Effect of the combinations of I and t_m on the R_{20} values (%). Four methods with similar total measuring times but different combinations of I and t_m are compared at Vent A and B with \diamond = 6-Y; \star =14-Z ; \circ = 16-X. These components represent highest, middle and lowest values, respectively. Results of other components lie between these ranges and were not shown to simplify the figure.

Only three velocity components (VB-6-y, VB-8-y and VB-16-y) had R_{20} values above 90%, even with the best performing method (10x10 method). However, some important considerations had to be made. Due to the variability of the wind a large part of the measured velocities in the vents can be lower than 0.5m/s especially in the X- and Z-direction. The use of a relative measurement error [4.4] can induce large errors when dealing with these low wind speeds. In Fig. 4-12 the influence of these low velocities on the R_{20} was examined by omitting the data below a certain velocity limit and recalculating the R_{20} . It can be seen that omitting the data below 0.05m/s already had a large impact on the results, especially for the X-components in Vent A. This is in contrast to the Y-components where the omission of the lower air velocities did not have a large impact.

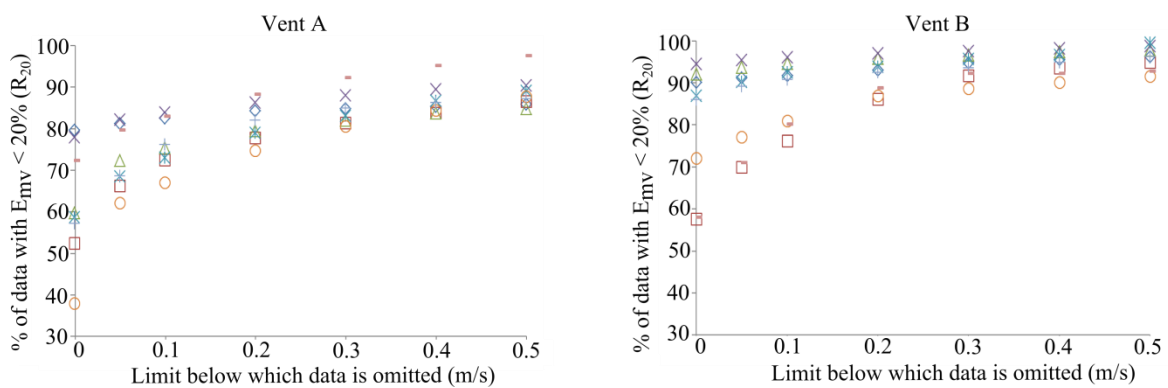


Fig. 4-12: Effect of low air velocities measured at the measuring volumes on the R_{20} values (%) for sampling method 10x10 (I x t_m). Different limits for the air velocity below which the data is omitted are shown for Vent A and B with \diamond = 6-Y; \square = 8-X; \triangle = 8-Y; \times = 14-Y; \star =14-Z ; \circ = 16-X; $+$ = 16-Y; $-$ = 16-Z.

It should be noted that the observed increase in R_{20} for the X- and Z-components by omitting low airflow velocities resulted from omitting a large part of the data. This can be seen in Fig. 4-13 where

the difference is shown between the complete dataset and a dataset where all measurements below 0.05m/s were omitted. Again the 10x10 method ($I \times t_m$) was applied. The total amount of data was divided into different ranges of the relative error E_{mv} . A substantial part of the data had an E_{mv} smaller than 10% even when all data was considered, especially in VB-8-y. The amount of data with an E_{mv} higher than 100% remained small for all elementary surfaces. However, it was clear that these high values of E_{mv} were more common in Vent A. When removing all data with an average velocity lower than 0.05m/s, the high E_{mv} values disappeared almost completely. Although this removal resulted in an increase of R_{20} , it also caused a considerable loss of data, especially for the X- and Z-components.

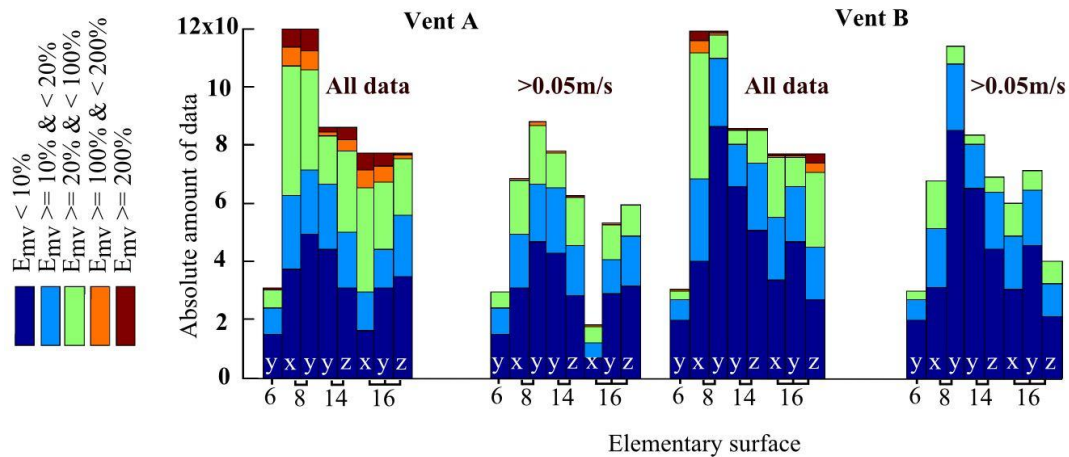


Fig. 4-13: The influence of omitting air velocities below 0.05m/s on the E_{mv} . The absolute amount of data in different ranges of E_{mv} are given. Data obtained by applying $t_m = 10$ s and $I = 10$.

The higher R_{20} values in Vent B suggest that a measurement in this vent would possibly be more reliable due to the sheltering effect of the test construction. Therefore, Vent B was chosen as the reference for the evaluation of the airflow rate measurement method (See [4.5]).

Only the best performing sampling method with $I = 10$, $t_m = 10$ and a total measuring time of 32min. was withheld for further experiments. The results attained within this time interval can give insight into the further applicability of the method for either airflow rate control systems or emission rate measurements. In case of emission measurements this time interval is certainly adequate, as generating average values at a daily basis could be sufficient (Estelles et al., 2010b). It must be noted that under highly variable wind conditions, it cannot be excluded that the selected sampling strategy might deliver unsatisfactory results.

4.3.2. Implementation and evaluation of the optimized sampling strategy

4.3.2.1. Experimental conditions

Experiments were conducted in the test room from April till November 2013. Fig. 4-14 gives the frequency distribution of the wind speed and the polar plot for the wind direction at the meteo mast during the airflow rate measurements. A mean wind speed of (2.4 ± 1.6) m/s was found. Although the wind was primarily blowing from South to South-West, a considerable amount of data was also

gathered for other wind directions. During this testing period 1005 airflow rates were computed and calculated according to the method developed in 4.3.1.

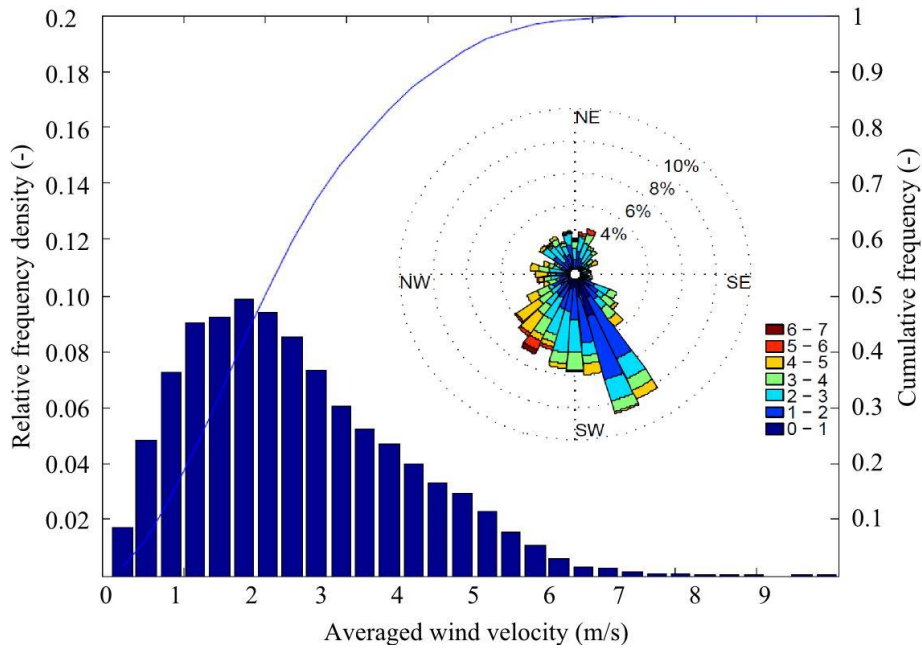


Fig. 4-14: Frequency distribution of the wind speeds (m/s) and polar plot of wind direction and wind speed frequency measured at the meteomast during all airflow rate experiments.

4.3.2.2. Influence of wind speed and incidence angle on the relative measurement error (E_q)

In Fig. 4-15 it is clear that the lowest air velocities, averaged in Vent A, usually resulted in higher relative measurement errors (E_q). As can be seen, the largest errors occurred for air velocities below 0,05m/s (between the dotted vertical lines). These data represented only 5% of the 1005 measured airflow rates. Five measurements with E_q 's over 100%, also with average air velocities below 0.05m/s, were omitted from Fig. 4-15. Outside these boundaries, the E_q remained for 96% of the data below $\pm 20\%$ with an average and standard deviation of $-1 \pm 11\%$. It was verified that setting the boundary higher than 0.05m/s would not result in a further improvement of the E_q . Setting the boundary at $\pm 0.15\text{m/s}$ for instance, resulted in an average E_q of $-0 \pm 9\%$. The improvement was deemed non-essential compared to the loss of data as only 70% of the data remained. There was no clear relation between the magnitude of the air velocities and the E_q ($R^2 = 0.42$, $y = 20.8x - 4.2$, data within the range of $|0,05\text{m/s}|$ was not accounted for). Therefore, no evidence was found that higher average air velocities in a vent in- or decreased the relative measurement error.

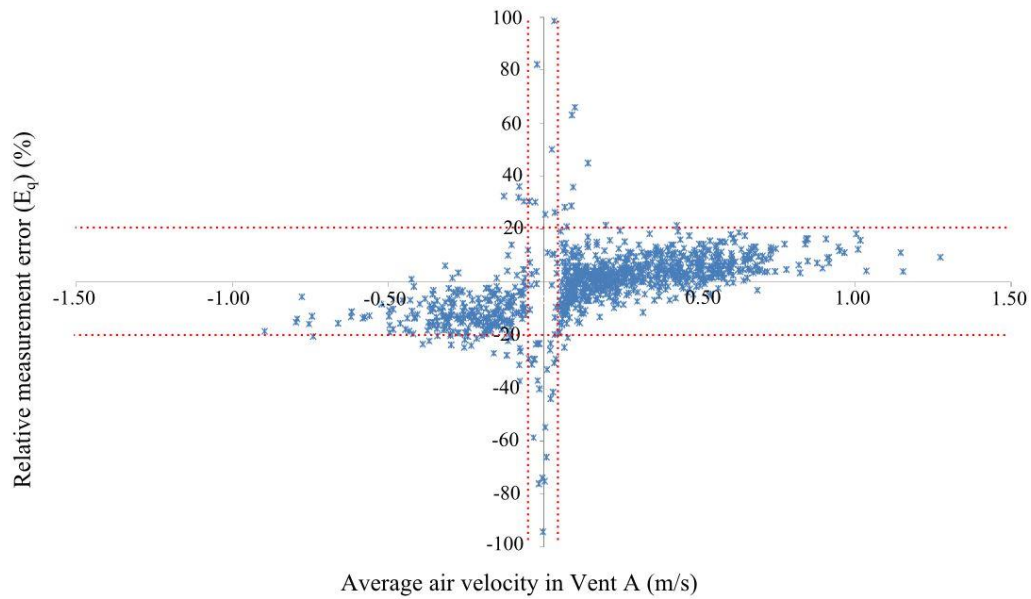


Fig. 4-15: Influence of the average air velocity in Vent A (m/s) on the relative measurement error (E_q , %). The dotted vertical lines represent the measurement limit at ± 0.05 m/s. The dotted horizontal lines represent the $\pm 20\%$ interval of E_q .

In Fig. 4-16 the relative measurement error is examined per wind incidence angle class. It can be seen that for most wind incidence angles the E_q remained between the limits of 20%. These results show that, although the optimal sampling method was obtained through measurements for a predominantly S to SW wind (see 4.3.1.1), the method was also capable of delivering satisfactory results for other wind directions. However, the ranges $45^\circ - 75^\circ$, $75^\circ - 105^\circ$, $255^\circ - 285^\circ$ and $285^\circ - 315^\circ$ show a larger spread of the error. It was assumed that this was due to complex airflow patterns caused by these wind incidence angles parallel to the vents.

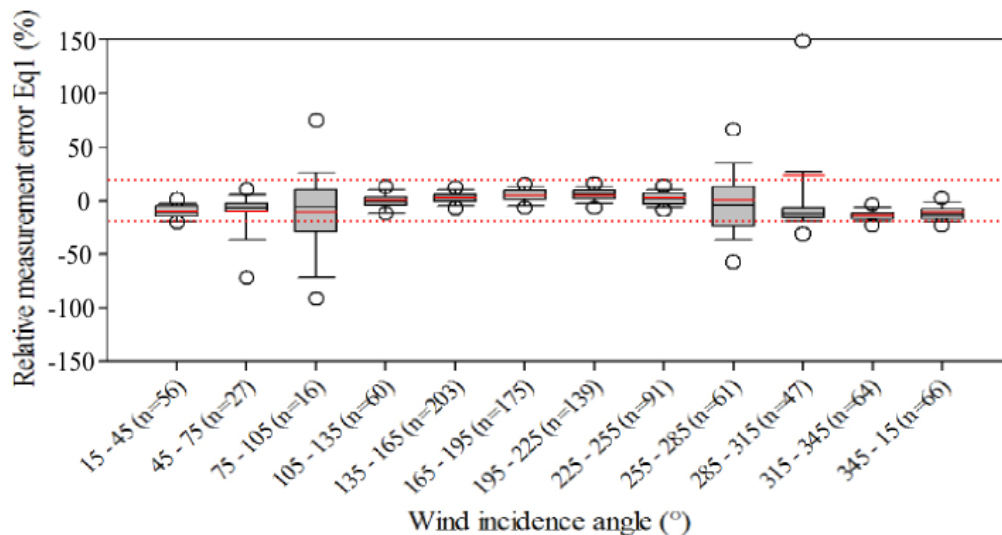


Fig. 4-16: Boxplot of the relative measurement error of the airflow rate in relation to the wind incidence angle for all data when calculated following equation [4-5]. Dotted red lines represent the 20% acceptance criterion, full red lines are the means and “n” are the number of airflow rate measurements.

It was concluded that for a broad range of wind incidence angles and speeds the acceptance criterion was fulfilled as the measuring method results in Eq's mainly below 20%. However, average air velocities below 0.05m/s and wind incidence angles close to 90° or 270° will result in higher Eq's.

4.3.2.3. Influence of 3D airflow information on the relative measurement error (E_q)

As can be seen in Fig. 4-4 the total virtual outflow area of 1.25m^2 (100%) consisted of three differently oriented subareas: 0.25m^2 (20%), 0.50m^2 (40%) and 0.50m^2 (40%) for the X- Y- and Z-components, respectively. From this percentage distribution it can be expected that the X-components contributed the least to the airflow rate (see also 4.3.2.5). Additionally, due to the flanges built around the vents, the most influential components are expected to be the Y- and Z-components through the front and bottom plane of the composed traverse plane, respectively. However, in Fig. 4-17 it is shown that the average E_q is strongly influenced by the addition of the X- and Z-components to the airflow rate determination. For these calculations 6 additional data points with relative errors higher than 200% have been removed from the data. These were due to the subdivision of the airflow rate into X-, Y- and Z-components resulting in very small airflow velocities. The average E_q over all wind incidence angles decreases from $8 \pm 29\%$ when only the Y-component was accounted for to $-5 \pm 10\%$ when also the Z-component was added to the airflow rate measurement. Adding the X-component resulted in an average E_q of $-1 \pm 10\%$. This strengthens the proof that measuring all components, as required by the Basic 3DS method in Chapter 3, is also advisable under conditions of natural ventilation, even with a flange around the vents. Removing the flange could result in more complex airflow patterns around the combined traverse plane and could increase the contributions of the X- and Z- components to the total airflow rate. However, as a flanged opening is not representative of vents in actual naturally ventilated animal houses, the influence of this flange and its removal should be further examined. It is also to be kept in mind that larger openings – as is the case in commercial animal houses - will show reduced edge effects.

Although in the studied cases the contribution of the X-components was perhaps too small to be of use in practice, they were considered to be necessary for a reference measurement technique in this installation. It is, however, expected that, as the size of the vent enlarges, the contribution of the Y-component will become even more predominant, rendering the X- and Z-components insignificant.

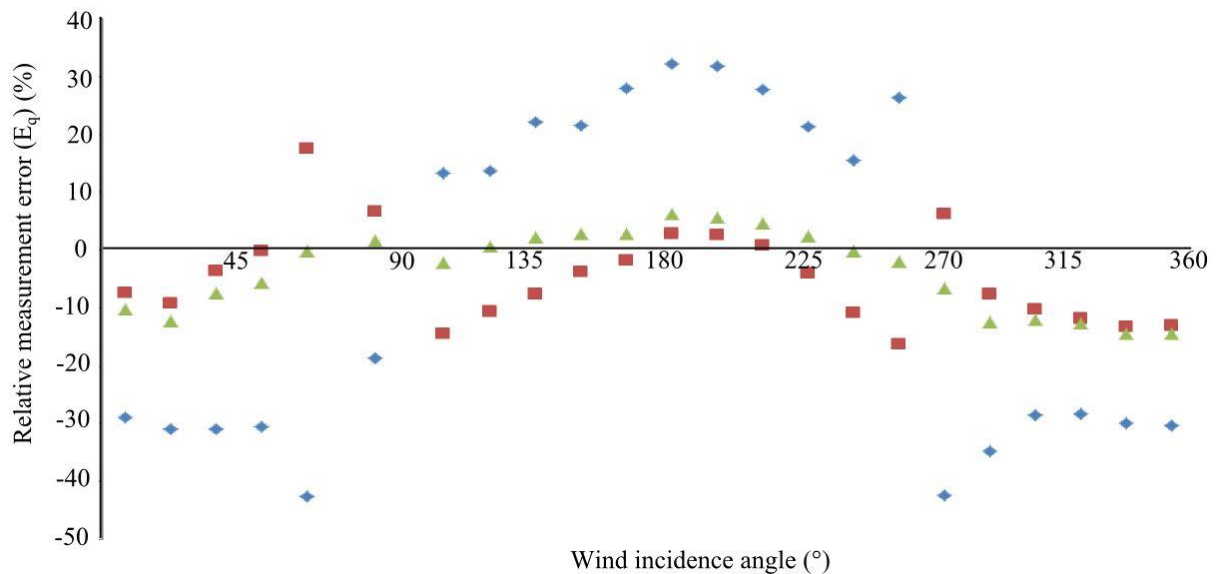


Fig. 4-17: The relative measurement error (E_q) as a function of the wind incidence when the X- and Z-components are added to the total airflow rate measurement. With \blacklozenge : E_q when only the Y-components are accounted for; \blacksquare : E_q with Y- and Z-components; \blacktriangle : E_q with X-, Y- and Z-components. Averages of the E_q 's are taken over 15° intervals. Data within the range of $[0,05\text{m/s}]$ and 6 additional data points with relative errors higher than 200% were not accounted for, 94% of the data remained.

4.3.2.4. *Influence of wind speed and incidence angle on airflow rate*

In Fig. 4-18 the airflow rates in relation to the wind incidence angle are shown for Vent A. A similar result was found for Vent B. Mostly positive airflow rates were found for wind incidence angles from 90° to 270° . For this range, Vent A and Vent B mainly acted as the in- and outlet, respectively. For other wind incidence angles negative airflow rates were induced. For both Vents A and B the largest airflow rates, up to $6000\text{m}^3/\text{h}$, were found at incidence angles around 180° and 360° , i.e., perpendicular to the vents, whilst the smallest were found around angles of 90° and 270° i.e. parallel to the vents. To see also the influence of the external wind velocity, the airflow rates were classified into 6 different categories according to the respective air velocities simultaneously measured at the metemast. The emerging pattern showed a clear dependency of the airflow rate on the external wind velocity and wind incidence angle. This confirms earlier studies where these are defined as two of the most influential parameters for the airflow rate in naturally ventilated buildings (Saha et al., 2013; Teitel et al., 2008b). Lower air velocities at the metemast combined with wind incidence angles between 105° and 255° (dotted lines L2 and L3) or above and below 285° (L4) and 75° (L1), respectively (see Fig. 4-18), result in small airflow rates. However, in the wind incidence angle intervals of 75° to 105° (L1 - L2) and 255° to 285° (L3 - L4), even for the higher wind velocities measured at the metemast, the airflow rates remained relatively small. In certain cases, especially when the wind is blowing parallel to the openings, a vent can be an in- and outlet simultaneously (Teitel et al., 2008b). As a consequence, it is possible that the mean airflow rate through an opening is very small or even zero, while in reality a significant amount could be entering the room. In the

alternative approach of calculating airflow rates and relative measurement errors, these situations are assumed to be accounted for (see 4.3.2.7). Although such conditions do not occur often when the animal house is built facing the predominant wind direction, they do present considerable difficulties when it comes to controlling the indoor airflow pattern. Obtaining an adequate and homogenous distribution of fresh air and temperature throughout the barn under these conditions is challenging as most control systems in ACNV act on the entire vent regardless of the possible duality of that vent. The data with an average velocity in Vent A of less than $|0,05\text{m/s}|$ is represented by the surface between the dotted vertical lines L5 and L6 in Fig. 4-18.

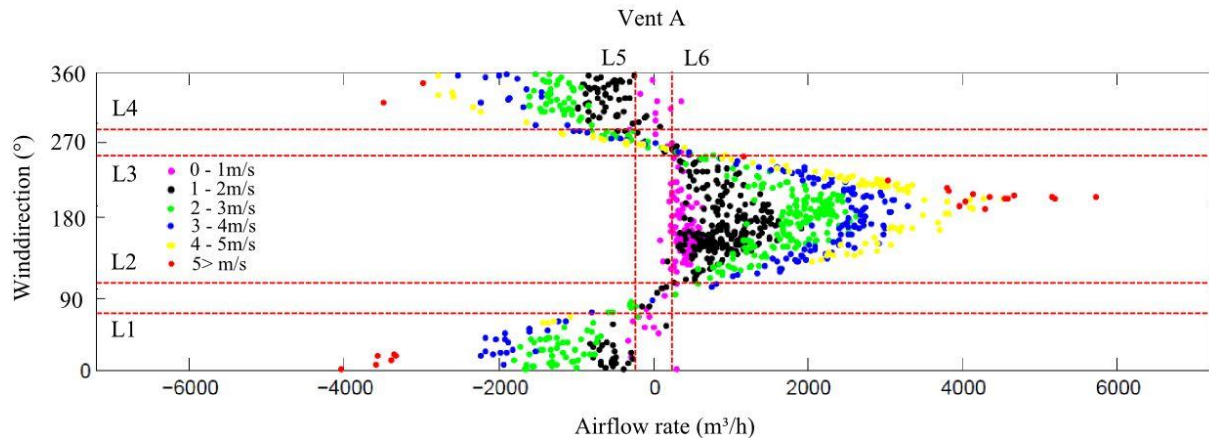


Fig. 4-18: Measured airflow rates in relation to the wind incidence angle for Vent A. The areas between dotted horizontal lines L1 to L2 and L3 to L4 represent wind incidence angles ranges of 75° to 105° and 255° to 285° respectively. The area between the dotted vertical lines L5 and L6 represent airflow rates with average air velocities in the vent lower than 0.05m/s . The wind speed at the meteoromast is represented by the different colours.

4.3.2.5. Influence of wind incidence angle on 3D airflow rate distribution

The relation between the airflow rates through the Y- and Z-planes were dependent on the wind direction. When Y-components were positive in Vent A (wind blowing from the SW), there was no strong relation between the airflow rates through the Z- and Y-planes (slope value = 0.07, $R^2 = 0.52$) (see Fig. 4-19, Vent A). This is caused by the more unidirectional pattern close to the inlet opening. However, with negative Y-components, i.e. Vent A acted as an outlet, a stronger effect was found (slope value = 0.33, $R^2 = 0.82$). This indicates that the Z-components had a larger influence in the vent that acted as an outlet. As the internal airflow meets the wall it has to travel alongside the wall to leave through the vent. Due to the flange around the border, only the bottom plane is unobstructed. Therefore, the Z-components measured in this plane, will contribute the more to an outflow rate. Comparable results were found for Vent B (See Fig. 4-19, Vent B, inlet: slope value = 0.11, $R^2 = 0.69$, outlet: slope value = 0.37, $R^2 = 0.93$).

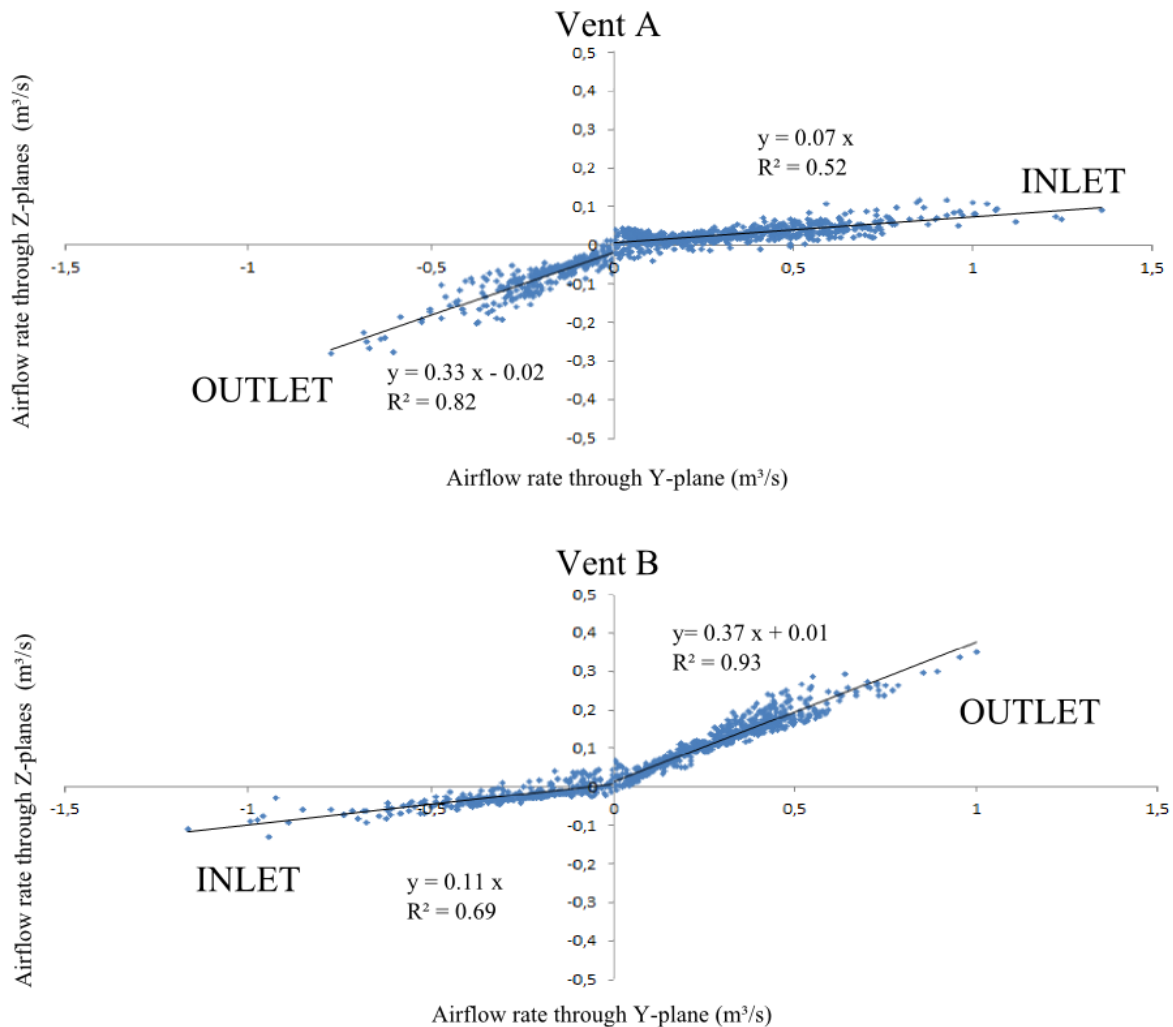


Fig. 4-19: Relation between the airflow rate through the top and bottom planes of the combined traverse plane (Z-planes) and the front plane (Y-plane) in both Vent A and Vent B. All components were averaged for the total duration of the airflow rate measurement period. The location of the planes can be found in Fig. 4-4.

The relative contributions of the airflow rates through the side planes (X-component), the top and bottom planes (Z- component) and front plane (Y- component) to the total airflow rate can be found in Table 4-3 for Vents A and B. The airflow rates were subdivided into 5 ranges of wind incidence angles (0-75°, 75-105°, 105-255°, 255-285°, 285-360°) measured at the meteomast. These ranges were chosen to set apart the influences of wind incidence angles almost parallel to the vents. In the range of 105° to 255°, where it is assumed that Vent A was the inlet, the respective X-, Y-, Z-component contributions to the total airflow rate were roughly 11%, 80% and 9%. When Vent A acted as an outlet (range 0° to 75° and 285° to 360°), the contribution of the Z-component was considerably larger with a distribution of roughly 4%, 67% and 29% for the X-, Y- and Z-components, respectively. As can be seen from the standard deviations (SD) these distributions were relatively stable and almost identical to the averages found for Vent B. For ranges 75° to 105° and 255° to 285°, where the wind incidence angle was almost parallel to the openings, similar averages were found. However, the larger standard deviations reveal an unsteady distribution between the respective components.

Table 4-3: All measured airflow rates were subdivided into their relative contributions (%) given by the X, Y Z-components (see Fig. 4-4). This data was subdivided into 5 wind incidence angle ranges and the average and standard deviation (SD) per range is given. Data within the range of $|0,05\text{m/s}|$ was not accounted for as these seemed to result in high relative measurement errors and, therefore, might wrongly influence the relative contributions.

Incidence angle (°)	Vent A				Vent B				#data
	X-comp. (SD)	Y-comp. (SD)	Z-comp. (SD)	In/Outlet	X-comp. (SD)	Y-comp. (SD)	Z-comp. (SD)	In/Outlet	
0-75	3.8 (2.3)	63.3 (5.1)	32.9 (6.0)	Outlet	7.9 (3.6)	83.5 (6.0)	8.6 (6.2)	Inlet	109
75-105	7.9 (15.0)	64.1 (23.7)	28.1 (37.7)	/	5.8 (6.6)	69.8 (25.8)	24.3 (31.9)	/	6
105-255	10.8 (4.0)	80.3 (8.2)	8.9 (7.7)	Inlet	5 (1.8)	66.7 (3.3)	28.3 (3.3)	Outlet	675
255-285	9.3 (11.9)	72.4 (15)	18.3 (25)	/	6 (5.9)	76.3 (27.3)	17.7 (32.5)	/	49
285-360	4.1 (3.1)	69.5 (6.2)	26.4 (5.2)	Outlet	5.9 (4.0)	86.4 (6.7)	7.7 (6.2)	Inlet	149

It is clear from Table 4-3 that the contribution of the X- and Z-components to the total airflow rate depended on whether a vent acted as the in- or the outlet. This implies that the airflow distribution through Vent A will be different from that in Vent B, creating two different velocity profiles. Both profiles are measured with the same method, delivering two similar airflow rates. This adds to the reliability of the method as the distribution of the airflow rate through the vents does not seem to influence the measurement result.

4.3.2.6. *Validity of chosen reference vent*

It must be noted that taking Vent B as the reference was based on the assumption that for all wind incidence angles Vent B would deliver a more reliable airflow rate measurement as it was sheltered at both sides from the external wind by the test facility. However, when the data was distributed amongst positive and negative airflow rates, different regression coefficients were found for data from Vents A and B (see Fig. 4-20). Although the correlation coefficient was very high in both cases ($R^2=0.99$), the slopes showed that the vent acting as the outlet always delivered smaller airflow rates than the inlet vent. This was similar to the results of Joo et al.(2014). However, the discrepancy between Vents A and B was larger when Vent A acted as an outlet. This was possibly caused by the more complex flow patterns at the leeward vent directly in contact with the outside environment (Nikas et al., 2010).

It was, however, impossible to determine which vent under- or overestimated the airflow rates for negative or positive airflow rates. Therefore Vent B was kept as the reference vent regardless of its function as the in- or outlet.

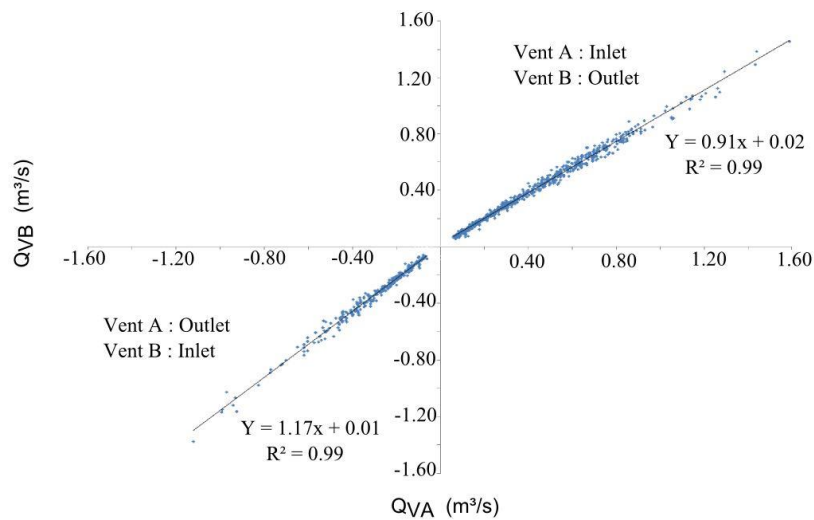


Fig. 4-20: Airflow rate measured in Vent A (Q_{VA}) in relation to the airflow rate measured in Vent B (Q_{VB}). Airflow rates measured at an inlet are higher than airflow rates measured at an outlet.

4.3.2.7. *Alternative approach to the evaluation of the measuring method*

Fig. 4-21 shows the results of the alternative method for calculating the relative measurement error (see 4.2.3). A considerable improvement of the variability of the relative measurement error was found in the wind incidence ranges $45^\circ - 75^\circ$, $75^\circ - 105^\circ$, $255^\circ - 285^\circ$ and $285^\circ - 315^\circ$. It is in these ranges that vents could possibly be an in- and outlet simultaneously. It seems that by differentiating the inflows from the outflows these situations are accounted for. An average E_{q_2} of $4 \pm 7\%$ was found. However, outside the abovementioned wind incidence ranges, both relative measurement error approaches (see equation [4.5] and [4.7]) delivered similar results. Comparable as to 4.3.2.6 it can be seen in Fig. 4-22 that the building's total outflow rates are lower than the total inflow rates. Therefore it was assumed that this was independent of the airflow rate calculation approach through equation [4.2] or [4.6], but inherent to the measuring method itself.

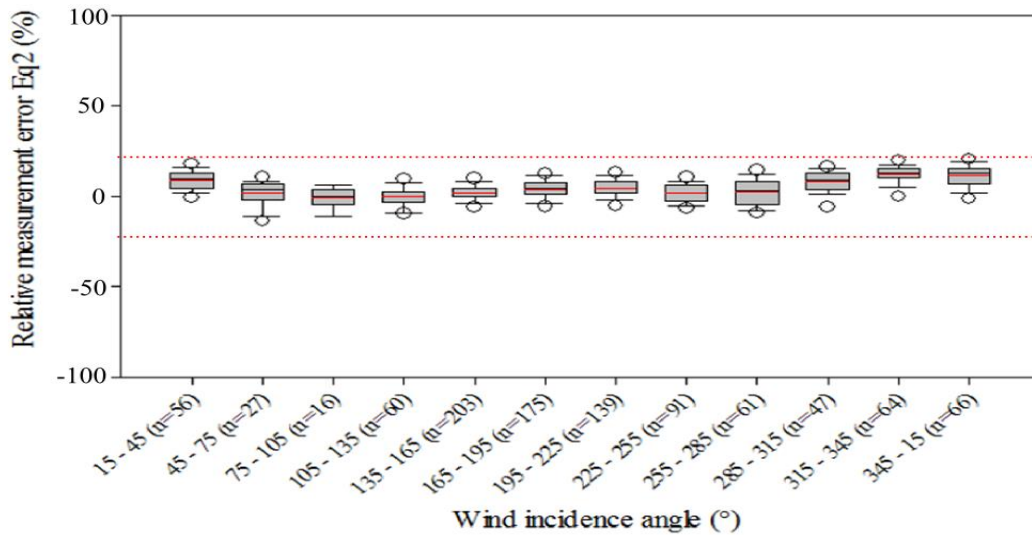


Fig. 4-21: Boxplot of the relative measurement error of the airflow rate in relation to the wind incidence angle when calculated following equation [4-7]. Dotted red lines represent the 20% acceptance criterion, full red lines represent the means.

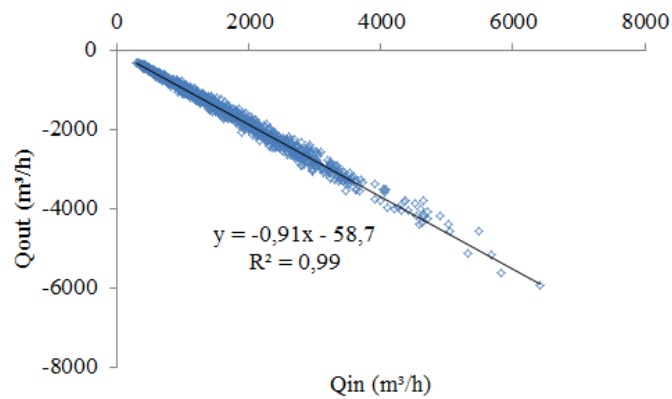


Fig. 4-22: Total inflow rate through the building (Q_m) in relation to the total outflow rate (Q_{out}).

4.4. Conclusions

A naturally ventilated test facility was built for the development of airflow rate measurement methods. The time-dependent airflow rates through a naturally ventilated vent were examined. The traverse based airflow rate measurement technique (Basic 3DS method) as developed in Chapter 3, was successfully adapted with a sampling method that could deal with the variable nature of naturally induced airflows. Optimal results were found when repeating the traverse movement 10 times whilst measuring each sampling point for 10s. The developed method was applied to both vents of a test room built inside the test facility.

The relative difference between the simultaneously measured airflow rates in both vents served as a tool to assess the accuracy of the method. A relative measurement error of 20% was deemed acceptable. For a wide range of average velocities in the vent and wind incidence angles, the average relative measurement error remained under $\pm 20\%$, i.e. $-1 \pm 11\%$. However, for wind incidence angles (almost) parallel to the vent a larger spread of the relative error was found. Calculating the relative

measurement error between the total building's inflow rates and the total outflow rates instead of between the airflow rate through Vent A and Vent B, reduces the relative measurement error. This was especially the case for wind angles close to 90° or 270° (i.e. parallel to the vents). This approach will be examined further in Chapter 5.

It was confirmed that measuring the X- and Z-components of the air velocity, additional to the Y-components normal to the inlet opening, was necessary to obtain satisfactory relative measurement errors. It was also shown that for an inlet the X-, Y- Z-component contributions to the total airflow were 11%, 80% and 9% respectively. For an outlet these respective contributions were roughly 5%, 65% and 30%. It was concluded at this stage that for the use as a reference technique none of the components could be omitted.

It must be noted that remaining below the self-imposed 20% limit allows us to move forward with this measuring method. It does not imply that this method, as is, will be applicable as a reference method. Especially for emission rate applications where the accuracy needs to be higher, more research is needed on how this relative measurement error can still be reduced or in what conditions (e.g. wind direction, vent size,...) lower measurement errors can be guaranteed.

The building and ventilation conditions under which the method was developed in this chapter (in particular the presence of the test room) were not yet similar to those found in a standard animal house. Therefore the method is not yet readily transferable to conditions in commercial animal houses. In Chapter 5 the technique developed and tested in Chapter 4 will be applied under conditions that are more comparable to those met in commercial animal houses i.e. larger vents and cross and ridge ventilation.

Chapter 5. Experiments under conditions of natural ventilation: Cross and ridge ventilated test facility*

*Adapted from: Van Overbeke, P., de Vogelee, G., Brusselman, E., Demeyer, P., Pieters, J.G., 2015. Development of a reference method for airflow rate measurements through rectangular vents towards application in naturally ventilated animal houses: Part 4:Cross and ridge ventilated test facility. Submitt. Publ.

5.1. Introduction

In Chapter 4 the procedure for a new measuring method for the ventilation rate in naturally ventilated buildings was described. The method's ability of coping with the continuously changing velocity profiles in the vents was examined. Although satisfying results were obtained in Chapter 4, the method has so far been applied to small openings only (0.5m×1.0m) in a naturally cross ventilated test room. However, cross ventilation alone rarely occurs in naturally ventilated animal houses, as they usually feature a ridge vent. The ridge plays an important role in the airflow patterns and might significantly affect the ventilation rate as well (Choinière et al., 1994; Scholtens et al., 2004). Therefore, in Chapter 5, the applicability of the method in situations more representative of commercial animal houses, i.e. cross and ridge ventilation, was examined. The method was applied to and validated for larger vent openings (0.5m×3.0m) and an additional measuring technique for the ventilation rate through the ridge was developed and validated.

5.2. Materials and Methods

5.2.1. Test facility

The wall of the test room was removed from the test facility (See Fig. 5-1). A detailed description of the test facility can be found in Chapter 4. Both concrete sidewalls have ventilation openings of 0.5m × 4.5m with a depth of 0.2m. The width of these vents can be changed by placing wooden boards that cover parts of the opening area. The ridge vent of 0.3m × 4.0m has upright flanges of 0.3m and can be sealed completely (see Fig. 5-2). During the monitoring period, no large obstructions were present in the area surrounding the test facility within a radius of 40m (see Chapter 4). A “standard blower door test” (ASTM international E 779-03) was performed at a pressurization of 4Pa to examine the airtightness of the building. Major leaks were visualized with smoke tests and sealed where possible.

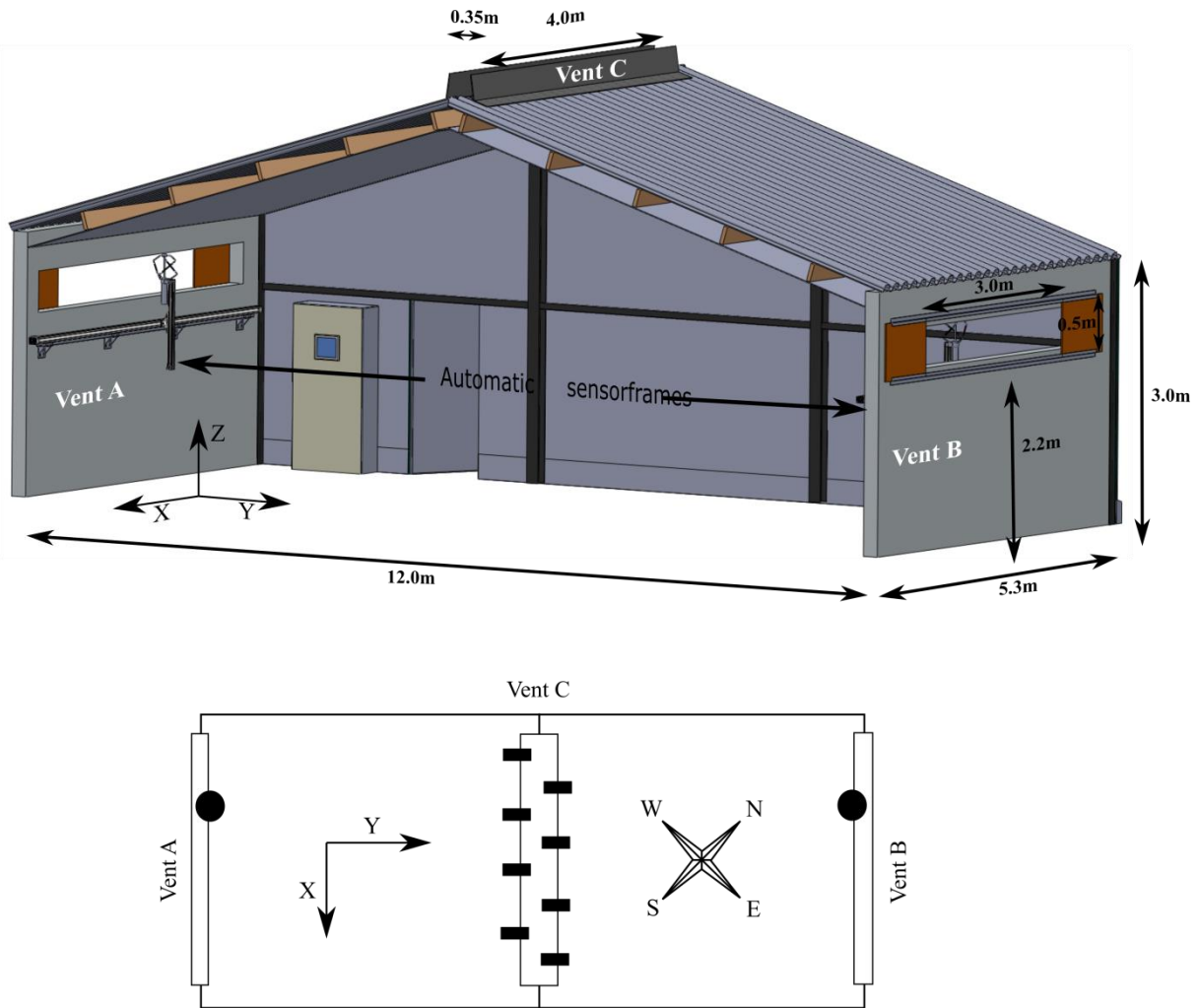


Fig. 5-1: 3D drawing of the test facility built at the Institute for Agricultural and Fisheries Research. An automatic sensorframe was installed at Vent A and B to allow an automated traverse movement of a 3D ultrasonic anemometer across the vent openings. Top view of the test facility with the X-Y coordinate system of the anemometers compared to the wind rose. ●: moving 3D ultrasonic anemometer in side vent; ■: static 2D ultrasonic anemometer in ridge.

5.2.2. Hardware configurations

An automatic sensor frame was developed and described in Chapter 3. This frame was used to perform an automated traverse movement by a 3D ultrasonic anemometer or 3DS (Thies® 4.3830.22.300, Göttingen, Germany) across the in- or outlet area of a vent. More detailed information concerning the frames can be found in Chapter 3. Two of these frames were positioned on the inner walls of the test facility beneath Vents A and B (Fig. 5-1).

In the experimental set-ups where the ridge was kept open (see 5.2.4), 8 2D ultrasonic anemometers or 2DS (Thies® 4.3820.02.300, Göttingen, Germany) were fixed inside the ridge. The positioning of these sensors can be seen in Fig. 5-2 A and B (side views) and C (top view). Holes were cut in the purlins in order to house the sensors. However, due to a lack of depth, the sensor heads were not located in the centre of the ridge but 2cm further away. This was the only feasible sensor set-up as other set-ups would cause larger flow obstructions.

In order to acquire more detailed information on the cross-sectioned air velocity profile through the ridge, 1D hotwire anemometers were used. A total of 9 hotwire anemometers were fixed across the width of the ridge (Fig. 5-2:B) (in the centre: TSI®, Air Velocity Transducer Model 8455, USA, Shoreview, and remaining hotwires: E+E Elektronik®, EE66-VC5K1000, Germany, Engerwitsdorf). A meteorological tower (meteomast) equipped with a 2DS at a height of 10m was installed South-East of the test facility. All sensors were connected to a datalogger (DataTaker® DT85M, Australia) through a serial interface (RS422). This allowed for a simultaneous readout of all sensors. The data was collected at 50Hz and 33Hz for the 2DS and 3DS, respectively, and stored as 1s averages. Hotwire anemometer readings were logged at 1Hz.

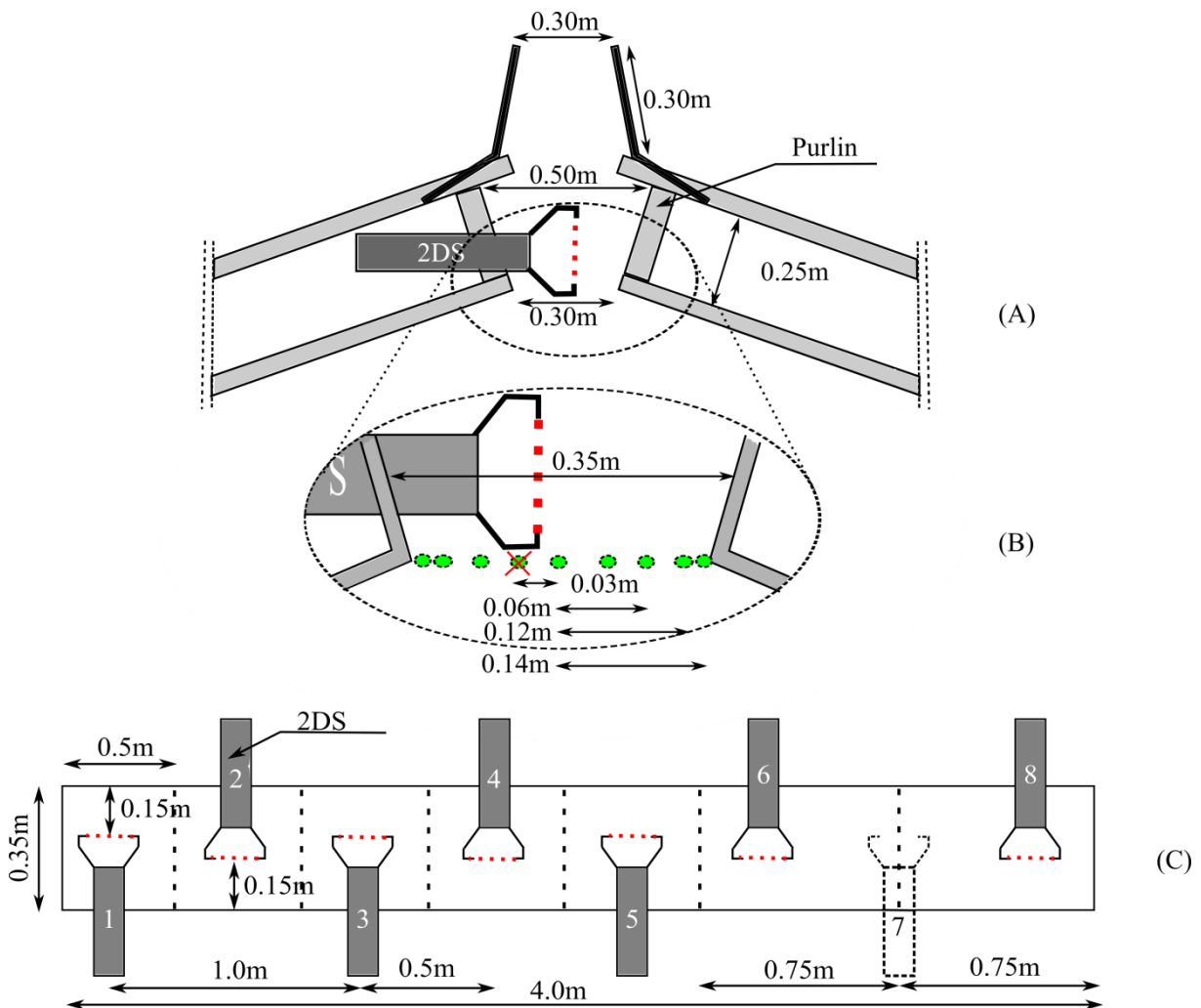


Fig. 5-2: **A:** Cross section of the ridge with an installed 2D ultrasonic anemometer. **B:** Green circles represent measurement locations of the 1D hotwire anemometers (not to scale). They are located beneath sensor 6. One of the hotwires malfunctioned and is marked with an \times . **C:** Top view of the ridge with 8 2D ultrasonic anemometers and their allocated outflow areas. Dotted red lines represent the measuring path of the 2D ultrasonic anemometer. Sensor 7 malfunctioned and was removed.

5.2.3. Ventilation rate measuring method

5.2.3.1. Data collection at side and ridge vents

Gathering the air velocity data at the side vents was performed by the method developed in Chapter 4. The method consisted of dividing the volume immediately downstream of the vent opening into cuboids with the size of the measuring head of the 3DS ($0.25\text{m} \times 0.25\text{m} \times 0.125\text{m}$, $L \times B \times H$), further referred to as measuring volumes. Each volume was sampled consecutively for 10s by a 3DS. Fig. 5-3:A illustrates how this method was applied to an opening of $0.5\text{m} \times 3.0\text{m}$. To capture the time dependent velocity profile, the complete vent was consecutively traversed 10 times. Hence each measuring volume was sampled for a total of 100s. More detailed information on the data collecting method can be found in Chapter 4.

For the ridge (Vent C) all measuring points were monitored simultaneously. Air velocity data at the ridge was collected over the same time period in which the side vents were traversed 10 times. 2D sensor 7 had to be removed from the ridge due to software errors and could not be replaced during further experiments. The ridge areas related to sensors 6 and 8 were widened to fill this gap (see Fig. 5-2:C). The width of the ridge was taken at the centre of the 2DS measuring path. Therefore the elementary surface area per 2DS was considered to be $0.35\text{m} \times 0.50\text{m}$ for sensors 1 to 5 and $0.35\text{m} \times 0.75\text{m}$ for sensors 6 and 8. Only the velocity component normal to these areas was utilized in the calculations.

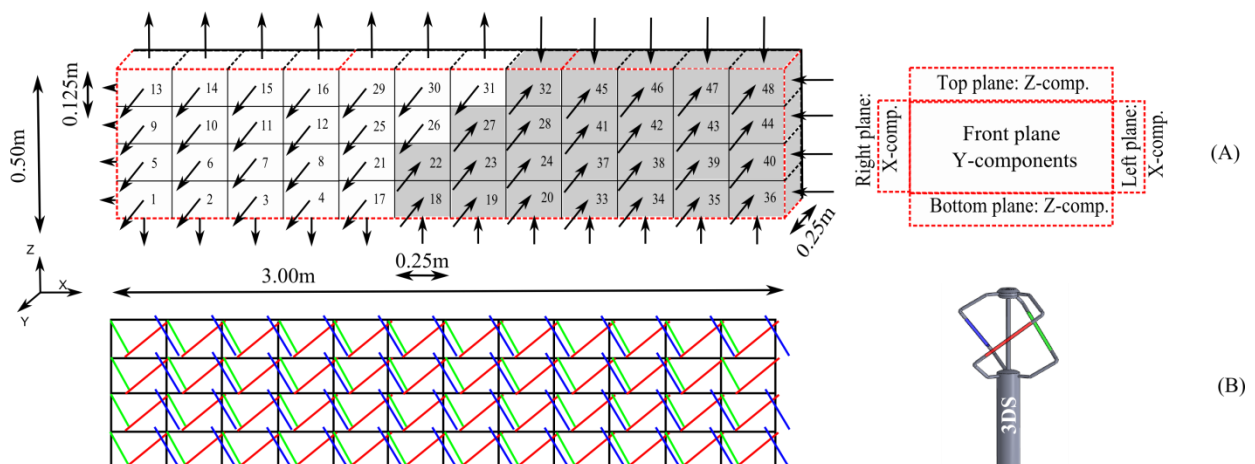


Fig. 5-3: A: Impression of a velocity profile measured in Side Vent B with North-Western winds. The vent is divided into 48 measuring volumes or 88 elementary surfaces. Arrows represent the velocity components sampled at each surface. Grey and white areas represent airflow flowing out of and in to the building, respectively. Airflow through grey surfaces is added to the total outflow rate (Q_{out}) airflow through white surfaces to the total inflow rate (Q_{in}); **B:** Side vent with the measuring paths of the 3D anemometer (green, red and blue lines) projected on the front plane in each of the 48 measuring volumes.

5.2.3.2. Determination of the ridge pipe factor

An additional consideration had to be made in view of the calculation of the in- and outflow rates through the ridge. An ultrasonic anemometer gives average wind speeds over its measuring paths. In Fig. 5-3:B and Fig. 5-2:C the measuring paths of the ultrasonic anemometers are projected on the

plane of the side vent (red, green and blue lines, 3DS) and ridge vent (dotted red line, 2DS), respectively. By moving the 3D sensor (see 5.2.3.1) most of the side vent area was covered by the paths. On the contrary, the coverage over the ridge area was much lower, requiring a different data processing method.

When the velocity profile in a vent is known, the average velocity (V_{avg}) can be found and multiplied by its related outlet area to obtain the airflow rate. However, only the velocity close to the longitudinal central axis (V_r) of the ridge was measured in this set-up. Assuming V_r to be representative of the total outflow area can lead to large inaccuracies of the airflow rate (Ozcan, 2011). The ratio between V_{avg} and V_r is represented by the pipe factor ($PF = V_{avg} / V_r$). For instance, the PF for a laminar flow through a wide rectangular channel is 2/3 (ASHRAE, 2009). However for a turbulent flow, which is expected in the ridge, determination of the PF is more complex and is dependent on the Reynolds number and roughness coefficient of the duct. A PF of 0.91 is given for a Reynolds number of 10^6 . Although the ridge is not a truly “smooth rectangular duct”, the expected value of the PF is thus situated between 0.66 and 0.91 (ASHRAE, 2009). Hotwire anemometer measurements in the ridge were carried out to give an estimate of the general shape of the velocity profile. All hotwire anemometers were calibrated. The measurements were taken directly beneath sensor 6 (see Fig. 5-2B). Sensors were positioned at the centre and at 0.03, 0.06, 0.12 and 0.14m to the left and right of the centre. The hotwire located at 0,03 cm to the left of the sensor malfunctioned and no valid data could be retrieved. All hotwires measured simultaneously at a frequency of 1Hz and results were based on 5 minutes averages. From these point measurements, a velocity profile was composed from which the V_{avg} was calculated. In this velocity profile, the velocity at the borders was considered zero. V_r was measured by the hotwire in the centre. A PF was calculated for each 5 minute measurement interval. It must be noted that in 2.3.4, where the ridge was simulated in a wind tunnel set-up, the low relative measuring errors inferred that additional measurements would not be necessary. However, the considerable difference in experimental conditions led to the belief that a more detailed study was needed.

5.2.3.3. Calculation of the ventilation rate

In Chapter 4 the airflow rates and associated relative measurement errors were calculated following two approaches: calculating the relative measurement error between (A) the building’s total inflow and total outflow rates and (B) between the airflow rate through Vent A and the airflow rate through Vent B. It was proven that approach (A) delivered better results for wind incidence angles close to 90° or 270° . It was assumed that in these cases the vents were simultaneously partly in- and outlet (Albright, 1990). Therefore, differentiating between in- and outflow rates was an essential step in the determination of the relative measurement error. Hence, approach (A) will be followed throughout this chapter.

The air velocities measured at the elementary surfaces were split into a subset for air velocities contributing to the inflow rate and a subset for air velocities contributing to the outflow rate. The time weighted averages of the inflow and outflow subsets are referred to as V_{i+} and V_{i-} , respectively. The same procedure was followed in the ridge vent but all measured air velocities were multiplied by the PF (see 5.2.3.2). As a final step, all elementary in- and outflow rates of all vents were summed into a total building inflow (Q_{in}) and outflow rate (Q_{out}), respectively (Equation [5.1])

$$Q_{in} = \sum_{j=1}^m \sum_{i=1}^n (V_{i+} A_i \cdot 3600)_j \quad [5.1]$$

With Q_{in} : the total building inflow rate (m^3/h); m : the number of vents (2 or 3 depending on whether or not the ridge is open); n : number of elementary surfaces in the vent (varying between 7 and 88 depending on the related vent and set-up); v_{i+} : the time weighted average of the velocity component contributing to the inflow rate through elementary surface “i” (m/s); A_i : the area of the elementary surface “i” for which the velocity component was measured (m^2). Equation [5.1] was also used to calculate the total building outflow rate (Q_{out} , m^3/h) by substituting v_{i+} to v_{i-} , which is the time weighted average velocity component contributing to the outflow rate through an elementary surface “i”.

The relative measuring error (E_q) between Q_{in} and Q_{out} (Equation [5.2]) was used as a measure for the accuracy of the method. Throughout the experiments the average value between Q_{in} and Q_{out} was taken as the reference ($Q_{avg} = (Q_{in} + Q_{out})/2$).

$$E_q = \frac{Q_{in} - Q_{out}}{Q_{avg}} 100 \quad [5.2]$$

As also stated in Chapter 4, the method was considered to be sufficiently accurate when the $|E_q|$ remained under 20% under a large variety of external wind conditions.

5.2.4. Imposed measurement conditions

In Chapter 4, the ventilation rate measuring method was validated for naturally ventilated openings of $0.5m \times 1.0m$ in a cross ventilated room. In Chapter 5, the final goal was to determine the airflow rates through the test facility featuring an open ridge and side vents of $0.5m \times 3.0m$. Therefore, three different set-ups of the test facility were examined (see Table 5-1).

In Set-up 1 the measuring method was applied to a wider vent, i.e. Vent A with an opening area of $0.5m \times 3.0m$ (see 5.3.2.1) and validated by considering Vent B with an opening area of $0.5m \times 1.0m$ as the reference. To allow the use of Vent B as the reference, this vent was set up in the same manner as was done in Chapter 4, i.e. with a flange of $1.14m \times 0.64m \times 0.30m$ bordering the vent. There it was shown that applying the measuring method to a flanged vent delivered satisfactory results. In

Chapter 4 it was also concluded that measuring the X- and Z- components at the borders of the $0.5\text{m} \times 1.0\text{m}$ vent was necessary to obtain the most accurate measuring method. In Set-up 1 this was re-evaluated with the wider Vent A. To allow for an even larger possible influence of the X- and Z- components, no flange was built around Vent A. In this set-up the ridge was closed.

In Set-up 2 the opening areas of Vents A and B were $0.5\text{m} \times 3.0\text{m}$ and the ridge was kept open. This allowed the validation of the measurement method in the ridge (see 5.3.2.2).

In Set-up 3 the width of Vent B was set to 1.0m in order to force more air towards the ridge in cases where Vent A was the inlet (see 5.3.2.3). This increased the ridge's relative contribution to the outflow rate. Set-up 3 was built to test the effect on the E_q of a predominantly ridge ventilated set-up as compared to Set-up 2. This allowed for an additional check of the ridge measurement method.

Table 5-1: Stepwise approach for validating the side vent and ridge airflow rate measuring methods. The size of the vents are shown in relation to the different set-ups.

	Side Vent A	Side Vent B	Ridge Vent C
Set-up 1	$0.5\text{m} \times 3.0\text{m}$	$0.5\text{m} \times 1.0\text{m}$	Closed
Set-up 2	$0.5\text{m} \times 3.0\text{m}$	$0.5\text{m} \times 3.0\text{m}$	$0.35\text{m} \times 4.0\text{m}$
Set-up 3	$0.5\text{m} \times 3.0\text{m}$	$0.5\text{m} \times 1.0\text{m}$	$0.35\text{m} \times 4.0\text{m}$

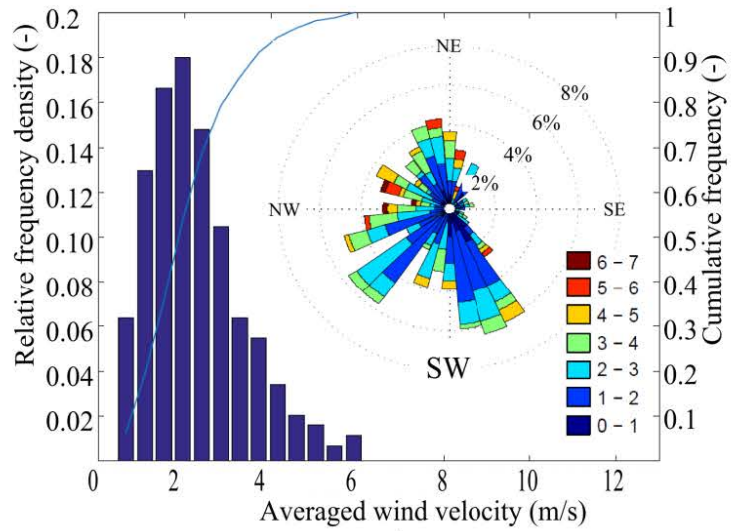
5.3. Results and Discussion

5.3.1. Experimental conditions

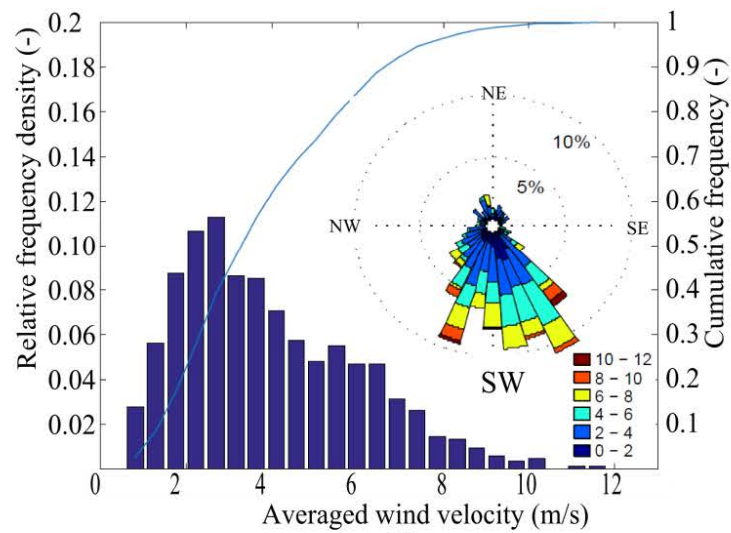
In Fig. 5-4 an overview is given of the wind conditions during the experiments in Set-ups 1, 2, and 3, and averages \pm standard deviations (SD) are provided in Table 5-2 for the total measuring period of each set-up. In Fig. 5-4, the distributions of the wind incidence angles are given in the polar plots together with the relative and cumulative wind speed frequencies. These parameters were measured at the meteomast and are based on the averages taken during 443, 833 and 710 airflow rate measurements in Set-ups 1, 2, and 3, respectively. The angle of 180° corresponds to the South-West direction. In Set-up 1, all directions except for south-east incidence angles were covered (Fig. 5-4:A). While, in Set-ups 2 and 3, only a relatively limited amount of data is coming from wind directions other than South to South-West (Fig. 5-4:B and C).

Table 5-2: Averages \pm standard deviation (SD) of wind speed and wind direction measured at the meteomast during the complete measuring period of Set-ups 1, 2 and 3.

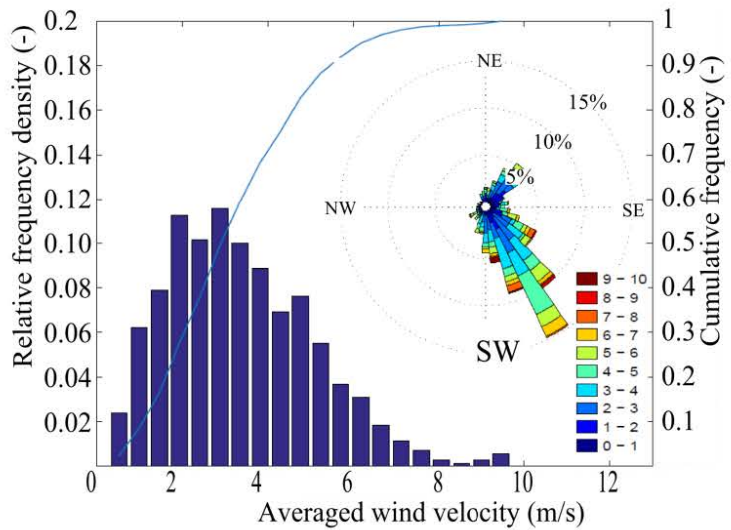
	Total measuring time (h)	Wind speed (m/s)	Wind direction ($^\circ$)	n
Set-up 1	708	2.3 ± 1.1	213 ± 92	443
Set-up 2	1333	3.9 ± 2.1	185 ± 65	833
Set-up 3	1136	3.4 ± 1.7	137 ± 71	710



A



B



C

Fig. 5-4 A, B and C: Relative and cumulative wind frequencies and polar plot of the wind direction measured at the meteomast during experiments in Set-up 1(A), Set-up 2 (B) and Set-up 3 (C) (See Table 5-1).

5.3.2. Evaluation and validation of the measuring method

5.3.2.1. Conditions of cross ventilation with closed ridge (set-up 1)

Relative measurement error

In Fig. 5-5:A the relative measurement error of the ventilation rate (E_q) as a function of wind incidence angle is shown. For all wind incidence angles E_q remained between $5 \pm 8\%$ which is below the established tolerance level of $\pm 20\%$. Therefore, it can be seen that the method developed in Chapter 4 was successfully adapted and transferred to the larger vent of $0.5\text{m} \times 3.0\text{m}$. In Fig. 5-5:A, a slight dependence of E_q on the wind incidence angle can be seen.

In Table 5-3 the relative contributions of Vents A and B to the total in- or outflow rates, classified amongst 4 ranges of wind incidence angles are shown. In the wind direction ranges of 135° to 225° and 315° to 45° a relatively stable contributions are found. Higher percentages suggest fixed in- and outlets in these situations. However, the contributions changes entirely in the ranges of 45° to 135° and 225° to 315° . These ranges contain wind directions parallel to the vents. A relative contribution to the inflow rate ranging from 34 to 69% for both Vents A and B indicates that these vents acted simultaneously as both in- and outlets. Nevertheless, as even in these complex situations E_q remained between $\pm 20\%$ (Fig. 5-5:A), it can be stated that the measurement method and data analysis were robust. In Fig. 5-6:A the change in relative in- or outflow contribution as a function of the wind incidence angle can be seen. From approximately 50° onward, the relative contributions begin to shift drastically to become stable again at around 120° . The amount of data for these wind directions was too low to see a clear start and end of this unstable region. However, the same trend is much clearer in the range of 225° to 315° , due to the larger amount of measuring points. There, the wind angle range in which the side vents shift from inlet to outlet and vice versa is approximately 250° to 300° .

Table 5-3: Relative contribution of Vents A and B to the total in- or outflow rate through the test facility for Set up 1, classified amongst 4 different ranges of wind incidence angles. Positive and negative values are relative inflow and outflow contributions, respectively.

Range ($^\circ$)	0 - 45 and 315 - 360	45 - 135	135 - 225	225 - 315
Vent A _{in} (%)	11 \pm 15%	58 \pm 32%	96 \pm 7%	69 \pm 34%
Vent B _{in} (%)	92 \pm 16%	41 \pm 34%	5 \pm 5%	34 \pm 33%
Vent A _{out} (%)	-82 \pm 8%	-53 \pm 23%	-19 \pm 11%	-44 \pm 26%
Vent B _{out} (%)	-15 \pm 9%	-48 \pm 25%	-79 \pm 9%	-53 \pm 24%
N	111	28	173	131

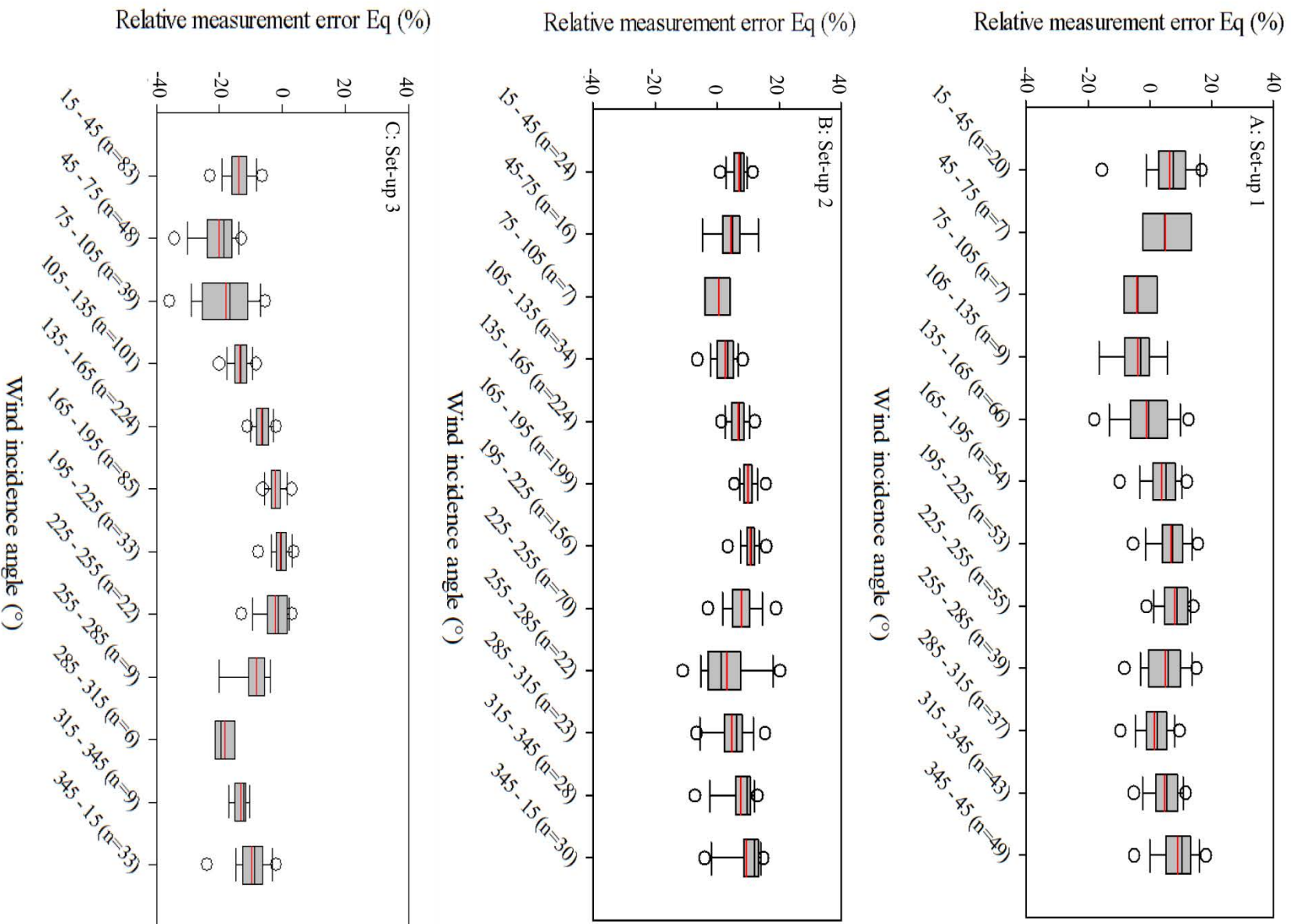


Fig. 5-5: Boxplots of relative measurement error as a function of wind incidence angle for set-ups 1 (A), 2 (B) and 3 (C) (See Table 5-1). The red lines in the boxes are averages.

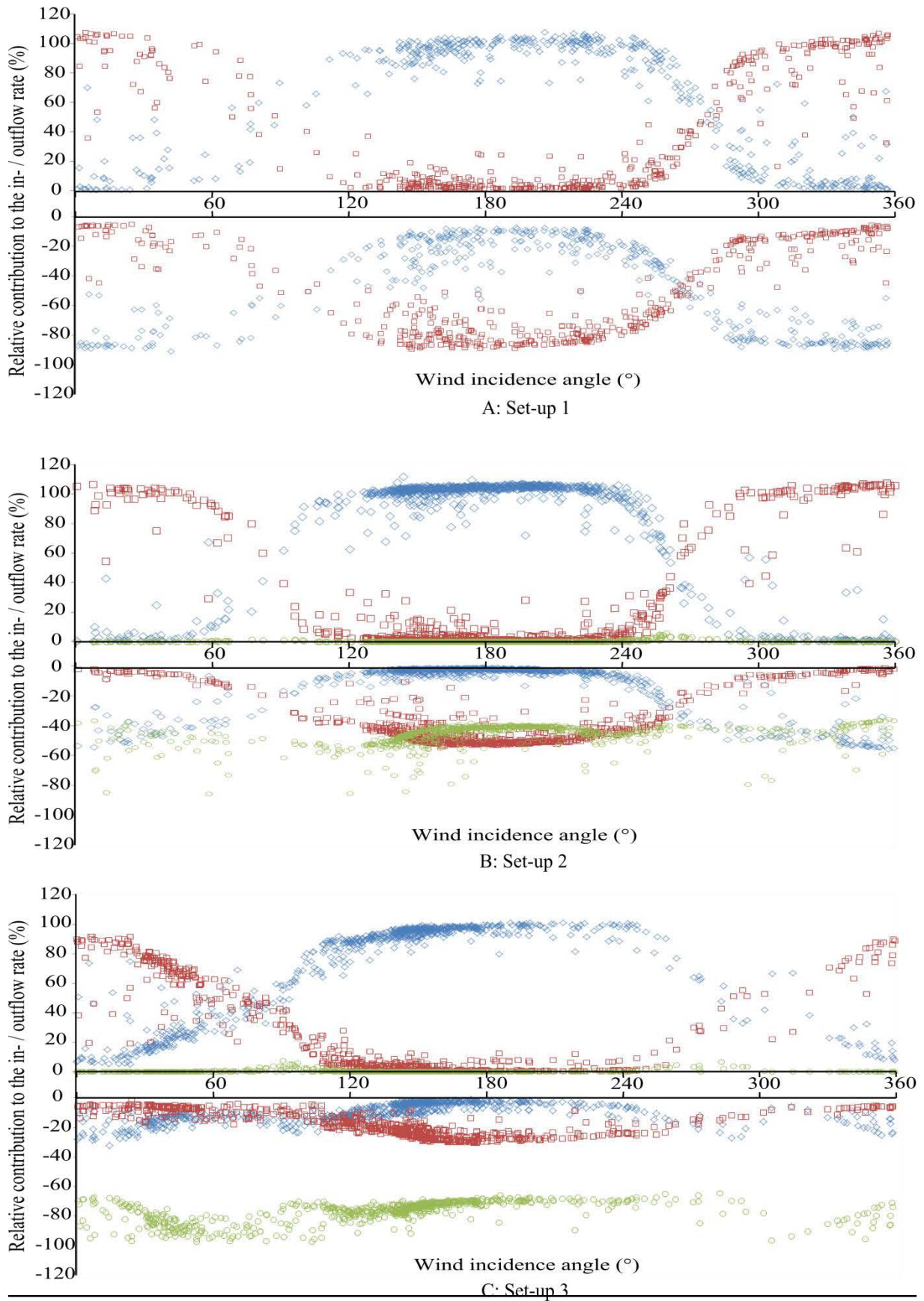


Fig. 5-6: Relative contributions of Vent A, B and C to the in- or outflow rate for set-ups 1 (A), 2 (B) and 3 (C) (See Table 5-1), with \diamond : flow through Vent A (blue); \square : flow through Vent B (red); \circ : flow through Vent C (green); positive and negative values are relative inflow and outflow contributions, respectively.

Need of 3D measurements

In Fig. 5-7: E_q values as a function of the wind incidence angle are shown, averaged over wind direction intervals of 30° . The in- and outflow rates measured in Vent A that are added to Q_{in} and Q_{out} , respectively, are calculated in 4 different ways. Namely, by accounting for different velocity components: (a) only the Y-components; (b) the Y- and X-components; (c) the Y- and Z-components and finally (d) all three components. Fig. 5-3 clarifies where these components were measured. The opening areas related to the Y- and Z- components (Y: front plane, Z: top and bottom plane) were considerably larger than those of the X-components (left and right plane). The in- and outflow rates in Vent B were calculated accounting for all components, as was recommended for this type of vent in Chapter 4. In Fig. 5-7 it can be seen that only accounting for the Y-components in Vent A resulted in larger relative measurement errors, in the range of $11 \pm 35\%$. Highest errors were found in cases where the wind was blowing perpendicular to the vents. Adding the Z-components to the calculation lowered the range of E_q to $5 \pm 8\%$. As seen in Fig. 5-7, this result is approximately equal to the result obtained by including all components. Therefore, including the Z-components was an essential part of the measuring method for this set-up. The X-component on the other hand, did not significantly alter the relative measurement error and, in the conditions of this study, could be omitted. However, for future study of flow patterns around the vents, all components deliver valuable information. The X-components are therefore not omitted in further measurements.

It must be noted that the large influence of the Z-components is partly attributable to the top and bottom planes being of almost equal area as the front plane (see Fig. 5-3:A). The larger the vent, the higher the influence of the front plane will be compared to that of the top and bottom plane. Therefore in very large vents, such as those found in cattle houses, measuring only the Y-component could be sufficient.

This statement seems to be in agreement with other studies where the ventilation rate in naturally ventilated buildings is determined by some anemometer measurement data multiplied by vent area. Also there, only the velocity component normal to the vent opening is usually considered (Joo et al., 2014; Molina-Aiz et al., 2009; Teitel et al., 2008a). However, compared to the present study, the applied vent areas related to the sampling points are much larger in these studies e.g. from 0.9m^2 (López et al., 2011a) and 2.1m^2 (Molina-Aiz et al., 2009) up to 110m^2 (Joo et al., 2014). Also measurements close to the vent's borders are mostly avoided in these studies. Air velocities are generally highest in the centre of the openings (Kiwani et al., 2012) as there is little influence of the vent's borders. Therefore these velocities can overestimate the in- and outflow rates when multiplied by the vent area. It is in such cases that applying mass conservation as a validation tool can be misleading as this overestimation cannot be identified. This might explain why, even when applying a low measurement density, the in- and outflow rates can still agree relatively well, e.g. within 12 to 19% (Joo et al., 2014), 1 to 28% (López et al., 2011b), -3 to 37% (Molina-Aiz et al., 2009) (percentages are calculated similar to equation [5.2]). Therefore, when the measurement set-up does

not sufficiently account for the spatial variability of the velocity profile, errors can occur which could remain undetected when validating with the mass conservation principle.

Although present study also relies on this principle, the reliability of our results was increased by the high measurement density and the large range of measurement conditions under which the method was validated.

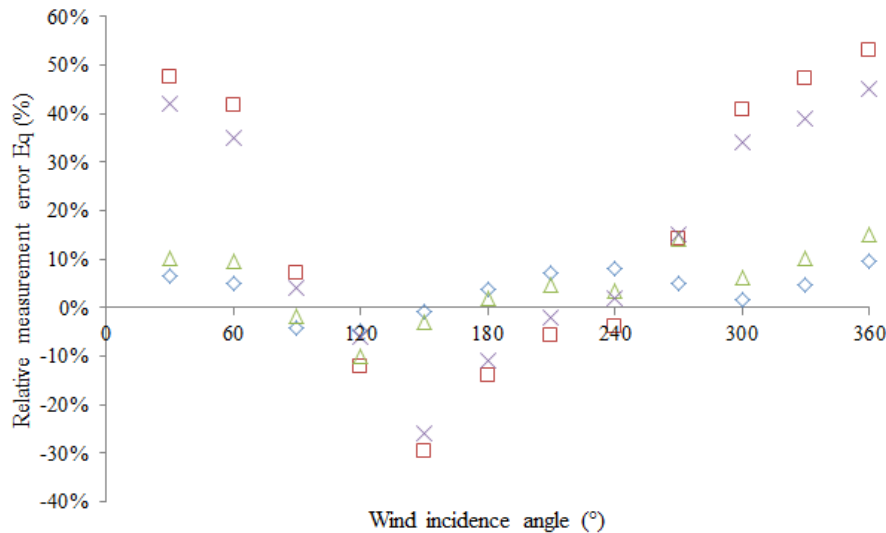


Fig. 5-7: The relative measurement error (E_q , %) as a function of wind incidence angle. The in- and outflow rates through Vent A are calculated with four different methods: \square : only accounting for the Y- velocity component (red); \triangle : accounting for the Y- and Z- velocity components (green); \times : accounting for the Y- and X- velocity components (purple); \diamond : accounting for all velocity components (blue). The in- and outflow rates through Vent B (needed for the calculation of E_q) were calculated accounting for all components. For each method the relative measurement errors (%) were calculated and averaged within intervals of wind incidence angles of 30° . (Set-up 1)

5.3.2.2. Conditions of cross and ridge ventilation (Set-up 2)

Pipe factor

In order to establish a PF value of the ridge, a total of 186 velocity profiles were determined with measurements carried out over a period of 4 days. In Table 5-4 the velocity profiles were subdivided into 8 V_r ranges, i.e. the wind velocity measured by the hotwire anemometer at the centre of the velocity profile in the ridge (Fig. 5-2:B). In Table 5-4 it can be seen that an increasing V_r resulted in a slight decrease in PF. Linear regression analysis indicated a rather weak, but present, correlation between the V_r and the associated PF's ($R^2=0.42$, $P<0.001$). In Fig. 5-8, where 7 of these velocity profiles are shown, it can be seen that a higher V_r resulted in profiles with a more “bullet shaped” profile. A lower V_r resulted in a more homogenous distribution of the air velocity. Although the profiles were not symmetrical, the velocity at the centre mostly remained the highest value.

The wind incidence angle during the tests varied between 105° and 168° ($N=152$) and between 284° and 314° ($N=22$). However, only the $105 - 168^\circ$ range was considered. Linear regression analysis showed a relatively weak correlation between wind incidence angle and the associated PF's ($R^2=0.27$, $P<0.001$). Nevertheless, one may notice that larger variations in wind incidence angles might have a significant effect on the shape of the velocity profile.

The ridge experiments indicated that the PF might be dependent on wind incidence angle and air velocity in the ridge. However, within the ranges of our measurements the correlations were weak. Hence, under the conditions met here, the PF was considered to be constant. Based on the average taken of all velocity profile measurements, a PF of 0.78 was withheld to calculate the airflow rates in set-ups 2 and 3.

Table 5-4: Pipe factors (PF, dimensionless) related to wind speeds at the centre of the velocity profile (V_r) measured in the ridge. N is the number of measurements within the associated range of V_r .

V_r range (m/s)	PF (SD)	N
0.50 to 0.74	0.79 ± 0.03	11
0.75 to 0.99	0.81 ± 0.04	46
1.00 to 1.24	0.79 ± 0.02	13
1.25 to 1.49	0.79 ± 0.02	14
1.50 to 1.74	0.77 ± 0.02	31
1.75 to 1.99	0.76 ± 0.02	21
2.00 to 2.24	0.75 ± 0.02	34
2.25 to 2.65	0.75 ± 0.02	16

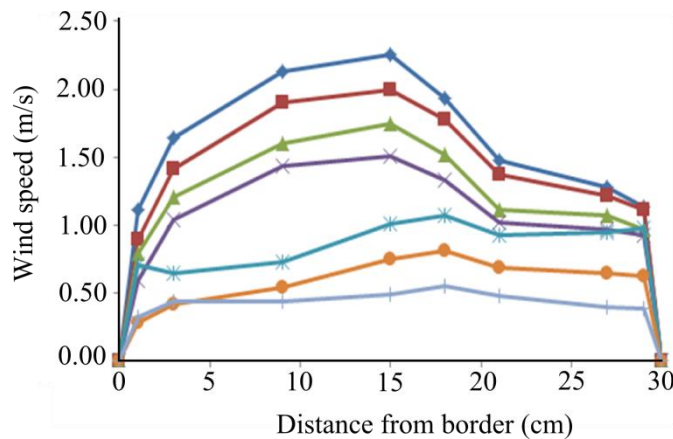


Fig. 5-8: Velocity profiles with different V_r (velocity in the centre of the profile, i.e. 15cm) measured in the ridge with $+$: 0.50m/s (light blue); \bullet : 0.75m/s (orange); $*$: 1.00m/s (blue); \times : 1.50m/s (purple); \blacktriangle : 1.75m/s (green); \blacksquare : 2.00m/s (red); \blacklozenge : 2.25m/s (dark blue). The velocities at the borders, i.e. at 0 and 30cm were assumed zero and do not represent measured values.

Relative measurement error

Values of E_q varied in the range of $8 \pm 5\%$ for the measurements in Set-up 2, thus successfully remaining below the $\pm 20\%$ limit. As this is in agreement to what was found in Set-up 1, the measurement method applied to the ridge was considered to be effective. Similar to Set-up 1, a dependence of E_q on the wind incidence angle can be seen in Fig. 5-5:B. Although in this set-up E_q

seems to reach lower values at wind incidence angles parallel to the vents, it presented an increased variability, as compared to Set-up 1.

In Fig. 5-6:B the relative contributions to the total inflow and outflow are shown. For all wind directions the contribution of the ridge to the inflow was nearly non-existent $0 \pm 1\%$. This means that the ridge can be considered a full and permanent outlet, independent of the wind incidence angle. A wind tunnel study by Choiniere and Munroe (1994) showed that at wind incidence angles close to 270° or 90° part of the ridge opening function fluctuated between in- and outlet. In present study it was assumed that the short length of the test facility's ridge compared to those found in commercial animal houses diminished this effect. The contribution of the ridge to the total outflow rate was relatively constant and therefore also independent of the wind incidence angle. The outflow contribution of the ridge varied in the range of $46 \pm 7\%$. Vents A and B showed a similar behaviour as in Set-up 1 where the in- or outlet character of the vents were determined by the wind incidence angle. Again the wind incidence ranges in which the inlets completely changed into outlets and vice versa were 50° to 120° and 250° to 300° . At approximately 90° and 270° there were cases in which both Vents A and B accounted for 50% of the inflow rate. The closer the wind incidence angle was to 180° or 360° , the higher the contribution to the inflow of Vent A or B, respectively. Fig. 5-6:B is summarised in

Table 5-5 where the data is classified amongst 4 ranges of 90° .

Table 5-5: Relative contribution of Vents A, B and C to the total in- or outflow rate through the test facility for set up 2, classified into 4 different ranges of wind incidence angles. Positive and negative values are relative inflow and outflow contributions, respectively.

	0-45° and 315-360°	45-135°	135-225°	225-315°
Vent A _{in} (%)	3 ± 7%	69 ± 37%	103 ± 5%	70 ± 37%
Vent B _{in} (%)	101 ± 9%	32 ± 37 %	2 ± 4%	32 ± 36 %
Vent C _{in} (%)	0 ± 0%	0 ± 0%	0 ± 0%	1 ± 1%
Vent A _{out} (%)	-46 ± 8%	-15 ± 13%	-3 ± 2%	-18 ± 15%
Vent B _{out} (%)	-4 ± 2%	-28 ± 13%	-48 ± 6%	-33 ± 14%
Vent C _{out} (%)	-46 ± 9%	-55 ± 8%	-44 ± 6%	-46 ± 6 %
N	82	57	579	115

5.3.2.3. *Conditions of cross and adapted ridge ventilation (Set-up 3)*

In Table 5-6 and Fig. 5-6:C it can be seen that the relative outflow rate contribution of the ridge was 20 to 30% higher than in Set-up 2. This effectively increased the contribution of the ridge measurement method on the relative measurement error. Values for E_q of $-9 \pm 7\%$ were found for the measurements in Set-up 3, remaining under the 20% limit. However, compared to Set-ups 1 and 2, a shift towards more negative values of E_q can be seen. In the ranges 45° - 75° , 75° - 105° and 275° - 315°

the values of E_q average around -20%. Although it is to be expected that in these ranges the measurement errors increase due to the more complex airflow patterns, it is not clear why this particular set-up seems to increase this effect. To determine whether the asymmetry of the side vent sizes was one of the influencing parameters, a more detailed view on velocity profiles and related indoor airflow patterns is necessary. It cannot be determined whether these negative values were due to an under- or overestimation of the inflow or outflow rate, respectively.

It should be noticed that the increase in the ridge's relative outflow contribution was only expected in situations where Vents A and B were full inlet and outlet, respectively. In such cases the outlet area through Vent B was 3 times smaller than that of the ridge. However, the relative outflow contribution of $77 \pm 7\%$ seemed to be approximately constant over all wind directions. Combined with the results found for Set-up 2, it can be inferred that the relative outlet contribution of the ridge was independent from the wind incidence angle, but strongly dependent on the side vents configuration. Experiments with more varied vent configurations should allow to derive the relation between the ridge's relative outlet contribution and the vent configuration.

In the range of $315^\circ - 45^\circ$, it was expected that Vent A would be completely an outlet with a relative inflow contribution of nearly 0%. However an inflow contribution of $20 \pm 14\%$ was found (see Table 5-6). This effect can also be seen in Fig. 5-6:C. There, the ranges in which Vents A and B changed from approximately 0 to 100% inlet contribution widened considerably towards 360° as compared to Fig. 5-6:A and B. This means that even with wind incidence angles near 360° , there existed cases where Vents A and B were still partially in- and outlets. These situations are more challenging for the measuring method and could be a partial explanation for the higher absolute values of E_q . This also suggests that the wind incidence angles in which a side vent can be considered a full in- or outlet is dependent on vent size configuration. Therefore, studies that rely on the assumption that a vent is a permanent outlet, e.g. for emission rate measurements, should account for this effect. In such cases, special care should be taken when the vent has a variable area, as when curtains are used.

Table 5-6: Relative contribution of Vents A, B and C to the total in- or outflow rate through the test facility for set up 2, classified into 4 different ranges of wind incidence angles. Positive and negative values are relative inflow and outflow contributions, respectively.

	0 - 45° and $315 - 360^\circ$	45 - 135°	135 - 225°	225 - 315°
Vent A _{in} (%)	$20 \pm 14\%$	$66 \pm 24\%$	$96 \pm 3\%$	$81 \pm 21\%$
Vent B _{in} (%)	$74 \pm 15\%$	$25 \pm 23\%$	$2 \pm 2\%$	$14 \pm 17\%$
Vent C _{in} (%)	$0 \pm 0\%$	$1 \pm 1\%$	$0 \pm 0\%$	$1 \pm 2\%$
Vent A _{out} (%)	$-17 \pm 6\%$	$-13 \pm 4\%$	$-5 \pm 3\%$	$-12 \pm 6\%$
Vent B _{out} (%)	$-7 \pm 3\%$	$-14 \pm 5\%$	$-25 \pm 4\%$	$-20 \pm 5\%$
Vent C _{out} (%)	$-82 \pm 7\%$	$-82 \pm 7\%$	$-73 \pm 4\%$	$-72 \pm 6\%$
N	125	188	360	37

5.4. Conclusions

A naturally ventilated test facility was adapted for cross and ridge ventilation schemes, to which an automated airflow rate measuring technique was applied. For the side vents, a technique developed in Chapter 4 was successfully adapted to larger vents ($0.5\text{m} \times 3.0\text{m}$) and a new technique was developed for the ridge. A validated pipe factor of 0.78 was attributed to the ridge. Detailed measurements of the velocity profiles in the vents were possible and the in- and outflow rates in each vent were processed separately.

It was found that the method for the side vents should account for all air velocity components, while the Y- and Z- components were essential to the calculations.

A relative measurement error between the building's total in- and outflow rate of $8 \pm 5\%$ was found for the most open set-up, successfully remaining below the self-imposed limit of 20%.

The relative contribution of a side vent to the building's total in- or outflow rate was dependent on the wind incidence angle. The range of wind incidence angles in which a side vent entirely contributed to an inflow or an outflow depended on the size of the vents. Outside these ranges, the vent gradually changed from completely contributing to the inflow rate to completely contributing to the outflow rate or vice versa, as a function of wind incidence angle.

The ridge had no considerable contribution to the inflow rate and was considered a complete and permanent outlet, independent of wind direction. Moreover, the relative contribution of the ridge to the total outflow rate was relatively constant since a standard deviation of only 7% was found throughout all measured wind incidence angles. However, measurements in two different set-ups showed that the ridge's relative outflow contribution was dependent on the side vents configuration.

Due to the complexity of the measuring technique it is practically and economically unfeasible to transfer the technique to a full size animal house. However, as the test facility is equipped with a validated measuring technique, it can be used for development, comparison and validation of new and existing airflow rate measuring techniques for use in naturally ventilated buildings. The design of these new techniques should be focussed on the possible transfer to very large vent sizes such as those found in cattle houses. Modelling is a possible way to reduce the complexity of the measuring technique. The test facility can be used to develop, validate and test such models. Although these models will probably not be directly transferable to other buildings, proving that certain modelling approaches work in the test facility can provide useful information to guide the research on full scale animal houses.

Chapter 6. Experiments under conditions of natural ventilation: complementary data-analysis towards reduced measurement techniques

6.1. Introduction

The method described in Chapter 5 was developed to give accurate measurements of the airflow rate through the test facility. It was essential for the correct functioning of this method to account for the possibility that a vent can function simultaneously as both an in- and outlet. This approach led to a technically complex installation which was not transferable to commercial animal houses. Although it was not within the scope of this research to develop such a directly transferable method, a first step towards a possible simplified measuring strategy was taken, which might lead to insights into the development of a more practical measuring technique.

Considering the actual ACNV systems in practise, it would be safe to assume that a farmer would be willing to install at least 1 static anemometer in an animal house for control purposes. However, the location of this sensor will be essential. In this chapter it is examined whether one static sensor could predict the airflow rate, and where the ideal location of this sensor would be.

Not only the airflow rate but also the velocity profile in the vents is important. For emission rate measurements it is necessary to know exactly where the outlets are situated at all times, as it is at these locations that the pollutant concentrations should be measured (Ogink et al., 2013). Pollutant concentrations measured at an inlet are in principle lower than those measured at the outlet. When an inlet is mistaken for an outlet due to incomplete knowledge of the velocity profile the emission rate will be largely underestimated. Additionally, measuring the air velocity at unrepresentative locations within a heterogeneous profile in a vent can lead to an under- or overestimation of the airflow rate. Therefore, the heterogeneity of the velocity profiles gathered in Chapter 5 (Set-ups 2 and 3) is studied.

6.2. Methods

6.2.1. Estimating the ventilation rate with 1 static 2D sensor

The aim was to find a method to estimate the airflow rate using only 1 static ultrasonic sensor. Two approaches were considered, i.e. using a 2D sensor placed within the test facility's vents (indoor sensor) and an external 2D sensor placed outdoors. The most suitable location of the indoor sensor had to be found. Therefore, firstly, the vent with the most constant relative contribution to the total airflow rate through the building was sought. Secondly, the measuring location within that vent was sought that had the most constant contribution to the airflow through that vent. The 2D-ultrasonic sensor on the meteoromast was taken as the outdoor sensor (see Fig. 4-2). This added to the simplicity as it was present during all measurements in Set-ups 2 and 3 (see Chapter 5) resulting in a large available dataset for this sensor.

6.2.2. Analysis of the velocity profiles

6.2.2.1. Relative effective outlet area

The area of a vent that acts as an outlet relative to the total area of that vent is referred to as the relative effective outlet area (A_{eff}). It was examined in which ranges of wind incidence angles the A_{eff} of a vent was close to 100%, which means that that vent was a complete outlet. As such it was also determined in what ranges of incidence angles the A_{eff} was most variable, resulting in a vent that was neither a complete in- or outlet.

6.2.2.2. Variability of the outlet velocity profile

Conducting emission rate measurements under conditions for which the A_{eff} differs significantly from 100% is not recommended without detailed velocity profile measurements. Otherwise, the uncertainty concerning the size and location of the outlets could lead to large errors. However, even when the A_{eff} is close to 100%, it cannot be assumed that a velocity profile is homogeneous. Measurements at unrepresentative locations within a heterogeneous velocity profile can lead to under – or overestimations of the airflow rate. Within a homogeneous velocity profile each measurement location within the vent would deliver the same relative contribution to the total airflow through that vent. It was examined if such profiles could be found in vents when the A_{eff} is higher than 95% and whether the wind incidence angle influences this homogeneity.

The high number of sampling locations in the side vents (12 rows of 4 measuring volumes for the 0.5m x 3.0m vent, see Fig. 5-3 in Chapter 5) makes it difficult to give a visual overview of the variability of the relative contributions of the different measurement locations. The profiles were simplified by taking the average velocity of the Y-components in each of the 12 columns and in each of the 4 rows to study the horizontal and vertical variability of the profile, respectively.

6.3. Results and discussion

6.3.1. Estimating the ventilation rate with 1 static 2D sensor

6.3.1.1. Indoor sensor

In all set-ups in Chapter 5 it was seen that the relative contribution to the in- or outflow rate of Vent A and Vent B both had large variations due to changing wind incidence angles (see Fig. 5-6, Chapter 5). Therefore, these vents are not a suitable location for the static anemometer. The ridge on the other hand did not have these large variations. For example, in Set-up 2, the highest inlet contribution of the ridge relative to the total inflow of the building was 6%, and in 95% of the measurements the contribution was lower than 1%. Therefore, the ridge was considered a complete and constant outlet. The relative outlet contribution of the ridge was $46 \pm 7\%$ and $77 \pm 7\%$ for Set-up 2 and 3, respectively. The relatively small standard deviation on these results underline the stability of the ridge's outlet contribution.

The measuring location within the ridge with the most constant contribution to the total outflow rate of the ridge can be found in Fig. 6-1. An average contribution of $12.5 \pm 1.4\%$ over all sensors was found. However, the variability of this contribution changed per sensor, while sensors 4 and 5 show the least. Sensor 4 was chosen for further processing. No data was available for sensor 7.

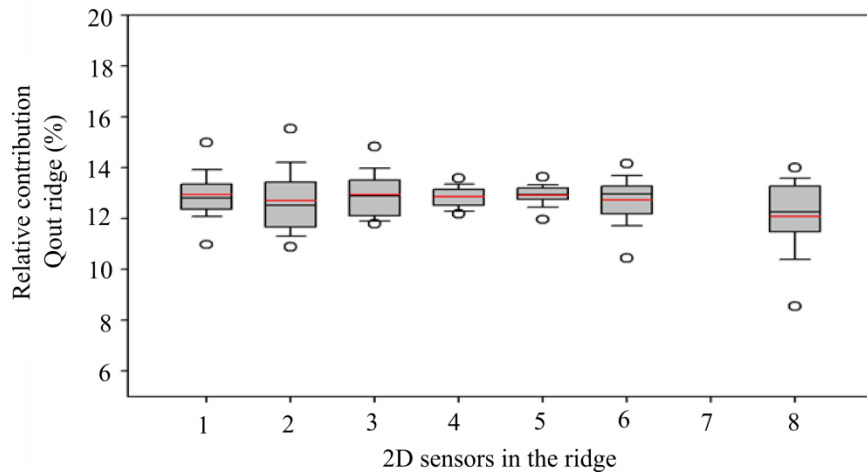


Fig. 6-1: The relative contribution to the outflow rate through the ridge ($Q_{out\ ridge}$) measured by each 2D ultrasonic sensor in that ridge. Data gathered from Set-up 2 in Chapter 5. Red horizontal lines indicate the means. Sensor 7 malfunctioned and did not deliver data.

A correlation coefficient of $R^2 = 0.97$ ($y = 9072x - 485$) and $R^2 = 0.99$ ($y = 6105x - 561$) between the average airflow rate ($Q_{avg} = (Q_{in} + Q_{out})/2$, for Q_{in} and Q_{out} see Chapter 5) and the air velocity measured by sensor 4 was found in Set-up 2 and 3, respectively. It was therefore concluded that one 2D-sensor in the ridge centre could be sufficient to give a good estimate of the airflow rate in Set-up 2 and 3. However, as was expected, the equation was clearly dependent on the set-up as the slope of the regression equation for Set-up 2 was 49% higher than the one for Set-up 3. This illustrates that these linear equations predicting the airflow rate will have to be determined case by case. Consequently the need for a more complex and accurate measuring system might remain for the validation or calibration of simplified measuring methods.

6.3.1.2. Outdoor sensor

Lo and Novoselac (2012) concluded that the ventilation rate of a naturally cross ventilated building correlates very well to the velocity component of the approaching wind which is normal to the inlet openings. This relation was confirmed for Set-ups 2 and 3 (Fig. 6-2) where the Y-component of the meteomast is shown in relation to Q_{avg} . However, it is clear that this relation will change according to different side vent configurations. For Set-up 2 it can be seen that two side vents of equal area resulted in a graph symmetrical about the Y-axis (Fig. 6-2). A difference in slope between the positive or negative Y-components of only 7% was found. In Set-up 3, where Vent A was 3 times the size of Vent B, the graph was clearly asymmetrical. Positive Y-components at the meteomast, i.e. wind blowing towards the largest vent, delivered on average more than twice the airflow rate as for negative Y-components. Considerably larger ventilation rates were found in Set-up 2, even for positive Y-

components. This was attributed to the internal pressure build-up caused by the smaller outlet area in Set-up 3 that counteracts the inflow of air. More different side vent configurations should be examined to determine how sensitive the airflow rate estimation model is to those changes in configuration. It must be noted that, especially for unequal vent sizes, the regression model should differentiate between positive and negative air velocities as these clearly induce a different slope steepness.

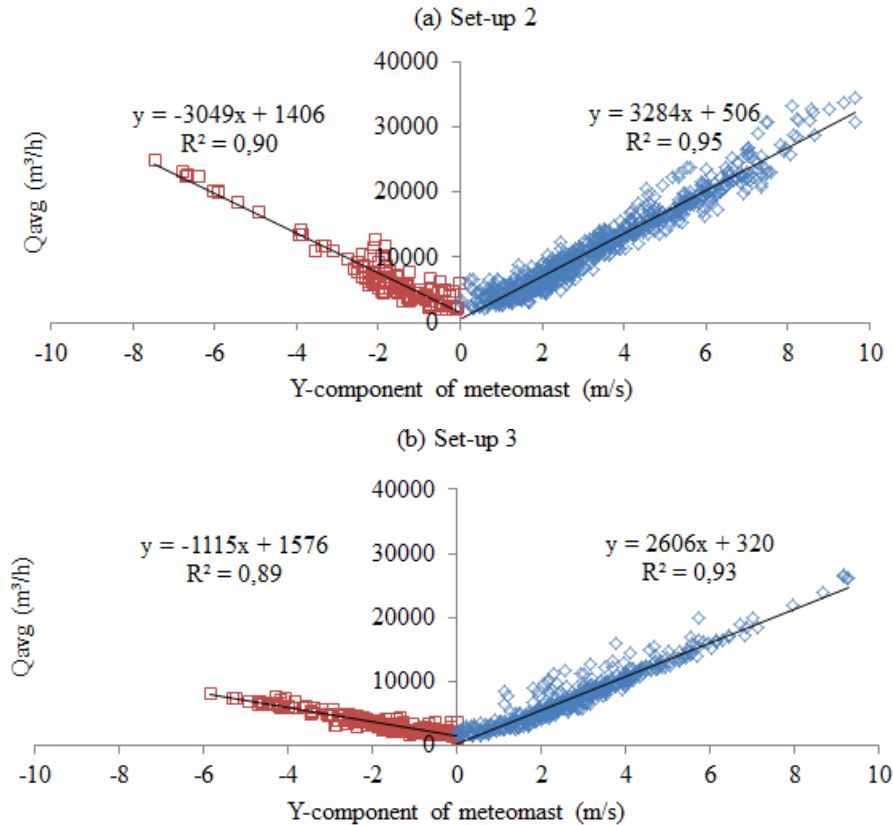


Fig. 6-2: The relation between the Y-component at the meteomast (m/s) and the average of the in- and outflow rates, Q_{avg} (m^3/h). A strong correlation is found and the linear regression equations are dependent on side vent configuration and direction of the Y-component. With (a): Set-up 2 and (b): Set-up 3. and \square : the negative Y-components measured at the meteomast \diamond : the positive Y-components measured at the meteomast.

6.3.2. Analysis of velocity profiles

6.3.2.1. *Relative effective outlet area*

During our experiments, as was proven in Chapter 5, the ridge can be assumed to have an A_{eff} of 100% irrespective of the wind incidence angle. However it must be noted that Choiniere and Munroe, (1994) and Choiniere et al. (1992) showed that with wind incidence angles close to parallel to the ridge, parts of the ridge can fluctuate between in- and outlet. Norton et al. (2009) even found that for wind incidence angles of 90° , 50% to 70% of the ridge area could act as an inlet (CFD simulation). This was not observed during our experiments, probably due to the relatively short length of the ridge in comparison to those in actual animal houses. In any case it is safe to state that a ridge vent is less variable than side vents. In Fig. 6-3:(a) the A_{eff} of the side vents in relation to the wind incidence angle

is given for Set-up 2. The vertical dotted lines show the ranges within which a side vent had an A_{eff} higher than 95% , i.e 120 to 240° and 290 to 50° for Vent B and A, respectively. All data points in the range of 120 to 240° that had a lower A_{eff} than 95% were due to very low average wind speeds ($\pm 0.1\text{m/s}$) in Vent B. In the range of 240 to 290° the A_{eff} was extremely variable, which agrees with the findings of Norton et al. (2009). In this relatively small range of 50° the A_{eff} dropped from 100 to 0% for Vent B and rose from 0 to 100% for Vent A. Not enough data was available for the 45 to 135° range, but still the same trend can be seen. For Set-up 3 it can be seen in Fig. 6-3:(b) that Vent A showed no characteristic range of wind incidence angles for which the vent was a complete outlet. Although this might be partly attributed to fewer data compared to setup 2, there is still a pattern visible that can support this statement. This implies that the wind incidence angle ranges for which vents were complete outlets, are dependent on the side vent configuration.

Fig. 6-3:(a) and (b) must not be confused with Fig. 5-6:B and C in Chapter 5. In Chapter 5 the relative contribution of a vent to the outflow rate was shown, while in present chapter the relative size of the outlet is given, both in relation to the wind incidence angle. Therefore, by combining the information delivered by these two types of figures, it is possible to determine how large the outlet area is and how it contributes to the total outflow rate under certain wind incidence angles. For example, in Set-up 2, with a wind incidence angle of 270°, 46% of Vent A acted as an outlet (Fig. 6-3:(a)) whilst 38% of the total outflow rate passed through that vent (Fig. 5-6:B). Such information can be very valuable for the set-up of emission rate experiments. During such experiments it cannot be expected that the wind incidence angle remains constant. Fig. 6-3:(a) shows that small variations in incidence angle can have a considerable impact on the in/outlet character of the vent when the wind direction is almost parallel to the vents (270°). Without a detailed measurement of the velocity profile, large errors can be made when vents are mistakenly considered to be complete in – or outlets. Therefore emission experiments should be avoided under such circumstances, unless the velocity profile is completely known.

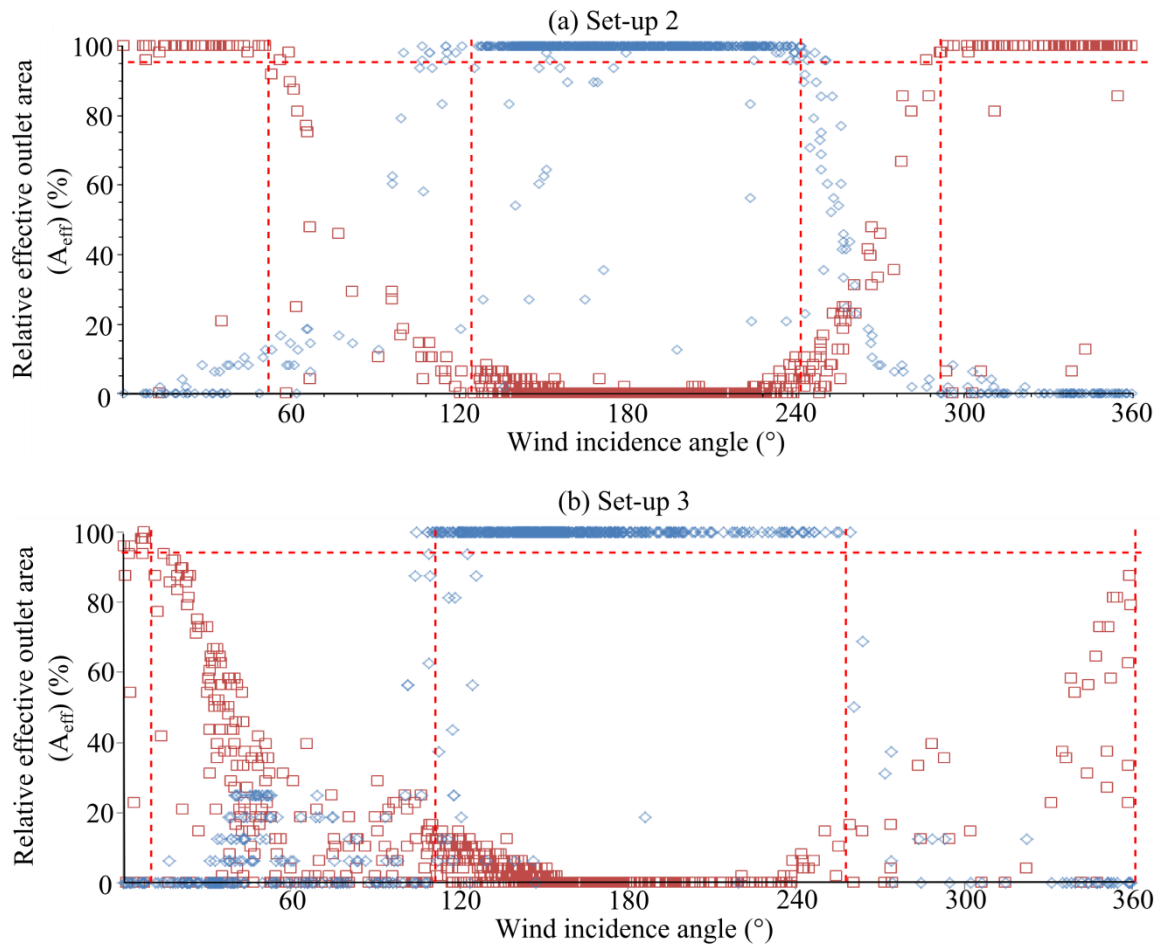


Fig. 6-3: The area of a vent acting as an outlet relative to its total area (A_{eff}) as a function of the wind incidence angle for set-up 2 (a) and 3 (b) with \diamond : A_{eff} of Vent B (blue); \square : A_{eff} of Vent A (red) Above the horizontal dotted line the A_{eff} is higher than 95%. The vertical dotted lines indicate the transition between zones with a stable A_{eff} and zones with a highly variable A_{eff} (visually determined).

6.3.2.2. Variability of the outlet velocity profile

Only the wind incidence ranges with A_{eff} higher than 95% were accounted for. As the ridge has a constant A_{eff} close to 100%, the complete range from 0 to 359° is discussed. However, for the side vents only the ranges 120° to 240° and 290° to 50° are discussed for Vent B and A, respectively, in Set-up 2.

Ridge

In Fig. 6-4 the influence of the wind incidence angle on the relative contribution to the ridge's outflow rate is shown for sensors 1, 5 and 8. The location of these sensors can be found in Fig. 5-2 in Chapter 5. The interlaying sensors S2, S3, S4 and, S6, gave similar patterns, with less variable contributions for sensors closer to the ridge's longitudinal centre. Over all wind incidence angles, the minimum and maximum contributions were 3% and 19%, 12% and 15%, 6% and 22%, for sensors S1, S5 and S8, respectively. This shows that although the ridge is a complete outlet, the velocity profiles are not homogeneous over all wind incidence angles. However, within the ranges of 120 to 210° and 315 to

45° even sensors S1 and S8, gave a relatively constant contribution as they remained within a range of 10 to 15% contribution. This infers that velocity profiles in these wind incidence ranges can be considered homogeneous.

The velocity profiles are comparable to the ones found by Choiniere and Munroe (1994). With wind incidence angles close to 90° or 270° the sensors at the sides reach a maximum or minimum relative contribution for the windward and leeward sensors, respectively. In Fig. 6-1 the relative contribution for all ridge sensors can be found.

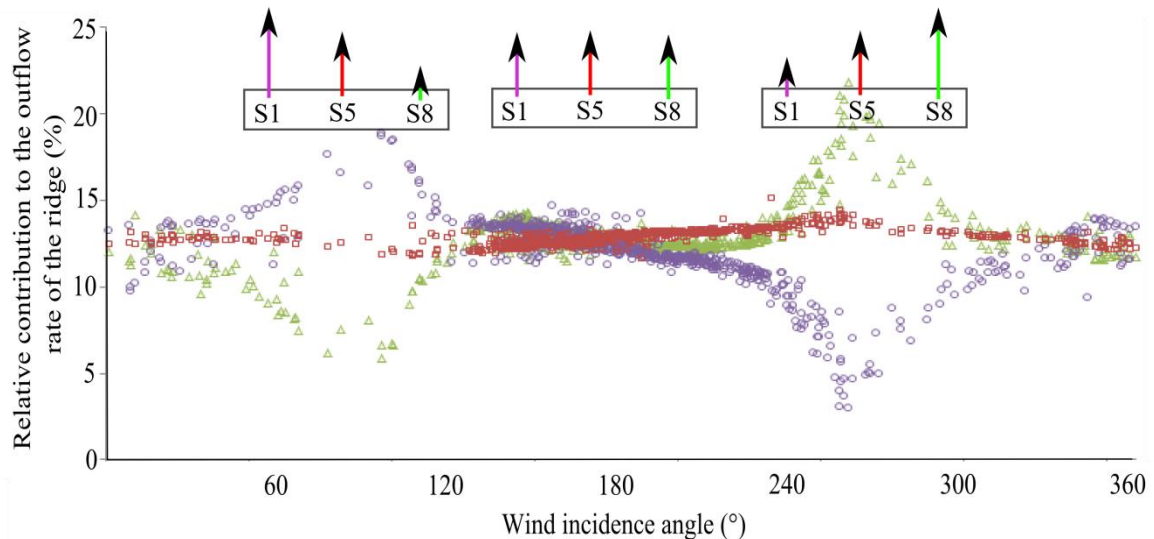


Fig. 6-4: The relative contribution of three 2DS sensors to the outflow rate through the ridge in function of the wind incidence angle, with: Δ : sensor 1 (green); \square : sensor 5 (red); \circ : sensor 8 (purple). Above, 3 schematic representations of the ridge with the coloured arrows representing the relative contribution of the three sensors influenced by the wind incidence angle. Data gathered from Set-up 2 (Chapter 5). Data from the other ridge sensors fall inside the range between the results from S1 and S8.

Side vents

In Fig. 6-5 the relative contributions of columns 1, 3, 5, 8, 10 and 12 to the outflow rate through Vent B is shown. It can be seen that the contributions of all columns remained mainly within 5 to 10% for wind incidence angles between 120° to 240°, with slightly lower contributions for the columns closer to the vent sides. This is visualised more clearly in the boxplot in Fig. 6-6 which again consists of all data from the wind incidence range 120° to 240° for Vent B (Set-up 2). Indeed all columns show a similar variability and in columns 1 and 12 the relative contribution decreases. In Fig. 6-7 the relative contribution of rows 1 to 4 to the outflow rate through Vent B is shown. On average a contribution of $21\pm 4\%$, $27\pm 2\%$, $28\pm 2\%$ and $24\pm 3\%$ was found for rows 1 to 4 respectively which is visualised more clearly in Fig. 6-8. This shows that the rows at the borders had a smaller contribution to the outflow rate than the rows at the centre which is attributable to the edge effects. Hence, a large part of the velocity profile can be considered to have a homogeneous distribution, i.e. the overlapping areas of columns 2 to 11 and rows 2 and 3 (see Fig. 6-9, green area) and can be accurately sampled with a lower measuring density. On the other hand, the remaining areas (red and blue) should each be

measured separately. It must be noted that these results are only valid in Set-up 2, within the wind incidence range where the A_{eff} was close to 100%.

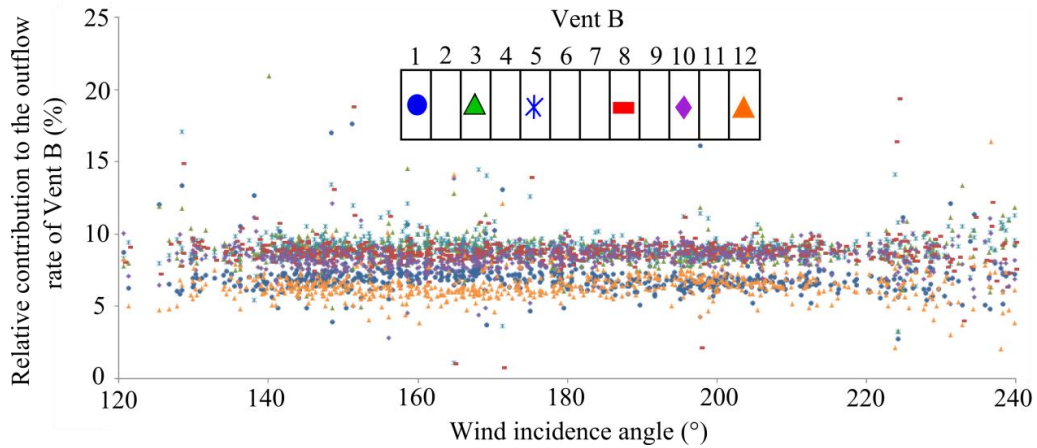


Fig. 6-5: Relative contribution to the outflow rate through Vent B for columns 1, 3, 5, 8, 10, 12. Added schematic representation of vent B illustrating the location of the twelve columns and associated symbols and colours. Data gathered from Set-up 2 (Chapter 5).

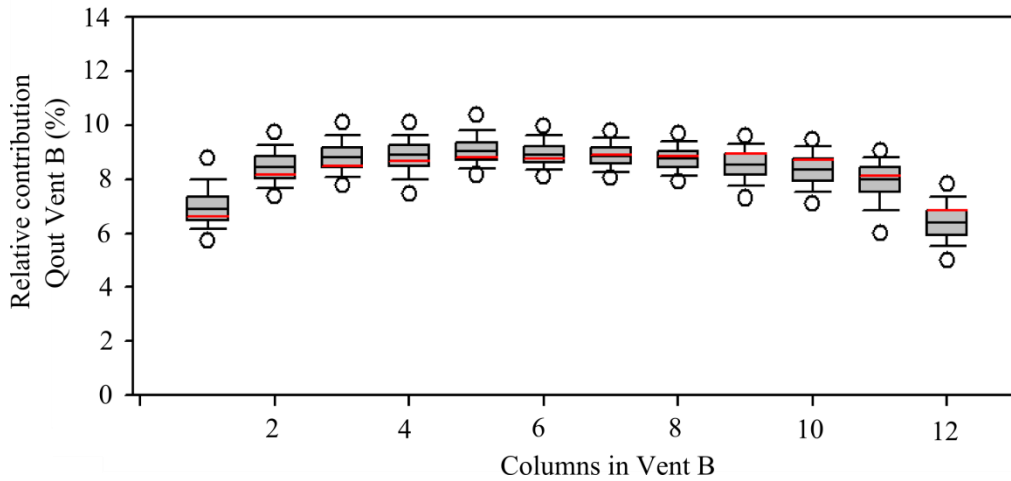


Fig. 6-6: Relative contribution to the outflow rate through Vent B (Q_{out}) for each column (see Fig. 6-5). Data gathered from Set-up 2 in the wind incidence angle range of 120° to 240° (Chapter 5). Red lines indicate the means.

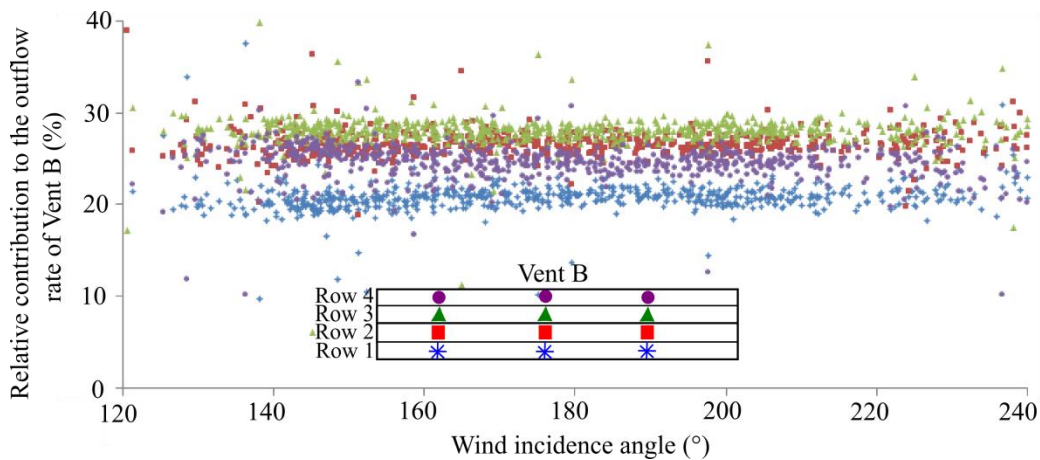


Fig. 6-7: Relative contribution to the outflow rate through Vent B for rows 1 to 4. Added schematic representation of vent B illustrating the location of the rows and associated symbols. Data gathered from Set-up 2 (Chapter 5).

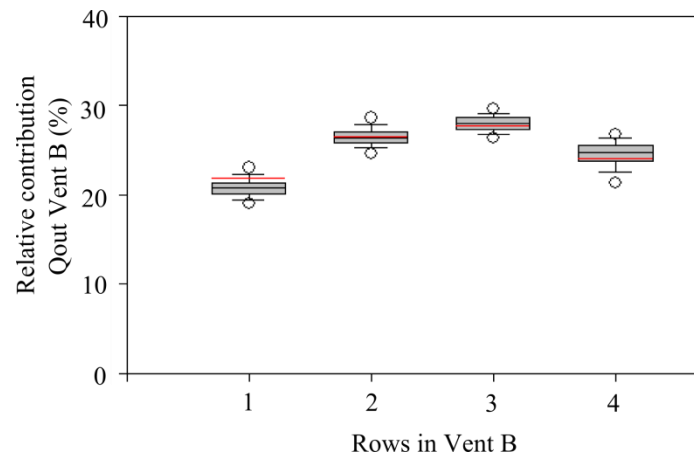


Fig. 6-8: Relative contribution to the outflow rate through Vent B for each row (see Fig. 6-7). Data gathered from Set-up 2 in the wind incidence angle range of 120° to 240° (Chapter 5). Red lines indicate the means.

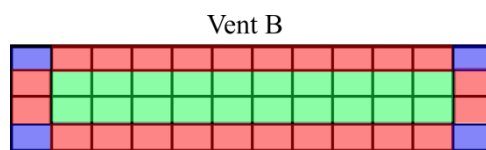
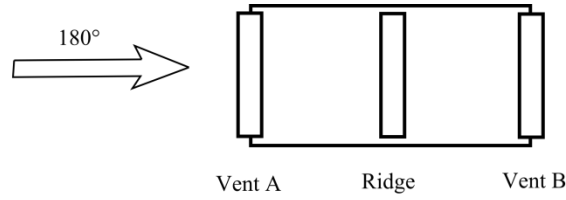


Fig. 6-9: Vent B divided into 9 different areas. All elementary surfaces within such an area have a similar and almost constant relative contribution to the outflow rate for wind incidence angles between 120° and 240° .

Illustrative examples of velocity profiles

From Fig. 6-10 to Fig. 6-13 the velocity profiles for both side vents and the ridge vent under conditions of different wind incidence angles and wind velocities are shown. It is clearly illustrated that wind incidence angles of 180° and 360° induce relatively heterogeneous profiles in the side outlet vent and the ridge. Also the decrease in air speed towards the borders of the side vents is visible. For the wind incidence angles of 90° and 270° , large differences in air velocity can be found along the length of the side vents and even in the ridge. Side vents became partial in – and outlets simultaneously under these conditions.



Wind incidence angle: 181° Wind velocity: 2.2m/s

Vent A

0.79	1.20	1.18	1.12	1.12	1.18	1.31	1.37	1.13	1.17	1.24	0.90
0.91	1.39	1.44	1.34	1.66	1.63	1.44	1.50	1.45	1.40	1.29	0.71
1.32	1.40	1.26	1.50	1.39	1.39	1.27	1.32	1.22	1.25	1.07	1.24
1.05	1.46	1.39	1.10	1.19	1.00	0.92	1.06	1.34	1.40	1.34	0.98

Vent B

-0.26	-0.32	-0.29	-0.27	-0.31	-0.35	-0.38	-0.40	-0.30	-0.32	-0.31	-0.33
-0.27	-0.44	-0.45	-0.44	-0.52	-0.54	-0.46	-0.48	-0.49	-0.40	-0.32	-0.30
-0.41	-0.45	-0.42	-0.50	-0.47	-0.48	-0.43	-0.39	-0.35	-0.37	-0.39	-0.43
-0.38	-0.40	-0.45	-0.42	-0.42	-0.43	-0.37	-0.36	-0.45	-0.48	-0.43	-0.28

Ridge

-0.74	-0.75	-0.77	-0.77	-0.77	-0.75	-0.74	-0.76
-------	-------	-------	-------	-------	-------	-------	-------

Wind incidence angle: 181° Wind velocity: 3.2m/s

Vent A

1.38	1.64	1.79	1.76	1.88	1.61	1.76	1.89	1.83	1.74	1.93	1.23
1.85	1.87	2.08	2.09	2.26	2.22	2.34	2.16	2.17	2.17	2.02	1.57
1.71	1.78	2.04	2.09	2.05	2.13	2.21	2.26	2.31	2.35	2.03	1.16
1.61	1.82	1.91	1.62	1.56	1.69	1.54	1.68	1.67	1.86	1.41	0.76

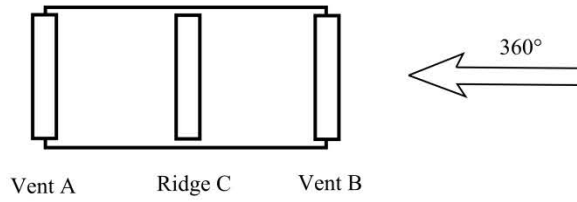
Vent B

-0.31	-0.38	-0.48	-0.45	-0.57	-0.54	-0.59	-0.55	-0.55	-0.49	-0.56	-0.50
-0.47	-0.61	-0.73	-0.73	-0.73	-0.71	-0.74	-0.70	-0.70	-0.71	-0.69	-0.59
-0.64	-0.71	-0.68	-0.65	-0.72	-0.72	-0.75	-0.76	-0.79	-0.75	-0.74	-0.47
-0.59	-0.69	-0.63	-0.61	-0.66	-0.58	-0.58	-0.58	-0.53	-0.52	-0.59	-0.37

Ridge

-1.08	-1.11	-1.14	-1.13	-1.12	-1.09	-1.08	-1.11
-------	-------	-------	-------	-------	-------	-------	-------

Fig. 6-10: Velocity profiles of Vents A and B and the ridge in Set-up 2, for wind incidence angles close to 180° for two different external wind speeds. Colours in the profiles are associated with the air velocities noted in each elementary measurement surface of the vents (Y-components). Positive and negative velocities(m/s) represent in- and outflows, respectively.



Wind incidence angle: 357° Wind velocity: 2.3m/s

Vent A

-0.19	-0.24	-0.25	-0.26	-0.30	-0.31	-0.29	-0.32	-0.35	-0.33	-0.31	-0.20
-0.27	-0.30	-0.30	-0.34	-0.34	-0.33	-0.37	-0.34	-0.37	-0.39	-0.35	-0.26
-0.25	-0.31	-0.32	-0.33	-0.40	-0.38	-0.37	-0.35	-0.35	-0.40	-0.35	-0.29
-0.15	-0.25	-0.27	-0.30	-0.26	-0.25	-0.26	-0.30	-0.30	-0.29	-0.32	-0.29

Vent B

0.39	0.96	1.05	1.18	1.24	1.12	1.12	1.15	1.15	1.15	1.24	1.27
0.44	0.88	1.14	1.32	1.30	1.23	1.30	1.32	1.27	1.28	1.34	1.45
0.29	0.78	1.19	1.39	1.36	1.29	1.32	1.23	1.23	1.28	1.28	1.35
0.09	0.47	0.87	1.01	0.64	0.67	0.62	0.66	0.72	0.74	0.76	1.13

Ridge

-0.62	-0.62	-0.62	-0.65	-0.66	-0.72	-0.70	-0.70
-------	-------	-------	-------	-------	-------	-------	-------

Wind incidence angle: 359° Wind velocity: 3.6m/s

Vent A

-0.46	-0.55	-0.61	-0.56	-0.57	-0.57	-0.58	-0.61	-0.53	-0.59	-0.58	-0.46
-0.54	-0.75	-0.75	-0.70	-0.72	-0.65	-0.65	-0.65	-0.67	-0.76	-0.76	-0.54
-0.60	-0.75	-0.74	-0.73	-0.65	-0.69	-0.75	-0.75	-0.79	-0.88	-0.82	-0.69
-0.41	-0.59	-0.56	-0.58	-0.64	-0.65	-0.65	-0.63	-0.81	-0.73	-0.80	-0.75

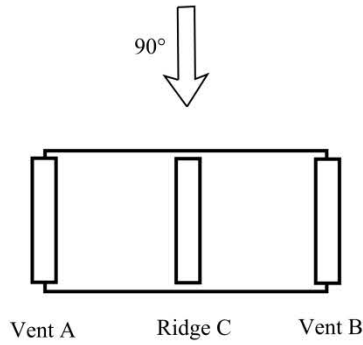
Vent B

1.26	2.04	1.97	1.57	1.74	1.67	1.76	1.43	1.60	1.64	1.77	1.71
1.34	2.08	2.36	2.26	2.13	2.10	1.97	2.02	2.13	2.29	2.42	1.79
1.87	2.37	2.35	2.32	2.07	2.09	2.19	2.29	2.45	2.49	2.63	2.25
1.17	1.72	1.75	1.60	1.74	1.57	1.72	1.61	2.04	1.97	2.23	2.13

Ridge

-1.12	-1.08	-1.04	-1.09	-1.02	-1.12	-1.05	-1.02
-------	-------	-------	-------	-------	-------	-------	-------

Fig. 6-11: Velocity profiles of Vents A and B and the ridge in Set-up 2, for wind incidence angles close to 360° for two different external wind speeds. Colours in the profiles are associated with the air velocities noted in each elementary measurement surface of the vents (Y-components). Positive and negative velocities (m/s) represent in- and outflows, respectively.



Wind incidence angle: 101° Wind velocity: 2.0m/s

Vent A

0.32	0.53	0.49	0.47	0.07	0.22	0.27	0.19	-0.02	0.08	0.03	-0.05
0.36	0.70	0.57	0.35	0.06	0.20	0.36	0.23	0.02	0.04	0.10	-0.05
0.32	0.56	0.41	0.36	0.22	0.28	0.26	0.30	0.01	0.16	0.08	-0.03
0.35	0.29	0.24	0.15	0.12	0.15	0.08	0.05	-0.03	0.43	0.40	0.34

Vent B

0.05	0.22	0.13	0.21	0.07	0.10	0.14	0.04	0.03	-0.00	0.00	0.01
0.07	0.19	0.20	0.24	0.06	0.16	0.08	0.06	0.02	0.06	-0.07	-0.01
0.19	0.21	0.13	0.17	0.03	0.25	0.11	0.08	0.05	-0.00	0.03	0.07
0.21	0.06	0.02	0.03	0.13	-0.01	0.02	-0.05	0.04	0.13	0.11	0.11

Ridge

-0.55	-0.55	-0.55	-0.51	-0.44	-0.39	-0.28	-0.26
-------	-------	-------	-------	-------	-------	-------	-------

Wind incidence angle: 92° Wind velocity: 3.0m/s

Vent A

0.54	0.40	0.30	0.40	0.18	0.00	-0.11	-0.02	-0.15	-0.33	-0.24	-0.13
0.79	0.63	0.44	0.53	0.15	0.14	0.03	0.09	-0.11	-0.28	-0.14	-0.09
0.80	0.41	0.29	0.22	0.34	0.34	0.11	-0.05	0.04	-0.12	-0.25	-0.09
0.73	0.26	0.28	0.33	0.35	0.36	0.17	0.08	0.18	0.13	0.21	0.00

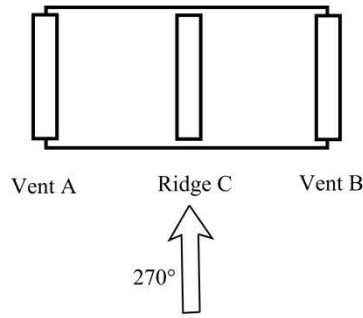
Vent B

0.60	0.43	0.29	0.28	0.29	0.27	0.17	0.09	0.13	0.22	-0.05	-0.12
0.72	0.56	0.49	0.32	0.31	0.33	0.36	0.44	0.21	0.07	-0.17	-0.00
0.76	0.80	0.77	0.73	0.42	0.30	0.54	0.50	0.22	0.16	-0.04	-0.11
0.87	1.06	1.00	0.96	0.86	0.43	0.58	0.44	0.23	0.30	-0.04	0.12

Ridge

-0.85	-0.85	-0.84	-0.76	-0.64	-0.53	-0.41	-0.33
-------	-------	-------	-------	-------	-------	-------	-------

Fig. 6-12: Velocity profiles of Vents A and B and the ridge in Set-up 2, for wind incidence angles close to 90° for two different external wind speeds. Colours in the profiles are associated with the air velocities noted in each elementary measurement surface of the vents (Y-components). Positive and negative velocities (m/s) represent in- and outflows, respectively.



Wind incidence angle: 279° Wind velocity: 2.1m/s

Vent A

-0.08	-0.03	-0.02	-0.04	-0.01	-0.01	0.05	0.12	0.12	0.08	0.15	0.26
-0.09	-0.09	-0.03	0.17	0.04	0.08	0.12	0.11	0.08	0.24	0.29	0.49
-0.02	-0.17	-0.03	0.04	0.06	0.12	0.09	0.14	0.37	0.33	0.31	0.48
0.11	-0.07	-0.01	-0.00	0.05	-0.03	0.10	0.00	0.31	0.25	0.34	0.22

Vent B

0.01	-0.06	0.02	0.07	0.13	0.20	0.25	0.15	0.39	0.30	0.23	0.50
-0.05	-0.06	0.03	0.11	0.27	0.23	0.26	0.36	0.25	0.29	0.45	0.58
0.05	0.04	-0.10	0.00	0.33	0.36	0.37	0.52	0.38	0.36	0.49	0.55
0.06	0.19	0.34	0.22	0.42	0.52	0.33	0.50	0.44	0.46	0.43	0.64

Ridge

-0.18	-0.25	-0.32	-0.40	-0.45	-0.52	-0.52	-0.55
-------	-------	-------	-------	-------	-------	-------	-------

Wind incidence angle: 268° Wind velocity: 3.0m/s

Vent A

-0.18	-0.13	-0.19	0.05	0.09	0.10	0.06	0.48	0.06	0.38	0.47	0.65
-0.11	-0.09	-0.06	0.00	0.15	0.12	0.13	0.29	0.39	0.58	0.81	1.08
-0.18	-0.09	0.05	0.19	0.25	0.16	0.47	0.31	0.65	0.90	0.77	1.08
-0.11	-0.04	0.10	0.13	0.23	0.27	0.42	0.33	0.72	0.66	0.83	0.82

Vent B

0.04	-0.17	-0.04	-0.04	-0.04	0.06	0.03	0.05	0.23	0.20	0.24	0.34
-0.05	-0.12	-0.09	-0.09	0.06	0.22	0.18	0.14	0.06	0.28	0.02	0.01
0.14	0.01	-0.14	-0.08	0.05	0.03	0.05	0.25	0.14	-0.03	0.15	0.12
0.02	-0.01	0.17	0.01	0.13	0.10	0.18	0.24	0.12	0.35	0.29	0.46

Ridge

0.07	-0.05	-0.18	-0.32	-0.44	-0.54	-0.61	-0.64
------	-------	-------	-------	-------	-------	-------	-------

Fig. 6-13: Velocity profiles of Vents A and B and the ridge in Set-up 2, for wind incidence angles close to 270° for two different external wind speeds. Colours in the profiles are associated with the air velocities noted in each elementary measurement surface of the vents (Y-components). Positive and negative velocities (m/s) represent in- and outflows, respectively.

6.4. Conclusions

As the developed methodology at this stage is too expensive and complex to be transferred to a commercial livestock building, an exploratory analysis was performed towards a more practical and reduced measuring technique. A strong correlation was found between the velocity component normal to the vents measured on a 10m high meteoromast and the total building's airflow rate. Also, a very strong correlation was found between an air velocity measurement in the longitudinal centreline of the ridge and the total building's airflow rate. Such findings could lead to simplified measuring methods for application in practice. However, it was also clear that all linear regression models found in this chapter were strongly dependent on the building's side vent configuration. This could imply that each set-up should be characterised by a different set of parameters. More research is necessary to examine the influence of different vent set-ups on the models.

The developed airflow rate measuring technique allows a detailed determination of the velocity profile in both side vents and the ridge vent. The ridge was a complete outlet independent of the wind incidence angle. Ranges of wind incidence angles were found (approximately 120° to 240° and 290° to 50° in Set-up 2) in which a side vent could be safely assumed to be a complete outlet. Within the range of 120° to 240°, it was shown that the outlet profiles in the side and ridge vents of Set-up 2 might be determined with a lower measuring density as large parts of the outlet area were characterised by similar relative outflow contributions. Needing less sampling locations would render the method more practical. By comparing Set-ups 2 and 3 it was found that these ranges changed according to the side vent configuration. This has to be taken into consideration when performing experiments in commercial animal houses where side vent configurations could change as a function of indoor climate requirements and outdoor climate conditions.

Knowledge concerning velocity profiles can be important for the correct implementation of emission rate experiments as gas concentration measurements should be taken at the outlet and corrected for background concentrations measured at the inlet. However, it must be noted that although a vent can be a complete outlet and might even have a homogenous velocity profile, it is not guaranteed that the gas concentration profile at that outlet is homogeneous. Therefore, a point measurement of the concentration taken at the outlet might not be representative of the whole opening (see 1.3.3). A homogeneous mixing of the pollutants throughout the whole animal house would, in principle, lead to strongly related velocity and concentration profiles. However, this cannot be assumed to be the case and should be checked by appropriate sampling throughout the building. Pollutant sampling locations in the outlet are thus subject to similar uncertainties as velocity measurements.

Chapter 7. General discussion and future perspectives

7.1. Development of the measuring method

As stated in the introduction there is a clear and urgent need for a reference technique for airflow rate measurements through naturally ventilated openings. Such a technique can play an essential role in the development of accurate emission rate measurement techniques and automatic control systems for the ventilation rate and indoor airflow patterns. The goal of this thesis was to develop a reference test platform, equipped with an accurate measurement method for velocity profiles and related airflow rates, where new and existing methods could be developed, validated, and calibrated. It must be noted that the focus of this thesis lies on the measurement of velocity profiles in the vents and the related airflow rates. Although indoor airflow patterns play a large role in the climate control of naturally ventilated animal buildings, they were not discussed in this thesis. A stepwise approach was followed, starting from controlled steady state experiments in a wind tunnel, up to experiments under varying wind conditions in a cross and ridge ventilated test facility in the open. The steady state wind tunnel experiments focused at the spatial variability of the velocity profile whilst the experiments in the test facility focused at the combined spatial and temporal variability.

7.1.1. Choice of building geometry

Takai et al. (2013) state that “ a better synergy between mathematical modelling, physical modelling and field measurements of ventilation rates in naturally ventilated livestock buildings is required”. Although experimental approaches such as scaled models in wind tunnels or CFD modelling can deliver valuable information, even then, experiments under conditions of natural ventilation are still essential as a validation tool. A choice had to be made between measurements in a full size mock up building or a real life commercial animal house. As this set-up was meant as a reference building where other techniques could be compared and developed, the commercial animal house was not a feasible option. In such a building the well-being of the animals has to be the main concern. Hence, the need to continuously adapt vent sizes to maintain an adequate indoor climate would make it difficult to perform long term measurements with fixed set-ups. Therefore the mock up building approach was followed. Such an approach has been used in other studies, but was predominantly focused at civil buildings (Lo and Novoselac, 2012; Park, 2013; Straw, 2000). These buildings evidently do not have the typical shape of an animal house with side vents, sloped roofs and ridge vents. As mentioned in the introduction, the building geometry can have a large influence on the ventilation rate and the airflow distribution. Therefore it was considered essential that the mock up building had the shape of a standard animal house. Hence, the test facility was based on a section of a pig house. Such a building was also present at the Silsoe research institute, i.e the Silsoe Structures Building, that was predominantly used to examine pressure distributions over the building envelope (Demmers et al., 2001; Richardson and Blackmore, 1995; Richardson et al., 1997).

7.1.2. Choice of measurement density

Most common direct measuring methods are based on sampling the air velocity in the vents and multiplying those results with the related vent area to obtain the in- and/or outflow rate (López et al., 2011a). As mentioned in the introduction the main source of uncertainty stems from the amount of sampling locations, i.e. the measurement density, that are deemed sufficient to deliver a representative average over the total vent area. Joo et al. (2014) stated that “establishing the minimum number of measurement points that do not compromise accuracy of emission rates at a reasonable cost” is a challenge for this type of measurement techniques. Knowing the lowest measurement density that delivers enough detail is only possible when the complete velocity profile is known. Therefore, to lower the uncertainty of such a direct measuring method, one should start with the highest measuring density that is practically and economically feasible.

Choosing ultrasonic anemometers has helped in obtaining high measuring densities. Unlike most of-the-shelf anemometers, the ultrasonic sensors do not give point measurements but the average velocities over their measuring paths (Barth and Raabe, 2011; Komiya and Teerawatanachai, 1993). The paths of the standard ultrasonic anemometers used in our study are relatively short ($\pm 0.2\text{m}$). However, when they are virtually concatenated by moving the sensor approximately one path length per sampling location, a high measurement density can be reached with a relatively low number of measurement locations compared to e.g. applying point measurements with a hotwire anemometer. This property of the sensors has not been used in most other studies concerning natural ventilation. Some examples can be found for the application in cylindrical gas distribution ducts (Drenthen and de Boer, 2001). The measurement density in our research was adapted to take maximum advantage of this effect. It is also at this point that our approach differs from other studies where the choice in measurement density seems to be predominantly driven by sensor availability or cost of the set-up due to the large size of the vents (Joo et al., 2014). The wind tunnel tests had proven that for a steady state velocity profile, the method took sufficient sampling points to accurately determine a heterogeneous velocity profile (Chapter 3). Therefore the same measurement density was adopted for measurements under conditions of natural ventilation.

Applying a large number of anemometers to reach this measurement density is not a feasible solution as this would possibly obstruct the airflow and certainly increase the total cost of the method. Already from the wind tunnel experiments it was decided that traversing a vent with one anemometer was the only viable option. Other studies have also applied this approach to larger vents (Boulard et al., 2000, 1997; López et al., 2011a; Molina-Aiz et al., 2009). However, varying outside conditions will result in time dependent measurements. The abovementioned studies handled these phenomena by: 1) measuring only at constant wind incidence angles and 2) normalising the measured air velocities using a fixed outside reference measurement. Naturally, a constant wind incidence angle does not occur and a certain amount of variation will be unavoidable. However, Campen and Bot (2003) showed that, in

the case of greenhouses, variations in wind incidence angle as small as 10° could change the airflow rate by up to 50% in some cases. This effect can also be observed in Chapter 4 Fig. 4-18. Furthermore, the stability of the wind incidence angle can be dependent on the region or season, influencing the time frame in which measurements can be performed with a nearly constant wind incidence angle. Some studies needed to discard large parts of their datasets as wind incidence angles were not optimal (Lengers et al., 2013). However, a reference airflow rate measuring technique should be reliable and applicable under all wind incidence angles. When the wind velocities are normalised to account for changing wind conditions the variations of the wind velocity in the vents are assumed to be directly proportional to the variations of an external fixed reference (Molina-Aiz et al., 2009). However, it cannot be excluded a priori that this proportionality might be dependent on the measuring location inside the vent and on the wind incidence angle. Therefore, it was chosen to develop a method that was independent of the stability of the wind incidence angle and had no need for the normalisation procedure. To take into account the temporal variability of the velocity profile, measuring each sampling location within the vent for 10s and repeating the complete vent traverse for 10 times was found to be the most satisfactory sampling strategy (Chapter 4).

7.1.3. Necessity of 3D air velocity measurements

The high measurement density (see 7.1.2) together with the need for continuous measurements imposed the automation of the anemometer's traverse movement. Consequently, the only practically feasible location for the ultrasonic sensor was directly behind the vent. At this location the flow could no longer be considered unidirectional. Indeed, in both the wind tunnel (Chapter 3) and test facility experiments (Chapter 4 and 5) it was shown that to obtain a measuring method that was independent of flow disturbances or profile shape, measuring the X- Y- and Z-components of the air velocity around the borders of the vent was necessary (with the Y-component normal to the in- or outflow plane and the Z-component the vertical velocity component). Doing so, the measuring method was able to account for the fanning out or narrowing of the flow depending on it being an in- or outflow, respectively. In some cases the airflow rate contributed by the Z-components was equal to 39% of the total airflow rate through that side vent when it was a complete outlet. On the other hand when a side vent was a complete inlet the relative contribution of the Z-components was less than 16% (see Chapter 4, Table 4-3). Therefore, our study showed that the relative contribution of the Z- components was also dependent on the wind incidence angle.

It must be noted that the necessity of a 3D measurement only applies to the measurements made at the edges of the vent, i.e. measuring the flow through the side, top and bottom planes of the combined traverse plane (Fig. 5-3). Therefore this aspect will possibly be less crucial in larger vents where the ratio of the vents' front plane area to the total area of the border planes is much higher. From the experiments in this thesis it was not possible to estimate when this ratio would be high enough to ignore these edge effects. However, it is assumed that in large vents, such as those typically found in

dairy farms, measuring velocity components other than normal to the vents would be unnecessary. In any case, there were no studies found where the ventilation rate was measured in large vents with more than the velocity component normal to the vents.

At least two studies experimented with small opening sizes where the ventilation rate was measured by an ultrasonic anemometer. Straw (2000) did measurements in a cross ventilated cubical structure with openings of 1.0m x 1.0m. He found that measuring only the normal velocity component in the centre of the vent and multiplying it to the vent area does not give a representative airflow rate. He used CFD to compensate for the low measuring density. Larsen (2006) carried out wind tunnel measurements in a cross ventilated full scale structure with vents of 0.15m x 0.86m. Again, only the normal velocity component was measured. However, the measurements were taken inside the vent opening (depth of 0.1m) instead of behind the opening. This might have prevented the airflow of fanning out at the measurement plane, possibly making the measurement of X- and Z-components unnecessary.

It must be noted that ridge measurements were taken within the ridge cross section. Therefore, similarly as Larsen (2006), only the velocity component normal to the outlet plane was taken into account.

7.1.4. Determining the accuracy of the measuring method

Currently there is no airflow rate measurement technique for naturally ventilated flows that is proven to be accurate enough to be considered the reference technique (Ogink et al., 2013). Without a reference there exist two main ways of estimating the accuracy of airflow rate measurement methods, i.e. comparison to other methods under the same circumstances (Kiwani et al., 2013), or by relying on the conservation of mass (López et al., 2011a; Molina-Aiz et al., 2009). Comparing methods of which none are suitable as reference techniques could evidently lead to large errors. When all methods give results that are in the range of realistic values, it is difficult to state which method performs better. Additionally, the range of realistic airflow rate values can be very large. Relying on the principle of mass conservation, which in our case translates into the inflow rate equalling the outflow rate, does not guarantee an accurate measurement technique. When measurements of both inflows and outflows have a similar under- or overestimation of the actual airflow, a closed balance could still fail to estimate the true absolute airflow rates. However, it cannot be avoided to use one of these methods as it is essential to obtain an idea of the accuracy of the developed method. As in all our experiments in the test facility the airflow rates through all vents were simultaneously measured, mass conservation was the logical approach.

It must be noted that side and ridge measurement methods have been tested under a large range of wind incidence angles and velocities and that these conditions strongly affected the velocity profiles in the vents (see Chapter 6 and section 7.1.5). It was also shown that the profile shape in the side vents caused by an inflow or an outflow was substantially different in terms of heterogeneity and

contribution of X- Y- and Z-components. Under all of these different external conditions, the different profiles in all vents were measured with such an accuracy that the relative difference between in- and outflow rates did not surpass the 20% limit. It was shown that wind incidence angles close to 90° or 270° induced complex velocity profiles in both side vents (Chapter 6). Although, in such cases the variation on the relative measurement error increased compared to incidence angles close to 180° or 360°, it still remained below the 20% limit. In any case, the extensiveness and variety of the performed experiments will reduce the risk that all in- and outflow rates were over- or underestimated similarly. Other studies where in- and outflow rates were compared as a validation tool found relative measurement errors of 12 to 19% (Joo et al., 2014), 1 to 28% (López et al., 2011b) and -3 to 37% (Molina-Aiz et al., 2009). However, none of the studies could give an in depth insight into the influence of the wind incidence angle on the relative measurement error, partly due to the lack of long-term measurements.

7.1.5. Measurement of velocity profiles

At the Silsoe research institute there exists a mock up building for natural ventilation measurements (“the Cube”) that can be turned towards different wind directions. Such a feature can be of great value as much of the research on natural ventilation concerns the effect of wind incidence angles on airflow rates or patterns (De Paepe et al., 2013; Nikolopoulos et al., 2012). Such a feature was infeasible in our case due to practical limitations. This meant that the amount of data that could be collected for the different wind directions was entirely dependent on the wind conditions. Evidently the largest amount of data was gathered for the predominant wind direction (South-West). It is important to have an in depth insight into these conditions as they are the most prevalent in practice. However, it was our aim to validate the method under a more or less continuous range of wind incidence angles, and not only the predominant one. When there are no obstructions in the surroundings of the building and the vent sizes and building geometry are symmetrical, the number of measurements can be reduced accordingly (Teclé et al., 2013). Hence, measurements in a range of 180° to 90° or 270° (with 180° equal to normal to the side wall) could be sufficient. However, this is rarely the case. The experiments in this thesis were continued until a sufficient amount of data was gathered for different combinations of wind speed and incidence angle. In total, more than 3000 sets of velocity profiles were measured and processed, gathered in 4 different naturally ventilated set-ups. Still, some wind incidence angles occurred so rarely that these were underrepresented in the data. However, due to the automation of our measuring technique allowing continuous measurements, the amount of data gathered from other than the predominant wind direction is considerably higher compared to other studies. Evidently, studies where anemometers were moved manually had a much more limited amount of data. For example López et al. (2011) and Molina-Aiz et al. (2009) each had only 4 complete airflow rate measurements. On the other hand studies where multiple static sensors were used, had large datasets but low measurement densities in the vents (Joo et al., 2015, 2014).

It must be noted that all data was gathered for wind effect only. Although stack and wind effect often occur simultaneously in animal houses (Zhang et al., 1989), it was not considered necessary to simulate the stack effect by adding heat sources in the test facility. The measurement method was developed to accurately determine the velocity profile through each vent, irrespective of the cause of this profile. Hence, adding heat sources might have an influence on the profiles themselves, but not on the accuracy of the measuring method.

Few studies have been found where the velocity profiles in the vents were studied in detail. Some studies delivered such information through CFD modelling (Nikas et al., 2010; Teitel et al., 2008b). Other studies in wind tunnels (Choiniere and Munroe, 1994; De Paepe et al., 2013; Larsen, 2006), or studies in full scale commercial greenhouses (López et al., 2011a) or livestock buildings (Kiwani et al., 2012) also delivered some information on the velocity profiles, albeit less detailed. And while the wind incidence angle is one of the most influential parameters of the profile shape, none of the abovementioned studies gives detailed profiles for more than a few distinct incidence angles. This is in contrast to our study where each pair of data points (relative inflow and outflow contribution) shown in Fig. 5-6 in Chapter 5 represents a complete and detailed measurement of the velocity profile (as shown in Chapter 6). The velocity profiles, and especially those in the side vents, were measured in more detail than in the mentioned studies (not accounting for CFD models). Additionally, measurements were carried out for a much larger range of wind incidence angles.

The velocity profiles found in our experiments followed similar patterns as those found in literature. Although the study of Choiniere and Munroe (1994) was performed in a wind tunnel, it was the most comparable study in terms of building geometry where the effect of different wind incidence angles (180°, 150°, 120° and 90°) on the airflow patterns in the ridge and side vents were studied. The profiles in the side vents were more or less homogeneous for wind incidence angles close to 180° or 360°. The variations in the profiles became larger as the wind incidence angle deviated further from 180° or 360° to reach the most complex profiles around 90° and 270°, where side vents acted simultaneously as in- and outlet (Norton et al., 2009). The velocity profiles in the ridge also showed larger variations towards incidence angles closer to 90° and 270°, albeit less pronounced.

The high degree of detail in which the velocity profiles were measured made it possible to make a more substantiated estimate of the wind incidence ranges in which vents remained complete in- or outlets. This is valuable information for emission rate measurements that need the exact locations of the outlets. For the side vents it was shown in Chapter 6 that there exists a wide range of wind angles, approximately 120° to 240°, where a vent is a complete outlet. However outside this range, the outlet can change into a complete inlet over a relatively small range of approximately 50°. This was in contrast to the findings in the ridge where it was shown that the ridge remained a complete outlet irrespective of the wind incidence angle. However, Choiniere and Munroe (1994) found that in some cases (incidence angles of 120° and 90°) part of the ridge could fluctuate between in- and outlet. This difference was attributed to the larger (relative) length of the ridge in their scale model.

It was also found that the relative contribution of the ridge to the total outflow rate was relatively constant (standard deviation: 7%) throughout all wind directions. Again this is very different from side vents that vary from 0% to 100% relative outflow contribution depending on the wind incidence angle. The independence of the relative outflow contribution of the ridge to the wind incidence angle makes it very promising for the development of measuring methods with a reduced number of measuring points (see 7.2.2)

7.2. *Transferability to commercial animal houses*

7.2.1. Experimental set-up

As the gable walls of the test facility are close to each other (5m), they will certainly have a considerable impact on the velocity profiles in the vents and the airflow patterns inside the building. This effect will be less pronounced for wind incidence angles normal to the vents (De Paepe et al., 2013) i.e. wind angles of 180° or 360°. For these conditions transferring the conclusions made in the test facility concerning velocity profile shape to wider commercial buildings might be possible. On the other hand, the more the wind incidence angle deviates from normal to the vents, the more influence the gable walls will have on patterns and profiles. In any case, the small width of the test facility will have made the velocity profiles more heterogeneous, therefore subjecting the measuring method to a worst case situation.

The measuring method in the side vents was not designed to be transferable to a commercial building. It is practically infeasible to automatically move a sensor across vents that can be tens of meters long. There are not only the technical and economical obstacles, but also the dangers of a continuously moving sensor near farmers and/or animals. Additionally, maintaining the absolute measuring density in these large vents, i.e. 32 samples per m², would lead to extremely high measuring times. Considering the small vents in the test facility as a scaled version of the large vents in commercial animal houses might lead to the assumption that 48 measuring locations, equally distributed over the vent area, would be an adequate measuring density. However, without validation measurements in larger vents there is no evidence that this approach would be satisfactory. In any case, as an automatic movement would not be possible and a manual movement would impede long term measurements, a large amount of static sensors would be necessary. It is clear that for commercial buildings a strongly reduced method is required. Additionally, as long as the method relies on non-simultaneous measurements, the temporal variability of the velocity profiles will be a source of inaccuracy. To account for this variability the vents are repeatedly traversed to obtain representative averages of the airflow rate. However, this resulted in a measuring method with an execution time of 1h32min. For future use in ACNV systems, this output frequency is much too low. Therefore developing a faster measurement method could not only further reduce the influence of profile fluctuations but also increase the applicability of the method. It must be noted that this only applies for the side vents as the

measurements in the ridge were performed with 7 static ultrasonic 2D sensor. In conclusion, to make the method transferable to commercial animal houses it will need to be based on few measuring points and deliver airflow rate values at a higher rate (see 7.2.2).

7.2.2. Reduced measurement methods through modelling

The experiments in the test facility have shown two reduced approaches that seem to be promising, i.e. estimating the airflow rate through measurements at the longitudinal centre of the ridge only (linear regression with $R^2 = 0.99$) or at a nearby meteomast (linear regression with $R^2 = 0.89$). Evidently, the linear model behind both approaches could only be found when the airflow rate is known beforehand, i.e. measured by the complex method. Although only two different cross/ridge ventilated set-ups were examined in Chapter 6, it was clear that the model was dependent on the side vents configuration. It is expected that every parameter that will have an influence on the airflow rate should be included in the model. These parameters can be subdivided into static parameters such as building geometry, building surroundings and pen configuration, and variable parameters such as wind incidence angle and speed, temperature differences between in- and outside of the building, vent permeability, amongst others. These parameters are discussed in the introduction. The large variability that can occur within these parameters and the possible interaction between them, infers that each building might need a unique calibration of the model for predicting the airflow rate accounting for external and internal governing climate conditions. This means that methods based on velocity measurements limited to the ridge or a meteomast will need to be calibrated and/or validated by another method that delivers more detail on the airflow rate distribution through all the vents. The downside of this conclusion is that the need for complex and detailed measurements cannot be discarded. However, it also shows that after a calibration / validation period, the complex method might be completely replaced by models and a relatively small number of sensors. For research purposes this would mean that part of the equipment can be recuperated after a certain time and used for other experiments, whilst long term measurement can be performed with a minimum of remaining equipment. For commercial purposes a supplier of ACNV systems could make the calibration equipment available for a certain time after which it is removed and installed on the next newly built animal house. Additionally, the more different animal houses are measured with the complex technique, the stronger the models can become. This might eventually shorten validation/calibration time to a minimum.

It must be noted that the models given in Chapter 6 do not give any information on the velocity profile. The complexity of the model will be dependent on the degree of detail in which the profile needs to be known. Avoiding black box modelling will provide insights into the many influential parameters. However, due to the large variety of parameters this might not be a feasible solution and applying modelling approaches such as response surface methodology (Shen et al., 2013) or artificial neural networks (Ayata et al., 2007; De Vogelee et al., 2014) could be more appropriate.

7.2.3. Development of new techniques

Due to the extensiveness of the experiments under a large variety of external conditions, a unique test platform was created. The in depth knowledge of the velocity profiles and the associated airflow rates through each vent, create possibilities for the development, the calibration and the validation of new airflow rate measurement techniques. These techniques need to be designed to allow the transferral to commercial animal houses. Although the test platform would not give definitive conclusions on how a new technique would perform in real life animal houses, it can give strong indications on its ability to cope with the highly variable conditions in the vents.

7.3. Future perspectives

The test facility can be used to develop, calibrate and validate new airflow rate measurement techniques. Ideally, as our method would act as a reference, a higher output frequency than that of the technique under development is needed. At the moment the developed method has an output rate of 1 per 92 minutes, due to the multiple traverses and the high number of sampling locations. In some cases this frequency could be a limitation for the development of new techniques, especially for airflow rate control techniques. When such a technique needs to be transferred to a commercial animal house, the complexity and total cost of the technique are important parameters. In any case, it is practically and economically infeasible to transfer the developed method as is, to a commercial animal house due to the method's complexity.

Both the increase in output frequency and the decrease in method complexity can be obtained by developing models that only need a small amount of input sensors. The extensive datasets that were gathered during our experiments can serve as the basis for such model development efforts. Ideally, the model should be able to predict the air velocity profiles and the related airflow rates in each vent. It is clear that such a model will at least need representative air velocity and wind incidence angle data as input parameters. The data gathered in our test facility can be used to determine the ideal location of the air velocity measurements and its relation with the profiles and airflow rates. As mentioned in the discussion, the ridge and meteomast are promising sampling locations. It must be clear that although the measurements in the test facility are a stepping stone towards measurements in commercial animal houses, there is no guarantee that the results and related models are transferable without additional research. For example, the ridge in the test facility has a very small length compared to those of commercial animal houses. It is possible that the amount of sensors needed to characterise the airflow through the vent will be proportional to the length of the vent. Evidently, the less measurement locations are needed, the cheaper the complete method. As a lower measurement density would be allowed, the need for moving sensors would decrease. The sensor movement was the main reason for the low output frequency of the method. An optimum has to be found between the amount of velocity profile detail that the model can deliver and the cost and practical feasibility of the method.

When focusing on the transferability of a predictive model to a commercial animal house, the influence of building geometry and location, vent size, internal pen design, heat sources a.o., on the model should be accounted for. The test facility can be used to gain insight into the variability or sensitivity of these models by examining variations on some of the influencing parameters. Although linear regression models often seemed to be satisfactory for the results in this thesis, accounting for parameters such as stack effect, pen design, vent size, and others, will significantly increase the complexity of the models. In a follow up project, the possible use of grey or black box modelling will be examined to cope with these additional parameters.

Even though the test facility can give insights into the sensitivity of a model, it cannot be assumed that the model would directly apply to commercial animal houses. Therefore, there is still a need for techniques based on direct measurements of the airflow rate and velocity profile, applicable in commercial animal houses, that can be used to calibrate the model. The test facility could be used as a test platform to develop and validate new or existing techniques that serve such a purpose. The focus must lie on the transferability of the developed methods to a commercial animal house, i.e. accounting for large vents, changing vent sizes, harsh environments, and others. There already exist several techniques to measure the airflow rate in naturally ventilated buildings (tracer gas tests, air velocity measurements combined with normalisation, differential pressures). These techniques could all be compared to the method developed in this thesis and where possible improved and validated or their shortcomings examined. New techniques such as the one described by Lule et al. (2014) can be examined and compared. This method is based on the heat dissipation from a line source to characterise the ventilation rate.

Research efforts should also go towards the design of the vent openings and related air guidance systems. They are primarily essential for the control of the airflow rate and possibly the airflow pattern. However, a well-designed vent might be able to reduce part of the turbulences caused by the vent's borders, thus improving the homogeneity of the velocity profiles. A more homogenised profile could possibly be determined by less measurement locations.

Additional to the knowledge of the velocity profiles and related airflow rates, the understanding of how these are linked to the internal airflow pattern is of much importance. As mentioned in the introduction, when an airflow pattern is properly guided, high airflow speeds over emitting surfaces could be avoided, reducing the release of NH_3 , whilst delivering an adequate indoor climate. Ideally the control of airflow rate and indoor airflow patterns should always go together. During experiments with different vent sizes, ultrasonic anemometers can be distributed inside the test facility to obtain information concerning airflow patterns. Especially cases where the side vents have different opening areas can be interesting as this is a much applied strategy in practice. Installing commercially available airflow valves or windscreens on the vents of the test facility could also be a possible research setup. However, the fixed relatively small size of the side vents could be an obstacle.

The test facility is also an ideal structure for the development and validation of CFD models, as the geometry is relatively simple and velocity profiles can be used as boundary conditions. A CFD model of the test facility and its immediate surroundings can be developed to gain insight in the different airflow patterns related to the airflow rate distributions through all vents. The model could be validated against measurements made in this thesis supplemented with measurements of the internal and external flows using 2D or 3D anemometers. The external flows are also of importance as these flows are responsible of negative pressures at the ridge which influences the flow pattern and rate. Also, as the maximum side vent size in the test facility is limited to 0.5m x 4.0m, a CFD model could be of use to simulate larger vent sizes and examine the effects on the airflow pattern. This might allow comparisons with the larger vents found in dairy farms.

Knowledge of the airflow rate and especially the velocity profiles in the vents are of great value for emission rate measurements as the location of the outlets needs to be known at all times. All progress made, whether through a modelling approach or the development of an accurate direct measuring technique, is a step closer to reliable and accurate emission measurements. The relation between gas concentration profiles in the vents and the velocity profiles might not be directly proportional, especially with an incomplete mixing of the pollutant and the indoor air. Therefore, also for the gas concentration profiles a high measurement density could be recommended. In the test facility the release of pollutants can be simulated. Detailed measurements of gas concentrations throughout the room combined with an airflow rate or pattern measurement can give insight into the relations between gas concentration distribution and air velocity patterns and profiles.

References

- Albright, L.D., 1990. Environment Control for Animals and Plants, ASABE Textbook. ASABE, St. Joseph, MI, U.S.A.
- Allard, F., 1998. Natural Ventilation in Buildings: A Design Handbook, James and James Ltd., London.
- Andonov, K., Daskalov, P., Martev, K., 2003. A New Approach to Controlled Natural Ventilation of Livestock Buildings. *Biosyst. Eng.* 84, 91–100. doi:10.1016/S1537-5110(02)00218-0
- ASHRAE, 2009. ASHRAE handbook: Fundamentals. Atlanta, USA. Am. Soc. Heating, Refrig. Air- Cond. Eng.
- ASTM international E 779-03, n.d. Standard Test Method for Determining Air Leakage Rate by Fan Pressurization.
- Ayata, T., Arcaklıoğlu, E., Yıldız, O., 2007. Application of ANN to explore the potential use of natural ventilation in buildings in Turkey. *Appl. Therm. Eng.* 27, 12–20. doi:10.1016/j.applthermaleng.2006.05.021
- Bangalee, M.Z.I., Miao, J.J., Lin, S.Y., Yang, J.H., 2013. Flow visualization, PIV measurement and CFD calculation for fluid-driven natural cross-ventilation in a scale model. *Energy Build.* 66, 306–314. doi:10.1016/j.enbuild.2013.07.005
- Banhazi, T.M., Seedorf, J., Rutley, D.L., Pitchford, W.S., 2008. Identification of Risk Factors for Sub-Optimal Housing Conditions in Australian Piggeries: Part 3. Environmental Parameters. *Am. Soc. Agric. Biol. Eng.* 14, 41–52.
- Barber, E.M., Ogilvie, J.R., 1982. Incomplete mixing in ventilated airspaces. Part 1 theoretical considerations. *Can. Agric. Eng.* 24, 25–29.
- Barth, M., Raabe, A., 2011. Acoustic tomographic imaging of temperature and flow fields in air. *Meas. Sci. Technol.* 22, 035102. doi:10.1088/0957-0233/22/3/035102
- Bartzanas, T., Kittas, C., Sapounas, A.A., Nikita-martzopoulou, C., 2007. Analysis of airflow through experimental rural buildings : Sensitivity to turbulence models 97, 229–239. doi:10.1016/j.biosystemseng.2007.02.009
- Berckmans, D., Goedseels, V., 1986. Development of new control techniques for the ventilation and heating of livestock buildings. *J. Agric. Eng. Res.* 33, 1–12. doi:10.1016/S0021-8634(86)80024-5

- Bjerg, B., Cascone, G., Lee, I.-B., Bartzanas, T., Norton, T., Hong, S.-W., Seo, I.-H., Banhazi, T., Liberati, P., Marucci, A., Zhang, G., 2013a. Modelling of ammonia emissions from naturally ventilated livestock buildings. Part 3: CFD modelling. *Biosyst. Eng.* 116, 259–275. doi:10.1016/j.biosystemseng.2013.06.012
- Bjerg, B., Liberati, P., Marucci, A., Zhang, G., Banhazi, T., Bartzanas, T., Cascone, G., Lee, I.-B., Norton, T., 2013b. Modelling of ammonia emissions from naturally ventilated livestock buildings: Part 2, air change modelling. *Biosyst. Eng.* 116, 246–258. doi:10.1016/j.biosystemseng.2013.01.010
- Bjerg, B., Sørensen, L.C., 2008. Numerical Simulation of Airflow in Livestock Buildings with Radial Inlet X, 1–11.
- Bjerg, B., Svidt, K., Zhang, G., Morsing, S., 2000. The Effects of Pen Partitions and Thermal Pig Simulators on Airflow in a Livestock Test Room. *J. Agric. Eng. Res.* 77, 317–326. doi:10.1006/jaer.2000.0596
- Blocken, B., 2014. 50 years of Computational Wind Engineering: Past, present and future. *J. Wind Eng. Ind. Aerodyn.* 129, 69–102. doi:10.1016/j.jweia.2014.03.008
- Boadi, D., Benchaar, C., Chiquette, J., Massé, D., 2004. Mitigation strategies to reduce enteric methane emissions from dairy cows: Update review. *Can. J. Anim. Sci.* 84, 319–335. doi:10.4141/A03-109
- Boulard, T., Kittas, C., Papadakis, G., Mermier, M., 1998. Pressure Field and Airflow at the Opening of a Naturally Ventilated Greenhouse. *J. Agric. Eng. Res.* 71, 93–102. doi:10.1006/jaer.1998.0302
- Boulard, T., Meneses, J.F., Mermier, M., Papadakis, G., 1996. The mechanics involved in the natural ventilation of greenhouses. *Agric. For. Meteorol.* 79, 61–77.
- Boulard, T., Papadakis, G., Kittas, C., Mermier, M., 1997. Air flow and associated sensible heat exchanges in a naturally ventilated greenhouse. *Agric. For. Meteorol.* 88, 111–119. doi:10.1016/S0168-1923(97)00043-9
- Boulard, T., Wang, S., Haxaire, R., 2000. Mean and turbulent air flows and microclimatic patterns in an empty greenhouse tunnel. *Agric. For. Meteorol.* 100, 169–181. doi:10.1016/S0168-1923(99)00136-7
- Brockett, B.L., Albright, L.D., 1987. Natural Ventilation in Single Airspace Buildings. *J. Agric. Eng. Res.* 37, 141–154.
- Bucklin, R.A., Nääs, I.A., Zazueta, F.S., Walker, W.R., 1991. Natural ventilation in swine housing. IFAS Bulletin 270. Florida Cooperative Extension Service, Institute of Food and Agric. Sciences, University of Florida.

- Calvet, S., Campelo, J.C., Estellés, F., Perles, A., Mercado, R., Serrano, J.J., 2014. Suitability evaluation of multipoint simultaneous CO₂ sampling wireless sensors for livestock buildings. *Sensors (Basel)*. 14, 10479–96. doi:10.3390/s140610479
- Calvet, S., Gates, R.S., Zhang, G., Estellés, F., Ogink, N.W.M., Pedersen, S., Berckmans, D., 2013. Measuring gas emissions from livestock buildings: A review on uncertainty analysis and error sources. *Biosyst. Eng.* 116, 221–231. doi:10.1016/j.biosystemseng.2012.11.004
- Campen, J., Bot, G.P., 2003. Determination of Greenhouse-specific Aspects of Ventilation using Three-dimensional Computational Fluid Dynamics. *Biosyst. Eng.* 84, 69–77. doi:10.1016/S1537-5110(02)00221-0
- Cao, X., Liu, J., Jiang, N., Chen, Q., 2014. Particle image velocimetry measurement of indoor airflow field: A review of the technologies and applications. *Energy Build.* 69, 367–380. doi:10.1016/j.enbuild.2013.11.012
- Carter, A.H., 2001. *Classical and statistical thermodynamics*. Prentice Hall, New Jersey, USA.
- Choiniere, Y., Blais, F., Munroe, J.A., 1988. A wind tunnel study of airflow patterns in a naturally ventilated building. *Can. Agric. Eng.* 293–297.
- Choiniere, Y., Munroe, J.A., 1994. A wind tunnel study of wind direction effects on airflow patterns in naturally ventilated swine buildings. *Can. Agric. Eng.*
- Choinière, Y., Munroe, J.A., 1990. Principles for natural ventilation for warm livestock housing, in: *Canadian Society of Agricultural Engineers*. Ontario, pp. 1–17.
- Choiniere, Y., Tanaka, H., Munroe, J.A., A., S.-T., 1992. prediction of wind induced ventilation for livestock housing. *J. Wind Eng. Ind. Aerodyn.* 44, 2563–2574.
- Choinière, Y., Tanaka, H., Munroe, J.A., -Tremblay, A.S., 1994. A wind tunnel study of the pressure distribution around sealed versus open low-rise buildings for naturally ventilated livestock housing. *J. Wind Eng. Ind. Aerodyn.* 51, 71–91. doi:10.1016/0167-6105(94)90078-7
- Chu, C.-R., Chiang, B.-F., 2013. Wind-driven cross ventilation with internal obstacles. *Energy Build.* 67, 201–209. doi:10.1016/j.enbuild.2013.07.086
- CIGR, 1992. 2nd Report of working Group on Climitazation of Animal Houses.
- Cooper, K., Parsons, D.J., Demmers, T., 1998. A Thermal Balance Model for Livestock Buildings for use in Climate Change Studies. *J. Agric. Eng. Res.* 69, 43–52. doi:10.1006/jaer.1997.0223
- Daskalov, P., Arvanitis, K., Sigrimis, N., Pitsilis, J., 2005. Development of an advanced microclimate controller for naturally ventilated pig building. *Comput. Electron. Agric.* 49, 377–391. doi:10.1016/j.compag.2005.08.010

- De Paepe, M., Pieters, J.G., Cornelis, W.M., Gabriels, D., Merci, B., Demeyer, P., 2013. Airflow measurements in and around scale-model cattle barns in a wind tunnel: Effect of wind incidence angle. *Biosyst. Eng.* 115, 211–219. doi:10.1016/j.biosystemseng.2013.03.008
- De Paepe, M., Pieters, J.G., Cornelis, W.M., Gabriels, D., Merci, B., Demeyer, P., 2012. Airflow measurements in and around scale model cattle barns in a wind tunnel: Effect of ventilation opening height. *Biosyst. Eng.* 113, 22–32. doi:10.1016/j.biosystemseng.2012.06.003
- De Vogeleer, G., Van Overbeke, P., Pieters, J.G., Demeyer, P., 2014. Assessing natural ventilation rates using a combined measuring and modelling approach, in: *International Conference of Agricultural Engineering - AgEng 2014 Zurich - Engineering for Improving Resource Efficiency*. pp. 1–8.
- Demmers, T.G.M., Burgess, L.R., Phillips, V.R., Clark, J. a., Wathes, C.M., 2000. Assessment of Techniques for Measuring the Ventilation Rate, using an Experimental Building Section. *J. Agric. Eng. Res.* 76, 71–81. doi:10.1006/jaer.2000.0532
- Demmers, T.G.M., Phillips, V.R., Short, L.S., Burgess, L.R., Hoxey, R.P., Wathes, C.M., 2001. Validation of Ventilation Rate Measurement Methods and the Ammonia Emission from Naturally Ventilated Dairy and Beef Buildings in the United Kingdom. *J. Agric. Eng. Res.* 79, 107–116. doi:10.1006/jaer.2000.0678
- DIN EN ISO, 5167-2:2004-01: Measurement of fluid flow by means of pressure differential devices inserted in circular cross-section conduits running full - Part 2: Orifice plates (ISO 5167-2:2003), n.d.
- Drenthen, J.G., de Boer, G., 2001. The manufacturing of ultrasonic gas flow meters. *Flow Meas. Instrum.* 12, 89–99. doi:10.1016/S0955-5986(01)00003-6
- EEA, 2014. Air pollution fact sheet 2014 - European Union (EU-28) [WWW Document].
- EFSA, 2009. Scientific report of EFSA prepared by the Animal Health and Animal Welfare Unit on the effects of farming systems on dairy cow welfare and disease. Annex to EFSA J. 1143, 1–7.
- EFSA, 2007. Scientific Opinion of the Panel on Animal Health and Welfare on a request from the Commission on Animal health and welfare in fattening pigs in relation to housing and husbandry. *EFSA J.* 564, 1–14.
- Estelles, F., Calvet, S., Ogink, N.W.M., 2010a. Effects of diurnal emission patterns and sampling frequency on precision of measurement methods for daily ammonia emissions from animal houses. *Biosyst. Eng.* 107, 16–24. doi:10.1016/j.biosystemseng.2010.06.007
- Estelles, F., Calvet, S., Ogink, N.W.M., 2010b. Effects of diurnal emission patterns and sampling frequency on precision of measurement methods for daily ammonia

- emissions from animal houses. *Biosyst. Eng.* 107, 16–24.
doi:10.1016/j.biosystemseng.2010.06.007
- Etheridge, D.W., 2012. *Natural Ventilation of Buildings: Theory, Measurement and Design.* John Wiley & Sons Ltd. doi:10.1037/009148
- Fiedler, M., Berg, W., Ammon, C., Loebstin, C., Sanftleben, P., Samer, M., von Bobrutski, K., Kiwan, A., Saha, C.K., 2013. Air velocity measurements using ultrasonic anemometers in the animal zone of a naturally ventilated dairy barn. *Biosyst. Eng.* 116, 276–285.
doi:10.1016/j.biosystemseng.2012.10.006
- Fracastoro, G.V., Mutani, G., Perino, M., 2002. Experimental and theoretical analysis of natural ventilation by windows opening. *Energy Build.* 34, 817–827. doi:10.1016/S0378-7788(02)00099-3
- Freire, R.Z., Abadie, M.O., Mendes, N., 2013. On the improvement of natural ventilation models. *Energy Build.* 62, 222–229. doi:10.1016/j.enbuild.2013.02.055
- Gates, R.S., Casey, K.D., Xin, H., Wheeler, E.F., Simmons, J.D., 2004. Fan Assessment Numeration System (FANS) Design and Calibration Specifications. *Am. Soc. Agric. Eng.* 47, 1709–1715.
- Graves, R.E., Brugger, M., 1995. *Natural Ventilation for Freestall Barns, Factsheet G-75,* Pennsylvania State University - College of Agricultural Sciences.
- Groot Koerkamp, P.W.G., Metz, J.H.M., Uenk, G.H., Phillips, V.R., Holden, M.R., Sneath, R.W., Short, J.L., White, R.P.P., Hartung, J., Seedorf, J., Schröder, M., Linkert, K.H., Pedersen, S., Takai, H., Johnsen, J.O., Wathes, C.M., 1998. Concentrations and Emissions of Ammonia in Livestock Buildings in Northern Europe. *J. Agric. Eng. Res.* 70, 79–95.
doi:10.1006/jaer.1998.0275
- Heber, A.J., Haymore, B.L., Duggirala, R.K., Keener, K.M., 2001. Air quality and emission measurement methodology at swine finishing buildings. *Am. Soc. Agric. Eng.* 44, 1765–1778.
- Heiselberg, P., 2006a. *Design of Natural and Hybrid Ventilation, DCE Lecture Notes No. 005,* Aalborg University - Department of Civil Engineering -Indoor Environmental Engineering, ISSN 1901-7286.
- Heiselberg, P., 2006b. *Modelling of Natural and Hybrid Ventilation, DCE Lecture Notes No. 004,* Aalborg University - Department of Civil Engineering -Indoor Environmental Engineering, ISSN 1901-7286.
- Hellickson, M.A., Hinkle, C.N., Jedele, D.G., 1983. Natural ventilation, in: *Natural Ventilation. In Ventilation of Agricultural Structures.* ASAE, St. Joseph, Mich., pp. 81–100.
- Hellickson, M.A., Walker, J.N., 1983. *Ventilation of agricultural structures. Monograph no. 6.* St. Am. Soc. Agric. Eng. 81–102.

- Hinz, T., Linke, S., 1998. A Comprehensive Experimental Study of Aerial Pollutants in and Emissions from Livestock Buildings. Part 1: Methods. *J. Agric. Eng. Res.* 70, 111–118. doi:10.1006/jaer.1997.0279
- Hoff, S.J., 2004. Automated control logic for naturally ventilated agricultural structures. *Appl. Eng. Agric.* 20, 47–56.
- Hoff, S.J., Jacobson, L.D., Heber, A.J., Ni, J., Zhang, Y., Koziel, J.A., Beasley, D.B., 2009. Real-Time Airflow Rate Measurements from Mechanically Ventilated Animal Buildings. *J. Air Waste Manage. Assoc.* 59, 683–694. doi:10.3155/1047-3289.59.6.683
- Hoxey, R.P., Richards, P.J., 1995. Full-scale wind load measurements point the way forward. *J. Wind Eng. Ind. Aerodyn.* 57, 215–224.
- Inard, C., Bouia, H., Dalicieux, P., 1996. Prediction of air temperature distribution in buildings with a zonal model. *Energy Build.* 24, 125–132. doi:10.1016/0378-7788(95)00969-8
- Industrial Emission Directive 2010/75/EU, 2015. Best Available Techniques (BAT) Reference Document for the Intensive Rearing of Poultry or Pigs.
- Innovatiesteunpunt, 2015. Energiewinst in limburg- Veehouderij.
- IPPC, 2003. Integrated Pollution Prevention and Control (IPPC): Reference Document on Best Available Techniques for Intensive Rearing of Poultry and Pigs.
- Ji, L., Tan, H., Kato, S., Bu, Z., Takahashi, T., 2011. Wind tunnel investigation on influence of fluctuating wind direction on cross natural ventilation. *Build. Environ.* 46, 2490–2499. doi:10.1016/j.buildenv.2011.06.006
- Joo, H.S., Ndegwa, P.M., Heber, a. J., Bogan, B.W., Ni, J.-Q., Cortus, E.L., Ramirez-Dorransoro, J.C., 2014. A direct method of measuring gaseous emissions from naturally ventilated dairy barns. *Atmos. Environ.* 86, 176–186. doi:10.1016/j.atmosenv.2013.12.030
- Joo, H.S., Ndegwa, P.M., Heber, A.J., Ni, J., Bogan, B.W., Ramirez-dorransoro, J.C., Cortus, E., 2015. Greenhouse gas emissions from naturally ventilated freestall dairy barns. *Atmos. Environ.* 102, 384–392. doi:10.1016/j.atmosenv.2014.11.067
- Kittas, C., Boulard, T., Papadakis, G., 1997. Natural ventilation of a greenhouse with ridge and side openings: sensitivity to temperature and wind effects. *Am. Soc. Agric. Eng.* 40, 415–425.
- Kiwan, A., Berg, W., Brunsch, R., Özcan, S., Müller, H., Gläser, M., Fiedler, M., Ammon, C., Berckmans, D., 2012. Tracer gas technique , air velocity measurement and natural ventilation method for estimating ventilation rates through naturally ventilated barns. *Agric Eng Int CIGR J.* 14, 22–36.
- Kiwan, A., Berg, W., Fiedler, M., Ammon, C., Gläser, M., Müller, H.-J., Brunsch, R., 2013. Air exchange rate measurements in naturally ventilated dairy buildings using the tracer gas

- decay method with ^{85}Kr , compared to CO_2 mass balance and discharge coefficient methods. *Biosyst. Eng.* 116, 286–296. doi:10.1016/j.biosystemseng.2012.11.011
- Kizil, U., Simsek, E., Lindley, J.A., 2002. Design of natural ventilation systems using a computer program, in: An ASAE Meeting Presentation.
- KMI, 2015. Karakteristieken van enkele klimatologische parameters [WWW Document]. URL <http://www.meteo.be/meteo/view/nl/360361-Parameters.html> (accessed 5.13.15).
- Komiya, K.-I., Teerawatanachai, S., 1993. Ultrasonic tomography for visualizing the velocity profile of air flow. *Flow Meas. Instrum.* 4, 61–65. doi:10.1016/0955-5986(93)90014-A
- Kurniadi, D., Trisnobudi, A., 2006. A Multi-Path Ultrasonic Transit Time Flow Meter Using a Tomography Method for Gas Flow Velocity Profile Measurement. Part. Part. Syst. Charact. 23, 330–338. doi:10.1002/ppsc.200601067
- Kyoto-Protocol, 1998. Kyoto Protocol to the United Nations Framework Convention on Climate Change. United Nations.
- Larsen, T.S., 2006. Natural Ventilation Driven by Wind and Temperature Difference, Doctoral dissertation. Aalborg University.
- Larsen, T.S.S., Nikolopoulos, N., Nikolopoulos, A., Strotos, G., Nikas, K.-S., 2011. Characterization and prediction of the volume flow rate aerating a cross ventilated building by means of experimental techniques and numerical approaches. *Energy Build.* 43, 1371–1381. doi:10.1016/j.enbuild.2011.01.015
- Lengers, B., Schiefler, I., Büscher, W., 2013. A comparison of emission calculations using different modeled indicators with 1-year online measurements. *Environ. Monit. Assess.* 185, 9751–9762. doi:10.1007/s10661-013-3288-y
- Linden, P.F., 1999. The fluid mechanics of natural ventilation. *Annu. Rev. Fluid Mech* 31, 201–38.
- Lo, L.J., Novoselac, A., 2012. Cross ventilation with small openings: Measurements in a multi-zone test building. *Build. Environ.* 57, 377–386. doi:10.1016/j.buildenv.2012.06.009
- López, A., Valera, D.L., Molina-Aiz, F., 2011a. Sonic anemometry to measure natural ventilation in greenhouses. *Sensors* 11, 9820–9838. doi:10.3390/s111009820
- López, A., Valera, D.L., Molina-Aiz, F.D., Peña, A., 2012a. Sonic anemometry measurements to determine airflow patterns in multi-tunnel greenhouses. *Spanish J. Agric. Res.* 10, 631. doi:10.5424/sjar/2012103-660-11
- López, A., Valera, D.L., Molina-Aiz, F.D., Peña, A., 2012b. Sonic anemometry to evaluate airflow characteristics and temperature distribution in empty Mediterranean greenhouses equipped with pad–fan and fog systems. *Biosyst. Eng.* 113, 334–350. doi:10.1016/j.biosystemseng.2012.09.006

- López, A., Valera, D.L., Molina-Aiz, F.D., Peña, A., 2011b. Effects of surrounding buildings on air patterns and turbulence in two naturally ventilated mediterranean greenhouses using tri-sonic anemometry. *Am. Soc. Agric. Biol. Eng.* 54, 1941–1950.
- Louwagie, L., 2015. 1700 Pigs die of suffocation. *Courth. news Serv.*
- Lule, I., Eren Özcan, S., Berckmans, D., 2014. Characterisation of ventilation rate in naturally-ventilated buildings using heat dissipation from a line source. *Biosyst. Eng.* 124, 53–62. doi:10.1016/j.biosystemseng.2014.05.009
- MB, 2004. 19 MAART 2004- Ministerieel besluit houdende vaststelling van de lijst van ammoniakemissiearme stalsystemen in uitvoering van artikel 1.1.2 en artikel 5.9.2.1bis van het besluit van de Vlaamse Regering van 1 juni 1995 houdende algemene en sectorale bepa.
- Mendes, L.B., Edouard, N., Ogink, N.W.M., van Dooren, H.J.C., Tinôco, I.D.F.F., Mosquera, J., 2015. Spatial variability of mixing ratios of ammonia and tracer gases in a naturally ventilated dairy cow barn. *Biosyst. Eng.* 129, 360–369. doi:10.1016/j.biosystemseng.2014.11.011
- Molina-Aiz, F.D., Valera, D.L., Peña, A. a., Gil, J. a., López, A., 2009. A study of natural ventilation in an Almería-type greenhouse with insect screens by means of tri-sonic anemometry. *Biosyst. Eng.* 104, 224–242. doi:10.1016/j.biosystemseng.2009.06.013
- Monteny, G., Hartung, E., 2007. Ammonia emissions in agriculture. DOI: 10.3920/978-90-8686-611-3.
- Monteny, G.-J., Bannink, A., Chadwick, D., 2006. Greenhouse gas abatement strategies for animal husbandry. *Agric. Ecosyst. Environ.* 112, 163–170. doi:10.1016/j.agee.2005.08.015
- Morsing, S., Ikeguchi, A., Bennetsen, J.C., Ravn, P., Okushima, L., 2002. Wind induced isothermal airflow patterns in a scale model of a naturally ventilated swine barn with cathedral ceiling. *Am. Soc. Agric. Eng.* 18, 97–101.
- Morsing, S., Strøm, J.S., Zhang, G.Ǻ., Kai, P., 2008. Scale model experiments to determine the effects of internal airflow and floor design on gaseous emissions from animal houses. *Biosyst. Eng.* 99, 99–104. doi:10.1016/j.biosystemseng.2007.09.028
- Mosquera, J., Monteny, G.J., Erisman, J.W., 2005. Overview and assessment of techniques to measure ammonia emissions from animal houses: the case of the Netherlands. *Environ. Pollut.* 135, 381–8. doi:10.1016/j.envpol.2004.11.011
- Nääs, I.A., Moura, D.J., Bucklin, R.A., Fialho, F.B., 1998. An algorithm for determining opening effectiveness in natural ventilation by wind. *Am. Soc. Agric. Eng.* 41, 767–771.

- Ndegwa, P.M., Hristov, A.N., Arogo, J., Sheffield, R.E., 2008a. A review of ammonia emission mitigation techniques for concentrated animal feeding operations. *Struct. Environ.* 100, 453–469. doi:10.1016/j.biosystemseng.2008.05.010
- Ndegwa, P.M., Joo, H.S., Heber, A.J., Ramirez-Dorronsoro, J.C., Cortus, E.L., Bogan, W.W., 2008b. A Method for Determination of Pollutant Emissions from Naturally Ventilated Freestall Dairy Barns, in: *Livestock Environment VIII*. pp. 237–244.
- NEC-Directive, 2001. Directive 2001/81/EC of the European parliament and of the council.
- Ngwabie, N.M., Jeppsson, K., Nimmermark, S., Swensson, C., Gustafsson, G., 2009. Multi-location measurements of greenhouse gases and emission rates of methane and ammonia from a naturally-ventilated barn for dairy cows. *Biosyst. Eng.* 103, 68–77. doi:10.1016/j.biosystemseng.2009.02.004
- Ngwabie, N.M., Vanderzaag, A., Jayasundara, S., Wagner-Riddle, C., 2014. Measurements of emission factors from a naturally ventilated commercial barn for dairy cows in a cold climate. *Biosyst. Eng.* 127, 103–114. doi:10.1016/j.biosystemseng.2014.08.016
- Nikas, K., Nikolopoulos, N., Nikolopoulos, A., 2010. Numerical study of a naturally cross-ventilated building. *Energy Build.* 42, 422–434. doi:10.1016/j.enbuild.2009.10.010
- Norton, T., Grant, J., Fallon, R., Sun, D., 2010. Optimising the ventilation configuration of naturally ventilated livestock buildings for improved indoor environmental homogeneity 45, 983–995. doi:10.1016/j.buildenv.2009.10.005
- Norton, T., Grant, J., Fallon, R., Sun, D., 2009. Assessing the ventilation effectiveness of naturally ventilated livestock buildings under wind dominated conditions using computational fluid dynamics. *Biosyst. Eng.* 103, 78–99. doi:10.1016/j.biosystemseng.2009.02.007
- Norton, T., Sun, D.-W., Grant, J., Fallon, R., Dodd, V., 2007. Applications of computational fluid dynamics (CFD) in the modelling and design of ventilation systems in the agricultural industry: a review. *Bioresour. Technol.* 98, 2386–414. doi:10.1016/j.biortech.2006.11.025
- Ntinis, G.K., Zhang, G., Fragos, V.P., Bochtis, D.D., Nikita-Martzopoulou, C., 2014. Airflow patterns around obstacles with arched and pitched roofs: Wind tunnel measurements and direct simulation. *Eur. J. Mech. B/Fluids* 43, 216–229. doi:10.1016/j.euromechflu.2013.09.004
- Ogink, N.W.M., Mosquera, J., Calvet, S., Zhang, G., 2013. Methods for measuring gas emissions from naturally ventilated livestock buildings : Developments over the last decade and perspectives for improvement. *Biosyst. Eng.* 116, 297–308. doi:10.1016/j.biosystemseng.2012.10.005
- Omland, Ø., 2002. Exposure and respiratory health in farming in temperate zones – a review of the literature. *Rev. Artic. AAEM Ann Agric Env. Med* 9, 119–136.

- Ozcan, S.E., 2011. Techniques to determine ventilation rate and airflow characteristics through naturally ventilated buildings, Doctoral dissertation, K. U. Leuven. K.U.Leuven. doi:ISBN 978-90-8826-205-0
- Özcan, S.E., Vranken, E., Berckmans, D., 2009. Measuring ventilation rate through naturally ventilated air openings by introducing heat flux. *Build. Environ.* 44, 27–33. doi:10.1016/j.buildenv.2008.01.011
- P. Karava, T. Stathopoulos, Athienitis, A.K., 2011. Wind Driven Flow Through Openings – A Review of Discharge Coefficients. *Int. J. Vent.* 3, 255–266.
- Papadakis, G., Mermier, M., Meneses, J.F., Boulard, T., 1996. Measurement and analysis of air exchange rates in a greenhouse with continuous roof and side openings. *J. Agric. Eng. Res.* 63, 219–227. doi:10.1006/jaer.1996.0023
- Park, J.S., 2013. Long-term field measurement on effects of wind speed and directional fluctuation on wind-driven cross ventilation in a mock-up building. *Build. Environ.* 62, 1–8. doi:10.1016/j.buildenv.2012.12.013
- Pearson, C.C., Owen, J.E., 1994. The Resistance to Air Flow of Farm Building Ventilation Components. *J. Agric. Eng. Res.* 57, 53–65.
- Perén, J.I., Hooff, T. Van, Leite, B.C.C., Blocken, B., 2015. CFD analysis of cross-ventilation of a generic isolated building with asymmetric opening positions : Impact of roof angle and opening location. *Build. Environ.* 85, 263–276. doi:10.1016/j.buildenv.2014.12.007
- Philippe, F.-X., Cabaraux, J.-F., Nicks, B., 2011. Ammonia emissions from pig houses: Influencing factors and mitigation techniques. *Agric. Ecosyst. Environ.* 141, 245–260. doi:10.1016/j.agee.2011.03.012
- Philippe, F.-X., Nicks, B., 2015. Review on greenhouse gas emissions from pig houses: Production of carbon dioxide, methane and nitrous oxide by animals and manure. *Agric. Ecosyst. Environ.* 199, 10–25. doi:10.1016/j.agee.2014.08.015
- Phillips, V.R., Lee, D.S., Scholtens, R., Garland, J. a., Sneath, R.W., 2001. A Review of Methods for measuring Emission Rates of Ammonia from Livestock Buildings and Slurry or Manure Stores, Part 2: monitoring Flux Rates, Concentrations and Airflow Rates. *J. Agric. Eng. Res.* 78, 1–14. doi:10.1006/jaer.2000.0618
- Randall, J.M., Sharp, J.R., Armsby, A.W., 1983. Cooling gradients across pens in a finishing piggery II. Effects on excretory behaviour. *J. Agric. Eng. Res.* 28, 261–268. doi:10.1016/0021-8634(83)90074-4
- Richards, P.J., Hoxey, R.P., 2012. Pressures on a cubic building—Part 1: Full-scale results. *J. Wind Eng. Ind. Aerodyn.* 102, 72–86. doi:10.1016/j.jweia.2011.11.004
- Richardson, G.M., Blackmore, P.A., 1995. The Silsoe Structures Building: Comparison of 1:100 model-scale data with full-scale data. *J. Wind Eng. Ind. Aerodyn.* 57, 191–201.

- Richardson, G.M., Hoxey, R.P., Robertson, A.P., Short, J.L., 1997. The Silsoe Structures Building : Comparisons of pressures measured at full scale and in two wind tunnels 72, 187–197.
- Rong, L., Nielsen, P. V, Zhang, G., 2009. Effects of airflow and liquid temperature on ammonia mass transfer above an emission surface: experimental study on emission rate. *Bioresour. Technol.* 100, 4654–61. doi:10.1016/j.biortech.2009.05.003
- Roy, J.C., Boulard, T., Kittas, C., Wang, S., 2002. Convective and Ventilation Transfers in Greenhouses, Part 1: the Greenhouse considered as a Perfectly Stirred Tank. *Biosyst. Eng.* 83, 1–20. doi:10.1006/bioe.2002.0107
- Saha, C.K., Ammon, C., Berg, W., Loebstin, C., Fiedler, M., Brunsch, R., von Bobrutski, K., 2013. The effect of external wind speed and direction on sampling point concentrations, air change rate and emissions from a naturally ventilated dairy building. *Biosyst. Eng.* 114, 267–278. doi:10.1016/j.biosystemseng.2012.12.002
- Samer, M., Loebstin, C., Fiedler, M., Ammon, C., Berg, W., Sanftleben, P., Brunsch, R., 2011a. Heat balance and tracer gas technique for airflow rates measurement and gaseous emissions quantification in naturally ventilated livestock buildings. *Energy Build.* 43, 3718–3728. doi:10.1016/j.enbuild.2011.10.008
- Samer, M., Loebstin, C., von Bobrutski, K., Fiedler, M., Ammon, C., Berg, W., Sanftleben, P., Brunsch, R., 2011b. A computer program for monitoring and controlling ultrasonic anemometers for aerodynamic measurements in animal buildings. *Comput. Electron. Agric.* 79, 1–12. doi:10.1016/j.compag.2011.08.006
- Schiffman, S.S., Auvermann, B.W., Bottcher, R.W., 2006. Health Effects of Aerial Emissions from Animal Production and Waste Management Systems. *Anim. Agric. Environ. Natl. Cent. Manure Anim. Waste Manag. White Pap.* 225–262.
- Scholtens, R., Dore, C.J., Jones, B.M.R., Lee, D.S., Phillips, V.R., 2004. Measuring ammonia emission rates from livestock buildings and manure stores—part 1: development and validation of external tracer ratio, internal tracer ratio and passive flux sampling methods. *Atmos. Environ.* 38, 3003–3015. doi:http://dx.doi.org/10.1016/j.atmosenv.2004.02.030
- Scholtensa, R., Doreb, C.J., Jonesb, B.M.R., Lee, D.S., Phillips, V.R., 2004. Measuring ammonia emission rates from livestock buildings and manure stores—part 1: development and validation of external tracer ratio, internal tracer ratio and passive flux sampling methods. *Atmos. Environ.* 38, 3003–3015.
- Shen, X., Zhang, G., Wu, W., Bjerg, B., 2013a. Model-based control of natural ventilation in dairy buildings. *Comput. Electron. Agric.* 94, 47–57. doi:10.1016/j.compag.2013.02.007
- Shen, X., Zhang, G., Wu, W., Bjerg, B., 2013b. Model-based control of natural ventilation in dairy buildings. *Comput. Electron. Agric.* 94, 47–57. doi:10.1016/j.compag.2013.02.007

- Shen, X., Zong, C., Zhang, G., 2012. Optimization of sampling positions for measuring ventilation rates in naturally ventilated buildings using tracer gas. *Sensors (Basel)*. 12, 11966–88. doi:10.3390/s120911966
- Sommer, S.G., Christensen, M.L., Schmidt, T., Jensen, L.S., 2013. *Animal manure recycling: Treatment and management*. Wiley, ISBN: 978-1-118-48853-9.
- Straw, M.P., 2000. *Computation and Measurement of Wind Induced Ventilation*, Doctoral dissertation. University of Nottingham.
- Strøm, J.S., Morsing, S., 1984. Automatically controlled natural ventilation in a growing and finishing pig house. *J. Agric. Eng. Res.* 30, 353–359. doi:10.1016/S0021-8634(84)80036-0
- Takai, H., Nimmermark, S., Banhazi, T., Norton, T., Jacobson, L.D., Calvet, S., Hassouna, M., Bjerg, B., Zhang, G.-Q., Pedersen, S., Kai, P., Wang, K., Berckmans, D., 2013. Airborne pollutant emissions from naturally ventilated buildings: Proposed research directions. *Biosyst. Eng.* 116, 214–220. doi:10.1016/j.biosystemseng.2012.12.015
- Teclé, A., Bitsuamlak, G.T., Jiru, T.E., 2013. Wind-driven natural ventilation in a low-rise building: A Boundary Layer Wind Tunnel study. *Build. Environ.* 59, 275–289. doi:10.1016/j.buildenv.2012.08.026
- Teitel, M., Liran, O., Tanny, J., Barak, M., 2008a. Wind driven ventilation of a mono-span greenhouse with a rose crop and continuous screened side vents and its effect on flow patterns and microclimate. *Biosyst. Eng.* 101, 111–122. doi:10.1016/j.biosystemseng.2008.05.012
- Teitel, M., Tanny, J., Ben-Yakir, D., Barak, M., 2005. Airflow patterns through roof openings of a naturally ventilated greenhouse. *Acta Hort.* 691, 663–670. doi:10.1016/j.biosystemseng.2005.07.013
- Teitel, M., Ziskind, G., Liran, O., Dubovsky, V., Letan, R., 2008b. Effect of wind direction on greenhouse ventilation rate, airflow patterns and temperature distributions. *Biosyst. Eng.* 101, 351–369. doi:10.1016/j.biosystemseng.2008.09.004
- UNECE, 2014. *Guidance document on preventing and abating ammonia emissions from agricultural sources*. EB.AIR 120.
- Van Buggenhout, S., Brecht, A. Van, Özcan, S.E., Vranken, E., Van Malcot, W., Berckmans, D., 2009. Influence of sampling positions on accuracy of tracer gas measurements in ventilated spaces. *Biosyst. Eng.* 104, 216–223. doi:10.1016/j.biosystemseng.2009.04.018
- Van Gansbeke, S., 2014. *Het ontwerp van melkveestallen*, Technische Brochure 31, Vlaamse Overheid, Beleidsdomein Landbouw en Visserij, Duurzame landbouwontwikkeling.
- van't Klooster, C.E., 1996. Animal-based control algorithm for natural ventilation in pig houses. *Am. Soc. Agric. Eng.* 39, 1127–1133.

- van't Klooster, C.E., Heitlager, B.P., 1994. Determination of Minimum Ventilation Rate in Pig Houses with Natural Ventilation based on Carbon Dioxide Balance. *J. agric. Engng Res* 57, 279–187.
- VDI2041, 2001. Measurement of Fluid Flow with Primary Devices: Orifice Plates and Nozzles for Special Applications: Orifices or Nozzles at the beginning or end of a pipe line. (reviewed 2001-04).
- Verlinde, W., Gabriels, D., Christiaens, J.P.A., 1998. Ventilation coefficient for wind-induced natural ventilation in cattle buildings: a scale model study in a wind tunnel. *Am. Soc. Agric. Eng.* 41, 783–788.
- Wang, K., Ye, Z., Li, H.U., 2010. Preliminary study of ammonia emissions from naturally ventilated fattening pig houses in the south-east China, in: XVIIth World Congress of the International Commission of Agricultural and Biosystems Engineering (CIGR). Québec, pp. 1–8.
- Wang, S., Deltour, J., 1999. Lee-side Ventilation-induced Air Movement in a Large-scale Multi-span Greenhouse. *J. Agric. Eng. Res.* 74, 103–110. doi:10.1006/jaer.1999.0441
- Wang, S., Yernaux, M., Deltour, J., 1999. A Networked Two-Dimensional Sonic Anemometer System for the Measurement of Air Velocity in Greenhouses. *J. Agric. Eng. Res.* 73, 189–197. doi:10.1006/jaer.1998.0403
- Webb, J., Menzi, H., Pain, B.F., Misselbrook, T.H., Dämmgen, U., Hendriks, H., Döhler, H., 2005. Managing ammonia emissions from livestock production in Europe. *Environ. Pollut.* 135, 399–406. doi:10.1016/j.envpol.2004.11.013
- Wu, W., Zhang, G., Kai, P., 2012. Ammonia and methane emissions from two naturally ventilated dairy cattle buildings and the influence of climatic factors on ammonia emissions. *Atmos. Environ.* 61, 232–243. doi:10.1016/j.atmosenv.2012.07.050
- Yu, H., Hou, C.-H., Liao, C.-M., 2002. Scale Model Analysis of Opening Effectiveness for Wind-induced Natural Ventilation Openings. *Biosyst. Eng.* 82, 199–207. doi:10.1006/bioe.2002.0072
- Zhang, G., Pedersen, S., Kai, P., 2010. Uncertainty analysis of using CO₂ production models by cows to determine ventilation rate in naturally ventilated buildings, in: XVIIth World Congress of the International Commission of Agricultural and Biosystems Engineering (CIGR). pp. 1–10.
- Zhang, J.S., Janni, K.A., Jacobson, L.D., 1989. Modeling Natural Ventilation by Combined Thermal Buoyancy and Wind. *Am. Soc. Agric. Eng.* 32, 2165–2174.
- Nikolopoulos, N., Nikolopoulos, A., Larsen, T.S., Nikas, K.-S.P., 2012. Experimental and numerical investigation of the tracer gas methodology in the case of a naturally cross-ventilated building. *Build. Environ.* 56, 379–388. doi:10.1016/j.buildenv.2012.04.006

Curriculum vitae

Personal Data

Name Philippe Van Overbeke
Date of birth January 14th,1986
Place of birth Ghent
Nationality Belgian
E-mail Philippe.vanoverbeke@ilvo.vlaanderen.be

Education

2011-present Doctoral Schools of Bioscience Engineering, Ghent University, Ghent
2004-2009 Master in Industrial Sciences- Electromechanics
1998-2004 Secondary school, Modern languages –Mathematics, K.A.Mariakerke,
Mariakerke

Professional Career

2009 – 2015 Researcher at the Institute for Agricultural and Fisheries Research (ILVO
Technology and Food Science Unit, Agricultural Engineering

Publications

International journals with peer review

Van Overbeke, P., Pieters, J. G., De Vogeleer, G., & Demeyer, P. (2014). Development of a reference method for airflow rate measurements through rectangular vents towards application in naturally ventilated animal houses: Part 1: Manual 2D approach. *Computers and Electronics in Agriculture*, 106, 31-41.

Van Overbeke, P., De Vogeleer, G., Pieters, J. G., & Demeyer, P. (2014). Development of a reference method for airflow rate measurements through rectangular vents towards application in naturally ventilated animal houses: Part 2: Automated 3D approach. *Computers and Electronics in Agriculture*, 106, 20-30.

Van Overbeke, P., De Vogeleer, G., Brusselman, E., Pieters, J.G., Demeyer, P.,(2015). Development of a reference method for airflow rate measurements through rectangular vents towards application in naturally ventilated animal houses: Part 3 : Application in a test facility in the open. Accepted in *Computers and Electronics in Agriculture*.

Van Overbeke, P., De Vogeleer, G., Brusselman, E., Demeyer, P., Pieters, J.G., (2015). Development of a reference method for airflow rate measurements through rectangular vents towards application in naturally ventilated animal houses: Part 4:Cross and ridge ventilated test facility. Submitted to *Computers and Electronics in Agriculture*

Conference proceedings

Van Overbeke, P., De Vogeleer, G., Pieters, J., & Demeyer, P. (2014). Development of a Reference Test Facility for the Validation of Naturally Ventilated Airflow Rate Measurement Techniques. In proceedings of the 18th World Congress of CIGR - International Commission of Agricultural and Biosystems Engineering, Beijing, China.

Van Overbeke, P., Pieters, J., De Vogeleer, G., & Demeyer, P. (2013). Development of a reference method for the measurement of the ventilation rate through rectangular ventilation openings using ultrasonic anemometers. In proceedings of the 11th Conference "Construction, Engineering and Environment in Livestock Farming, Vechta, Germany.

Van Overbeke, P., De Vogeleer, G., Demeyer, P., & Pieters, J. (2013). Development of a real life measuring technique for the ventilation rate of naturally ventilated animal houses. In proceedings of 18th National Symposium on Applied Biological Sciences, Ghent, Belgium.

De Vogeleer, G., **Van Overbeke, P.**, Pieters, J. G., & Demeyer, P. (2014). Assessing natural ventilation rates using a combined measuring and modelling approach. In proceedings of International Conference of Agricultural Engineering - Engineering for Improving Resource Efficiency. The European Society of Agricultural Engineers (EurAgEng), Zurich, Switzerland

De Vogeleer, G., Pieters, J., **Van Overbeke, P.**, & Demeyer, P. (2013). Field test facility for the development of a reference method for ventilation rate and emission measurements in naturally ventilated pig houses. In proceedings of the 11th Conference "construction, engineering and environment in livestock farming", Vechta, Germany

Vulgarising literature

Van Overbeke, P., D'Hoop, M., Van Ransbeeck, N., & Demeyer, P. (editor) (2010). Code van goede praktijk voor emissiearme stalsystemen in de varkenshouderij. Instituut voor Landbouw- en Visserijonderzoek.

Van linden, V., Dekeyser, D., **Van Overbeke, P.**, Baets, B., Löffel, J., & Degroote, T. (2011). Code van goede praktijk voor het energie-efficiënt gebruik van mechanische ventilatie in de intensieve veehouderij: Onderdeel van een ADLO-demonstratieproject rond energiezuinigheid in de Vlaamse Land- en Tuinbouw. Instituut voor Landbouw- en Visserijonderzoek.

Scientific Activities

Oral presentations at conferences

17 09 2014 Development of a Reference Test Facility for the Validation of Naturally Ventilated Airflow Rate Measurement Techniques - 18th World Congress of CIGR - International Commission of Agricultural and Biosystems Engineering, Beijing, China.

25 09 2013 Development of a reference method for the measurement of the ventilation rate through rectangular ventilation openings using ultrasonic anemometers - 11th Conference "Construction, Engineering and Environment in Livestock Farming, Vechta, Germany.